^{18}F-Labeling of Small Molecules and Peptides

Von der Fakultät für Mathematik, Informatik und Naturwissenschaften der RWTH Aachen University zur Erlangung des akademischen Grades eines Doktors der Naturwissenschaften genehmigte Dissertation

vorgelegt von

Master of Science

H. Jens Rickmeier

aus Ahlen

Berichter: Professor Dr. Tobias Ritter

Universitätsprofessor Dr. Carsten Bolm

Tag der mündlichen Prüfung: 13. September 2019

Zusammenfassung

Bis 2018 hat die Food and Drug Administration (FDA) nur zehn Positronen-Emissionstomographie (PET)-Tracer zugelassen, von denen sechs in den letzten sieben Jahren entwickelt wurden. Die geringe Menge an zugelassenen PET-Tracern ist zum Teil auf das Fehlen allgemeiner Methoden zur Herstellung von potenziellen Tracern zurückzuführen. Die Halbwertszeit, der am häufigst verwendeten Radionuklide, liegt unter zwei Stunden. Daher sollte das Radionuklid möglichst spät in der Synthese eingeführt werden. Die hohe Dichte an funktionellen Gruppen kann die Reaktivität von Fluorid verringern und Reagenzien oder Katalysatoren deaktivieren. Es werden neue Methoden benötigt, die eine hohe strukturelle Komplexität tolerieren und damit den Zugang zu neuen Tracern ermöglichen.

Die Gruppe von Professor Tobias Ritter hat die robuste Ruthenium-vermittelte Radiodeoxyfluorierung von Phenolen entwickelt. Das erste Kapitel dieser Arbeit beschreibt ein verbessertes Verfahren für die Ruthenium-vermittelte Radiodeoxyfluorierung, das es uns ermöglicht hat, dass sonst unzugängliche [^{18}F]Atorvastatin herzustellen. Unter basischen Bedingungen wurde eine selektive Komplexierung des 4-Hydroxyphenylsubstituenten gegenüber anderen Arylsubstituenten in Hydroxy-Atorvastatin erreicht. Die Verwendung protischer polarer Lösungsmittel ermöglichte eine nahezu quantitative Elution von [^{18}F]Fluorid von der Anionenaustauschkartusche. Diese Verbesserungen der Methode erlaubten es uns, [^{18}F]Atorvastatin in 20% radiochemischer Ausbeute zu isolieren und wir konnten zeigen, dass es im Menschlichen- und Rattenserum stabil ist.

Peptide sind eine vielversprechende Plattform für die Entwicklung von PET-Tracern, da sie sehr selektive Bindungseigenschaften und eine schnelle Entfernung aus dem Blutkreislauf aufweisen können. Darüber hinaus ermöglicht die schnelle Synthese von Derivaten durch Festphasen-Peptidsynthese (SPPS) das schnelle Screening einer Strukturdatenbank. In den letzten zehn Jahren wurden viele Methoden zur Polypeptidmarkierung mit [^{18}F]Fluorid entwickelt, die jedoch alle die Einführung einer prosthetischen Gruppe erfordern, welche die Eigenschaften des Peptids verändert. Der zweite Teil dieser Arbeit berichtet über ein Verfahren, in dem durch

Radiodeoxyfluorierung eines Tyrosinrestes in einem Peptid die Einbringung von 4-[^{18}F]Fluorphenylalanin-Seitenketten ernöglicht wird. Durch den Austausch eines Wasserstoff- oder Hydroxysubstituenten in der nativen Peptidstruktur mit Fluor-18 werden die sterischen Eigenschaften des Peptids kaum verändert und damit seine biologischen Funktionen sehr wahrscheinlich nicht verändert. Die vorgestellte Methode toleriert alle 20 kanonischen Aminosäuren, ermöglicht die Markierung am C-Terminus, N-Terminus oder innerhalb des Peptids und der Markierungsvorläufer kann druch einen neuartigen, rutheniumhaltigen Aminosäurebausteins per SPPS synthetisiert werden.

Abstract

As of 2018, the Food and Drug Administration (FDA) has approved just ten positron-emission-tomography (PET)-tracers, of which six have been developed in the last seven years. The overall low quantity of approved PET-tracers can be partly attributed to the lack of general methods to access potential tracers. The half-life of commonly used radionuclides is below two hours; therefore, the radionuclide should be introduced in the last step of the synthesis. The high density of functional groups on advanced molecular structures can lower the reactivity of fluoride, and can deactivate reagents and catalysts. New methods are required that tolerate high structural complexity and thereby permit access to new tracers.

The group of Ritter has developed the highly functional group tolerant ruthenium-mediated radio-deoxyfluorination of phenols. The first chapter of this thesis describes an improved procedure for the ruthenium-mediated radio-deoxyfluorination, which has allowed us to obtain the otherwise inaccessible [^{18}F]atorvastatin. Under basic conditions, selective complexation to the 4-hydroxyphenyl substituent over other aryl substituents in hydroxy-atorvastatin was achieved. The use of protic polar solvents enabled almost quantitative elution of [^{18}F]fluoride from the anion exchange cartridge without the need for inversion. These improvements of the method allowed us to isolate [^{18}F]atorvastatin in 20% radiochemical yield and we could show that it is stable in human and rat serum.

Peptides are a favorable platform for the development of PET-tracers, because they can show very selective binding and rapid clearance from the bloodstream. Additionally, rapid synthesis of derivatives by solid phase peptide synthesis (SPPS) enables for the fast screening of a structural library. Over the last decade, many methods for polypeptide labeling with [^{18}F]fluoride have been developed, however, all require the introduction of a prosthetic group that changes the properties of the peptide. The second part of this thesis reports a method that provides access to peptides containing 4-[^{18}F]fluoro-phenylalanine side chains by radio-deoxyfluorination of a tyrosine residue bearing a traceless transition metal activating group. By merely exchanging one hydrogen or hydroxyl substituent of the native peptide structure with fluorine-18, the steric properties of the

peptide are barely altered and thus its biological functions are likely preserved. The presented method tolerates all 20 canonical amino acids, allows the labeling on the C- terminus, N- terminus or within the peptide, and enables the labeling precursor to be easily accessed by SPPS using a novel ruthenium-containing amino acid building block.

In memory of my father Heinrich Rickmeier

TABLE OF CONTENT

Notes

The work presented in this thesis was carried out from October 2015 until June 2019 at the Max Planck Institut für Kohlenforschung, under the supervision of Prof. Dr. Tobias Ritter.

Parts of this dissertation were published and have been reproduced with permission.

Gonçalo S. Clemente, **Jens Rickmeier**, Tryfon Zarganes-Tzitzikas, Farinha I. Antunes, Riemer H. J. A. Slart, Alexander Dömling, Tobias Ritter, Philip H. Elsinga, "Automated Radiosynthesis of [^{18}F]Atorvastatin via Ru-mediated ^{18}F-deoxyfluorination: a prospective PET-Imaging Tool for the Assessment of Statin related Mechanisms of Action" , *J. Labelled Compd. Radiopharm.* **2019**, *62*, S84–S85.

Jens Rickmeier, Tobias Ritter, "Site-Specific Deoxyfluorination of Small Peptides with [^{18}F]Fluoride" *Angew. Chem. Int. Ed.*, **2018**, *57*, 14207–14211.

"Reagent and process for the site-specific deoxyfluorination of peptides", Tobias Ritter and **Jens Rickmeier**, EP18181055.7, **2018.**

In addition to the work presented in this thesis, additional research conducted during my doctoral studies has been published as contributions to the following publications:

Gonçalo S. Clemente, Farinha I. Antunes, **Jens Rickmeier**, Ben L. Feringa, Philip H. Elsinga, Tobias Ritter, "Automated Synthesis of 5-[^{18}F]fluoro-Tryptophan via Deoxyfluorination of a Phenol-derived Ru-coordinated Complex", *Eur. J. Nucl. Med. Mol. Imaging*, **2018**, *45* (1), S223–S223.

List of Abbreviation

3D	three-dimensional
α	alpha particle
A	amount of activity
Å	ångström
Ac	acetyl
acetyl-CoA	acetyl-coenzyme A
Ala	alanine
Aq	aqeous
Ar	aryl
Arg	arginine
Asn	asparagine
Asp	aspartic acid
AY	activity yield
β^+	positron
Bn	benzyl
Boc	*tert*-butyloxycarbonyl
Bq	becquerel
br	broad
^{t}Bu	*tert*-butyl
c.a.	carrier added
calcd	calculated
COD	1,5-cyclooctadiene
Cp	cyclopentadienyl
CT	computer tomography
CuAAC	copper(I)-catalyzed azide alkyne cycloaddition
Cys	cysteine
d	doublet
DCM	dichloromethane
DCC	*N*,*N*′-dicyclohexylcarbodiimide
DCE	dichloroethane
DFI	2,2-difluoro-1,3-dimethylimidazolidine
diCy-18-cr-6	dicyclohexano-18-crown-6
DIPEA	diisopropylethylamine
DMF	*N*,*N*-dimethylformamide
DMSO	dimethylsulfoxide
DOTA	1,4,7,10-tetraazacyclododecane-1,4,7,10-tetraacetic acid
DTT	dithiothreitol
EC	electron capture
EI	electron ionization
equiv	equivalent
EOB	end of bombardment
ESI	electrospray ionization
EtOH	ethanol
eV	electronvolt
FBAM	*N*-[6-(4-fluorobenzylidene)aminooxyhexyl]maleimide
FDA	Food and Drug Administration
[^{18}F]FDG	2-deoxy-2-[^{18}F]fluoroglucose
Fmoc	fluorenylmethoxycarbonyl
g	gram
GC	gas chromatography
Gln	glutamine

Glu	glutamic acid
Gly	glycine
HBTU	2-(1*H*-benzotriazol-1-yl)-1,1,3,3-tetramethyluronium-hexafluorophosphate
HCl	hydrochloric acid
HFIP	1,1,1,3,3,3-hexafluoro-2-propanol
His	histidine
HOBt	1-hydroxybenzotriazol
HPLC	high-performance liquid chromatography
HMG-CoA	*β*-hydroxy *β*-methylglutaryl-coenzyme A
HRMS	high-resolution mass spectrometry
ICP-MS	inductively coupled plasma mass spectrometry
Ile	isoleucine
^{iPr}ImCl	2-chloro-1,3-bis(2,6-diisopropylphenyl)imidazolium chloride
J	coupling constant
K_{222}	Kryptofix [2.2.2] = 4,7,13,16,21,24-hexaoxa-1,10-diazabicyclo[8.8.8]hexacosane
L	liter
Leu	leucine
Lys	lysine
m	multiplet
M	moles per liter
MA	molar activity
mAbs	monoclonal antibodies
Me	methyl
MeCN	acetonitrile
MeOH	methanol
Met	methionine
MG11	Minigastrin 11
mol%	mole percent
m.p.	melting point
MRI	magnetic resonance imaging
MS	molecular sieves
n	amount of substance
N	neutron
NaDT	sodium decatungstate
n.c.a.	no carrier added
n.d.	not determined
NFSI	*N*-fluorobenzenesulfonimide
NHS	*N*-hydroxysuccinimide
ν	neutrino
NMR	nuclear magnetic resonance
NpTMAF	neopentyltrimethylammonium fluoride
NpTMAOx	bis(neopentyltrimethylammonium) oxalate
Nu	nucleophile
OSu	*N*-oxysuccinimide
OTf	triflate
P	proton
Pbf	2,2,4,6,7-pentamethyldihydrobenzofuran-5-sulfonyl
PBS	phosphate-buffered saline
PET	positron-emission-tomography
PivCN	pivalonitrile
PG	protecting group
Ph	phenyl
Phe	phenylalanine
PMB	4-methoxybenzyl
ppb	parts per billion

ppm	parts per million
^{i}Pr	isopropyl
Pro	proline
q	quartet
QMA	quaternary methyl-ammonium
R	arbitrary organic substituent
RCY	radiochemical yield
RT	room temperature
s	singlet
sat.	saturated
S_EAr	electrophilic aromatic substitution
Ser	serine
[^{18}F]SFB	*N*-succinimidyl-4-[^{18}F]fluorobenzoic acid
SiFA	silicon fluoride acceptor
S_NAr	nucleophilic aromatic substitution
t	triplet
TEA	tetraethylammonium
TBA	tetrabutylammonium
TFA	trifluoroacetic acid
THF	tetrahydrofuran
TIPS	triisopropylsilane
TLC	thin-layer chromatography
Tmob	2,4,5-trimethoxybenzyl
Thr	threonine
Trp	tryptophan
Trt	trityl
Tyr	tyrosine
UV	ultraviolet
Val	valine
vis	visible
X	halogen or *pseudo* halogen

Acknowledgment

First and foremost I would like to express my gratitude to Prof. Dr. Tobias Ritter for giving me the opportunity to do my doctoral studies in his group and for giving me the confidence and the freedom to design and perform my own projects. I would also like to thank him for teaching me how to select experiments that allow key hypotheses of a project to be tested and how to adjust the direction of a project accordingly. I would like to thank him for interesting scientific discussions and for invaluable feedback on my communication and leadership skills. Finally, I want to thank him for giving me the opportunity to work on interdisciplinary projects with collaborators/experts from a wide range of areas.

I am grateful to Prof. Dr. Carsten Bolm for the examination of this doctoral thesis. I am thankful to Matthew Tredwell for teaching me how to work with fluorine-18 and for being a great training partner for running competitions. I have to thank all members of the Ritter research group for helpful discussions and the creation of an enjoyable research environment. Special thanks go to Jonas Börgel, Heejun Lee, and Matthew Plutschack, with whom I shared my office with and with whom I had invaluable scientific discussions with.

I want also to thank all the talented technicians, visiting students and doctoral students with whom I had the chance to work with, for their helpful support. I want to highlight the work of Nele Kronau, who helped me to discover additives to improve the elution efficiency of fluorine-18, and Sonja Irene Klein, who helped me to expand the substrate scope of the peptide labeling project. For the successful collaboration in the development of a theranostic peptide pair I want to thank Nicola Breen. Working with them was a great learning process for me and I hope they learned as much as I did.

Special thanks go to all the collaborators with whom I could work with throughout my time in the Ritter laboratory. I want to take the chance to thank in particular Gonçalo Santos Clemente, for performing the biological tests with [^{18}F]atorvastatin.

I would like to thank Jonas Börgel, Matthew Plutschack, Florian Berger, and Nicola Breen for carefully proofreading this manuscript and thereby improving its quality considerably.

Also I want to thank Sylwia Falk for all her support with bureaucratic problems and for helping me with the organization of events. I would also like to thank Joseph Cornella for enabling me to invite inspiring speakers to the Institute.

The greatest thanks are due to my family, who always listened to me and unconditionally support me. Beside my parents I would like to thank Lisa for her endless patience and understanding. Without your support, I would not have achieved what I have.

I. Introduction

I.1. Nuclear Imaging

I.1.1. Key discoveries toward positron-emission-tomography (PET)

George de Hevesy, also known as “the father of nuclear medicine”, was the first to use radioactive tracers to study biochemical processes.[1] He proposed that the great sensitivity to measure radioactivity and the similar chemical behavior of isotopes of the same element would make radioactive isotopologues promising tracers to study *in vivo* behavior.[2] In his initial experiments, he studied the absorption and translocation of lead in plants by immersing the roots of *Vicia Faba* in a solution of radioactive lead-212 nitrate and subsequently measuring the relative activity of the roots, stem, leaves, and fruits of the plants.[1] He also showed that this technique could be translated to animals while studying the phosphorus metabolism in rats.[3] George de Hevesy received the Nobel Prize in chemistry in 1943 for discovering that radioactive isotopologues can be used to study *in vivo* processes and for the application of this technique.[2]

The next important milestone toward the development of PET was Irène Curie’s discovery that the irradiation of a boron-10 sample with alpha particles affords a new radioactive element with a half-life of 14 minutes.[4] This was the first observation that artificial radioactive isotopes can be synthesized by bombardment of elements with light particles. E. Lawrence *et al.* built the first particle accelerator, also known as a cyclotron, and demonstrated that artificial radioactive substances can be synthesized by bombarding samples with accelerated deuteron particles. This technology was a key invention to PET because, for the first time, it allowed the reliable and on demand synthesis of artificial isotopes without the need of another radioactive sample.[5]

I.1.2. **Principle of PET**

Positron-emission-tomography is a non-invasive imaging technique that enables the visualization of radiolabeled molecules *in vivo* and can be used to diagnose diseases, study biochemical processes and develop drugs.[6] Unlike other imaging techniques that give anatomical images of the body, such as magnetic resonance imaging (MRI), X-ray and computer tomography (CT), PET is a functional imaging modality.[7] As such, it visualizes the spatial distribution of tracer molecules and thereby gives information about biological processes such as metabolism, receptor concentration or transport across cell membranes. An abnormal change of these processes is common in diseases and can occur before anatomical changes can be observed, enabling an earlier diagnosis of diseases.[8] The high sensitivity of PET (10^{-11} M – 10^{-12} M) allows the use of small amounts of tracer molecules (ng quantities) that typically have no relevant influence on biological systems at low concentration.[6] Since PET-images provide only the spatial concentration of the tracer, it is often combined with complimentary anatomical imaging techniques, such as CT, to enable precise localization of the tracer within the body. In addition, spatially-resolved information about γ-ray scattering obtained by the CT-scan enables a higher spatial resolution in PET (1 – 6 mm).[9]

PET-tracers are typically administered by inhalation or by intravenous injection to avoid time consuming uptake into the bloodstream via the gastrointestinal tract.[8] The blood stream transports the tracer to the target, to which the tracer tightly binds. In order to get a high target-to-background ratio, non-bound tracer molecules need to be cleared from the bloodstream before imaging. Upon beta-plus-decay of the neutron-deficient radionuclide in the tracer, one proton (P) is converted into a neutron (N), and a neutrino (ν) and a positron (β^+) are emitted (Figure 1).[10] The positron migrates through the tissue and loses kinetic energy by collision with other atoms. Once the kinetic energy of the positron is below 10 eV, it recombines with an electron to form a positronium that, upon annihilation, emits two γ-rays with an energy of 511 keV at an angle almost 180° to each other.[11] The small deviation of 180° is a result of the remaining kinetic energy of the positronium. The emitted γ-rays are detected by a scintillation detectors placed

around the patient. If two opposite detectors measure an impact with 511 keV within a short time frame the signal is valid. The signals are then converted by a computer into a 3D-image of the absolute tracer concentration.[7]

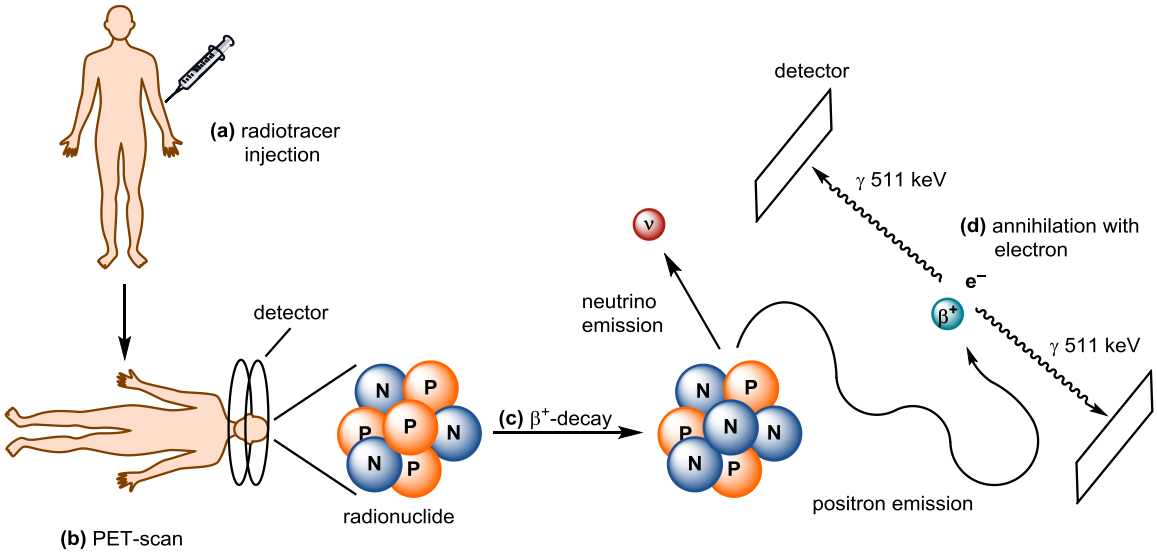

Figure 1. General principle of PET.[12]

The most commonly used PET-tracer is [^{18}F]fluorodeoxyglucose ([^{18}F]FDG, **7**), with major applications in oncology.[13] Structurally, [^{18}F]FDG is a glucose analog in which the hydroxyl-substituent in the two-position is exchanged with its bioisostere fluorine-18. Therefore, [^{18}F]FDG is metabolically similar to glucose and can be used to image glucose metabolism. Glucose transporters internalize [^{18}F]FDG into the cells, where it is phosphorylated by hexokinase at the oxygen in six-position.[12] The next step of the glycolysis cascade, the isomerization of glucose to fructose, cannot occur with [^{18}F]FDG due to the absence of the hydroxyl substituent in the two-position, so it is captured in the cell. Due to its high polarity the not trapped [^{18}F]FDG is rapidly cleared from the bloodstream through the bladder. Many types of cancer have upregulated glucose transporter and hexokinase expression and, therefore, [^{18}F]FDG accumulates faster in cancerous tissue than in healthy tissue.[14] Therefore, unusually high glucose uptake may indicate cancer. Despite the high cost of this imaging technique, it has found widespread applications and has resulted in a dense cyclotron infrastructure.[13]

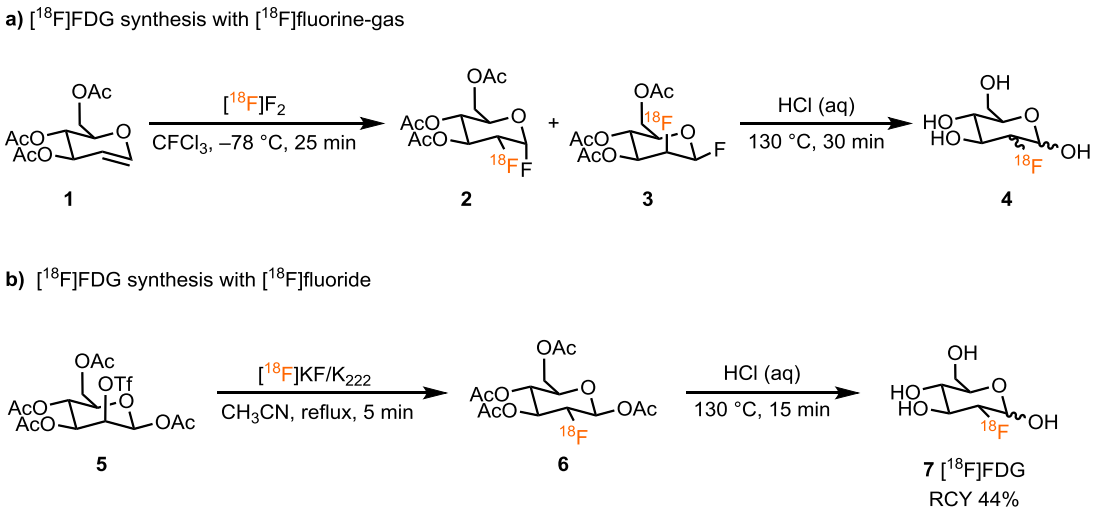

Scheme 1. Synthesis of [^{18}F]fluorodeoxyglucose.[15]

In 1978, [^{18}F]FDG was first synthesized in a two-step procedure starting from 3,4,6-tri-O-acetyl-*D*-glycal (**1**). In the first step [^{18}F]fluorine gas was added to the enol **1** to afford **2** and **3** in a 4:1 ratio (Scheme 1 a). The subsequent purification, and hydrolysis with aqueous (aq) hydrochloric acid (HCl) afforded [^{18}F]FDG in 8% radiochemical yield (RCY).[15a] Due to the utility of [^{18}F]FDG, the synthesis sequence was continuously improved. Hamacher *et al.* reported the state of art procedure starting from [^{18}F]fluoride, which is easier to handle than [^{18}F]fluorine gas (Scheme 1 b). In the first step, the triflate substituent in **5** is displaced via nucleophilic substitution with [^{18}F]fluoride, followed by the removal of acetyl protecting groups under acidic or basic conditions to afford [^{18}F]FDG in 44% RCY.[15b, 16]

I.1.3. **Radionuclides**

Despite fluorine-18 being the most commonly used radioisotope in PET-imaging, it is not always the ideal radionuclide for all kinds of tracers. The ideal half-life of the radionuclide depends on the biochemical process that should be visualized by a tracer molecule. Radiolabeled monoclonal antibodies (mAbs) often show an optimal tumor-to-background ratio 2–4 days post injection and require radionuclides with appropriate half-lives ($t_{½}$), such as iodine-124 ($t_{½}$ = 4.18 days, Table 1).[17] However, other biological processes can be visualized relatively quickly. For example, blood flow is imaged with [^{15}O]water, which has a half-life of two minutes.[18] In general, the half-life of the radionuclide needs to be long enough for the tracer to reach an optimal

target-to-background ratio, while being as short as possible to minimize the radiation dose for the patient. The ideal radionuclide for PET-imaging should decay only via positron emission and the energy of the positron should be as low as possible to achieve maximal spatial resolution and minimal radiation dose for the patient (Table 1).[19] Furthermore, the radionuclide needs to be easily accessible to enable a reliable and cost efficient synthesis of tracers.

Table 1. Properties of important PET radionuclides.[20]

nuclide	half-life	max. positron energy [MeV]	max. linear range in H_2O [mm]	max. molar activity [GBq·µmol^{-1}]	production method	decay mode (%)
^{11}C	20.3 min	0.96	4.1	3.4 x 10^5	^{14}N(p,α)^{11}C	β^+(99.8) EC(0.2)
^{13}N	9.97 min	1.19	5.4	6.9 x 10^5	^{16}O(p,α)^{13}N	β^+(100)
^{15}O	2.03 min	1.72	8.2	3.4 x 10^6	^{14}N(d,n)^{15}O	β^+(99.9) EC(0.1)
^{18}F	109.8 min	0.64	2.4	6.3 x 10^4	^{18}O(p,n)^{18}F ^{20}Ne(d,α)^{18}F	β^+(97) EC(3)
^{64}Cu	12.7 h	0.66	2.5	9 x 10^3	^{64}Ni(p,n)^{64}Cu	β^+(25) EC(75)
^{68}Ga	68.3 min	1.90	10	1.0 x 10^5	^{68}Ge(EC)^{68}Ga	β^+(90) EC(10)
^{124}I	4.18 days	2.14	14	1.2 x 10^3	^{124}Te($d,2n$)^{124}I	β^+(25) EC(75)

Most of the commonly used radioisotopes are synthesized by a cyclotron, a compact particle accelerator. The production of [^{18}F]fluoride begins with conversion of dihydrogen in an electric current into hydride anions (Figure 2).[5] The hydride anions are accelerated by an electric field on a spiral trajectory between two D-shaped hallow metal chambers. Once the hydride anion reaches the desired kinetic energy, it passes through a foil of carbon, the so-called stripper, where it is oxidized to a proton. The proton emitted from cyclotron hits a target of [^{18}O]water and combines with the nucleus, while a neutron is emitted.

Nitrogen-13 is produced in the cyclotron by the nuclear reaction ^{16}O(p,α)^{13}N and is available as nitrate or nitrite in water. The [^{13}N]nitrate can be subsequently reduced with the Devarda's alloy to afford [^{13}N]ammonia, the only FDA approved PET-tracer containing nitrogen-13.[21] In patients

with suspected or existing coronary artery disease [^{13}N]ammonia is used to image the myocardial perfusion. The short half-life of 9.97 minutes requires on site production of the tracer.

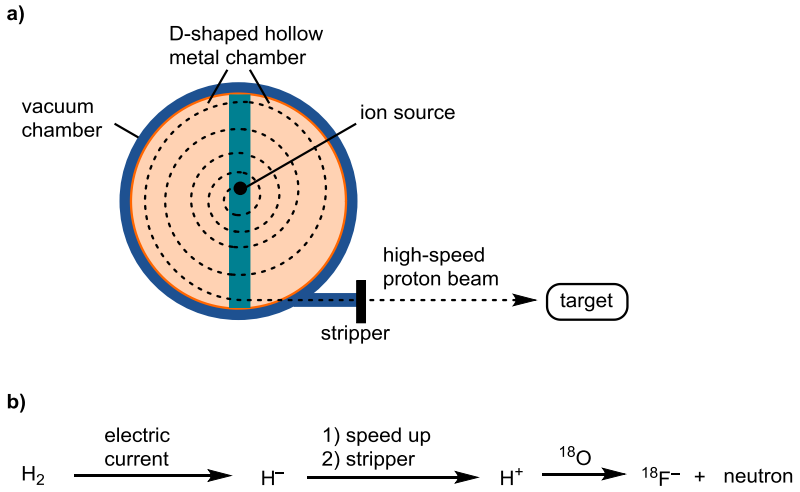

Figure 2. Cyclotron production of fluorine-18.[22]

Carbon-11 has a half-life of 20.3 minutes, allowing PET-imaging times of more than one hour. Since carbon is among the most abundant elements in natural products and pharmaceuticals, its radioactive isotope can be used to label them without affecting their biological behavior.[23] This can be crucial, for example, for investigating the pharmacokinetic profile of drugs. Despite the short half-life of 20.3 minutes, carbon-11 can be used in multistep syntheses. Carbon-11 is synthesized by proton bombardment of nitrogen-14, which emits an alpha particle to afford carbon-11 (^{14}N(p,α)^{11}C). Targets containing [^{14}N]nitrogen-gas and dihydrogen afford [^{11}C]CH_4, which can be further converted by gas-solid iodination to [^{11}C]methyliodide. Carbon-11 is most commonly introduced in organic molecules by electrophilic alkylation.[24] The only FDA approved carbon-11 containing PET-tracer is [^{11}C]choline. It is used to diagnose prostate cancer and brain tumors.

Metallic positron emitters are typically attached to the target molecule via bifunctional chelators. The chelator labeling approach is most commonly used for labeling of large molecules (molecular weight (MW) > 1000 g·mol^{-1}), as they tend to show smaller changes in binding affinities upon introduction of the chelator and the radioactive metal (MW ≈ 500 g·mol^{-1}).[25] A major advantage of labeling with metallic radionuclides is the possibility to attach various radioactive metals with different physical properties to the same tracer precursor. Gallium-68 is a commonly used

metallic-radionuclide with a half-life of 68.3 minutes. Different to previously mentioned radionuclides, gallium-68 is obtained from a $^{68}Ga/^{68}Ge$ generator. In the generator germanium-68 (half-life 271 days) decays by electron capture to gallium-68 that can be extracted with a ligand from the generator.[26] The only FDA-approved PET-tracer containing a metallic radionuclide is NETSpot, a receptor-binding peptide used to image neuroendocrine tumors that cannot be imaged with [^{18}F]FDG.[27]

Fluorine-18 has a longer half-life (109.8 min) than other organic radionuclides such as ^{11}C, ^{13}N and ^{15}O, which permits the imaging of slower biochemical processes and the shipment of tracers from a nuclear pharmacy to the imaging site. The maximum positron energy of fluorine-18 ($E_{\beta+}$ = 0.64 MeV) is among the smallest of commonly used positron emitters. Thus, fluorine-18 also has a low positron range in water (2.4 mm). The low positron range of fluorine-18 merely impacts the spatial resolution since current ultra-high spatial resolution cameras have a maximal spatial resolution of 3–4 mm for human PET scanner and 1–2 mm for small animal PET scanner. However, the positron range increases drastically as one moves from dense tissue to lung tissue, affording the positron energy as a major limiting factor in spatial resolution.[28] Despite fluorine being the thirteenth most abundant element in the earth crust, it is extremely rare in natural products.[29] However, fluorine has shown privileged properties in drug development, and as of 2018, 45% of FDA-approved drugs contain at least one carbon fluorine bond.[30] Drugs containing fluorine can be labeled by a formal isotope exchange between fluorine-19 and fluorine-18 without affecting their pharmacodynamics. Fluorine is frequently used in drug design as a bioisostere of hydrogen and hydroxyl substituents.[31] The van der Waals radius of fluorine is intermediate (1.47 Å) compared to oxygen (1.52 Å) and hydrogen (1.20 Å). Fluorine is the most electronegative element (Pauling electronegativity of 4.0) that induces a strong dipole to the C–F bond. This is more similar to the C–O bond (Pauling electronegativity of oxygen, 3.4) than to the less polarized C–H bond. Due to the high electronegativity, the lone pairs of fluorine in the C–F are not available as hydrogen bond acceptors. The inability to act as a hydrogen bond acceptor and donor are the major differences between fluorine and hydroxyl substituents in organic molecules.[32] As

of 2018 six out of ten FDA approved PET-tracers contain fluorine-18, among which only Vizamyl contains an aryl fluorine-18 bond (Figure 3). Vizamyl is a diagnostic agent that can be used to estimate the amount of β-amyloid plugs in the brain, and a negative scan indicates low likelihood of Alzheimer's disease.[33]

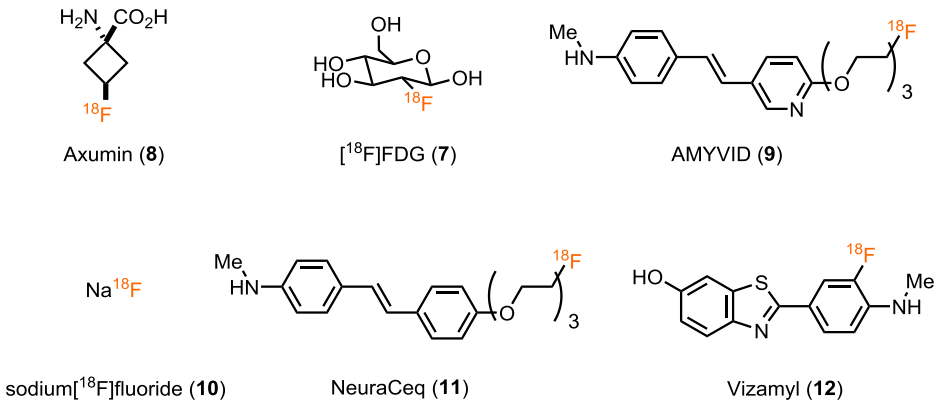

Figure 3. Fluorine-18 containing FDA approved PET-tracer.[27]

I.1.1. **Molar activity**

In radiochemistry, the terms molar- and specific activity are used interchangeably, but specific activity is defined as the amount of activity (A) in Becquerel (Bq) divided by its mass.[34] This definition is inconvenient to apply with PET-tracers, because they are typically obtained in small quantities (ng) that cannot be weighed. The molar activity (MA) is defined as the activity per mole (n) (Equation 1), and the amount of substance can be determined by UV/Vis spectroscopy according to the Lambert-Beer law. However, this technique can only be applied to analytically pure samples or samples with known impurities.

Equation 1 $$\mathrm{MA} = \frac{A}{n}$$

I.2. General considerations for labeling with fluorine-18

The major challenge in radiochemistry is the race against time. As a general rule-of-thumb, the time between the end of bombardment (EOB) and injection of the tracer should be less than three isotope-half-lives.[8] Therefore, labeling with fluorine-18 should be performed in less than 5.5 hours. This limited synthesis time requires the formation of difficult to synthesize carbon fluorine bonds at a late stage. In organic chemistry, reagents and substrates are often used in almost equimolar amounts; in radiochemistry, on the other hand, non-radioactive reagents and substrates are typically used in large excess to increase the reaction rate. Human imaging with [^{18}F]FDG requires about 370 MBq (≈ 6 pmol) of labeled tracer, which is synthesized from 10-100 µmol of substrate and non-radioactive reagents.[35] Due to the large excess of reagents, the reaction is pseudo-first-order in fluorine-18.[35] However, the use of a large excess of reagents is not entirely favorable since even small amounts of impurity in the reagents can react with fluorine-18 in an unfavorable way, preventing the reaction. An additional challenge is that the amount of activity required for human imaging is not suitable for manual handling. Therefore, it is crucial that the labeling procedure can be performed in a shielded hot cell by an automated radiochemical synthesizer.

Two general types of precursor are available for fluorine-18 labeling; no carrier added (n.c.a.) [^{18}F]fluoride and carrier added (c.a.) [^{18}F]fluorine gas. The major difference between those two precursors in classical organic synthesis is that fluorine gas is a strong electrophile and fluoride is typically a poor nucleophile. [^{18}F]fluorine gas is produced via bombardment of neon-20 with deuterium cations to afford fluorine-18 cations.[36] Today, a small amount of fluorine gas is added to the target to trap the fluorine-18 cations by isotope exchange with the fluorine-19 gas. Because just one of the two fluorine atoms in [^{18}F]F_2 can react as electrophilic fluorine, and there is chemically almost no difference between the isotopes, the maximum achievable RCY is 50%.[37] Another potential problem is that [^{18}F]F_2 is diluted with fluorine-19 to give roughly an overall ratio of 1:100,000 (0.5 GBq·µmol^{-1}), which is considered low molar activity. Injecting 370 MBq of a tracer with low molar activity (0.5 GBq·µmol^{-1}) means that about 6 µmol of a fluorinated

substrate are injected to the patient. This large amount of substrate can lead to toxic side effects and a poor signal-to-noise ratio due to the saturation of receptors present in low concentration.[19] In a few facilities, electrophilic fluorine-18 sources with high molar activity (50 GBq·µmol^{-1}) were produced, but the procedure is not widespread since it requires specialized equipment.[38]

The labeling of potential tracers in high molar activity can be achieved with [^{18}F]fluoride. Bombardment of [^{18}O]H_2O with protons affords nucleophilic [^{18}F]fluoride via $^{18}O(p,n)^{18}F$ reaction. Using this technique, [^{18}F]fluoride is routinely produced in high molar activity (1,900 GBq·µmol^{-1}), which is still more than an order of magnitude below the theoretical maximum molar activity (63,000 GBq·µmol^{-1}).[36] The amount of fluorine-19 responsible for the dilution is very low and can result from minor impurities in reagents. Furthermore, part of the fluorine-19 can be washed in by radiolysis of fluorine containing polymers, such as Teflon.[39]

I.3. Arene labeling with [^{18}F]fluorine gas

Fluorine gas is a very strong electrophilic fluorinating reagent, and its fluorine-18 isotopolog can be accessed with a cyclotron. Despite the low molar activity of [^{18}F]fluorine-gas, it has in the past found vast applications to synthesize otherwise inaccessible ^{18}F-labeled aromatic compounds via electrophilic aromatic substitution (S_EAr). One of the few PET-tracers routinely produced via electrophilic ^{18}F-fluorination is [^{18}F]F-*L*-DOPA. Treatment of *L*-DOPA with [^{18}F]fluorine gas affords a mixture of all three potential constitutional isomers in overall low RCY (Scheme 2).[40] The low yield and selectivity can be attributed to the high reactivity of fluorine gas, which can lead to the formation of side products, such as quinones. The yield and the selectivity can be increased using less reactive [^{18}F]AcOF.[41] However, decomposition of starting material and the formation of constitutional isomers results in a lengthy and time consuming purification, which reduces the RCY by decay of the product. The minute polarity difference between aromatic C–H and C–F bonds, which results in a difficult separation, creates an additional problem for direct C–H fluorination reactions.[40, 42]

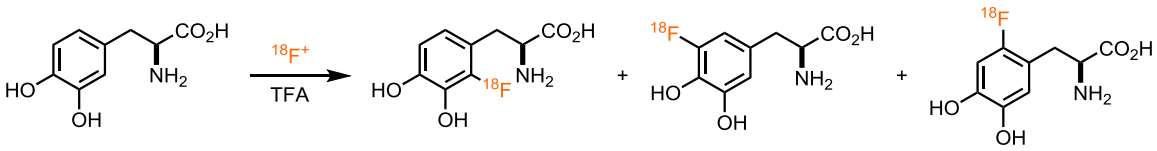

L-DOPA (**13**)		2-[^{18}F]fluoro-*L*-DOPA	5-[^{18}F]fluoro-*L*-DOPA	6-[^{18}F]fluoro-*L*-DOPA
$^{18}F^{+}$ Reagent	RCY			
[^{18}F]F_2	10%	75.2	24	0.8
[^{18}F]AcOF	15%	88.9	9.7	1.4

Scheme 2. Labeling of *L*-DOPA with electrophilic fluorine-18.[40, 43]

Regioselective electrophilic ^{18}F-fluorination of arenes can be achieved by fluorodemetallation of precursors such as arylstannanes. Treatment of trimethyl(*para*-trifluoromethylphenyl)stannane with [^{18}F]AcOF affords **14** in 35% RCY (Scheme 3).[44] More electron-rich arenes tend to give higher yields. The reaction is regiospecific for electron-poor arenes, but trimethyl(4-methoxyphenyl)stannane affords two constitutional isomers of **17** in a 70:12 ratio, which results in a time consuming separation. The general lower molar activity and the high reactivity of F_2 reduces the overall utility of methods using [^{18}F]fluorine gas.

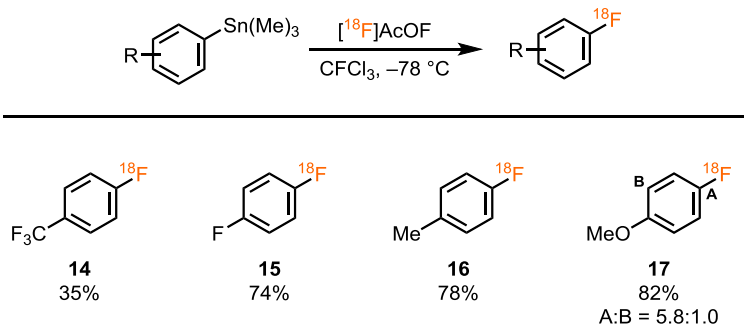

14 35% **15** 74% **16** 78% **17** 82% A:B = 5.8:1.0

Scheme 3. Fluorine-18 labeling of aryl stannanes.[44]

I.4. Arene labeling with [^{18}F]fluoride

I.4.1. Processing of [^{18}F]fluoride

Most labeling methods use [^{18}F]fluoride obtained from a cyclotron in an aqueous solution of [^{18}O]water. The aqueous solution contains various impurities such as free radicals that can result in side reactions, metal ions that can deactivate [^{18}F]fluoride, and anions that can compete in nucleophilic displacements.[45] The purification of [^{18}F]fluoride typically begins by trapping of [^{18}F]fluoride on a quaternary methyl-ammonium (QMA) anion exchange cartridge, and subsequent washing of the cartridge to remove impurities (Figure 4). The [^{18}F]fluoride is afterwards eluted with an aqueous solution containing large cations such as cesium, Kryptofix® 222 (K_{222}) potassium complex or quaternary alkyl-ammoniums.[46] The salts of fluoride and large soft cations have higher solubility in organic solvents and render fluoride more nucleophilic than salts of fluoride with small hard cations due to weaker interactions between fluoride and the cation.[47] Fluoride can form exceptionally strong hydrogen bonds to protic solvents, especially with water (the hydration energy of fluoride in water is 105 kcal·mol^{-1}).[48] The strong hydrogen bonding interactions between fluoride and protic solvents, which are lost upon nucleophilic substitution, lower the nucleophilicity of fluoride.[49] Water is typically removed after elution under an argon stream, and the water content is further reduced by azeotropic drying with acetonitrile. Basic conditions during the drying process are critical, because it avoids formation of [^{18}F]HF, which can react with the glassware or be released as gaseous [^{18}F]HF.[35, 50] The whole process takes roughly twenty minutes, but even after azeotropic drying the remaining solid contains small amounts of water. Thus, radiolabeling methods must tolerate small quantities of water.

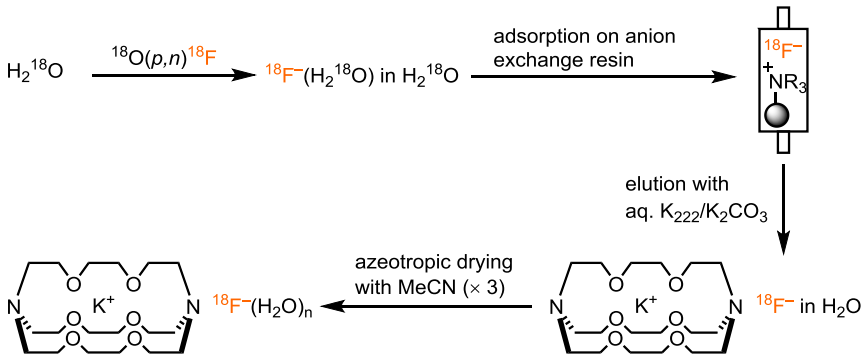

Figure 4. General method for processing of [^{18}F]fluoride.[19]

I.4.2. ^{18}F-labeling via nucleophilic aromatic substitution

The introduction of fluoride to aromatic compounds on an industrial scale is most commonly done via nucleophilic aromatic substitution (S_NAr).[51] Nucleophilic fluorination is generally preferred over electrophilic fluorination because of the higher selectivity, and lower cost of fluoride sources. Nucleophilic aromatic substitution cannot occur via an S_N2 mechanism, similar to aliphatic compounds, because the σ* orbital of the C–LG bond is buried in the aromatic ring (Scheme 4). The classic textbook example for nucleophilic aromatic substitution proceeds via the two-step addition-elimination mechanism. The lone pair of the nucleophile (Nu) attacks the vacant π* orbital of the arene to form a tetrahedral intermediate, called Meisenheimer complex.[52] The tetrahedral intermediate typically is higher in energy than both starting material and product, because the aromaticity is broken and a full negative charge is deposited on the arene. In the second step, the leaving group is expelled and the overall substitution product is obtained.

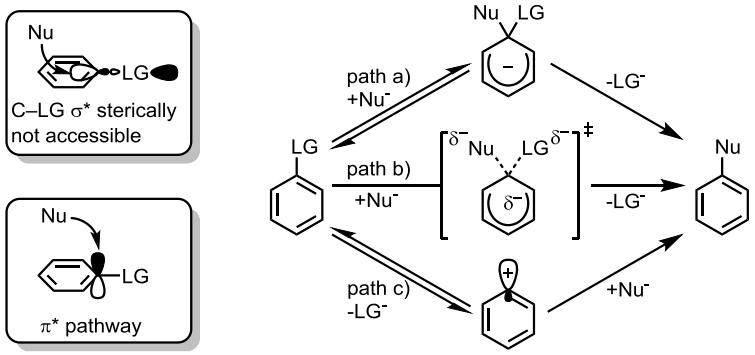

Scheme 4. Three mechanistic pathways for nucleophilic aromatic substitution. Path a) addition-elimination b) concerted c) elimination-addition.

Radiolabeling of an arenes with [^{18}F]fluoride via an addition-elimination mechanism requires strong inductive- or mesomeric electron withdrawing groups in the *ortho*- or *para*-position to stabilize the full negative charge deposited on the arene in the Meisenheimer complex. The relative rate of the radiolabeling correlate well with electron withdrawing properties of the substituents.[53] The influence of the leaving group is smaller, but it can also further decrease the electron density in the *ipso* position, so that the rate of nucleophilic attack increases with more electron withdrawing substituents (I<Br<Cl<NO_2=NMe_3^+<F).[54] The ionic trimethylammonium leaving groups are particularly preferred for ^{18}F-fluorination via S_NAr, as the ionic precursor is more polar than the neutral [^{18}F]fluoroarene, which facilitates product purification.[55] When less activated arenes such as anilinium **18** are subjected to the reaction, the trimethylammonium leaving group undergoes mainly a competing S_N2 side reaction to afford 4-bromo-dimethylaniline and [^{18}F]fluoromethane (Scheme 5).[56] The [^{18}F]fluoromethane formed during the reaction is released as a gas, lowering the RCY and posing a potential safety hazard. Exchanging the trimethylammonium leaving group with a nitro substituent afforded **20** in less than 0.5% RCY (Scheme 5).[57] A major side product formed was the debromofluorinated arene.

The selectivity and reactivity toward S_NAr on the nitro rather than the bromine substituent can be increased by the introduction of temporary activation groups. The group of Coenen introduced an aldehyde *ortho* to the nitro substituent on the arene, which could increase the selectivity and thus the RCY to 70%.[58] In a second step, the carbonyl group is removed using the Wilkinson's catalyst to give **20** in overall 37% RCY. The temporary activation group strategy provides access to otherwise difficult to obtain compounds, but increases the number of steps. The increased number of steps can result in worse reproducibility and longer reaction times, which can reduce the RCY due to decay of fluorine-18.

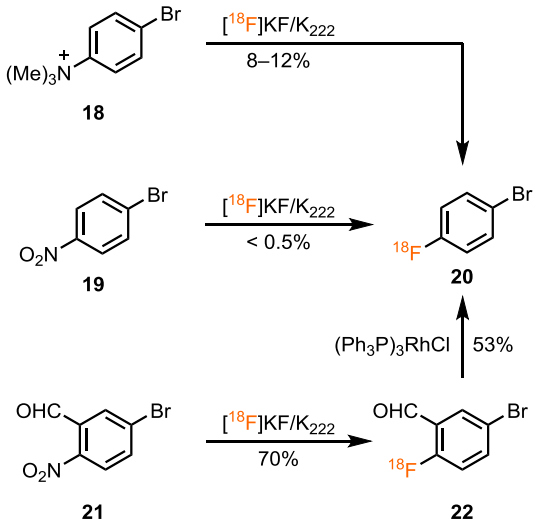

Scheme 5. Synthesis 4-bromo-[^{18}F]fluorobenzene.[57-58]

I.4.3. ^{18}F-labeling of aryl diazoniums

At the other end of the mechanistic spectrum of S_NAr reactions is the elimination-addition mechanism (Scheme 4 path b). This mechanism is quite rare because it proceeds through the high-energy phenyl cation intermediate. The most prominent example is the decomposition of aryl diazonium tetrafluoroborates to aryl fluorides.[59] The reaction rate is much less dependent on the substituents on the arene and permits to access an electronically broad spectrum of fluorinated arenes.[60] This reaction, developed by Balz and Schiemann, was translated to radiochemistry in 1971 by the group of Wolf.[61] More than 20 year later, the strategy was used to label dopamine with fluorine-18. In the first step the isotope exchange between tetrafluoroborate diazonium **23** and [^{18}F]HF was performed, the subsequent thermal decomposition and purification afforded 5-[^{18}F]fluoro-dopamine (**25**) in an overall RCY of 24%. (Scheme 6).[62] As previously mentioned under the reaction conditions, diazonium **24** decomposes to a phenyl cation that abstracts one fluoride from the tetrafluoroborate counter-ion to afford aryl fluoride **25**. Since the tetrafluoroborate anion contains four fluorides, of which just one is transferred and the trifluoroborane byproduct evaporates, the maximum radiochemical yield is limited to 25%.[53] A further disadvantage of the reaction is that the products are typically obtained in low molar activity, since the exchange of fluorine-19 with fluorine-18 can only partially take place due to the large excess of precursor **23** used.

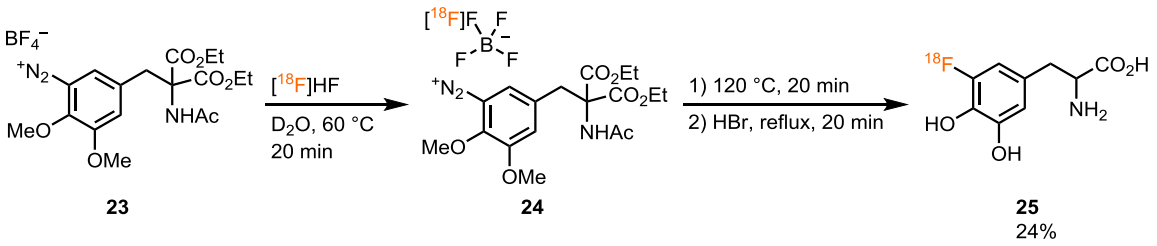

Scheme 6. Fluorine-18 labeling of aryl diazonium.[62]

I.4.4. **Radio-deoxyfluorination**

The deoxyfluorination of phenol is an attractive reaction as it allows the conversion of a hydroxyl substituent with its bioisostere fluorine. The displacement of hydroxyl substituents via S_NAr is unfavorable for two reasons: firstly, because hydroxide is a bad leaving group, and secondly, because basic fluoride can lead to deprotonation, and thus further deactivate the arene toward S_NAr. Therefore, the deoxyfluorination of phenols is typically a two-step process consisting of converting the hydroxyl group into a good leaving group, followed by nucleophilic aromatic substitution. In 2002, the group of Hayashi reported on the 2,2-difluoro-1,3-dimethylimidazolidine (DFI, **27**)-mediated deoxyfluorination of phenols (Scheme 7).[63] In the first step, the hydroxyl substituent is converted into uronium bifluoride, which is a good leaving group. In a subsequent step, the arene is attacked by fluoride and a highly exergonic expulsion of corresponding urea occurs. Despite the good leaving group properties of urea, only electron-poor arenes could be deoxyfluorinated. More electron-rich arenes such as phenol formed the key uronium bifluoride intermediate, but subsequent aryl fluoride formation does not take place.

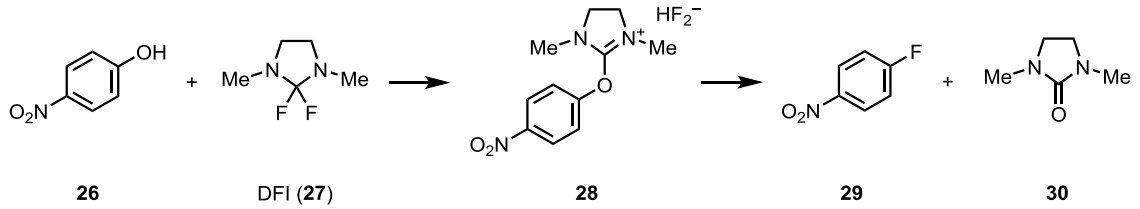

Scheme 7. DFI-mediated deoxyfluorination of phenols via an aryl uronium.[63]

In 2011, Ritter *et al.* reported on the deoxyfluorination of phenols using the PhenoFluor reagent (**31**), which has a similar scaffold to DFI and also takes advantage of the strongly exothermic formation of the corresponding urea as a driving force (Scheme 8).[64] Despite the common

uronium intermediate, the PhenoFluor-mediated deoxyfluorination proceeds efficiently for both electron-poor and electron-rich arenes such as **29** and **17**. The reaction is highly functional group tolerant and substrates containing ketones **33**, esters **34**, and unprotected primary amines **32** could be obtained in high yields. Furthermore, heterocycles and complex structures are tolerated under the reaction condition and the estrone analog **33** and cinchona alkaloid analog **34** could be accessed in high yields.

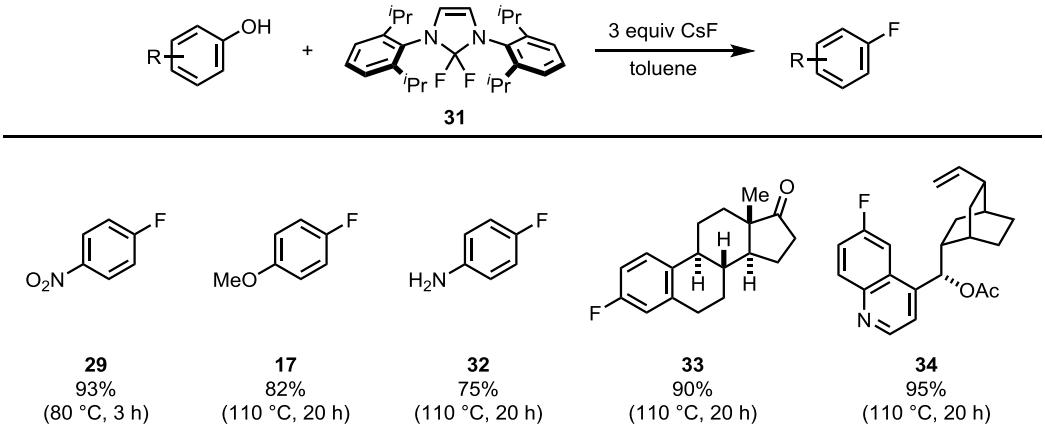

29 93% (80 °C, 3 h) **17** 82% (110 °C, 20 h) **32** 75% (110 °C, 20 h) **33** 90% (110 °C, 20 h) **34** 95% (110 °C, 20 h)

Scheme 8. PhenoFluor-mediated deoxyfluorination of phenols.[64]

The electronically diverse substrate scope is atypical for S_NAr reactions that proceed through an addition-elimination mechanism (typical Hammett-value ρ = 3–8) (Scheme 9 a).[65] Constanze N. Neumann and Tobias Ritter showed that the electronically diverse substrate scope is the result of a concerted mechanism. The uronium fluoride **35** is in equilibrium with imidazoline **36** (Scheme 9 c). From the tetrahedral intermediate **36**, deoxyfluorination proceeds with an activation barrier between 20–25 kcal·mol^{-1} via a four-center transition state in a concerted fashion, where the C–O bond is broken simultaneously with the formation of the C–F bond (Scheme 9 b). As a result of the concerted mechanism, only a partial negative charge is localized on the arene, and the reaction has little dependence on the electronics of the arene (Hammett-value ρ = 1.8) compared to an addition-elimination mechanism. Traditionally, nucleophilic aromatic substitution with fluoride requires polar solvents for the solvation of metal fluorides. In the S_NAr transition state, desolvation of fluoride contributes significantly to the activation energy required.[65] Therefore, deoxyfluorination with PhenoFluor is highest yielding in aprotic unpolar solvents since desolvation contributes to a smaller extent to the reaction barrier and the fluorine is part of

imidazoline **36**. Furthermore, fluorine in **36** is non-basic and this prevents side reactions which can degrade the substrate.

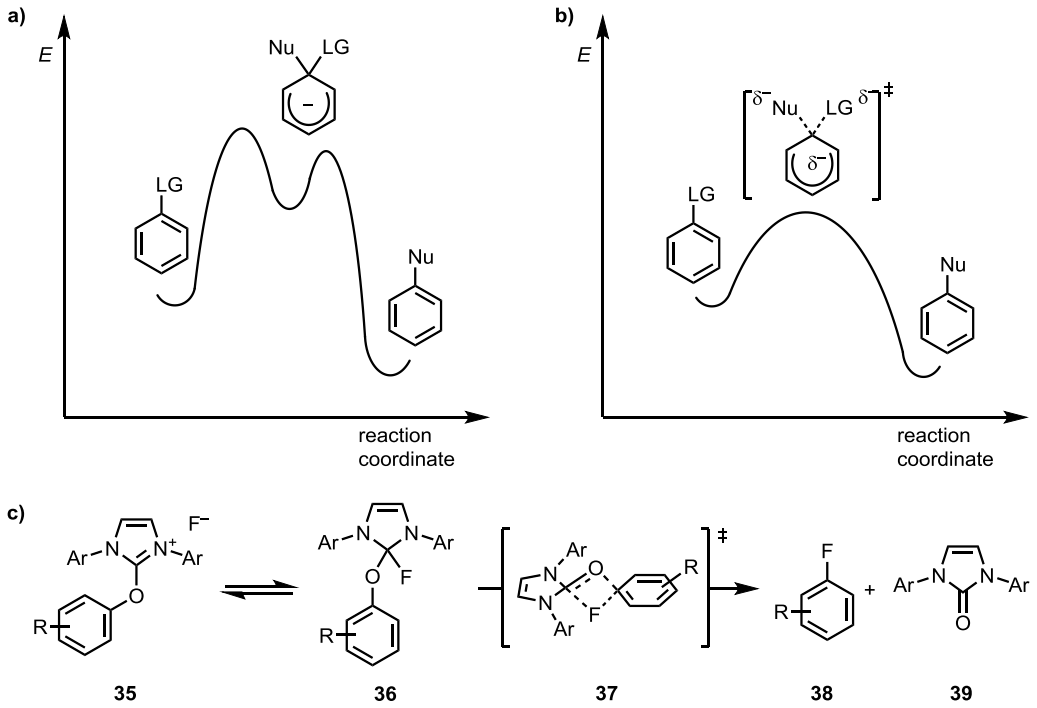

Scheme 9. a) Energy profile of nucleophilic aromatic substitution via addition-elimination mechanism. b) Energy profile of concerted nucleophilic aromatic substitution. c) Intermediates in the concerted nucleophilic aromatic substitution.[65]

Neumann and Ritter also translated the PhenoFluor-mediated deoxyfluorination of phenols to a method using [^{18}F]fluoride.[65] A central challenge in the translation was that the PhenoFluor reagent contains two fluorine-19 atoms that would lower the molar activity during radiolabeling. The use of chloroimidazolium chloride **40** (^{iPr}ImCl) omits the two fluorine-19 atoms and provides access to the uronium chloride intermediate (Scheme 10). In the second step, the chloride counter-ion is replaced via an anion exchange cartridge with [^{18}F]fluoride to form key intermediate [^{18}F]**35**. Heating the uronium [^{18}F]fluoride affords the fluorine-18 labeled arene in high RCY. The reaction has a similar functional group tolerance as the cold reaction, and tolerates primary amides, esters, secondary amines, and heterocycles. The high functional group tolerance can be potentially attributed to the non-basic organic-fluorine in the tetrahedral intermediate. Different to the PhenoFluor-mediated deoxyfluorination, the reaction highly depends on the electronics and only works with electron-poor arenes and heteroarenes. Electron-rich arenes shift the equilibrium

from fluoroimidazoline **36** to uronium fluoride **35**. In the ionic form, the fluoride is more reactive and can undergo unproductive side reactions with the reaction vial. Complete sequestration of fluoride is not possible in the cold reaction because an excess of cesium fluoride is used, but in radiochemistry [^{18}F]fluoride is the limiting reagent. Therefore, the [^{18}F]fluoride can be sequestered before it can undergo productive aryl fluoride bond formation.

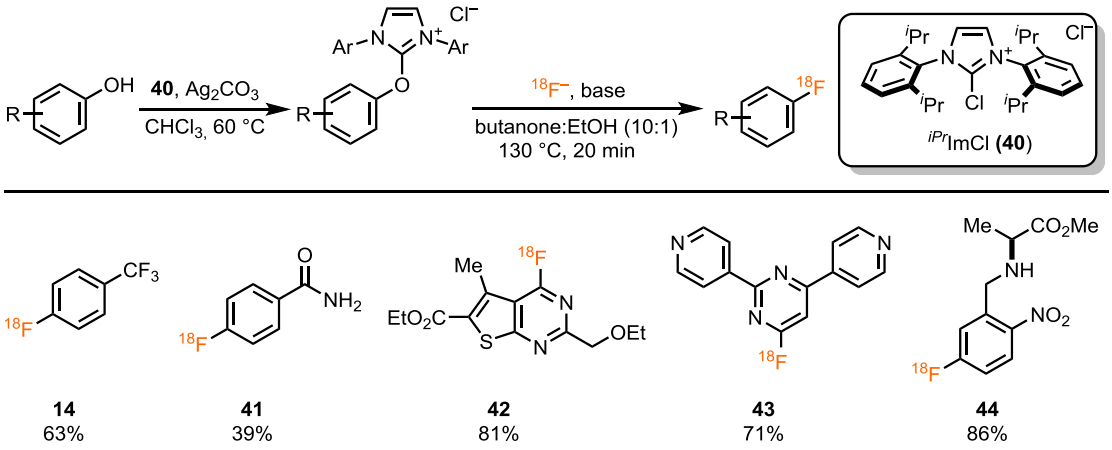

Scheme 10. Radio-deoxyfluorination with ^{iPr}ImCl.[65]

I.4.5. **Ruthenium-mediated radio-deoxyfluorination of phenols**

η^6-coordination of a transition metal to an arene can drastically alter the properties of the arene.[66] The electron density on the complexed arene is reduced, resulting in an increased acidity of aromatic and benzylic protons, and increased electrophilicity, making the complexed arene more susceptible to nucleophilic attack.[67] Furthermore, the rate of oxidative addition and the rate of solvolysis for substituents in benzylic position is increased (Figure 5 a).[68] For the sake of the thesis we will focus on the enhanced electrophilicity.

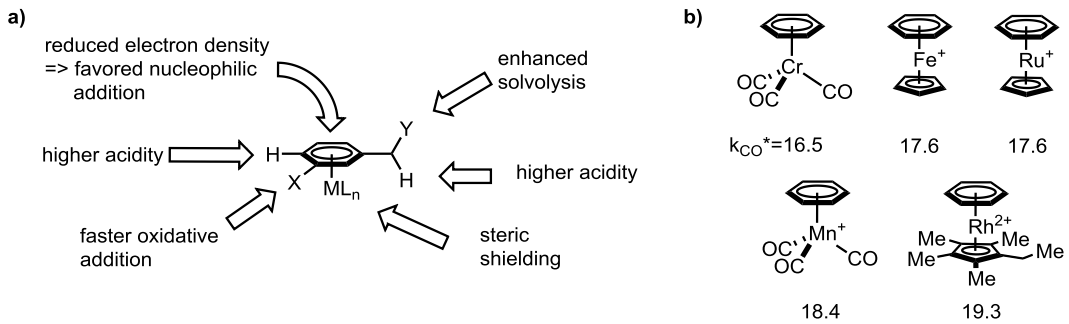

Figure 5. Arene activation by η^6-coordination.[66]

The extent of arene activation toward nucleophilic attack by η^6-coordination is dependent on the metal center and the ligands. Generally, more positively charged metal-centers withdraw more electron density and activate the arene more toward nucleophilic attack.[66] For example, the electron density removed by complexation to chromium tricarbonyl is comparable to one nitro substituent in the *para* position, manganese tricarbonyl is comparable to two nitro substituents and rhodium(Cp*) is similar to three nitro groups (Figure 5 b).[66, 69] A quantitative description of the activation by η^6-coordination is given by the reactivity parameter k_{CO}^*, which represents the C–O stretching constant in a tris carbonyl analog of the η^6-arene complex (Figure 5 b). Higher values represent more activated arenes.

While chlorobenzene is a bad substrate for S_NAr, chromium complex **45** undergoes nucleophilic aromatic substitution with sodium methoxide at 50 °C (Scheme 11).[70] The displacement of a halide requires the reversible nucleophilic attack on the arene, since kinetically the addition to the proton substituted position is favored ($k_1 > k_2$). The rate of the reverse reaction (k_{-1}) depends on the leaving abilities of the nucleophile. Nucleophiles that are bad leaving groups, such as alkyl anions, favor formation of the cyclohexandienyl adduct and the extrusion barely occurs ($k_1 >> k_{-1}$). The addition of weaker nucleophiles, such as methoxide, is reversible and efficient nucleophilic aromatic substitution occurs.[69]

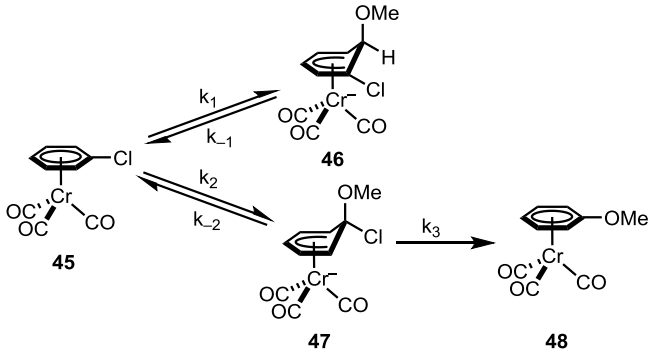

Scheme 11. Potential intermediates of nucleophilic aromatic substitution on η^6-activated arenes.[66]

The synthetic utility of η^6-mediated S_NAr was highlighted by its application in the total synthesis of vancomycin (Scheme 12).[71] Ruthenium was complexed to phenylalanine analog **49**, and the resulting complex was subsequently deprotected with trifluoroacetic acid (TFA) to afford **50** in 58% yield. Primary amine **50** engaged in effective amide coupling to afford **51** in high yield. The

ruthenium-mediated macrocyclization was performed using 2,6-bis(*tert*-butyl)phenoxide as non-nucleophilic base to afford macrocycle **52** in 88% yield. The ruthenium complex was removed afterwards by irradiation with UV-light for 24 hours in acetonitrile.

The Ritter group was the first to use the activation of arenes through η^6-coordination to ruthenium to enable labeling with fluorine-18.[72] They showed that electron-rich phenols could be radio-deoxyfluorinated with ^{iPr}ImCl if the phenol is coordinated to a ruthenium complex (Scheme 13 a). The complexation of ruthenium cyclopentadienyl to an arene is roughly worth the activation of two nitro substituents.[69] The lower electron density on the arene and the columbic repulsion of the two positive charges shifts the equilibrium even for electron-rich phenols to the side of the tetrahedral intermediate, from which the productive radio-deoxyfluorination can occur (Scheme 13 a). The ruthenium-mediated radio-deoxyfluorination of phenols begins with the formation of the ruthenium η^6-phenol complex by heating a mixture of ruthenium precursor **57** and the desired phenol in ethanol at 85 °C for 30 minutes. Fluorine-18 was eluted into a vial with a mixture of ruthenium η^6-phenol complex and ^{iPr}ImCl, and the vial was heated to 125 °C for 30 min to afford the decomplexed fluorine-18 labeled arene.

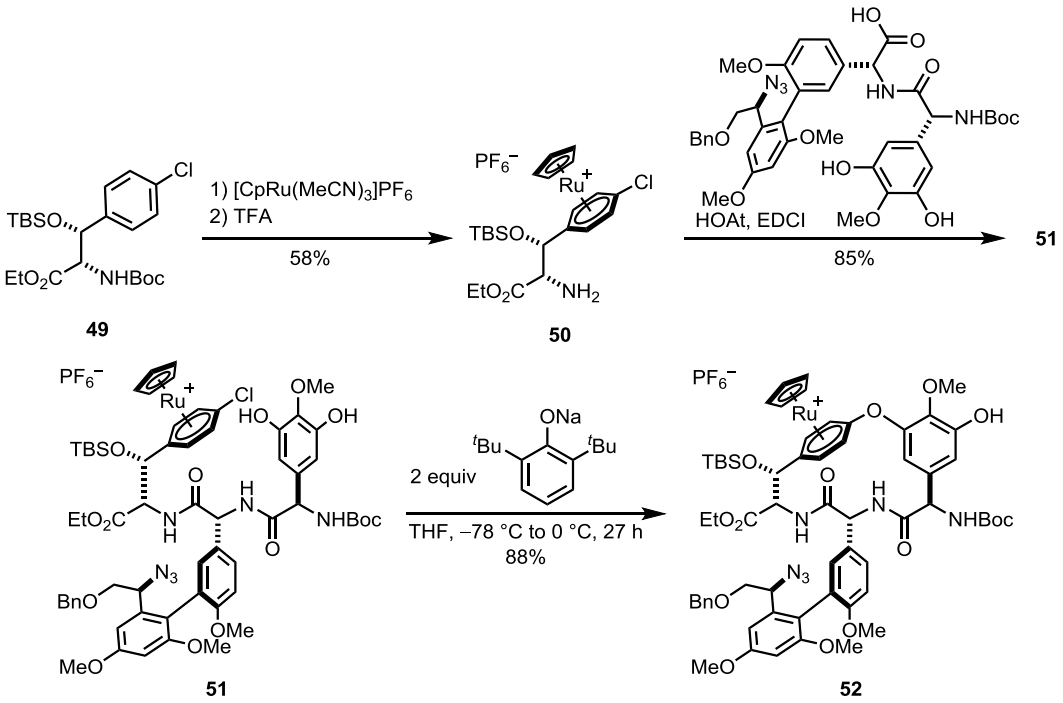

Scheme 12. Application of η^6-mediated S_NAr in the synthesis of vancomycin.[71]

This procedure allowed for the radio-deoxyfluorination of electron-rich arenes such as *para*-methoxy phenol, and heteroarenes such as 5-hydroxy indole derivative (Scheme 13 b). Furthermore, even complex structures such as ezetimibe were labeled in the presence of protic functional groups, such as secondary alcohols. During the reaction no special precautions toward air and moisture were required. It was shown that the RCY of the reaction highly depends on the reactor pressure and size. The use of a 10 mL vial instead of a 3 mL vial decreased the yield for labeling of **60** by threefold. This can be problematic because the ELIXYS automated synthesizer can just fit 5 mL vials. By using self-made adapters to fit 3 mL vials into the ELIXYS system, it was possible to label and isolate **60** in 24% RCY and the product was obtained in high molar activity (93 GBq·µmol^{-1}), sufficient for receptor imaging. Computational mechanistic investigations suggest that the reaction does not proceed via a concerted nucleophilic aromatic substitution, but rather via an addition-elimination mechanism. The reason for this is the strong stabilization of the negative charge in the cyclohexadienyl complex. Overall, the reaction combines the excellent functional group tolerance of the ^{iPr}ImCl-mediated radio-deoxyfluorination with the substrate scope of the PhenoFluor reaction.

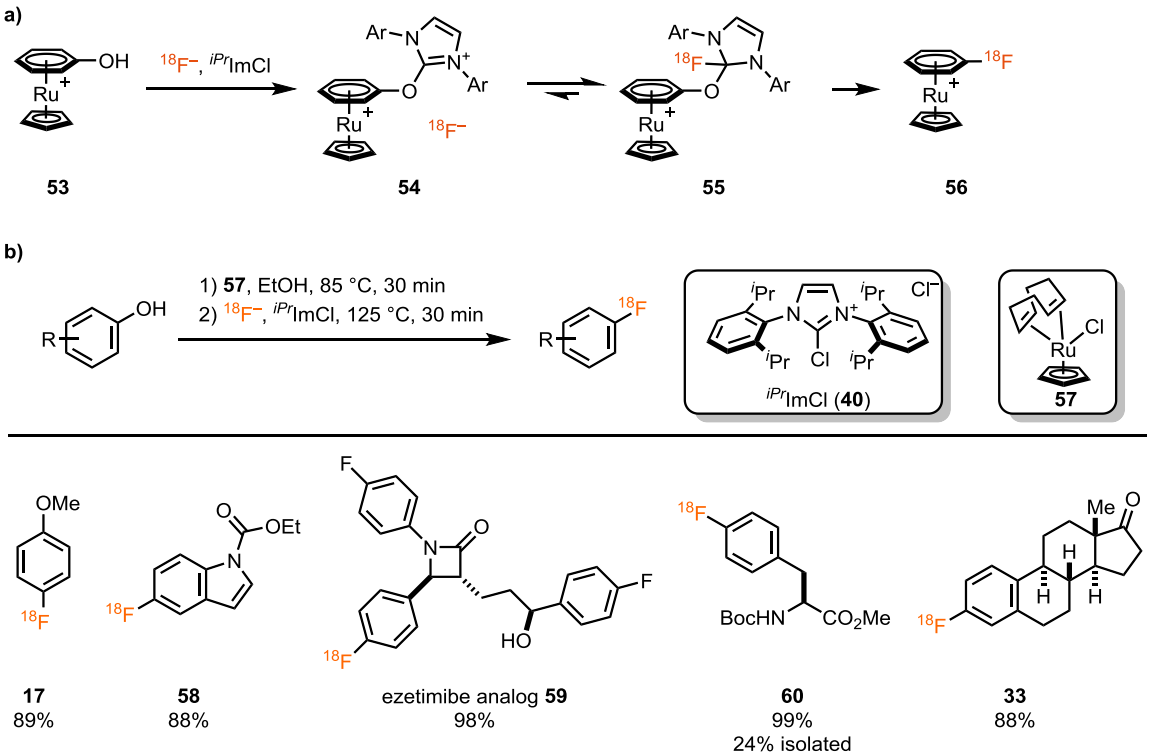

Scheme 13. Ruthenium-mediated radio-deoxyfluorination of arenes.[72]

I.4.6. ^{18}F-labeling of diaryliodoniums

The first air and moisture stable diaryliodonium salt was isolated in 1894.[73] Since then, many reports on nucleophilic aromatic substitution on diaryliodonium salts with various nucleophiles such as alkoxides, amides and fluoride have been reported.[74] Pike *et al.* were the first to translate the cold fluorination of diaryliodonium salts to labeling with [^{18}F]fluoride.[75] In stark contrast to the examples discussed in chapter I.4.2, nucleophilic aromatic substitution of diaryliodoniums has a small positive Hammett slope ($\approx \rho = 1.2$) and the substrate scope is little dependent on the electronics of the arene.[76] Despite this, the electronic structure of the arenes in unsymmetrical diaryliodoniums is the main factor determining which arene is labeled.[75] To a smaller extent, the selectivity for C–F bond formation between the two arenes depends on the steric properties of the arene and favors labeling of the more sterically hindered arene. Pike *et al.* proposed that the more bulky arene preferentially occupies the equatorial position on the trigonal bipyramidal substituted diaryliodonium, and is thus preferentially labeled by the apical fluoride (Scheme 14 a).[77] Most labeling precursors are valuable material. In order to prevent the use of two equivalents in the labeling reaction, various dummy arenes were designed. Among the most prominent examples are 2-thienyl substituents. Treatment of aryl(2-thienyl)iodoniums with K_{222} potassium [^{18}F]fluoride at 130 °C affords the labeled arene and 2-iodothiophene as a byproduct (Scheme 14 b). Electron-rich arenes such as **17** could be obtained in 29% RCY and the more electron-poor arenes such as **62** in 62% RCY. The electronically diverse substrate scope is a big advantage compared to other methods; however, aryl(2-thienyl)iodonium salts are difficult to synthesize and purify, and often show limited stability under ambient conditions.[78]

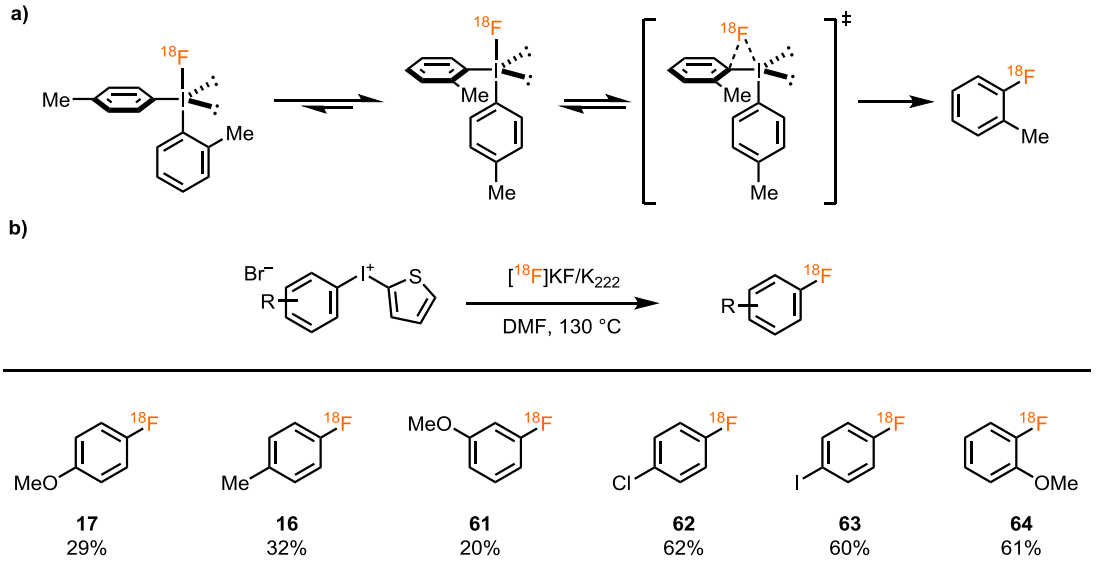

Scheme 14. a) Mechanism of ^{18}F-labeling of diaryliodonium. b) Substrate scope of ^{18}F-labeling of diaryliodonium.[76]

Sanford *et al.* developed the copper-catalyzed coupling of diaryliodoniums with fluoride. In contrast to the uncatalyzed fluorination of diaryliodoniums, the chemoselectivity between the two aryl substituents mainly depends on the steric bulk and favors labeling of the sterically less hindered arene.[79] In the proposed mechanism, copper(I) undergoes a chemoselective oxidative addition to the sterically less hindered aryl iodonium bond, followed by reductive elimination from copper(III) fluoride.[80] Most notably, the fluorination of mesityl(2-thienyl)iodonium without a catalyst affords mesityl fluoride in 98:2 selectivity, whereas in the catalyzed reaction 2-fluorothiophene is formed with 99:1 selectivity.[79] The method was translated to the use of [^{18}F]fluoride and the reaction proved to have a substrate scope covering a broad range of electronics on the arene (Scheme 15).[78] Furthermore, the reaction tolerates many functional groups such as esters, amides and ketones. Using this methodology, even complex molecules such as [^{18}F]F-DOPA analog **67** could be accessed in 30% RCY. The use of the iodonium tetrafluoroborate precursor afforded [^{18}F]F-DOPA analog **67** in low molar activity (11 GBq·µmol^{-1}), likely due to the well-known fluorine exchange between fluorine-18 in solution and the fluorine-19 in the tetrafluoroborate.[81] The use of iodonium tosylate precursor, which cannot release fluorine-19, increased the molar activity of the product to 148 GBq·µmol^{-1} albeit lowering the RCY to 17%.

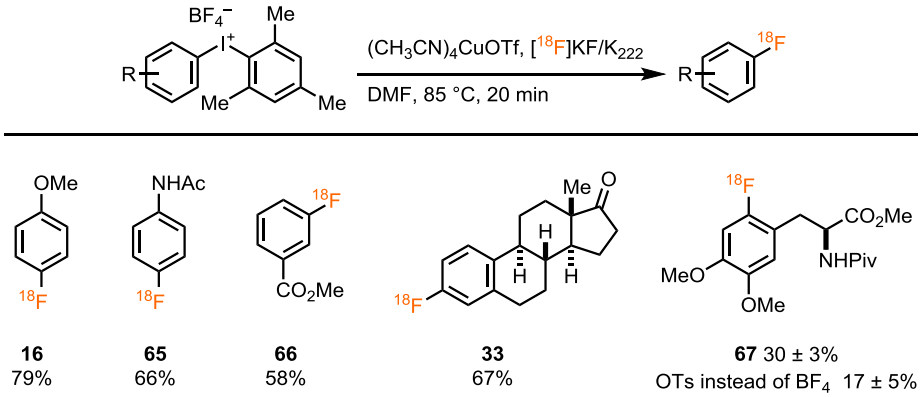

Scheme 15. Copper-mediated radio-fluorination of mesityl(aryl)iodonium salts.[78]

I.4.7. ^{18}F-labeling of aryl boronic acids

The use of arylboronic acids as starting material is favorable because they are non-toxic and readily accessible at a late stage via transition metal catalyzed C–H activation or via Suzuki Miyaura borylation.[82] The copper-catalyzed cross-coupling of arylboronic acids with heteroatoms was developed simultaneously by Chan, Evans, and Lam.[83] The Chan-Evans-Lam coupling evolved into one of the most versatile cross couplings, capable of forming otherwise difficult to introduce bonds such as C–N, C–O and C–Cl under mild conditions using inexpensive copper reagents.[84] Hartwig *et al.* were able to show that a copper-mediated C–F bond formation is possible using F^+ sources such as 1-fluoro-2,4,6-trimethylpyridinium.[85] Hartwig and many other showed the feasibility of the introduction of fluorine via cross coupling, but required the use of electrophilic fluorine. The use of expensive F^+ reagents is not feasible in large-scale application and is furthermore unfavorable for PET-imaging due to its low molar activity. The Gouverneur group was the first to report on the fluorine-18 labeling of arylboronic esters using [^{18}F]fluoride in a copper-mediated Chan-Evans-Lam type reaction.[86] It was proposed that copper (II) captures [^{18}F]fluoride and undergoes transmetallation with the arylboronic ester. The resulting aryl copper(II) fluoride disproportionates to copper(I) and aryl copper(III) fluoride, which has been shown to undergo facile C–F reductive elimination.[80] The copper-mediated ^{18}F-labeling works well on electron-rich and electron-poor arenes, tolerates many functional groups such as ethers, nitro, and amides, and tolerates substituents in the *ortho*-position (Scheme 16). Substrates containing protic functional groups such as phenols **69** or secondary amides resulted in a low

RCY (< 10%), probably owing to the competitive C–O or C–N bond formation. The poor compatibility of protic functional groups is highlighted in the attempt to label a single *tert*-butyloxycarbonyl (Boc) protected [^{18}F]F-DOPA precursor to afford **71** in 5% RCY, while the double boc-protected precursor afforded **72** in 83% RCY (Scheme 16). An additional potential problem is that the arylboronic ester precursor can undergo further side reactions, such as protodeborylation and oxidation to the phenol, resulting in a challenging purification. The presence of oxygen in the reaction vial can reduce the formation of these side products.

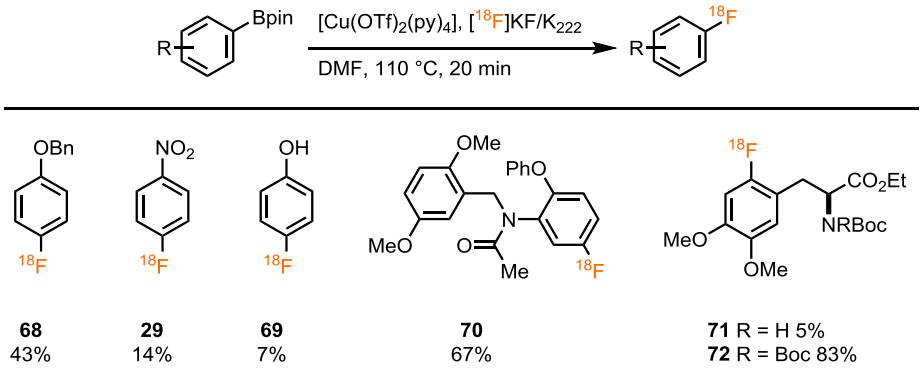

68 43%
29 14%
69 7%
70 67%
71 R = H 5%
72 R = Boc 83%

Scheme 16. Copper-mediated ^{18}F-labeling of arylboronic esters.[86]

I.5. Peptide labeling

For decades, labeled antibodies were considered the “magic bullet” in tracer development, due to their highly specific binding.[87] Initial enthusiasm about antibody labeling decreased due to several disadvantages associated with their high molecular weight/large size. Large molecule such as antibodies can be sequestered by reticuloendothelial cells, and often optimal target-to-background ratios are achieved after 2–4 days.[87] This long imaging times require the use of long lived radio nuclides and result in higher radiation exposure of the patients.

IUPAC refers to peptides as amino carboxylic acids that are covalently linked by amide bonds without restriction in size. In the following thesis, “peptide” will refer to polymeric structures containing 2–50 amino acids. Similar to antibodies, peptides can show as well high and very specific binding.[88] In contrast to antibodies, peptides have a lower molecular weight, which offers several additional advantages. The lower molecular weight permits fast diffusion to the target cells and rapid blood clearance. Many receptor-binding peptide tracers are internalized into the cells upon binding to G-coupled proteins. A combination of these properties can result in high target-to-background ratios in a short amount of time. Another advantage is that peptides can be conveniently accessed via automated solid phase peptide synthesis (SPPS). Naturally occurring peptides often show low stability in serum (somatostatin biological half-life = 2 min) and are therefore not suitable tracers. However, there are several known ways to increase their stability such as cyclization, introduction of unnatural amino acids and modification of the C– and N–termini.[89] In addition, peptides are typically non-immunogenic.[90] The only FDA approved peptide PET-tracer, NETSpot (Galium-68-DOTATATE), is used to image the somatostatin receptor, which is overexpressed in neuroendocrine tumors (Figure 6).[91] These neuroendocrine tumors cannot be imaged with [^{18}F]FDG, highlighting the necessity of this NETSpot tracer.

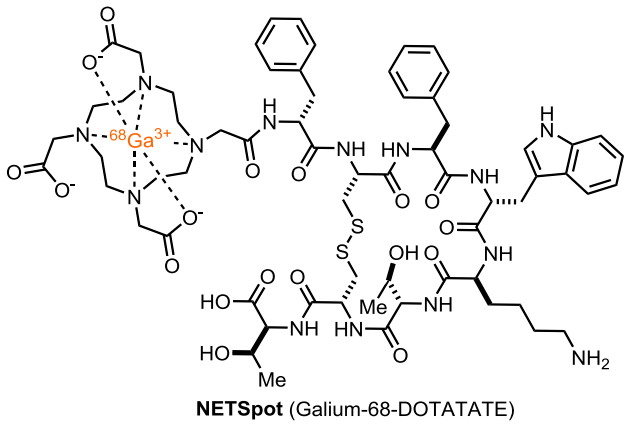

Figure 6. Structure of NETSpot.

Labeling of peptides is a unique challenge due to the high density of functional groups, such as acidic functional groups, the presence of various nucleophiles, and stereocenters, which require mild labeling conditions.[92] Most peptide labeling strategies uses small bifunctional molecules that can be both easily labeled and attached to peptide. Those linkers are referred to as prosthetic groups; analogous to the prosthetic group of proteins, which consist of "the non-amino acid portion of a conjugated protein".[93] Peptide labeling methods can be divided into four main strategies: direct labeling of activated peptides, indirect labeling of activated peptides, indirect labeling of unactivated peptides, and direct labeling of unactivated peptides via C–H fluorination (Scheme 17).

I.5.1. **Direct labeling of activated peptides**

The direct labeling of activated peptides enables the introduction of the radionuclide in the last step of the synthesis and avoids time-consuming multi-step synthesis. The introduction of prosthetic groups, such as DOTA ligands, is a prominent approach since it allows complexation to positron emitting metals such as gallium-68, copper-64, and copper-68, under mild condition.[94] The main advantage of this approach is the ease of labeling and flexible introduction of various radionuclides with different half-lives. Small receptor-binding peptides typically have a molecular weight around 1,000 g·mol^{-1} and the introduction of a metal-chelator complex (500 g·mol^{-1}) has the potential to alter the biological behavior of the peptide, such as the internalization rate.[95] It was shown in a competing binding experiment that the IC_{50} of octreotide increased by almost an

order of magnitude upon addition of an ytterbium-DOTA complex (see Figure 6 for a structurally similar example).[96]

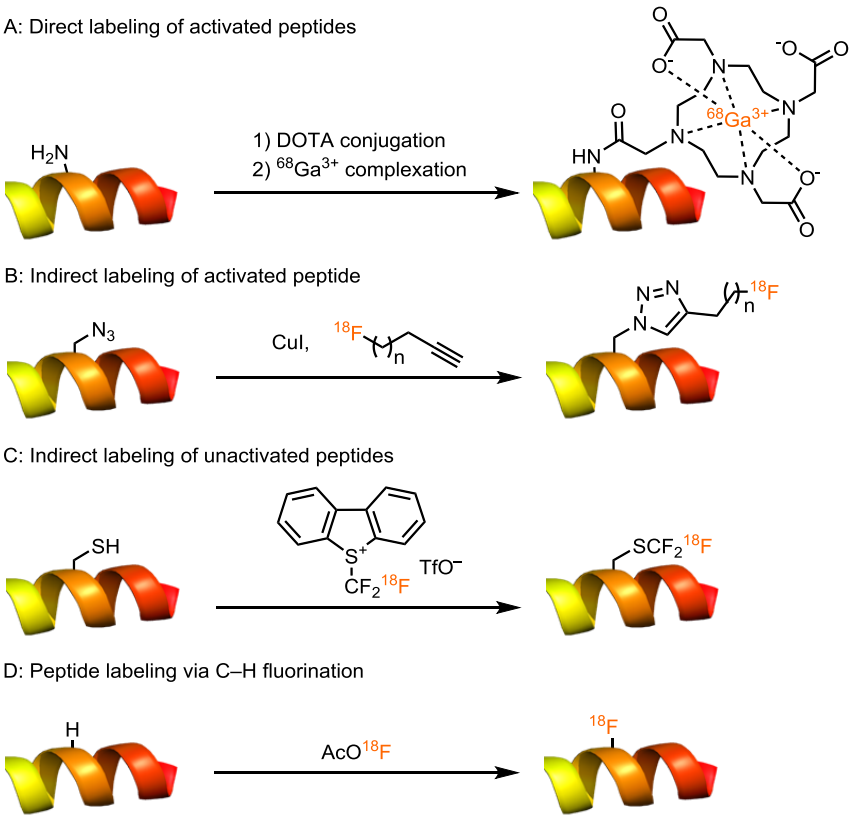

Scheme 17. Peptide labeling strategies.

Fluorine-18 labeling of peptides has gained growing interest due to the favorable half-life of 109.8 min, which enables multistep synthesis, permits distribution of tracers, and is long enough to allow imaging over several hours. Low concentration of peptide-receptors demands tracers in high molar activity (37–370 MBq·µmol^{-1}) and restricts labeling to the use of [^{18}F]fluoride.[97] Labeling with nucleophilic [^{18}F]fluoride is challenging because of the harsh reaction conditions typically required and the high functional group density in peptides.[98] To circumvent harsh labeling conditions, unnatural functional groups capable of capturing [^{18}F]fluoride under mild conditions can be introduced to the peptide. It is to be expected that the introduction of smaller organic prosthetic groups will change the properties of the peptides to a smaller extent than large metal-chelator complexes.[99]

Silicon has a high fluorine affinity and forms strong silicon fluorine bonds (129 kcal·mol^{-1}), which is advantageous for mild labeling.[100] Rosenthal *et al.* were the first to synthesize

[^{18}F]fluorotrimethylsilane and evaluated its use for animal experiments. However, during *in vivo* evaluation they observed rapid hydrolysis to give [^{18}F]fluoride.[101] The released ionic [^{18}F]fluoride is taken up by the bones and lead to unnecessary radiation exposure of patients and for PET-tracers not targeting skeletal PET, the target-to-background ratio is decreased. Fast hydrolysis can prevent imaging if the tracer is hydrolyzed before it can reach the target. The hydrolysis of Si–F bonds proceeds by nucleophilic substitution via a pentacoordinated silicate **74** (Scheme 18 a). The bulkier and more electron donating the substituents on silicon are, the slower the rate of hydrolysis. The reason for this is that the pentacoordinated intermediate **74** is destabilized by bulkier substituents due to steric clash.[102]

Höhne *et al.* found that bis-*tert*-butyl-phenyl substituted fluorosilanes are stable in human serum for more than 300 hours, and applied the silicon fluoride acceptor (SiFA) approach to label bombesin derivate **76** (Scheme 18 b).[103] The radio-dehydrofluorination of peptide silane precursor **76** was performed under acidic conditions at 110 °C. Bombesin analog **77** could be isolated in 13% decay corrected (d.c.) RCY and was stable in phosphate-buffered saline (PBS) and human serum. However, *in vivo* experiments showed that the lipophilic prosthetic group drastically changed the biodistribution of **77** and thus low and unspecific uptake of **77** was observed.[103]

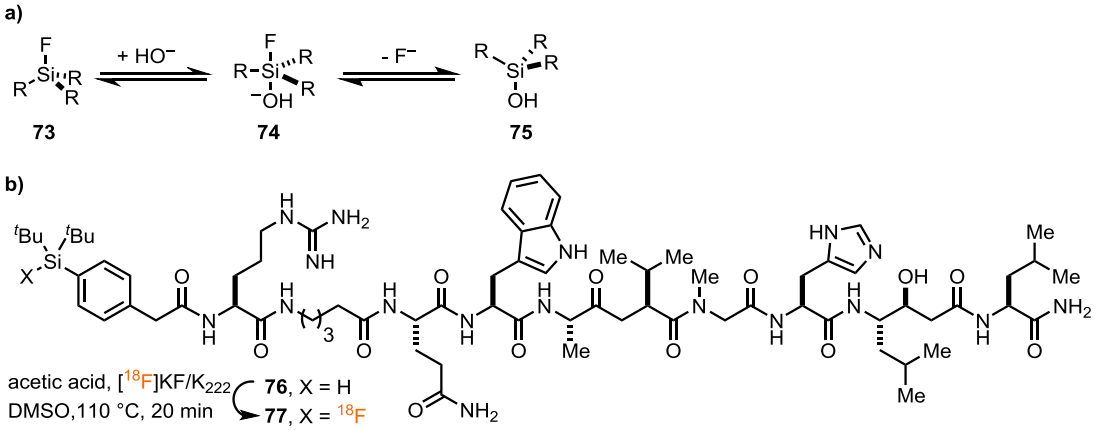

Scheme 18. a) SiFA hydrolysis. b) Application of SiFA labeling on bombesin.[103]

Perrin *et al.* developed boron acceptors that allow for the trapping of [^{18}F]fluoride under acidic aqueous conditions to form trifluoroborates. Similar to silicon, boron can form strong covalent

bonds with fluorine (bond dissociation energy = 125 kcal·mol^{-1}), but the anionic trifluoroborate prosthetic group is rather hydrophilic.[100a] Despite the thermodynamically favorable B–F bond formation, aryl trifluoroborates hydrolyze at high dilution in water due to the large excess of water.[104] Hydrolysis occurs via a dissociative pathway, in which the sp^3-hybridized borate is transformed to the sp^2-hybridized borane, which can be destabilized by bulky *ortho* substituents. Hammett analysis showed a slightly negative value ($\rho \approx -1$) for the rate of hydrolysis, which resulted in the design of **79** containing electron withdrawing substituents in the *ortho* and *para* position and a linker in *meta* position to the trifluoroborate (Scheme 19).[105] The electron withdrawing substituent led to an increased solvolytic half-life of ~1000 min. Arylboronic ester **78** can be converted to the aryl trifluoroborate **79** under mildly acidic conditions in the presence of [^{18}F]KHF$_2$ (Scheme 19).[106] An additional advantage of trifluoroborate substituents is the bio-orthogonality. However, **79** can also lead to a change in the properties of the peptides by introducing a negative charge on the peptide.

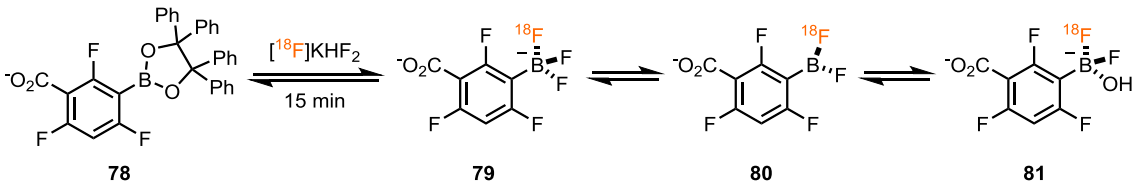

Scheme 19. Fluorine-18 labeling via formation of aryltrifluoroborate.[106]

The group of Perrin found an inverse correlation between the pK_a of alkyl carboxylic acids and the hydrolytic stability of their alkyltrifluoroborate analogs. The correlation arises from the negative charge that needs to be stabilized in both equilibriums.[107] Acetic acid has a pK_a of 4.81 and the solvolytic half-life of its trifluoroborate analog is 2–3 minutes.[107] In order to overcome previous limitations of charged prosthetic group, the Perrin group designed ammoniummethylene-BF$_3$ (AMBF$_3$, **82**), which as a betaine analog (pK_a of carboxylic acid analog 1.84) should be stable and overall non-charged.[108] AMBF$_3$ has a solvolytic half-life of more than 11 days and can be easily introduced to azide containing peptides via copper(I)-catalyzed azide alkyne cycloaddition (CuAAC). Labeling of **83** is achieved via an ion exchange reaction under acidic conditions at 80 °C. TATE analog **83** could be labeled with this protocol in 20% RCY. Despite the presence of

fluorine-19 in the precursor **83**, the labeled peptide **84** was obtained in high molar activity (111 GBq·µmol^{-1}). The high molar activity could be achieved due to the use of small amounts of precursor **83** (50 nmol). The utility of this methodology was highlighted by the 5-fold higher binding affinities of TATE analog **84** to sstr2 receptor compared to clinically used ^{68}Ga-DOTATATE.[109] Automated radiolabeling procedures are crucial for human imaging since large amounts of the tracer are required. Due to otherwise slow reaction rate the fluoride exchange labeling of $AMBF_3$ analogs is typically performed in small reaction volumes (1.5 µL), which can be difficult to handle with automated synthesizer.

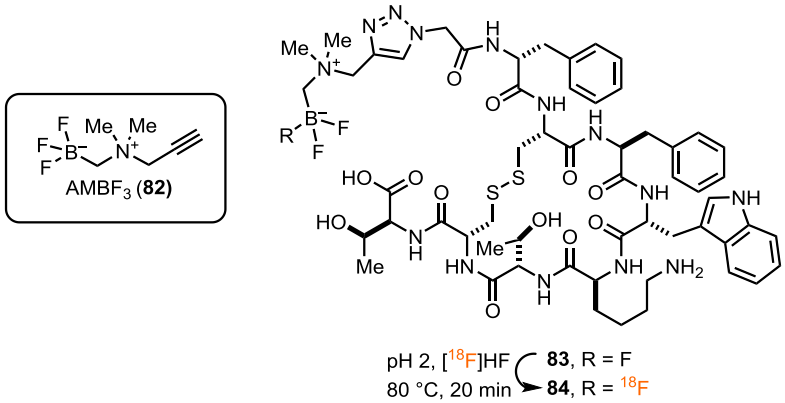

Scheme 20. $AMBF_3$ labeling of TATE analog.[109]

I.5.2. **Indirect labeling of activated peptides**

In the indirect labeling of activated peptides a small bifunctional molecule is first labeled and afterwards attached to a preactivated peptide containing an artificial substituent allowing orthogonal attachment. Indirect labeling takes advantage of robust prosthetic groups that can be labeled under harsh reaction conditions and can be afterwards, attached to a pre-functionalized site of the peptide under mild conditions. The pre-functionalized site often contains a functionality that enables orthogonal conjugation of the prosthetic group in the presence of common functional groups in peptides. Azides, as well as alkynes, are stable toward water, oxygen and most organic synthesis conditions, making them ideally suited for late stage coupling.[110] Due to the orthogonality to biological functional groups, CuAAC has found wide application in protein and peptide modification, and was first used in peptide labeling with fluorine-18 by Sutcliffe and

Marik.[111] The fluorine-18 containing prosthetic group 5-[^{18}F]fluoro-1-pentyne (**86**) was synthesized by nucleophilic substitution of 5-tosyl-1-pentyne (**85**) at 100 °C with [^{18}F]fluoride (Scheme 21). Alkyne **86** was purified by distillation, and in a second step conjugated to the peptide at room temperature (RT) to afford **87** in 97% RCY. One concern with using [^{18}F]alkylfluorides is always the potential for release of [^{18}F]fluoride through nucleophilic substitution or metabolism.

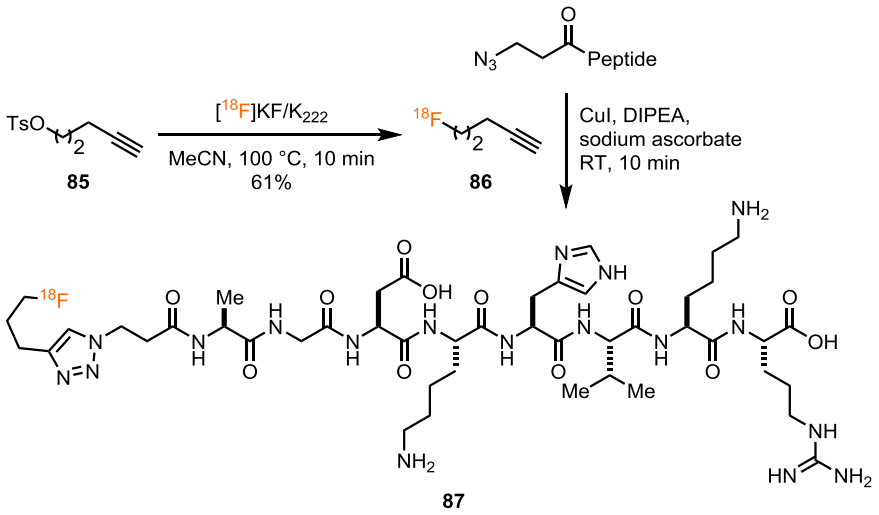

Scheme 21. CuAAC labeling of peptides.[111]

In contrast to standard CuAAC conditions, in the previous example the CuI was used in large excess compared to the amine base to obtain high yields in the cycloaddition. For cell studies and human imaging, an almost quantitative removal of copper is required to avoid cytotoxic side effects by copper.[112] Copper-free alkyne azide cycloaddition can be achieved with highly strained alkynes. The energy gained by strain release lowers the transition state for cycloaddition and permits triazole formation with azides at room temperature.[113] The first copper-free click labeling of peptides was demonstrated by Feringa *et al.* and was applied to label bombesin.[114] In the first step, [^{18}F]fluoroazide **89** was synthesized via S_NAr from **88**. After purification, **89** was conjugated in 31% RCY to peptide **90** containing a strained alkyne. One advantage of this labeling strategy is the possibility to scavenge non-labeled precursor by an azide containing resin.[115] Different to the copper catalyzed reaction, the strain promoted reaction afforded both triazole constitutional isomers, which were not separated. The formation of a product mixture is

not suitable in human imaging, and difficult to separate mixtures lead to a decreased RCY due to time-consuming purifications.

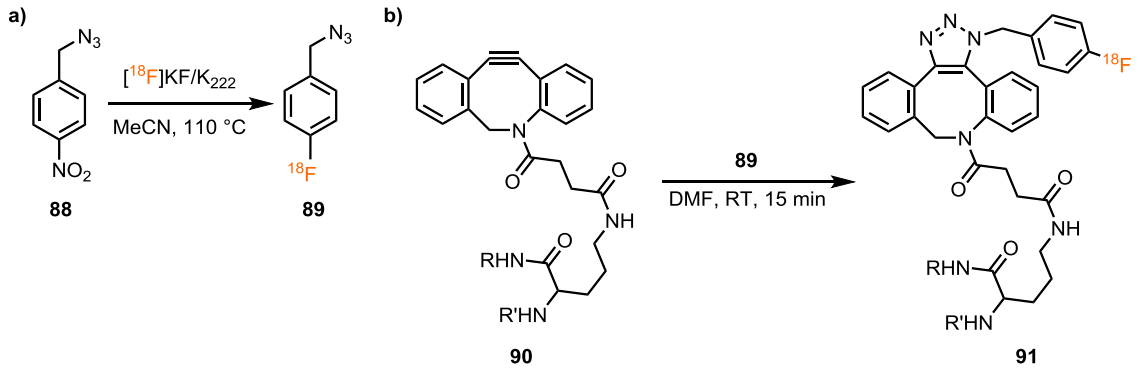

Scheme 22. Aromatic click labeling of peptides. R = Pyr-Gln, R' = Leu-Gly-Asn-Gln-Trp-Ala-Val-Gly-His-Leu-Met-NH_2.[114]

I.5.3. **Indirect labeling of unactivated peptides**

The indirect labeling of unactivated peptides also uses bifunctional prosthetic groups, which can first be labeled and then attached to a native functional group in the peptide. This can be advantageous as tracer development often starts from unlabeled compounds with high binding affinities.[116] Labeling approaches for the introduction of fluorine-18 to the native peptide structure are preferred since they allow quick access to labeled analogs of the most promising tracer candidates. Indirect labeling approaches of unactivated peptides can be divided in two subclasses: One is used to label peptides at the cysteine side chains, and the other is used to label primary amines. Among the most prominent reagents for the installation of a prosthetic group in peptides is *N*-succinimidyl-4-[^{18}F]fluorobenzoic acid ([^{18}F]SFB, **94**) (Scheme 23). The synthesis of [^{18}F]SFB begins with the nucleophilic aromatic substitution of aryl ammonium **92** with n.c.a. [^{18}F]fluoride, followed the by oxidation of aldehyde **93** to the carboxylic acid, which is converted using *N*,*N*′-Dicyclohexylcarbodiimide (DCC) an *N*-hydroxysuccinimide (NHS) to [^{18}F]SFB in overall 25% RCY in roughly 100 min.[117] [^{18}F]SFB can be conjugated to the peptide of choice at pH 8.5 at room temperature, and full conversion is commonly achieved within 15 minutes (Scheme 23).[118] For a long time, [^{18}F]SFB was the most commonly used prosthetic groups for peptide and protein labeling under mild conditions. However, a major drawback of the method is

labeling of peptides containing more than one primary amine, since differentiation using [^{18}F]SFB labeling can be very challenging. Thiols are scarcer among peptides and, if present, often just one cysteine can be found in receptor-binding peptides. Thus, labeling strategies targeting cysteine often show selective labeling. [^{18}F]FBAM (**96**) is among the most commonly used reagents for the selective installation of a fluorine-18 labeled prosthetic group on cysteine. The cysteine adds to the maleimide substituent in [^{18}F]FBAM via Michael-addition (Scheme 23).[119] Since most radiotracers are developed from non-radioactive lead compounds a minimal perturbation of its structure upon labeling is desirable.[120] However, also this method introduces quite large lipophilic prosthetic groups such as SFB and FBAM that can alter the properties of the peptide.[120]

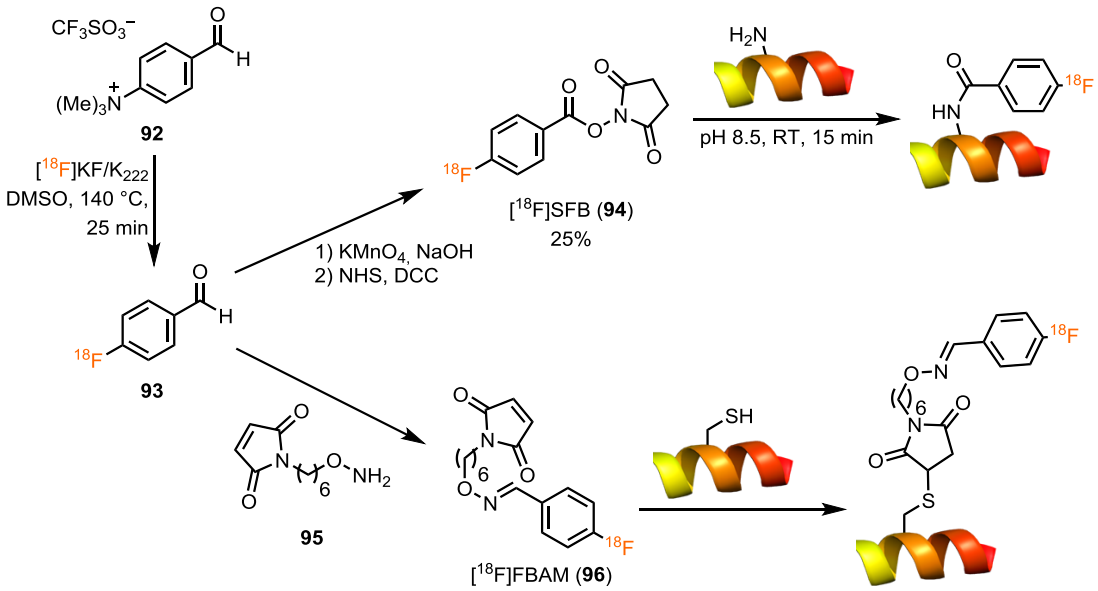

Scheme 23. Synthesis and application of [^{18}F]FBAM and [^{18}F]SBF.[117, 119]

In 2018, the Gouverneur group reported the synthesis of the [^{18}F]Umemoto reagent in a two-step protocol from nucleophilic [^{18}F]fluoride.[121] Substitution of bromide in **97** with [^{18}F]fluoride, followed by oxidative cyclization with oxone and triflic anhydride affords 5-[^{18}F](trifluoromethyl)dibenzothiophenium trifluoromethanesulfonate (**99**) in 5% RCY (Scheme 24 a). Despite the use of [^{18}F]fluoride as a precursor, the molar activity of **99** was 0.08 GBq·µmol^{-1}. The low molar activity is potentially a result of fluoride leaching of starting material **97** under labeling conditions in step 1. The reagent **99** enables the ^{18}F-trifluoromethylation of cysteine and

homocysteine. For example using this method, even complex structure such as amyloid-β-fragment **100** could be obtained in 30% RCY (Scheme 24 b). This method permits chemoselective labeling in the presence of nucleophilic amino acids such as tyrosine, lysine, and arginine, and tolerates the presence of all 20 canonical amino acids. However, peptides containing histidine or tryptophan resulted in the formation of a second radiolabeled side product, which potentially results from N or C trifluoromethylation of those amino acids. *In vivo* biodistribution of cRGDfC([^{18}F]CF_3) (**101**) showed no bone uptake and demonstrated stability of the prosthetic group.

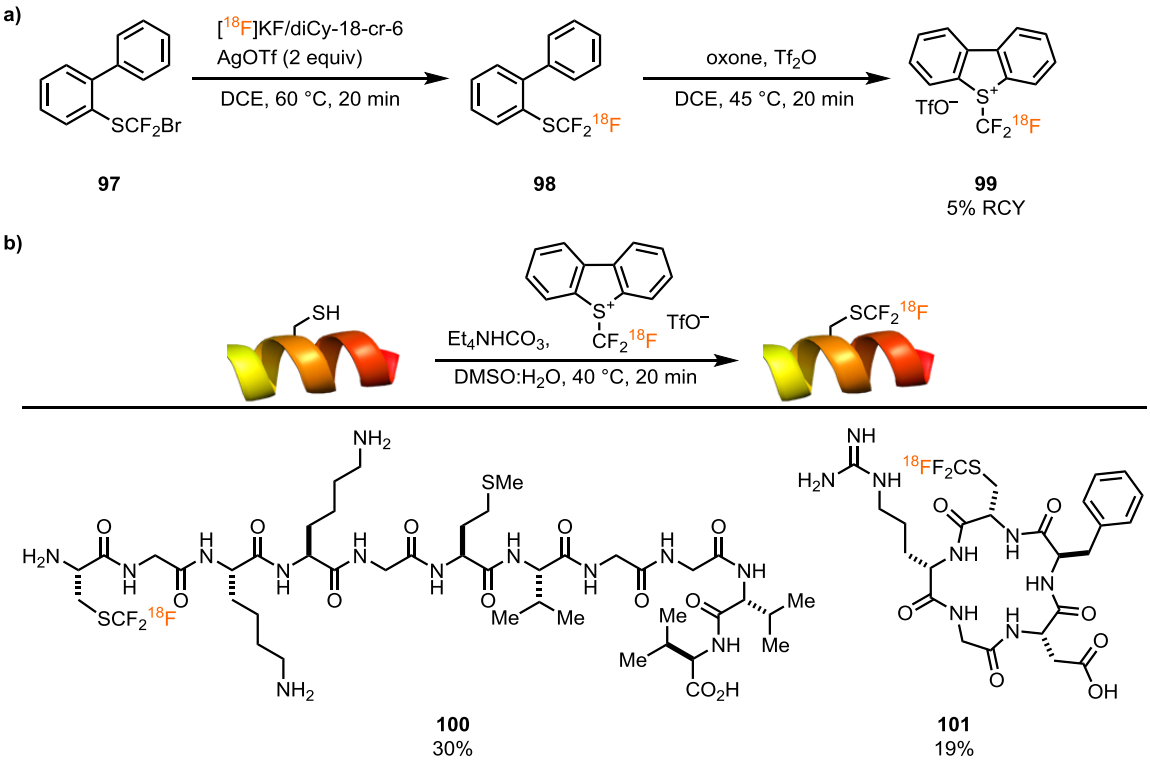

Scheme 24. Peptide labeling with the [^{18}F]Umemoto reagent.[121]

I.5.4. **Direct labeling of unactivated peptides**

The direct C–H ^{18}F-fluorination of peptide is advantageous, due to minimal perturbation in the structure of the peptide. Even though electrophilic ^{18}F-labeling of aromatic amino acids has found numerous applications, just one reported method for ^{18}F-fluorination of peptides via electrophilic aromatic substitution is known. The group of Hatano used [^{18}F]AcOF to label the aryl substituent on phenylalanine in cyclic peptide **102** (Scheme 25).[122] The labeled peptide **103** was obtained in

22% RCY as a mixture of three constitutional isomers and doubly fluorinated products. The two major products are 2-[^{18}F]F-cRGD and 4-[^{18}F]F-cRGD (**103**), which were obtained in a ratio of almost 1:1. However, it was not possible to determine the exact product ratio because 3-[^{18}F]F-cRGD could not be separated from 4-[^{18}F]F-cRGD. The low selectivity limits the applicability of this methods since more than 98% radiochemical purity of the tracer is required for human imaging, and the larger the peptide, the more difficult the purification of isomers becomes.[8] Another limitation of this method is that methionine, cysteine and tryptophan can be oxidized by [^{18}F]AcOF,[123] and [^{18}F]AcOF can just be obtained in low molar activity. For these reasons, a peptide labeled via this approach may not be suitable for imaging of receptors at low concentration.[97]

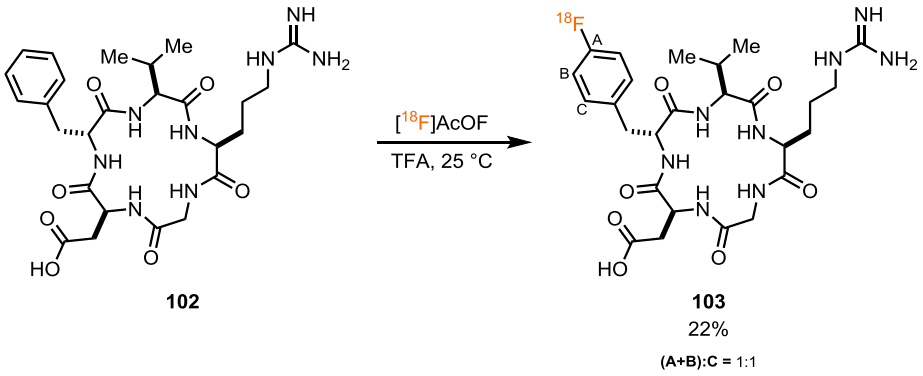

Scheme 25. Fluorine-18 labeling of peptides with [^{18}F]AcOF.[122]

The Groves group disclosed a method for labeling of benzylic C–H bonds with [^{18}F]fluoride, using manganese(salene) complex **104**, and iodosylbenzene as a terminal oxidant.[124] It was proposed that the manganese complex **104** is able to capture [^{18}F]fluoride from the solution and being oxidized by iodosylbenzene to **106** (Scheme 26 a). The manganese oxo complex **106** favors abstraction of the benzylic hydrogen over other weak C–H bonds, such as at tertiary carbon hydrogen bond. The resulting radical abstracts the [^{18}F]fluorine atom from the complex to afford the benzylic fluoride. The method enables labeling of complex drug molecules, such as protected dopamine and celestolide, in good RCY (Scheme 26 b). The chiral manganese salene complex **104** barely allows the control of enantioselectivity, and ^{18}F-celestolide **110** was obtained in 25% enantiomeric excess (ee). This method can also be used to label the fully protected enalaprilat tripeptide in 46% RCY, but the ratio of diastereomeric products was not determined. Separation

of diastereomers of large peptides can be difficult and time consuming, and thus lowering the RCY by decay or preventing isolation of pure tracer. Furthermore, the method was so far not shown to be amendable to labeling of larger peptides.

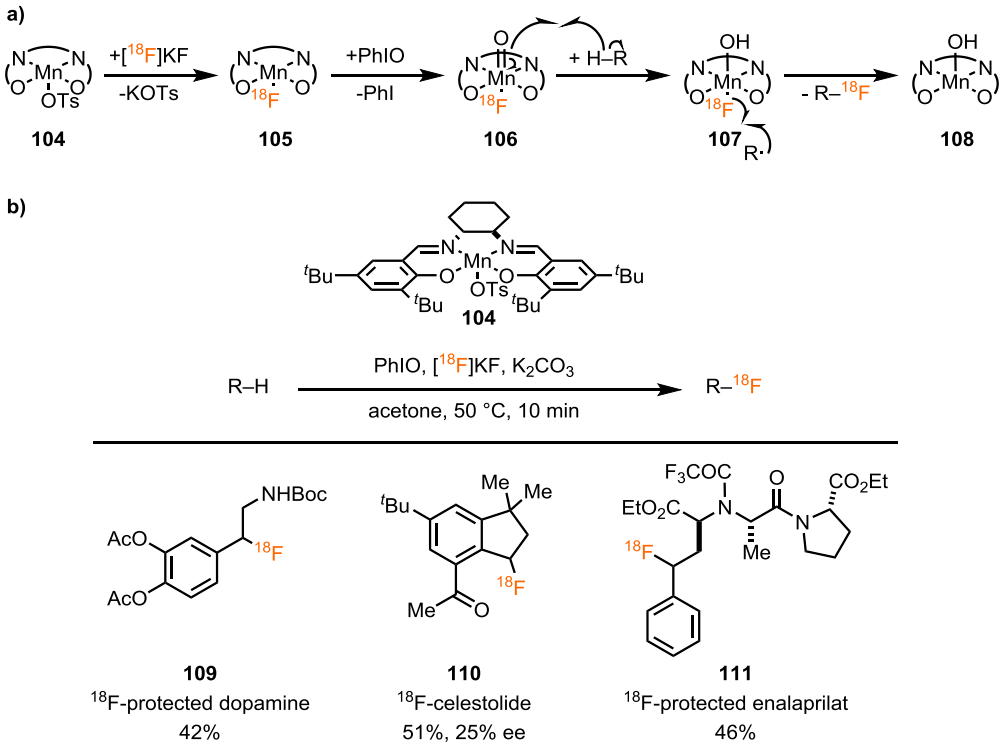

Scheme 26. a) Mechanism of the manganese-mediated benzylic radio-fluorination. b) Substrate scope of the benzylic C–H radio-fluorination.[125]

Britton and co-workers have developed the UV-light promoted labeling of leucine side-chains in unprotected peptides (Scheme 27).[126] The UV-light activated sodium decatungstate (NaDT) selectively abstracts a hydrogen atom in a branched position, followed by quenching of the carbon centered radical with [^{18}F]*N*-fluorobenzenesulfonimide ([^{18}F]NFSI).[127] Leucine labeling is favored over other canonical amino acids containing tertiary carbons hydrogen bond, but double fluorination has also been observed in substrates containing leucine and additional valine or isoleucine substituents.[128] Phenylalanine side chains containing weak benzylic C–H bonds are tolerated and do not lead to competitive benzylic ^{18}F-fluorination. Oxidizable amino acids such as cysteine and methionine are not tolerated and lead to formation of the corresponding sulfoxide and many other side products. Tyrosine, containing an electron-rich arene in the side chain, slows down the rate of reaction, while a tryptophan side chain prevents the reaction. Overall, it could be

shown that 15 of the 20 canonical amino acids are tolerated under the reaction condition. Labeling of ZJ-43 afforded **112** in 24% RCY and hexapeptide **113**, the longest sequence evaluated, was obtained in 8% RCY (Scheme 27). The use of the electrophilic fluorination reagent [^{18}F]NFSI, synthesized in 10% RCY from [^{18}F]fluorine gas, leads to low molar activity (1.3–5.3 MBq·mol^{-1}).[127] Furthermore, [^{18}F]fluorine gas is difficult to handle and not all radio pharmacies have the equipment to work with [^{18}F]fluorine-gas.

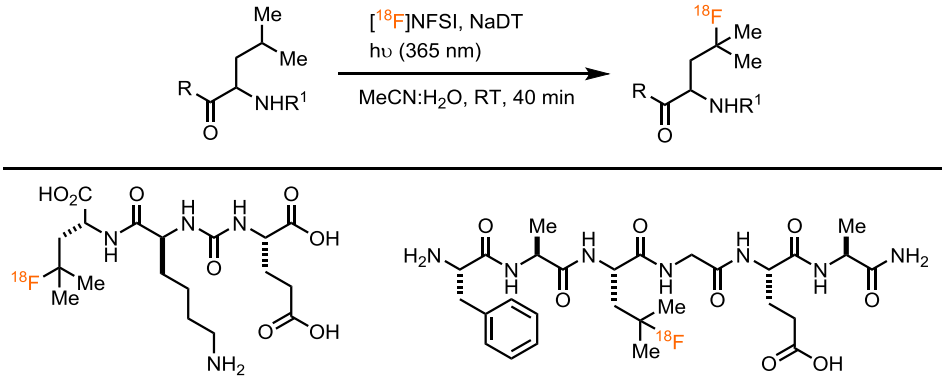

Scheme 27. Peptide labeling by C–H fluorination on leucine.[128]

II. Radio-deoxyfluorination of ruthenium phenol complexes

This chapter includes work that was published in Journal of Labelled Compounds and Radiopharmaceutical (*J. Labelled Compd. Radiopharm.* **2019**, *62*, S84-S85) and was taken with permission.[129] The target molecule was selected by Prof. Dr. Alexander Dömling, Prof. Dr. Philip H. Elsinga and Prof. Dr. Tobias Ritter. The author of this thesis designed and executed the synthesis toward [^{18}F]atorvastatin and optimized the reaction conditions. Gonçalo dos Santos Clemente performed the automated synthesis of [^{18}F]atorvastatin and performed the binding studies.

II.1. Why atorvastatin labeling?

In this chapter, we report on the synthesis of [^{18}F]atorvastatin through ruthenium-mediated radio-deoxyfluorination. Cardiovascular diseases, such as strokes, are among the leading causes of death worldwide.[130] As early as 1951, a correlation between high cholesterol level in the bloodstream and the likelihood of developing cardiovascular diseases could be made.[131] The endogenous cholesterol synthesis starts with the transformation of acetyl-coenzyme A (acetyl-CoA) to *β*-hydroxy *β*-methylglutaryl-CoA (HMG-CoA, **114**). Thioester **114** is then reduced in the liver to mevalonate (**115**) by the HMG-CoA reductase (Scheme 28 a). The reduction is the rate-limiting step in the endogenous cholesterol synthesis. Endo *et al.* found that Mevastatin (**117**), a mevalonate analog, was able to lower the cholesterol level in rats.[132] The competitive binding of mevastatin to the HMG-CoA reductase leads to its inhibition and is responsible for the cholesterol-lowering properties.

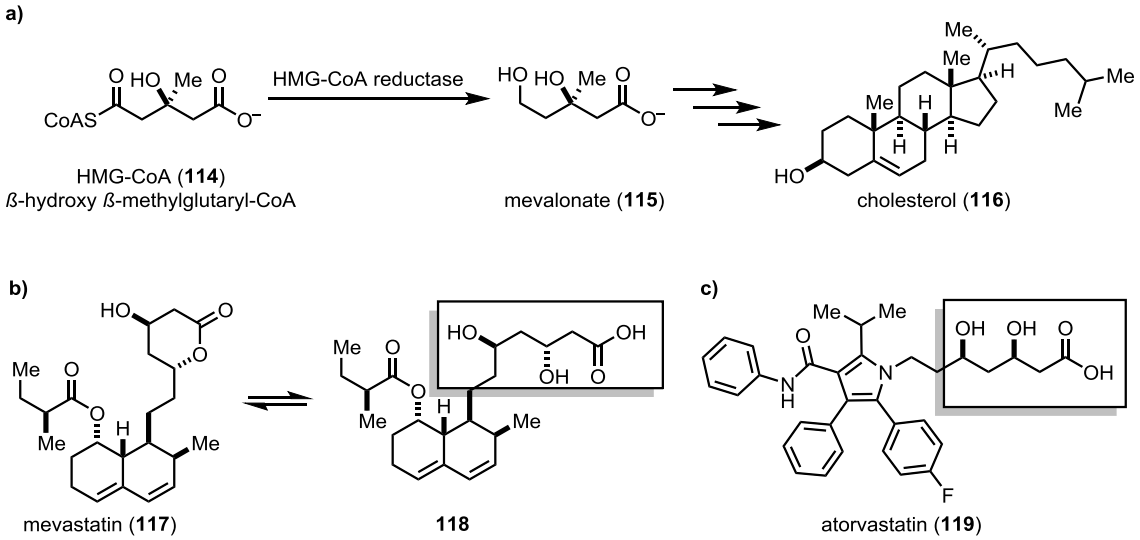

Scheme 28. a) endogenous cholesterol synthesis. b) structure of mevastatin. c) structure of atorvastatin.[132]

Atorvastatin, marketed by Pfizer under the brand name Lipitor, was the second most prescribed drug in the USA in 2016.[133] Like other statins, it is a lipid-lowering agents that slows down endogenous cholesterol synthesis and is used in the primary and secondary prevention of cardiovascular disease. Atorvastatin contains a *beta-delta*-dihydroxycarboxylic acid residue that mimics mevalonate, and assists in binding to the active site of HMG-CoA reductase. Besides lowering cholesterol levels, statins are associated with several positive side effects, for example on the immune system, the central nervous system, and the respiratory system.[134] These cholesterol-independent effects are called pleiotropic effects. Some of these effects can be attributed to other downstream endogenous synthesis products using mevalonate.[135] However some pleiotropic effects of atorvastatin cannot be assigned to lower mevalonate levels and it is proposed that binding of atorvastatin to other proteins might be the origin.[136] [^{18}F]Atorvastatin will give us the opportunity to investigate the biodistribution of atorvastatin and possibly help to understand the origin of some pleiotropic effects. In addition, we will be able to investigate whether a different *in vivo* distribution of atorvastatin can be correlated with patients who respond or do not respond to atorvastatin treatment.[137]

II.2. Synthesis of [^{18}F]atorvastatin

Atorvastatin has a plasma elimination half-life of 7 hours, and to study its biodistribution, it needs to be labeled with a radionuclide that allows imaging over several hours.[138] A suitable isotope is fluorine-18, having a half-life of 109.8 min. Labeling of atorvastatin without changing its steric and electronic properties is essential to obtain meaningful data. The formal exchange of fluorine-19 with fluorine-18 will have negligible effects on the *in vivo* behavior of the drug.[37] We envisioned accessing the fluorine-18 isotopologue of atorvastatin by ruthenium-mediated radio-deoxyfluorination (Figure 7). Ruthenium is crucial for the radio-deoxyfluorination, because arenes with electron-releasing substituents cannot be labeled with ^{iPr}ImCl alone. The unknown phenol derivative of atorvastatin was thought to be accessible via Paal-Knorr pyrrole synthesis in a similar way to the reported synthesis of atorvastatin.[139] In our retrosynthetic analysis we thought that the key 1,4-diketone intermediate **121** could be synthesized from *α,β*-unsaturated ketone **123** and aldehyde **124** via a Stetter reaction.

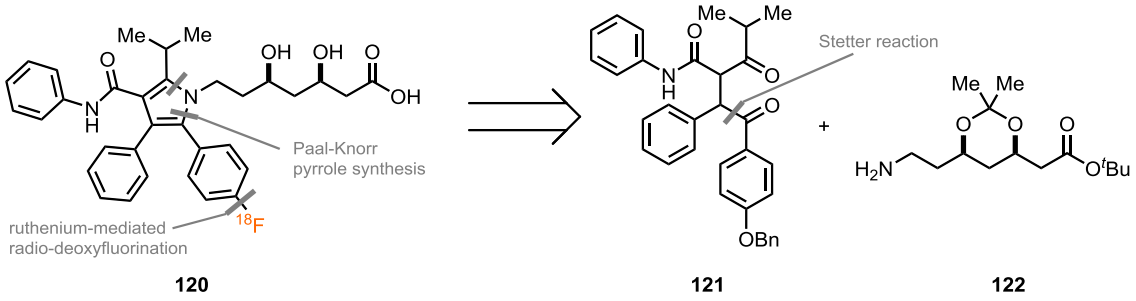

Figure 7. Retrosynthetic analysis of [^{18}F]atorvastatin.

At first, 1,4-diketone **121** was obtained via the Stetter reaction between *α,β*-unsaturated ketone **123** and aldehyde **124** catalyzed by thiazolium **125** (Scheme 29).[140] The poor yield of 16% is mainly attributed to low conversion, and the remaining starting materials could be recovered. The low yield of the Stetter reaction could not be increased by an increased catalyst loading. Next, diketone **121** was condensed with the commercially available primary amine **122** in a pivalic acid catalyzed Paal-Knorr condensation to afford pyrrole **126** in 63% yield.[141] Finally, removal of the benzyl protecting group by palladium on carbon catalyzed hydrogenolysis afforded the phenol **127**.

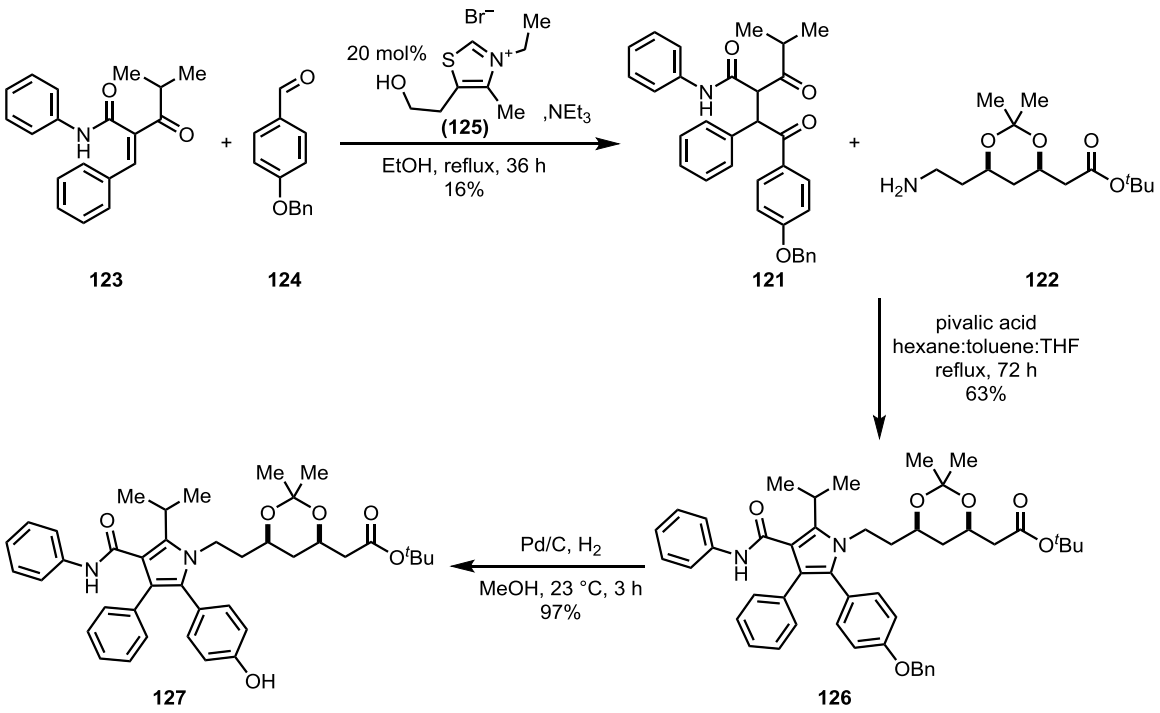

Scheme 29. Synthesis of [^{18}F]atorvastatin precursor **127**.

Following the previously published protocol on ruthenium-mediated radio-deoxyfluorination of phenols, we heated phenol **127** with ruthenium precursor **57** at 85 °C for 30 min to form the ruthenium phenol complex (Scheme 30). ^{iPr}ImCl was added to the reaction mixture, and the resulting mixture was used to elute the [^{18}F]fluoride from a quaternary methyl-ammonium (QMA) cartridge. The cartridge was once more eluted with a mixture of DMSO and acetonitrile into the same vial, which was then sealed and heated at 130 °C for 30 min. Despite the fact that most functional groups in phenol **127**, such as amides and esters, have been proven to be compatible with the ruthenium-mediated radio-deoxyfluorination, analysis of the reaction mixture by radio-TLC and radio-HPLC led to the conclusion that no [^{18}F]fluoride was consumed and no labeled organic product was formed.

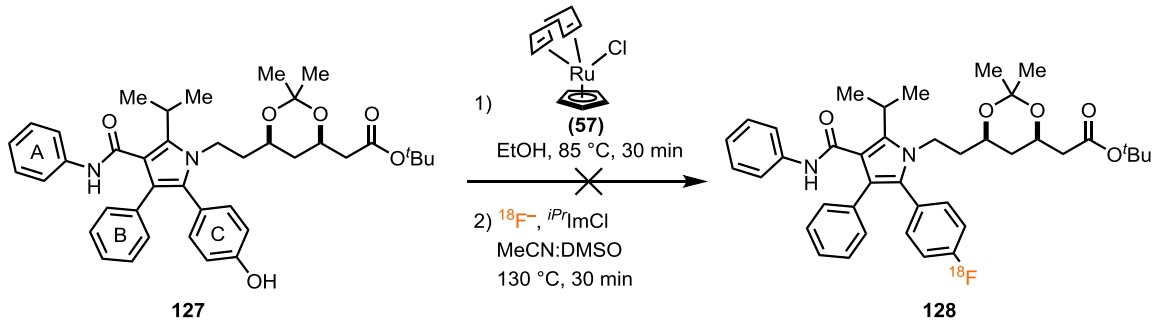

Scheme 30. Ruthenium-mediated radio-deoxyfluorination of hydroxyl-atorvastatin **127**.

Initial LC-MS examination of the reaction mixture showed a low conversion of **127** and mainly complexation to the wrong aryl substituent, leading to the conclusion that the phenol **127** was too electron-rich to undergo radio-deoxyfluorination with ^{iPr}ImCl without η^6-activation. Atorvastatin analog **127** contains three aromatic rings that could potentially form an η^6-complex to ruthenium. The complexation of ruthenium with the most electron-rich arene is thermodynamically favored. However, we believe that complexation of ring A is kinetically favored because it is the least sterically hindered arene and the amide substituent can act as a directing group. Due to the difficult complexation and because ruthenium precursor **57** is not commercially available, we thought improving the protocol and re-evaluating other ruthenium precursors.

II.3. New ruthenium precursor and complexation conditions

The ruthenium complex **57** was previously synthesized from commercially available ruthenium trichloride in a four-step procedure in 16% overall yield (Scheme 31).[72] Complex **57** is not commercially available and the synthesis procedure is lengthy and uses highly toxic cyclopentadienylthallium. The use of difficult to access ruthenium precursor **57** diminishes the utility of the ruthenium-mediated radio-deoxyfluorination methodology developed in our laboratory.

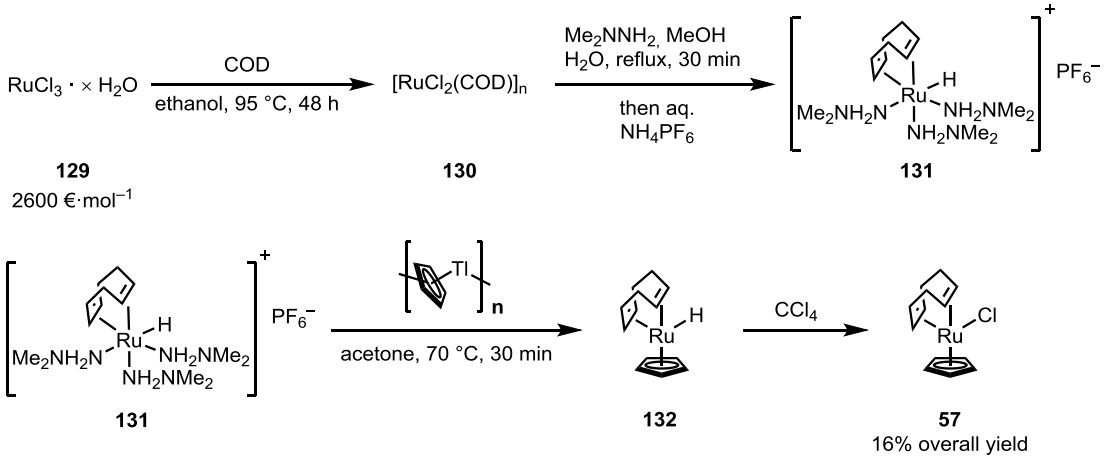

Scheme 31. Synthesis of ruthenium precursor **57**.[72]

When reviewing the literature, we found that ruthenium complex **134** could be a suitable ruthenium precursor.[142] Complex **134** is air and moisture stable, and can be stored on the bench

for several months without decomposition. In addition, **134** can be synthesized from ruthenium trichloride in a two-step procedure (Scheme 32).[143] The reductive complexation of cylopentadiene to ruthenium trichloride in the presence of zinc afforded ruthenocene (**133**) in almost quantitative yield. One cyclopentadienyl substituent of **133** can be selectively exchanged with naphthalene in the presence of strong Lewis acids. Quenching the reaction mixture with hydrogen peroxide in the presence of sodium triflate allowed for the extraction of **134**. The overall two-step procedure affords **134** in 71% overall yield. Although tetrafluoroborate and hexafluorophosphate analogs of complex **134** were widely used in literature, these anions tend to exchange fluorine-19 with fluorine-18 under harsh conditions, making them impractical precursors for radiolabeling with fluorine-18. We made ruthenium precursor **134** commercially available, which significantly increases the practicality of the ruthenium-mediated radio-deoxyfluorination.

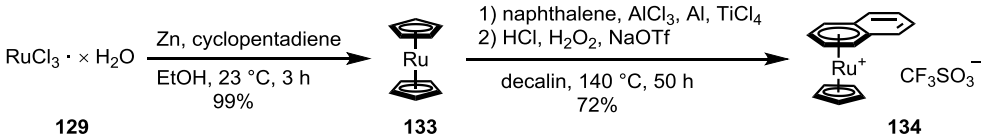

129 **133** **134**

Scheme 32. Synthesis of [(Cp)Ru(η^6-naphthalene)]OTf (**134**).

Attempts to complex **134** in ethanol to phenol **127** almost exclusively led to complexation to the undesired aryl substituent **A** (Table 2, entry 1). Changing the solvent to a mixture of dichloroethane (DCE) and acetonitrile (MeCN) led to a slight shift in the product ratio to 1:4, but still favored complexation to arene **A** (entry 3). It was speculated that the deprotonation of the phenol may alter selectivity, as the anionic phenoxide could be attracted to the positively charged ruthenium. After initial Ru–O bond formation, the arene **C** is in close proximity to ruthenium and can preferentially form the desired η^6-complex **135**. Additionally, complex **135** should have a stronger ruthenium arene bond, leading to a thermodynamically more favorable product. In the presence of one equivalent of potassium *tert*-butoxide the selectivity for complexation in DCE:MeCN increases to 1:1 (entry 7) and in *iso*-propanol almost exclusive complexation to the 4-hydroxyphenyl substituent was observed (entry 8). Complex **135** was isolated in 79% yield under the presented condition, and 11% of starting material **127** was recovered. Isolation of

complex **135** as a zwitterion was preferred to avoid formation of stoichiometric amounts of acid during the radio-deoxyfluorination.

Table 2. Optimization of complexation conditions.[a]

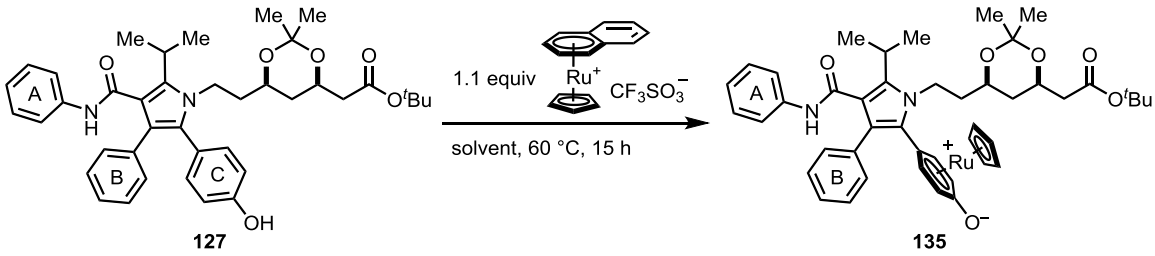

entry	solvent	additive	product ratio (C:A)[b]	yield[c]
1	ethanol	–	n.d.	< 5%
2	acetone	–	n.d.	< 5%
3	9 DCE : 1 MeCN	–	1:4	15
4	9 NO_2Me : 1 MeCN	–	1:6	< 5%
5	^{i}PrOH	–	< 1:10	0%
6	acetone	KO^{t}Bu	> 10:1	67%
7	9 DCE : 1 MeCN	KO^{t}Bu	1:1	21%
8	^{i}PrOH	KO^{t}Bu	> 10:1	79%[d]

[a] Reachtion conditions: All reaction were performed on 0.1 mmol scale in 500 µL solvent.[b] Product ratios were determined by ^{1}H-NMR analysis.[c] Yields were determined by ^{1}H-NMR analysis using mesitylene as an internal standard.[d] Isolated yield.

With access to ruthenium complex **135,** we have re-evaluated the radio-deoxyfluorination with ^{iPr}ImCl. The [^{18}F]fluoride was eluted from the QMA cartridge with a solution of ruthenium complex **135** and ^{iPr}ImCl in ethanol and acetonitrile, and the cartridge was subsequently eluted with a mixture of acetonitrile and DMSO into the same vial. The mixture was heated in a sealed vial at 130 °C for 30 minutes to afford **128** in 37% RCY (Table 3, entry 1). The published ruthenium-mediated radio-deoxyfluorination requires 8.7 µmol of substrate, but using complex **135** just 2 µmol of substrate were required. The use of smaller quantities of precursor is advantageous as they are often valuable and the purification of less material tends to be easier. The low RCY is attributed to the low conversion of [^{18}F]fluoride, formation of side products and inefficient elution of [^{18}F]fluoride. The major side product of the reaction is most likely the radio-

deoxyfluorinated, but still complexed, atorvastatin analog. Acetonitrile was a critical co-solvent for decomplexation of the arene, but has a low boiling point (83 °C) compared to the reaction temperature 130 °C. Higher boiling nitrile solvents such as benzonitrile (PhCN) and pivalonitrile (PivCN) increased the conversion and purity of the reaction to give an overall RCY of 45% and 47%, respectively (entry 2, 3). The exchange of DMSO as a co-solvent with 1,2-dimethoxybenzene increased the RCY to 58% (entry 5). We think that 1,2-dimethoxybenzene (veratrole) can act as a bidentate flat ligand that facilitates the decomplexation. Furthermore, veratrole can trap any released ruthenium to form stable η^6-complexes. The exchange of veratrole as a co-solvent with 1,4-dimethoxybenzene, which cannot act as a bidentate ligand, led to a significant drop in RCY to 34% (entry 6). The use of only veratrole or pivalonitrile as solvents lowered the RCY, highlighting the complementary properties (entry 7, 8). Lowering the reaction temperature to 110 °C resulted in a drastic drop of the RCY, as did shortening the reaction time to 10 minutes (entry 9, 10, 11). Increasing the reaction volume to 2 mL decreased the RCY to 8%, while decreasing the overall volume to 100 µL had little effect on the reaction (entry 12, 13).

With the new solvent conditions, an almost quantitative conversion of the [^{18}F]fluoride to **128** was observed, but the elution efficiency dropped from 74% to 59%. This trend might be a result of the lower polarity of the solvents.

Table 3. Optimization of solvent, temperature, and time.[a]

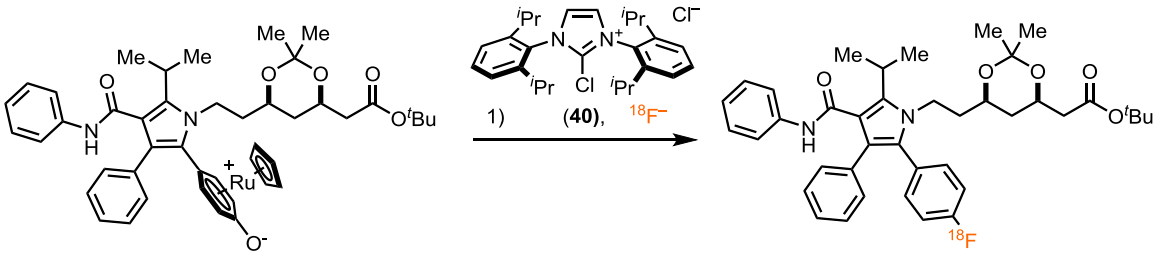

135 (2 µmol) **128**

entry	solvent	change of reaction conditions	TLC conversion	HPLC purity	elution efficiency[b]	RCY[c]
1	1EtOH: 4MeCN: 4DMSO	–	72%	70%	74%	37%
2	1EtOH: 4PhCN: 4DMSO	–	91%	81%	60%	45%
3	1EtOH: 4PivCN: 4DMSO	–	86%	90%	60%	47%
4	1EtOH: 4PivCN: 4NMP	–	57%	92%	49%	26%
5	**1EtOH: 4PivCN: 4veratrole**	**–**	**98%**	**100%**	**59%**	**58%**
6	1EtOH: 4PivCN: 4(*p*-methoxyanisole)	–	88%	63%	61%	34%
7	veratrole	–	85%	61%	30%	16%
8	PivCN	–	80%	63%	35%	18%
9	1EtOH: 4PivCN: 4veratrole	110 °C	47%	19%	59%	5%
10	1EtOH: 4PivCN: 4veratrole	20 min	85%	50%	64%	27%
11	1EtOH: 4PivCN: 4veratrole	10 min	72%	31%	56%	12%
12	1EtOH: 4PivCN: 4veratrole	2 mL	70%	24%	51%	8%
13	1EtOH: 4PivCN: 4veratrole	100 µL	99%	100%	55%	55%

[a] Reaction conditions: **135** (2.0 µmol), **40** (6.0 µmol), 130 °C, 30 min.[b] Determined by measuring the activity on the cartridge before and after elution.[c] Determined by multiplying radio-TLC conversion of fluorine-18 with radio-HPLC purity, with the elution efficiency.

Commonly used additives to elute [^{18}F]fluoride from the cartridge, such as tetraethylammonium bicarbonate, had detrimental effects on the reaction and lowered the conversion of [^{18}F]fluoride to 0% (Table 4, entry 1). In general, various bicarbonates and carbonates were found to have a detrimental effect on the reaction. Potentially formed imidazolium bicarbonate salts may decompose to the corresponding urea, and thus deactivate the reagent. Other additives that contain non-basic anions, such as tetrabutyl ammonium chloride and bis(neopentyltrimethylammonium) oxalate (NpTMAOx), had almost no effect on the elution efficiency, but rather lowered the

conversion and the purity of the product (entry 2, 3). To further explore the influence of anions on the reaction and elution, the reaction mixture was pre stirred with silver triflate and silver acetate before elution, which can exchange the counter-ion of ^{iPr}ImCl. Both additives increased the elution efficiency, but the RCY dropped, due to either low conversion or potential slow decomplexation (entry 4, 5). Protic solvents can form strong hydrogen bonds with fluoride, which leads to an increased solubility of fluoride salts. In most radiochemistry reactions, [^{18}F]fluoride is eluted from the cartridge with an aqueous solution of K_{222} and potassium bicarbonate. Due to the low reactivity of fluoride in water, water needs to be azeotropically removed in a time consuming process. In order to avoid azeotropic drying and at the same time benefit from the favorable elution properties of protic solvents, we evaluated various alcohols that can be easily removed under an argon stream.[144] Elution of fluorine-18 with a mixture of ruthenium complex **135** and ^{iPr}ImCl in methanol increased the elution efficiency to 95% (entry 6). The resulting solution was evaporated for 5 minutes at 80 °C under a stream of argon. Afterwards a mixture of pivalonitrile and veratrole was added and the solution was heated to 130 °C for 30 minutes. Despite a slightly lower conversion of fluorine-18, the overall RCY increased to 75%. The use of longer and branched alcohols as elution solvents decreased the elution efficiency (entry 7, 8). The use of more acidic alcohols such as hexafluoroisopropanol (HFIP), which can form even stronger hydrogen bonds to fluoride, results in low elution efficiency (entry 9). Scott and Sanford reported that preconditioning of QMA cartridges with different anions had a strong influence on the elution efficiency and the RCY of the copper-mediated radio-fluorination of arylboronic acids.[145] Cartridges pretreated with potassium oxalate resulted consistently in the highest yields (entry 6). The use of potassium chloride for preconditioning cut the elution efficiency almost in half (entry 10). Preconditioning of the cartridge with potassium bicarbonate and potassium triflate also resulted in an overall lower RCY (entry 11, 12). The use of Waters QMA light cartridges containing 130 mg of anion exchange resin, compared to Chromafix cartridges containing 45 mg resin, resulted in almost no change in RCY.

Table 4. Optimizing elution efficiency.[a]

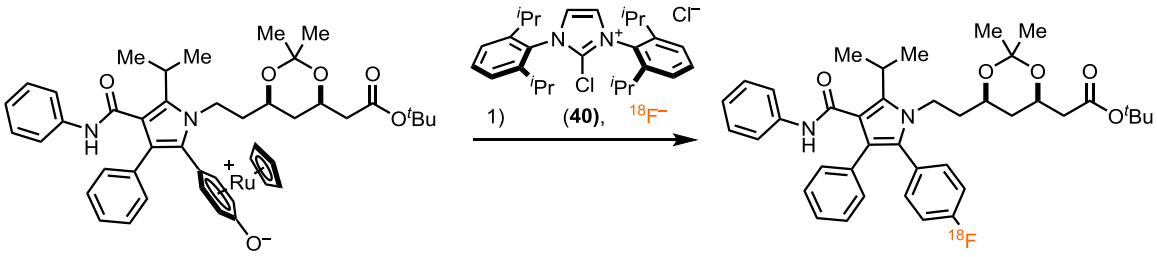

135 (2 µmol) **128**

entry	eluent solvent	additive	cartridge	TLC conversion	HPLC purity	elution efficiency[b]	RCY[c]
1	EtOH:PivCN	TEA bicarbonate	Chromafix oxalate	0%	0%	62%	0%
2	EtOH:PivCN	TBA chloride	Chromafix oxalate	91%	82%	62%	46%
3	EtOH:PivCN	NP oxalate	Chromafix oxalate	52%	71%	54%	20%
4	EtOH:PivCN	silver triflate	Chromafix oxalate	69%	36%	65%	16%
5	EtOH:PivCN	silver acetate	Chromafix oxalate	29%	82%	67%	16%
6	**methanol**	**–**	**Chromafix oxalate**	**88%**	**90%**	**95%**	**75%**
7	ethanol	–	Chromafix oxalate	94%	96%	79%	71%
8	*tert*-butanol	–	Chromafix oxalate	89%	83%	23%	17%
9	HFIP	–	Chromafix oxalate	86%	86%	60%	44%
10	methanol	–	Chromafix chloride	95%	88%	53%	44%
11	methanol	–	Chromafix bicarbonate	68%	85%	78%	45%
12	methanol	–	Chromafix triflate	78%	72%	74%	42%
13	**methanol**	**–**	**Waters QMA oxalate**	**90%**	**93%**	**93%**	**78%**

[a] Reaction conditions: **135** (2.0 µmol), **40** (6.0 µmol), 130 °C, 30 min.[b] Determined by measuring the activity on the cartridge before and after elution.[c] Determined by multiplying radio-TLC conversion of fluorine-18 with radio-HPLC purity (n = 2) with the elution efficiency.

To obtain [^{18}F]atorvastatin, the ketal and ester protecting groups on **128** need to be removed in subsequent steps (Scheme 33). The two-step deprotection protocol consists of acidic removal of the ketal protecting group using 6 M HCl at 60 °C for 5 minutes, followed by saponification of the ester using sodium hydroxide at 60 °C for 5 minutes. Using this overall three-step, one-pot protocol, it was possible to obtain [^{18}F]atorvastatin (**120**) in 20% decay-corrected RCY after preparative HPLC purification. After purification, the product was obtained in ≥ 95% radiochemical purity and in high molar activity 112 ± 77 GBq·µmol^{-1}.[129]

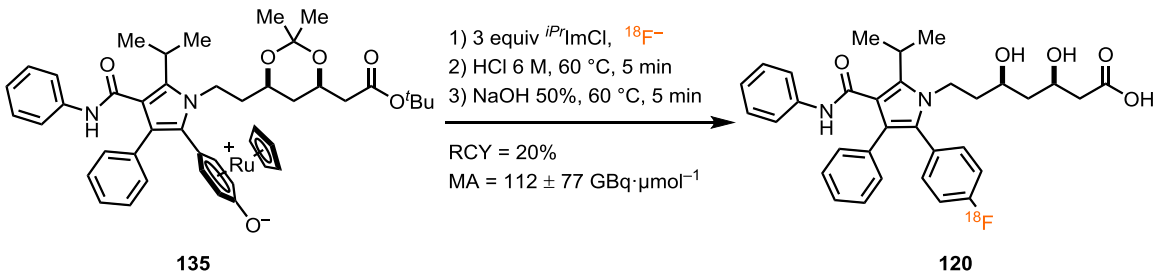

Scheme 33. Synthesis of [^{18}F]atorvastatin.[129]

Human imaging typically requires around 300 MBq of radioactive material, and the manual handling of these large amounts of activity is not possible. In order to access sufficient activity of [^{18}F]atorvastatin, the protocol was translated to the automated synthesis model Synthra RNplus. Initial automation experiments were successful and **120** could be isolated in 5% RCY.[129]

II.4. *In vitro* analysis of [^{18}F]atorvastatin

Before starting *in vivo* experiments, we investigated the behavior of [^{18}F]atorvastatin *in vitro*. The three-hour incubation of **120** in human serum and rat serum at 37 °C lead to no signs of decomposition. An ideal PET-tracer would exclusively bind the target. However, this exclusive binding is typically not possible. A high plasma protein binding can lead to a low target-to-background ratio, due to the high background radiation. The plasma protein binding in the serum of rats with a normal diet was 16.7%, and in rats with a high fat diet it was 13.8%. Furthermore, it could be shown that more [^{18}F]atorvastatin was bound to liver homogenates of rats with high calorie diet than of rats with low calorie diet.

II.5. Conclusion and outlook

In this chapter, we present an optimized protocol for the ruthenium-mediated radio-deoxyfluorination of phenols and overcome several of the previous known and unknown shortcomings. The selective complexation of ruthenium complex to the 4-hydroxyphenyl substituent against other arenes present in **127** was achieved under basic conditions. Furthermore, we were able show that the use of complexed precursor enabled us to reduce the amount of material used in fluorine-18 labeling from 8.7 µmol to 2 µmol. Major losses of fluorine-18 in the

previous protocol were attributed to low elution efficiency. Almost quantitative elution of [^{18}F]fluoride was achieved with ^{iPr}ImCl in methanol, followed by drying under a stream of argon. The elution efficiency of this protocol is comparable to elution with the well-established mixture of K_{222} and potassium bicarbonate, but circumvents time-consuming azeotropic drying. Furthermore, the inversion of the cartridge is no longer necessary and the RCY is no longer dependent on vial size or pressure, allowing easier translation to various automated synthesis models. Initial results show the feasibility of *in vivo* imaging with [^{18}F]atorvastatin. A major downside of the protocol is the high reaction temperature required for the decomplexation of ruthenium. The development of ruthenium complexes with an easy to trigger decomplexation functionality would be of great benefit to the protocol. Furthermore, the development of a good manufacturing practice (GMP) protocol would be a major step forward toward the first in human imaging studies using this methodology. The Elsinga laboratory at the University of Groningen is currently working on human imaging with [^{18}F]atorvastatin.

III. [18]F-Labeling of peptides

This chapter includes work that was published in Angewandte Chemie (*Angew. Chem. Int. Ed.* **2018**, *57*, 14207–14211) and was taken with permission.[146] The idea of the project was set out by Prof. Dr. Tobias Ritter and the author of this thesis. The author of this thesis designed and conducted experiments that led to the development of the site-specific radio-deoxyfluorination of small peptides with [^{18}F]fluoride. The manuscript was prepared in cooperative work between Prof. Dr. Tobias Ritter and the author of this thesis.

III.1. Project design

Receptor-binding peptides are a rapidly growing class of PET-tracers used in non-invasive diagnosis, in oncology, and the study of biochemical processes.[147] The use of peptides bears the inherent advantage of facile access by automated solid phase peptide synthesis, potential high binding affinity and rapid blood clearance.[97] A critical aspect to peptide labeling is that the labeling method should result in a minimal perturbation of the structure of the peptide. Labeling without changing the properties of the peptides can be achieved with carbon-11, nitrogen-13, and oxygen-15 labeled structures, but the half-lives of 20 minutes or less of these isotopes mitigates utility of those radionuclides toward PET-imaging with peptide-tracers.[148] Labeling with radioactive metals with sufficiently long half-lives such as gallium-68 or copper-64 requires the attachment of prosthetic groups that can drastically change the properties of the peptide. Although successful examples of peptide labeling via prosthetic groups are known, this requires in-depth knowledge of the binding site.[147] In contrast to radiometals, fluorine-18 can be introduced without the need of prosthetic groups and can result in small structural modifications, as it is considered a bioisostere of a hydrogen or a hydroxyl substituent. In addition, favorable nuclear properties such as low positron energy, preferential beta-plus-decay and, especially the half-life of 109.8 minutes makes it an ideal radionuclide for peptide labeling.[149] Despite the demand for methods to label polypeptides by simply exchanging one hydrogen or hydroxyl functionality with [^{18}F]fluoride, no method was able to achieve this goal. The reason for the lack of methods can be

attributed to the high density of functional groups and the lability of the structure. In our previous publications on ruthenium-mediated radio-deoxyfluorination of arenes,[72] we have shown that most functional groups common in peptides are well tolerated. Therefore, we thought that it might be possible to use the high functional group tolerance of the ruthenium-mediated radio-deoxyfluorination to achieve peptide labeling by formal exchange of a hydrogen/hydroxyl substituent with fluorine-18.

III.2. Building block design, synthesis and application

Introduction of fluorine-18 on arenes is often preferred over alkanes due to the higher metabolic and chemical stability.[126] Among the 20 canonical amino acids are four aromatic amino acids: phenylalanine, tyrosine, tryptophan, and histidine (Figure 8). It was found that the introduction of fluorine on aromatic side chains has little effect the on protein function, and up to 80% of tryptophan in Escherichia coli could be exchanged for 5-F-tryptophan while little effect on the growth of the bacterium being observed.[150] Similar results were found for the replacement of phenylalanine with 4-fluoro-phenylalanine.[151] In our previous publication on the ruthenium-mediated radio-deoxyfluorination of phenols, our group disclosed the radio-deoxyfluorination of protected tyrosine, which is not possible without ruthenium coordination. Thus, and because the resulting 4-fluoro-phenylalanine is an analog of phenylalanine and tyrosine, we decided to investigate the introduction of 4-[[18]F]fluoro-phenylalanine into peptides.[72]

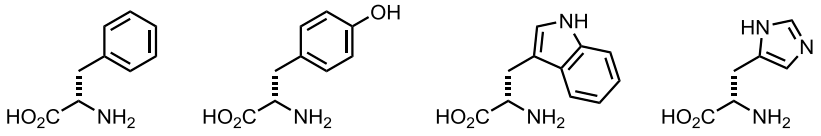

136 phenylalanine **137** tyrosine **138** tryptophan **139** histidine

Figure 8. Aromatic amino acids.

Since unprotected carboxylic acids tend to lower the RCY, most likely by protonation of [[18]F]fluoride to afford unreactive [[18]F]hydrogen fluoride, they need to be protected during labeling. To avoid this and other side reactions with labile functional groups, we focused on the labeling of fully protected peptides, which are as easily accessible by solid phase peptide

synthesis as unprotected peptides. Even though Kudinov *et al.* were able to show that selective complexation of ruthenium to aromatic side chains in peptides is feasible, no chemoselectivity in peptides containing more than one aromatic side chain has been shown.[152] The introduction of ruthenium as building block **140** during SPPS therefore has two advantages: First, ruthenium can be introduced chemoselectively on one tyrosine side chain and second, it reduces the numbers of steps required to access the labeling precursor (compared to peptide synthesis, selective deprotection, selective complexation). Building block **140** was synthesized in a two-step procedure by blue LED-light-mediated arene exchange on ruthenium precursor **141** with tyrosine,[152a] followed by protection of the primary amine using Fmoc-*N*-hydroxysuccinimide (Fmoc-OSu) (Scheme 34). The product was extracted from the aqueous solution as a zwitterion, which was precipitated once to obtain the analytically pure building block **140** in 75% yield. We did not observe erosion of the ee of tyrosine during the synthesis and if the building block **140** is stored in the freezer it was stable for several months, also without erosion of the ee.

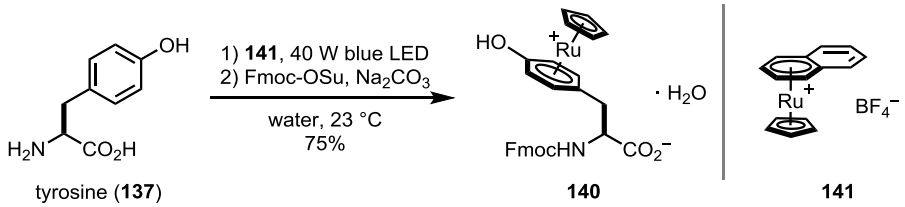

tyrosine (**137**) **140** **141**

Scheme 34. Fmoc-Tyr(RuCp)-O (**140**) synthesis.[146]

In a standard coupling experiment, HBTU was added to a vial containing **140**, HOBt and DIPEA in equimolar amounts in DMF (Scheme 35). After 5 minutes activation time, the mixture was added to a growing peptide on solid support. Typical coupling efficiencies of around 80% were achieved. Extended activation times of building block **140**, as they are usual for other amino acids, led to degradation of building block **140**. No ruthenium leaching from the building block was observed during SPPS and the unprotected ruthenium-bound phenol did not engage in any side reaction. The reason for both is probably the strong ruthenium-arene bond and the strong electron withdrawing properties of ruthenium, rendering the phenol less nucleophilic.[153] Solid phase peptides synthesis was typically performed on a 2-chlorotrityl resin, which allows the fully protected peptide to be cleaved from the resin using a mixture of 20% hexafluoroisopropanol

(HFIP) in dichloromethane. The fully protected ruthenium-containing peptide can be purified by preparative high-performance liquid chromatography (HPLC) under mildly acidic conditions. The resulting clean precursor can be stored on the bench for several months without decomposition. We found that the ruthenium-cyclopentadienyl-fragment can be selectively introduced in this way and no migration of ruthenium to other arenes was observed.

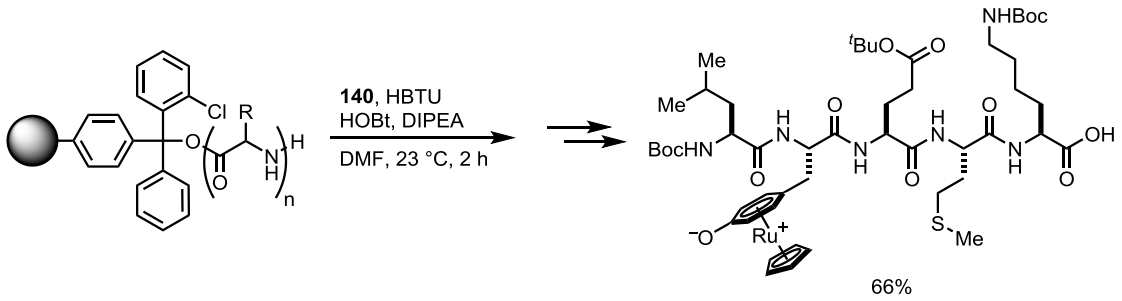

Scheme 35. Application of **140** in SPPS.

III.3. Radiolabeling of ruthenium peptide complexes

Typically radiochemical labeling with [^{18}F]fluoride begins with trapping of [^{18}F]fluoride on a QMA cartridge, followed by elution with an aqueous solution of K_{222} and potassium bicarbonate. Afterwards, water removed by azeotropic drying. This procedure takes 20 minutes and lowers the RCY by 12% through to the decay of fluorine-18. On the contrary, our protocol elutes the fluorine-18 with a mixture of the zwitterionic peptide-ruthenium complex and ^{iPr}ImCl in a mixture of ethanol and pivalonitrile. The cartridge was eluted again with a mixture of pivalonitrile and veratrole into the same vial, which was then sealed with a Teflon-lined cap and heated to 130 °C for 30 minutes to afford the labeled and fully protected peptide. Using this protocol, **143** was obtained in 34% RCY (Table 5, entry 1). The low yield is the result of low purity as well as low elution efficiency. The addition of quaternary alkyl-ammonium halides and mesylates increased the elution, but led to formation of side products, and thus overall lowered the RCY (entry 2, 3 and 4). The presence of more basic anions in the reaction mixture, such as bicarbonate, led to low conversion of fluorine-18 (entry 5).

Table 5. Optimization of the elution efficiency.[a]

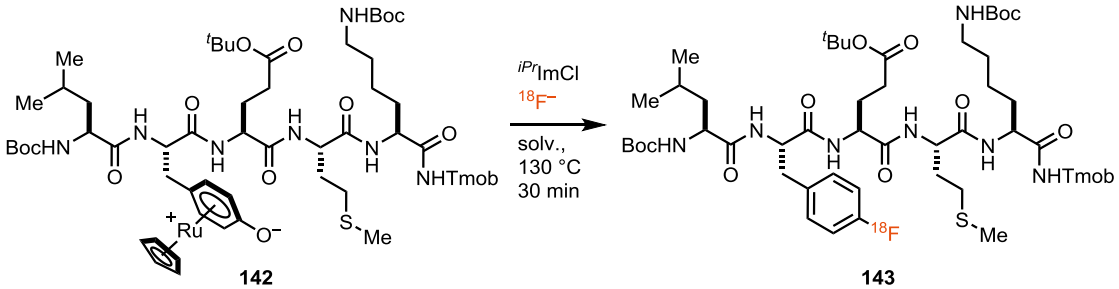

entry	eluent solvent	additive	TLC conversion	HPLC purity	elution efficiency[b]	RCY[c]
1	ethanol:pivalonitrile	–	97%	75%	47%	34%
2	ethanol:pivalonitrile	TBA chloride	100%	54%	76%	41%
3	ethanol:pivalonitrile	TBA iodide	100%	52%	85%	44%
4	ethanol:pivalonitrile	TBA OMs	100%	62%	78%	48%
5	ethanol:pivalonitrile	TEA bicarbonate	8%	62%	86%	4%
6	**ethanol:pivalonitrile**	**NpTMA oxalate**	**100%**	**93%**	**76%**	**71%**
7	ethanol:pivalonitrile	K_{222}, $K_2C_2O_4$	91%	84%	74%	57%
8	MeOH	–	93%	64%	92%	55%

[a] Reaction conditions: **142** (5.0 µmol), **40** (15 µmol) solv. = pivalonitrile:veratrole:ethanol (450 µL, 4:4:1, v:v:v).[b] Determined by measuring the activity on the cartridge before and after elution.[c] Determined by multiplying radio-TLC conversion of fluorine-18 with radio-HPLC purity.

A potential reason for the low purity could be due to decomposition of the ammonium salts. Above room temperature, anhydrous tetrabutylammoniumfluoride (TBAF) is unstable both in solid state as well as in solution.[154] The main decomposition pathway is a Hofmann-elimination (E2 reaction) (Scheme 36). Seppelt *et al*. developed neopentyltrimethylammonium fluoride (NpTMAF) as a stable source of naked and anhydrous fluoride, that cannot decompose by Hofmann-elimination due to the lack of β-hydrogen, but is still highly soluble in organic solvents.[155] Solid samples of NpTMAF decompose to fluoromethane at temperatures above 145 °C by S_N2 reaction. The use of neopentyltrimethylammonium oxalate (NpTMAOx) as an additive increased the elution efficiency to 76% while having no detrimental side effect on conversion or purity (entry 6). The use of a mixture of K_{222} and potassium oxalate proved to be equally effective in increasing the elution efficiency (entry 7). Although the product was obtained in lower purity, the use of these reagents allows a more facile GMP approval, as these reagents are commonly

used in radiochemistry. Almost quantitative elution of [^{18}F]fluoride in protic solvents was achieved, but the purity of the product was lowered (entry 8).

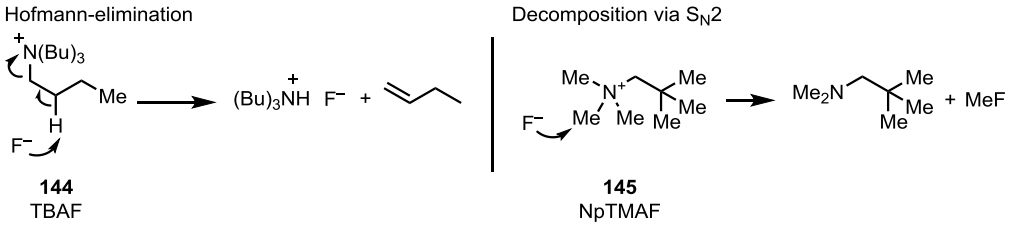

Scheme 36. Decomposition pathways of ammonium fluorides.[156]

Despite the high reaction temperature and the long reaction time, no extensive decomposition was observed (Figure 9). The only fluorine-18 containing side product that is formed has a very similar retention time to that of peptide ruthenium complex **142**. If the reaction time is shortened to 10 minutes, the amount of fluorine-18 labeled side product at 9.7 min increases to 74%, and if the reaction temperature is lowered to 100 °C, the amount increases to 98 % (Table 6, entry 2 and 3). The fact that the side product converts with extended reaction time and higher reaction temperature to the labeled peptide **143**, and the similar retention time to peptide ruthenium complex **142** leads to the assumption that it might be the radio-deoxyfluorinated, but still complexed peptide. This side product is easy to separate and does not pose a problem in purification.

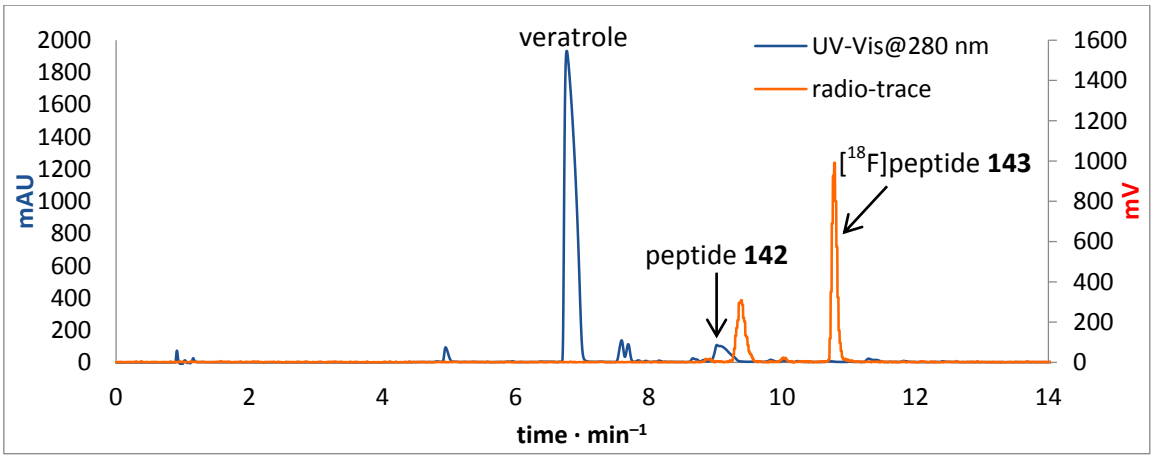

Figure 9. HPLC trace of crude reaction mixture.

In a clinical setting, the use of rigorously anhydrous solvents cannot be guaranteed. In order to underline the robustness of the presented method against water, we added 10 µL of exogenous water to the 450 µL reaction mixture, which resulted in a minor drop of RCY from 87% to 78%

(entry 4). Furthermore, no special precautions toward air were required. Lowering the amount of precursor used from 5 µmol (6.5 mg) to 2.5 µmol (3.2 mg) results in an acceptable decrease in RCY to 35%, and even as little as 1.5 µmol (1.9 mg) is sufficient to obtain **143** in acceptable yields (entry 5, 6). The lower amounts of precursor resulted in a stronger deviation of the results. Thus, all subsequent experiments were conducted with 5 µmol ruthenium peptide complexe. The size of the reaction vial did not have an influence on the RCY, leading to a more facile automation of the process (entry 7, 8).

Table 6. Modification of standard conditions.[a]

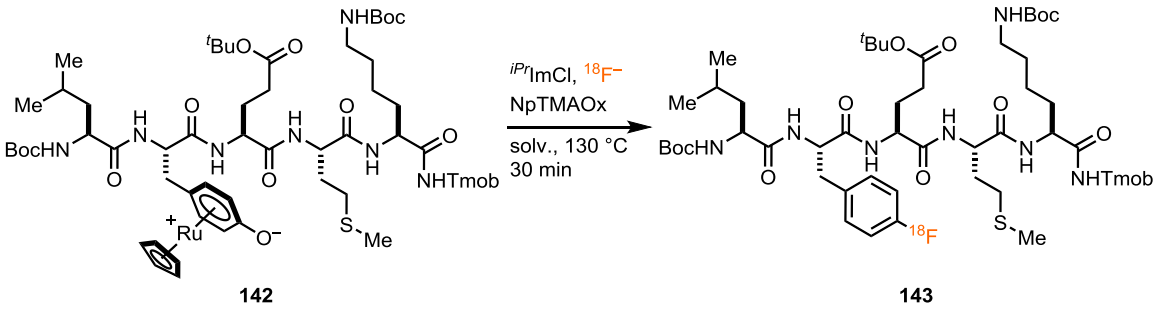

142 **143**

entry	change of reaction conditions	TLC conversion	HPLC purity	elution efficiency[b]	RCY[c]
1	none	100%	93%	76%	71%
2	100 °C	68%	3%	61%	1%
3	10 min	94%	26%	65%	16%
4	10 µL H_2O added	100%	78%	57%	45%
5	3 µmol of **142**	95%	53%	70%	35%
6	1.5 µmol of **142**	92%	47%	65%	28%
7	20 mL vial	100%	91%	80%	73%
8	2 mL vial	100%	96%	70%	67%

[a] Reaction conditions: **142** (5.0 µmol), NpTMAOx (14 µmol), **40** (15 µmol) solv. = pivalonitrile:veratrole:ethanol (450 µL, 4:4:1, v:v:v).[b] Determined by measuring the activity on the cartridge before and after elution.[c] Determined by multiplying radio-TLC conversion of fluorine-18 with radio-HPLC purity (n = 2).

III.4. Substrate scope

Most peptide PET-tracers do not contain protecting groups, and thus an additional deprotection step is required after labeling of protected peptides. The labeling of unprotected peptides would be inherently advantageous as it would reduce the overall number of steps of the labeling protocol. Furthermore, the complexation of ruthenium to tyrosine side chains in unprotected peptides is known, which would allow the labeling of native peptides.[157] Subjecting the ruthenium peptide complex **146** to our standard labeling conditions led to the formation of **147** in 12% RCY (Scheme 37). However, a messy radio HPLC-trace was observed, probably due to decomposition of the labeled product and precursor. The formation of a complex product mixture can lead to time consuming purification and would reduce the benefit of this approach. Therefore, we decided to focus on the labeling of protected peptides and add a deprotection step to the protocol.

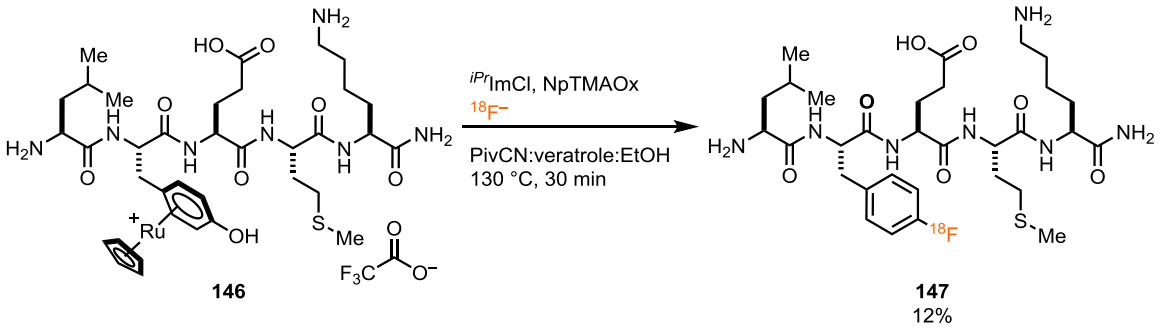

Scheme 37. Deoxyfluorination of unprotected peptide **146**.

A common deprotection mixture used in SPPS is a combination of TFA, 1,4-dithiothreitol (DTT), water, and triisopropylsilane (TIPS). All protecting groups common to SPPS with Fmoc strategy can be removed under acidic conditions as well as the trimethoxybenzyl (Tmob) protecting group on the C-terminal amide. The highly reactive intermediates formed during deprotection, such *tert*-butyl cations, must be quenched with nucleophilic scavengers, such as water and DTT. The second effect of DTT is that it is able to reduce sulfoxides and disulfides. The general procedure for the ruthenium-mediated peptide [18]F-labeling starts with trapping of [18]F]fluoride on a QMA cartridge that was preconditioned with potassium oxalate. The [18]F]fluoride was eluted with a mixture of the peptide ruthenium complex, *iPr*ImCl, and

NpTMAOx in a solution of ethanol and pivalonitrile into a 4 mL vial. The cartridge was eluted a second time with a mixture of veratrole and pivalonitrile into the same vial, which was closed with a Teflon-coated cap and was heated at 130 °C for 30 minutes. Afterwards, the reaction mixture was concentrated to dryness under a stream of argon at 80 °C, followed by addition of a mixture of TFA (0.44 mL), DTT (35 mg), water (25 µL), and TIPS (13 µL). The reaction mixture was heated to 50 °C for 10 minutes, subsequently diluted with a methanol:water mixture, and purified by preparative HPLC.

The radiochemical yield was determined by comparing the amount of activity prior to trapping on the QMA cartride with the activity of isolated, analytically pure material. This way of analysis provides the most reproducible results as it takes into account losses due to the release of gaseous side products such as [^{18}F]HF or [^{18}F]methylfluoride. Losses due to the reaction of [^{18}F]HF with the borosilcate glass are not taken into account by radio-TLC. Therefore, isolated RCY are typically lower than RCY determined by HPLC and TLC. This more precise measurement and the additional second step resulted in the generally lower yields compared to those determined previously.

The model substrate **147**, which contains an oxidatively labile methionine side chain and protected carboxylic acids could be isolated in 20% decay corrected (d.c.) RCY, which is only a quarter of the TLC/HPLC results measured before (Scheme 38). Minigastrin 11 (MG11) is an analog of the human gastrin and binds to the gastrin receptor, which is overexpressed in some cancer types such as medullary thyroid cancer. MG11 was previously labeled by ligation to a DOTA indium-111 complex for single photon emission computer tomography.[158] We were able to isolate fluorine-18 labeled MG11 analog **148** after ruthenium-mediated radio-deoxyfluorination in 24% d.c. RCY. Despite the presence of two tyrosine side chains in the precursor, we were able to selectively form just one product, leading to the assumption that chemoselective labeling was achieved. Cyclic peptide **149,** containing the Arg-Gly-Asp (RDG) triard which is popular in $\alpha_v\beta_3$ receptor imaging, could be isolated after labeling in 25% d.c. RCY. The fluorinated analog of neuromedine B **150** could be isolated after labeling and deprotection in 29% d.c. RCY. The

decapeptide **150** was the longest sequence evaluated, and more extensive decomposition was observed compared to other peptides. Thus, we think that our method is most applicable for labeling of small peptide sequences, which benefits most from labeling methods with minimal perturbation of structure. Most receptor-binding peptide PET-tracers contain C-terminal primary amides because this motif mimics the native peptide structure better and because peptides tend to have higher metabolic stability toward carboxypeptidases.[159] Octapeptide **151** containing a C-terminal carboxylic acid could be isolated in 11% d.c. RCY, starting from a precursor containing a non-protected C-terminal carboxylic acid. The protection of the carboxylic acid as an acid labile *p*-methoxybenzyl (PMB) ester increased the isolated d.c. RCY to 39%. Due to the high reaction temperature, we were afraid of epimerization of the peptides. Even though no excessive decomposition was observed, we used pentapeptide **152** as a model substrate, containing a histidine residue that can facilitate racemization by serving as an internal base.[160] If the product is compared with authentic reference samples of both potential diastereomers, no epimerization within the limits of detection could be observed. Overall, we could show that all 20 canonical amino acids are tolerated and that 4-[^{18}F]fluoro-phenylalanine could be introduced on the C-, N-terminus or within the peptide structure. The robustness of the method is highlighted by the use of one set of reaction conditions that allows for the rapid evaluation of tracer candidates.

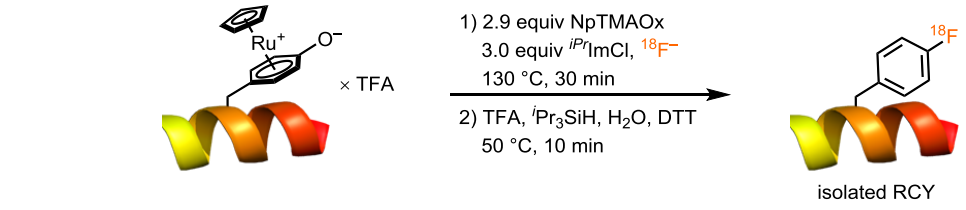

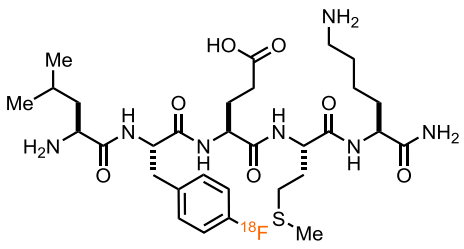

H-Leu-Phe(4-[^{18}F]F)-Glu-Met-Lys-NH_2 (**147**)
20% (n=2)

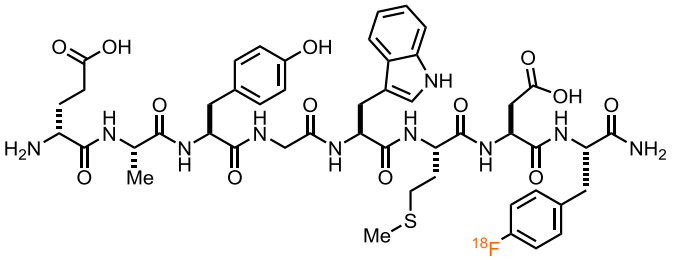

H-*D*-Glu-Ala-Tyr-Gly-Trp-Met-Asp-Phe(4-[^{18}F]F)-NH_2 (**148**)
MG11 analog
24% (n=3)

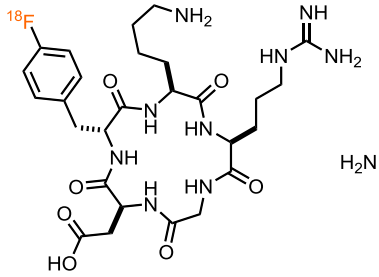

c(Asp-*D*-Phe(4-[^{18}F]F)-Lys-Arg-Gly) (**149**)
c(RGDfk) analog
25% (n=2)

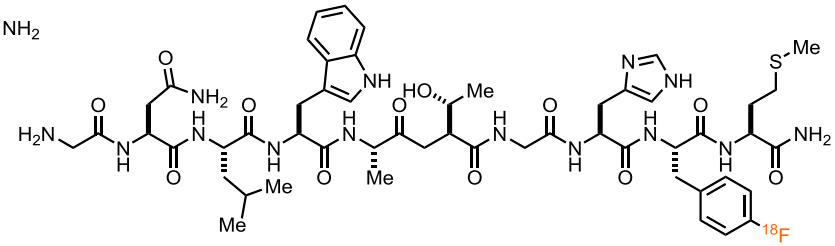

H-Gly-Asn-Leu-Trp-Ala-Thr-Gly-His-Phe(4-[^{18}F]F)-Met-NH_2 (**150**)
Neuromedin B analog
29% (n=2)

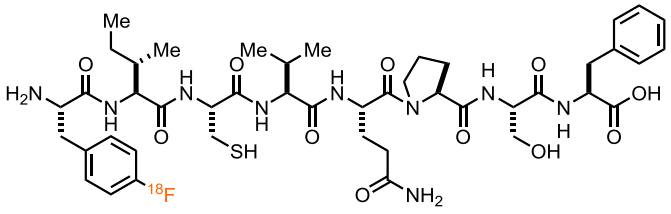

H-Phe(4-[^{18}F]F)-Ile-Cys-Val-Gln-Pro-Ser-Phe-OH (**151**)
free acid precursor 11% (n=2)
PMB ester precursor 39% (n=2)

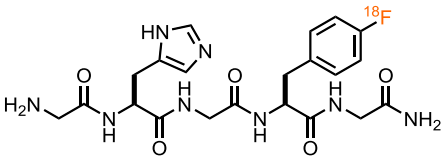

H-Gly-His-Gly-Phe(4-[^{18}F]F)-Gly-NH_2 (**152**)
39% (n=2)

Scheme 38. Substrate scope of peptide labeling.[146]

III.5. Automated labeling

First attempts to translate the ruthenium-mediated radio-deoxyfluorination of peptides to the ELIXYS FLEX/CHEM platform, connected to a PURE/FORM purification and reformulation unit (Sofie Bioscience) afforded **147** in low RCY. The RCY could be increased to 21% by changing the reaction temperature from 130 °C to 150 °C (Scheme 39). The difference in reaction temperature could be due to the adapter used to fit a 3 mL Vial into the synthesizer. The adapter might transfers heat slowly, resulting in a temperature difference between target and reaction temperature.[161] Within 99 minutes, 11.4 GBq of [^{18}F]fluoride could be converted to 1.28 GBq of **147**, formulated in a mixture of ethanol and saline, ready to use for biological experiments.

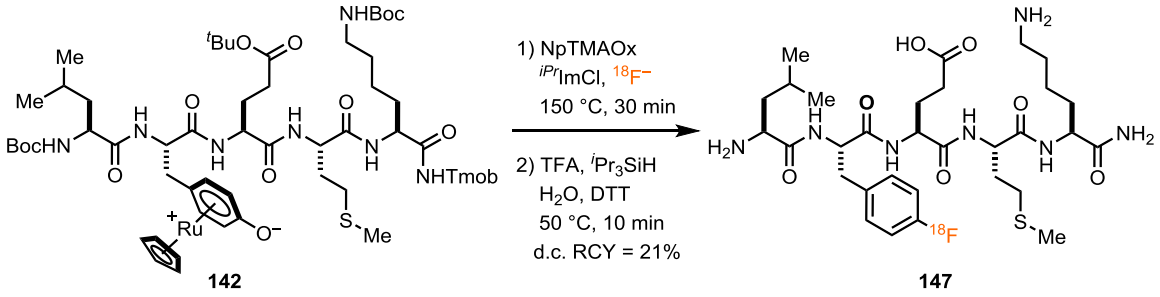

Scheme 39. Automated synthesis of **147**.[146]

High molar activity is crucial in peptide labeling, as the receptors are often present in low concentrations. The use of excessive amounts of hexafluorophosphate counter-ions during SPPS has the potential to contaminate the precursor with hexafluorophosphate anions, which can leach out fluorine-19 and decrease the molar activity. Nevertheless, **147** could be obtained high molar activity 99 GBq·µmol^{-1}. The molar activity of peptide **147** cannot only be lowered by dilution with fluorine-19, but also by the presence of side products or precursors that cannot be separated. The separation of precursor and labeled product gets more difficult with increasing size of the peptide. As previously mentioned, the retention time of complexed peptide is quite different to the decomplexed peptide, because the ionic ruthenium complex drastically changes the polarity of the peptide. Under our reaction conditions, we found that the fluorinated product was almost completely decomplexed while the precursor stays complexed to ruthenium, due to the stronger bond. This allowed for the facile separation of the precursor from the labeled peptide (Figure 10).

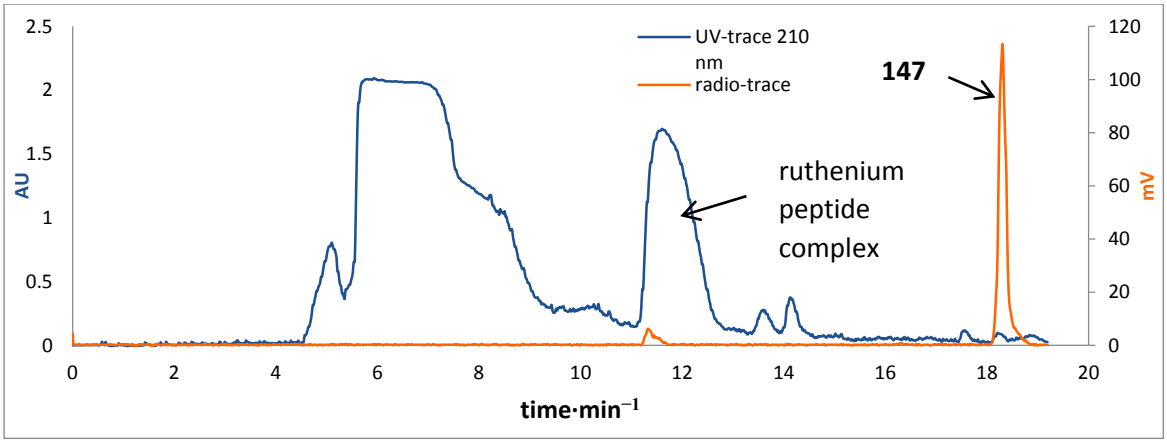

Figure 10. HPLC-trace of preparative HPLC purification of **147**.

The separation of ruthenium from the radiolabeled peptide is crucial, as the specific limit considered safe for human injection is 10 µg per day. The reformulated sample obtained after automated synthesis contained 1.8 µg of ruthenium, which is well below the limit. The ruthenium content in the reformulated sample could be further reduced to 0.09 µg by additional C-18 purification before preparative HPLC or by the use of metal scavenger resins such as Quadrasil AP to 0.11 µg, which is threefold as high as the blank sample.[162]

III.6. Conclusion and outlook

Overall, we have reported the first general protocol to formally exchange a single hydrogen or hydroxyl substituent in the native polypeptide structure with a single fluorine-18 (Scheme 40). This methodology avoids the use of large prosthetic groups. Instead, simply exchanging one hydrogen/hydroxyl substituent of the native peptide structure with fluorine-18, allows for minimal structural perturbation of the peptide and therefore, a minimal change of the behavior *in vivo*. We could show that the method tolerates all 20 canonical amino acids, is operationally simple, and tolerates water and air. The transformation is enabled by a traceless activation of a tyrosine residue by coordination in η^6-binding mode to ruthenium. The labeling precursors can be easily accessed by applying novel amino-acid building block **140** in SPPS. For facile adoption of the method to other research groups and clinical application we made amino acid building block **140** commercially available. This protocol can provide reliable access to novel tracer candidates, which may facilitate the development of novel peptide-PET-tracers.

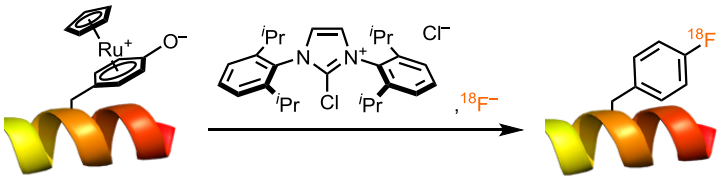

Scheme 40. General reaction scheme.

A major limitation of the described procedure is the high reaction temperature, which leads to minor degradation of smaller peptides, but with increasing size, the degradation rate increases, and side products become more difficult to separate. This limits the utility of the method to small peptide labeling. Furthermore, tertiary structures of proteins would degrade at 130 °C.[163] The development of novel ruthenium ligands that enable labeling and decomplexation at lower temperature would be beneficial. Another limitation of the substrate scope is that the native peptide must contain a phenylalanine or tyrosine that can be replaced with 4-[^{18}F]fluoro-phenylalanine.

The extension to tryptophan labeling would drastically increase the substrate scope. Another possible advantage could be a lower reaction temperature, since polycyclic arenes can be decomplexed at lower temperatures. The development of a ruthenium-containing tryptophan building block for SPPS is more challenging, since complexation of ruthenium to tryptophan creates a stereocenter on ruthenium (Figure 11). Initial results show that the tryptophan ruthenium complex is obtained as a diastereomeric mixture that is difficult to separate and, if applied in SPPS, would afford the peptide as a diastereomeric mixture. Because the purification is the major challenge in SPPS, introduction of a building block as a diasteromeric mixture is not acceptable.

A more attractive option would be the introduction of the ruthenium complex after synthesis and purification of the peptide containing the artificial 5-hydroxy-tryptophan residue. It has already been shown that under certain conditions, rhodium can selectively complex to tryptophan.[152b] The resulting diasteromeric mixture of peptide ruthenium complex could then be subjected to radio-deoxyfluorination without purification, because both precursors will merge to one product after labeling with [^{18}F]fluoride and subsequent decomplexation.

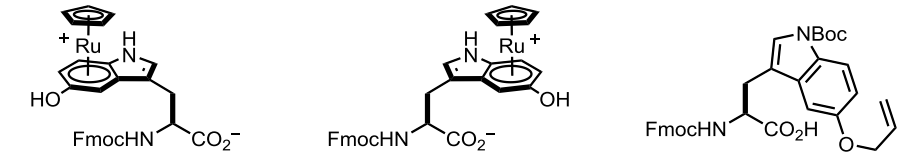

153 Fmoc-*S*-Trp-S_p-(RuCp)-OH

154 Fmoc-*S*-Trp-R_p-(RuCp)-OH

155 Fmoc-5-allyloxy-Trp(Boc)-OH

Figure 11. Potential building blocks for tryptophan labeling.

IV. Experimental part

IV.1. Atorvastatin labeling

IV.1.1. Materials and methods

All air- and moisture-insensitive reactions were carried out under an ambient atmosphere and monitored by thin-layer chromatography (TLC) or liquid chromatography-mass spectrometry (LC-MS). High-resolution mass spectra were obtained using *Q Exactive Plus* from *Thermo*. Concentration under reduced pressure was performed by rotary evaporation at 23–40 °C at an appropriate pressure. Purified compounds were further dried under vacuum (10^{-6}–10^{-3} bar). Yields refer to purified and spectroscopically pure compounds. All air- and moisture-sensitive manipulations were performed using oven-dried glassware (130 °C for a minimum of 12 hours), including standard Schlenk and glove-box techniques under an atmosphere of argon, although they can operate equally under an atmosphere of nitrogen.[164] Irradiation of photochemical reactions were carried out using a 40 W blue LED (Kessil A 160WE Tuna Blue).

Solvents

Acetonitrile, dichloromethane, 2,3-dimethoxybenzene (veratrole), and methanol were purchased from Sigma-Aldrich and used as received. Peptide grade dimethylformamide (DMF) and piperidine were purchased from Iris-Biotech and used as received. Ethanol (≥99.8%) was purchased from Honeywell and used as received. Trimethylacetonitrile (98+%) was purchased from Alfa Aesar and used as received. Anhydrous solvents were obtained from Phoenix Solvent Drying Systems. All deuterated solvents were purchased from Euriso-Top.

Chromatography

Thin layer chromatography (TLC) was performed using EMD TLC plates pre-coated with 250 µm thickness silica gel 60 F_{254} plates and visualized by fluorescence quenching under UV light. Flash chromatography was performed using silica gel (40–63 µm particle size) purchased from

Geduran. Preparative high-performance liquid chromatographic separation was executed on Shimadzu Prominence Preparative HPLC system.

Spectroscopy and Instruments

NMR spectra were recorded on a Bruker *Ascend*™ 500 spectrometer operating at 500 MHz, 471 MHz, and 126 MHz, for ^{1}H, ^{19}F, and ^{13}C acquisitions, respectively. Chemical shifts are reported in ppm with the solvent residual peak as the internal standard. For ^{1}H NMR: $CDCl_3$, δ 7.26; CD_3OD, δ 3.31; $(CD_3)_2SO$, δ 2.50; CD_3CN, δ 1.94. For ^{13}C NMR: $CDCl_3$, δ 77.16; CD_3OD, δ 49.00; $(CD_3)_2SO$, δ 39.52; CD_3CN, δ 1.32.[165] ^{19}F NMR spectra were referenced using a unified chemical shift scale based on the ^{1}H resonance of tetramethylsilane (1% v:v solution in the respective solvent).[166] Data is reported as follows: s = singlet, d = doublet, t = triplet, q = quartet, m = multiplet, br = broad; coupling constants in Hz; integration. Liquid chromatography-mass spectroscopic data were obtained on Agilent 1260 Infinity Automated LC/MS Purification System.

Starting materials

Ruthenium(III) chloride (metal content: 38%–43% ruthenium) was purchased from Johnson Matthey and used without purification. 2-Chlorotrityl chloride resin (2CTC resin) (100–200 mesh, 1% DVB, 1.6 $mmol \cdot g^{-1}$), Fmoc-Rink-Amide-2CT resin (200–400 mesh, 1% DVB, 0.68 $mmol \cdot g^{-1}$), diisopropylethylamine (DIPEA), 2-(1*H*-benzotriazol-1-yl)-1,1,3,3-tetramethyluronium-hexafluorophosphat (HBTU), 1-hydroxybenzotriazol (HOBt), Fmoc-*L*-Ala-OH·H_2O, Fmoc-*L*-Arg(Pbf)-OH, Fmoc-*L*-Asn(Trt)-OH, Fmoc-*L*-Asp(^{t}Bu)-OH, Fmoc-*L*-Cys(Trt)-OH, Fmoc-*L*-Glu(^{t}Bu)-OH·H_2O, Fmoc-*L*-Gln(Trt)-OH, Fmoc-Gly-OH, Fmoc-*L*-His(Trt)-OH, Fmoc-*L*-Ile-OH, Fmoc-*L*-Leu-OH, Fmoc-*L*-Lys(Boc)-OH, Fmoc-*L*-Met-OH, Fmoc-*L*-Phe-OH, Fmoc-*L*-Pro-OH·H_2O, Fmoc-*L*-Ser(^{t}Bu)-OH, Fmoc-*L*-Thr(^{t}Bu)-OH, Fmoc-*L*-Trp(Boc)-OH, Fmoc-*L*-Tyr(^{t}Bu)-OH, and Fmoc-*L*-Val-OH were purchased from Iris-Biotech. Aluminium powder (~325 mesh, 99.7%) was purchased from Strem chemicals. Fmoc-4-fluoro-*L*-phenylalanine (Fmoc-Phe(4-F)-OH), Fmoc-4-fluoro-*D*-phenylalanine (Fmoc-*D*-Phe(4-F)-OH), Fmoc *N*-hydroxysuccinimide ester (Fmoc-OSu), *D*-tyrosine (98%), dithiothreitol (DTT), and

trifluoroacetic acid (99%) were purchased from ABCR. Potassium oxalate monohydrate, triisopropylsilane, and *L*-tyrosine (98%) were purchased from Sigma Aldrich. 2,4,6-Trimethoxybenzylamine was purchased from Enamine. Kryptofix® 222 was purchased from Merck and used as received.

All substrates and reagents were used as received from commercial suppliers unless otherwise stated

IV.1.2. **Experimental Data**

Bis(cyclopentadienyl)ruthenium(II) (133)

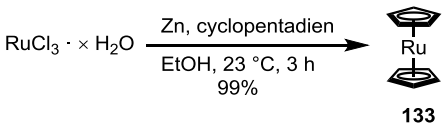

133

A two-neck round-bottom flask (500 mL) equipped with a Teflon-coated magnetic stirring bar and a thermometer, was charged with ruthenium trichloride hydrate ($RuCl_3 \times H_2O$, 12.3 g, 47 mmol, 1.0 equiv) and absolute ethanol (0.14 L, c = 0.34 M). The reaction flask was placed in an ice bath, and the reaction mixture was cooled to 0 °C, then cyclopentadiene (39 mL, 31 g, 0.47 mmol, 10 equiv)[167] was added via syringe to the dark red solution. Zinc dust (~325 mesh, 99.9% (metals basis), 31 g, 0.47 mmol, 10 equiv) was added over 60 minutes in 10 portions to the stirred solution, and the temperature was kept between 0 °C and 10 °C during the addition. The reaction mixture was stirred at 0 °C for 30 minutes, then the ice bath was removed, and stirring was continued for 3 hours. The suspension was filtered over a 60 mL Büchner funnel with micro porosity (code M), and the metallic grey solid was washed with hot toluene (100 °C, 4 × 0.14 L). The filtrate was concentrated on a rotary evaporation to dryness, and the brown residue was then dissolved in toluene (0.5 L) at 23 °C and passed through a plug of silica gel (20 g), which was subsequently rinsed with toluene (0.25 L). The resulting yellowish solution was concentrated *in vacuo* to dryness to afford ruthenocene (**133**) as a pale yellow solid (10.8 g, 46.7 mmol, 99% yield).

Note: Ruthenium(III) chloride solid (metal content: 38%–43% ruthenium) was purchased from Johnson Matthey and used without purification.

Melting point:[168] 199 °C.

NMR Spectroscopy:[169]

^{1}H NMR (500 MHz, $CDCl_3$, 25 °C, δ): 4.56 (s).

^{13}C{^{1}H} NMR (126 MHz, $CDCl_3$, 25 °C, δ): 70.1.

HRMS-EI (m/z) calc'd for $C_{10}H_{10}Ru$ $[M]^+$, 231.98197; found, 231.982042; deviation: –0.32 ppm.[170]

[(Cp)Ru(η^6-naphthalene)]·CF_3SO_3 (134)

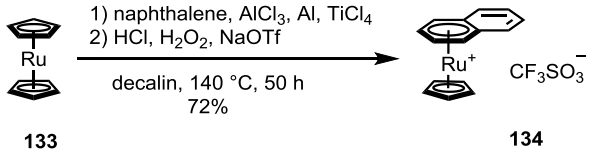

133 **134**

Under inert atmosphere, an oven-dried two-neck round-bottom flask (1000 mL) equipped with a reflux condenser and a Teflon-coated egg-shaped magnetic stirring bar was charged with ruthenocene (**133**) (10.7 g, 46.3 mmol, 1.00 equiv), naphthalene (59.3 g, 0.463 mol, 10.0 equiv), $AlCl_3$ (6.17 g, 46.3 mmol, 1.00 equiv), and aluminum powder (~325 mesh, 99.7%, 624 mg, 23.1 mmol, 0.500 equiv). Then dry decalin (0.25 L, c = 0.19 M) was added, followed by dropwise addition of $TiCl_4$ (2.53 mL, 4.39 g, 23.1 mmol, 0.500 equiv) via a syringe. The resulting red suspension was heated to 140 °C and was then stirred for 50 hours at 140 °C. The oil bath was removed, and after cooling to room temperature, the reaction mixture was poured onto a mixture of ice (0.3 kg), aqueous concentrated HCl-solution (66 mL), and H_2O_2 (50% solution in H_2O, 46 mL). The aqueous layer was separated from the organic layer with the aid of a separatory funnel, and the aqueous layer was washed with pentane (2 × 0.1 L). The combined organic layers were extracted with water (50 mL). The combined aqueous layers were added back to the reaction flask, and then sodium triflate (15.9 g, 92.5 mmol, 2.00 equiv) was added to the combined aqueous layers. The resulting orange solution was stirred for 15 minutes, and then the suspension was extracted with dichloromethane (5 × 0.24 L). The combined organic layers were dried over sodium sulfate, filtered, and concentrated *in vacuo* to dryness. The brown residue was dissolved in dichloromethane (30 mL) and then added dropwise through a syringe-filter to vigorously stirred diethyl ether (300 mL). The suspension was filtered through a 60 mL Büchner funnel with micro porosity (code M), and the pale yellow solid was washed with diethyl ether (2 × 30 mL), and dried *in vacuo* to afford **134** as a yellow solid (15.1 g, 34.1 mmol, 72% yield).

Melting point: 112 °C.

NMR Spectroscopy:[171]

^{1}H NMR (500 MHz, $CDCl_3$, 25 ºC, δ): 7.76 (dd, *J* = 6.7, 3.2 Hz, 2H), 7.59 (dd, *J* = 6.8, 3.1 Hz, 2H), 7.19–7.06 (m, 2H), 6.63–6.28 (m, 2H), 5.06 (s, 5H).

^{13}C{^{1}H} NMR (126 MHz, $CDCl_3$, 25 ºC, δ): 131.6, 129.5, 97.2, 86.5, 84.1, 80.2.

^{19}F NMR (471 MHz, $CDCl_3$, 25 ºC, δ): −78.1.

HRMS-EI (m/z) calc'd for $C_{15}H_{13}Ru$ $[M-OTf]^+$, 295.00553; found, 295.00563; deviation: 0.35 ppm.

Elemental Analysis calc'd for $C_{16}H_{13}F_3O_3RuS$: C, 43.34; H, 2.96; found: C, 43.31; H, 2.94.

UV/vis Spectroscopy (H_2O, 23°C): 360 nm (ε = 673 $M^{-1}\cdot cm^{-1}$).

[^{18}F]Atorvastatin precursor 1,4-diketone 121

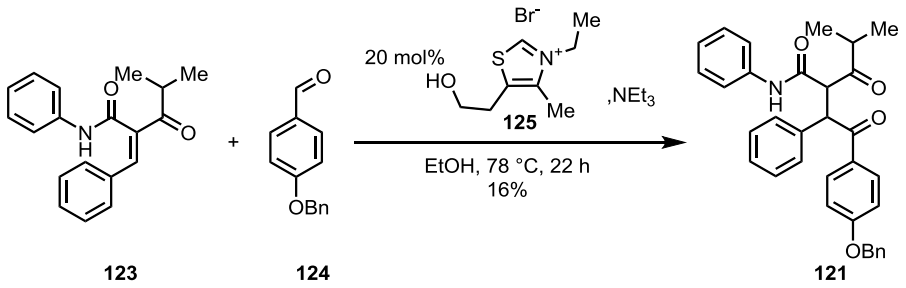

A 50 mL one-neck round-bottom flask equipped with a Teflon-coated magnetic stirring bar and a reflux condenser was charged with 3-ethyl-5-(2-hydroxyethyl)-4-methylthiazolium bromide(**125**) (0.860 g, 3.41 mmol, 0.200 equiv), 2-benzyliden-N-phenyl-isobutyloyl-acetamid (**123**) (5.00 g, 17.0 mmol, 1.00 equiv), 4-benzyloxybenzaldehyde (**124**) (3.98 g, 18.8 mmol, 1.10 equiv), triethylamine (2.61 mL, 1.90 g, 18.8 mmol, 1.10 equiv), and absolute ethanol (10 mL, 1.7 $mol\cdot L^{-1}$). The reaction mixture was heated at reflux. After 15 hours a second portion of 3-ethyl-5-(2-hydroxyethyl)-4-methylthiazolium bromide (**125**) (0.860 g, 3.41 mmol, 0.200 equiv) was added, and the reaction mixture was stirred and heated at reflux for additional 7 hours. Isopropanol (35 mL) was added to the reaction mixture at 78°C, and the oil bath was removed. After 12 hours the

solid was collected by filtration and dried *in vacuo* to afford **121** as colorless solid (1.38 g, 2.72 mmol, 16%).

R_f = 0.44 (EtOAc:Hexane, 3:7, v:v).

NMR Spectroscopy:

^{1}H NMR of major stereoisomer (500 MHz, DMSO-d_6, 25 °C, δ): 10.15 (s, 1H), 8.05–7.97 (m, 2H), 7.45–7.39 (m, 2H), 7.41–7.37 (m, 2H), 7.38–7.32 (m, 3H), 7.32–7.27 (m, 2H), 7.26–7.17 (m, 4H), 7.17–7.08 (m, 1H), 7.08–7.04 (m, 2H), 7.05–6.96 (m, 1H), 5.40 (d, *J* = 11.0 Hz, 1H), 5.17 (s, 2H), 4.85 (d, *J* = 10.9 Hz, 1H), 2.90 (hept, *J* = 6.9 Hz, 1H), 1.16 (d, *J* = 7.0 Hz, 3H), 0.94 (d, *J* = 6.6 Hz, 3H).

^{13}C{^{1}H}NMR of major stereoisomer (126 MHz, DMSO-d_6, 25 °C, δ): 207.9, 196.1, 165.1, 162.2, 138.1, 136.4, 135.8, 131.1, 128.8, 128.6, 128.5, 128.0, 127.8, 127.4, 123.9, 119.6, 114.7, 69.5, 62.9, 51.6, 18.8, 18.0.

HRMS-EI (m/z) calc'd for $C_{33}H_{31}N_1O_4Na$ $[M+Na]^+$, 528.21453; found, 528.21503; deviation: –0.96 ppm.

[^{18}F]Atorvastatin precursor pyrrole 126

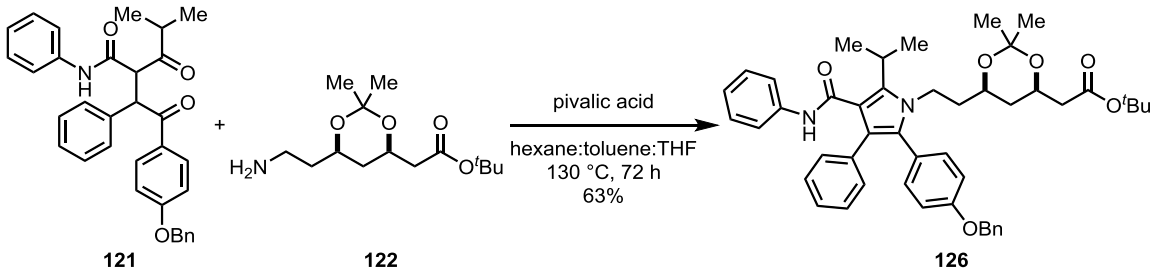

A 50 mL one-neck round-bottom flask equipped with a Teflon-coated magnetic stirring bar and a reflux condenser was charged with diketone **121** (1.27 g, 2.51 mmol, 1.00 equiv), amino ester **122** (0.891 g, 3.26 mmol, 1.30 equiv), pivalic acid (0.576 mL, 5.01 mmol, 2.00 equiv), and a mixture of THF:toluene:heptane (1:1:4, 42 mL, 0.06 mol·L^{-1}). The reaction mixture stirred at 130 °C oil bath temperature for 72 hours. The solvent was removed and the residue was purified by silica flash chromatography using EtOAc and hexane [1:3]. Pyrrole **126** was isolated as white solid (1.17 g, 2.51 mmol, 63%).

R_f = 0.58 (EtOAc:Hexane, 3:7, v:v).

NMR Spectroscopy:

^{1}H NMR (500 MHz, $CDCl_3$, 25 °C, δ): 7.46–7.42 (m, 2H), 7.42–7.37 (m, 2H), 7.36–7.32 (m, 1H), 7.23–7.15 (m, 7H), 7.13 (d, *J* = 8.5 Hz, 2H), 7.09 (d, *J* = 8.5 Hz, 2H), 6.98 (t, *J* = 7.3 Hz, 1H), 6.92 (d, *J* = 8.2 Hz, 2H), 6.89 (s, 1H), 5.04 (s, 2H), 4.17 (dtd, *J* = 9.0, 6.5, 2.2 Hz, 1H), 4.09 (ddd, *J* = 15.2, 10.5, 5.1 Hz, 1H), 3.90–3.81 (m, 1H), 3.69 (td, *J* = 8.4, 7.8, 1H), 3.59 (p, *J* = 7.1, 1H), 2.39 (dd, *J* = 15.9, 7.1 Hz, 1H), 2.25 (dd, *J* = 15.2, 6.0 Hz, 1H), 1.79–1.62 (m, 2H), 1.60–1.56 (m, 1H) 1.55 (dd, *J* = 7.1, 2.2 Hz, 6H), 1.44 (s, 9H), 1.37 (s, 3H), 1.35–1.33 (m, 1H) 1.32 (s, 3H), 1.06 (q, *J* = 11.9 Hz, 1H).

^{13}C{^{1}H} NMR (126 MHz, $CDCl_3$, 25 °C, δ): 170.3, 165.1, 158.4, 141.3, 138.6, 136.8, 135.1, 132.8, 130.6, 129.8, 128.7$_1$, 128.6$_5$, 128.3, 128.1, 127.6, 126.4, 124.8, 123.5, 121.5, 119.6, 115.2, 114.6, 98.7, 80.7, 70.0, 66.6, 66.0, 42.6, 40.9, 38.2, 36.1, 30.0, 28.2, 26.2, 21.9, 21.7, 19.8.

HRMS-ESI (m/z) calc'd for $C_{47}H_{54}N_2O_6Na$ $[M+Na]^+$, 765.38741; found, 765.38799; deviation: −0.76 ppm.

Hydroxy-defluoro-Atorvastatin derivative 127

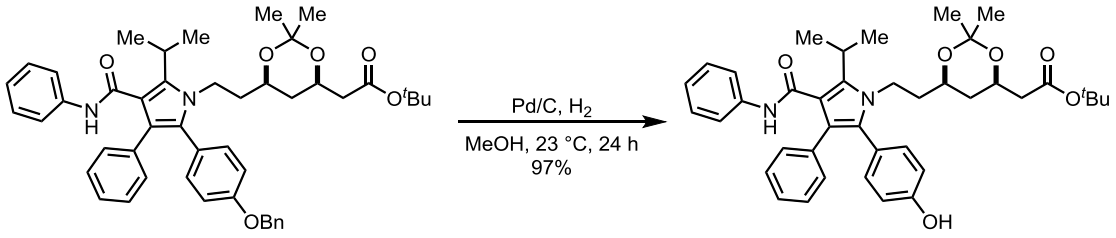

126 **127**

A round-bottom flask (100 mL) equipped with a septum and a magnetic stirring bar was charged with pyrrole **126** (765 mg, 1.03 mmol, 1.00 equiv), palladium on carbon (10 w%, 110 mg, 103 µmol, 0.100 equiv), and methanol (50 mL, 0.02 mol·L^{-1}). Argon was bubbled through the reaction mixture for 5 minutes while stirring. Afterwards, dihydrogen was bubbled through the reaction mixture for 10 minutes while stirring. The reaction mixture was stirred under dihydrogen atmosphere at 23 °C for 24 hours. Argon was bubbled through the reaction mixture for 5 min

while stirring. The reaction mixture was filtered through a Celite plug, and the Celite plug was washed with methanol (2 x 5 mL). The filtrate was concentrated under vacuum. A round-bottom flask (10 mL) equipped with a septum and a magnetic stirring bar was charged with pale yellow filtrate, *p*-toluenesulfonic acid (1.96 mg, 10.3 µmol, 1.00 mol%), 2,2-dimethoxypropan (190 µL, 161 mg, 1.54 mmol, 1.50 equiv), and acetone (2 mL). The reaction mixture was stirred at 23 °C for 2 hours. The resulting suspension was diluted with DCM (20 mL), and the solution was washed with saturated aqueous sodium bicarbonate solution (10 mL) and saturated aqueous sodium chloride solution. The organic layer was dried over sodium sulfate, filtered, and concentrated *in vacuo* to dryness to afford **127** as a pale yellow powder (653 mg, 1.00 mmol, 97% yield).

R_f = 0.33 (EtOAc:Hexane, 3:7, v:v).

NMR Spectroscopy:

^{1}H NMR (500 MHz, $CDCl_3$, 25 ºC, δ): 7.21–7.10 (m, 7H), 7.06 (d, *J* = 7.9, 2H), 7.03 (d, *J* = 8.4, 2H), 6.98 (t, *J* = 7.3 Hz, 1H), 6.91 (s, 1H), 6.77 (d, *J* = 8.3, 2H), 6.43 (br, 1H), 4.17–4.10 (m, 1H), 4.05 (ddd, *J* = 15.1, 10.3, 5.3 Hz, 1H), 3.82 (ddd, *J* = 14.9, 10.0, 5.6 Hz, 1H), 3.66 (tt, *J* = 11.1, 5.3, 1H), 3.57 (p, *J* = 7.1, 1H), 2.37 (dd, *J* = 15.1, 7.2 Hz, 1H), 2.23 (dd, *J* = 15.1, 5.8 Hz, 1H), 1.72–1.62 (m, 2H), 1.51 (dd, *J* = 7.1, 4.9 Hz, 6H), 1.44 (s, 9H), 1.35 (s, 3H), 1.31 (s, 3H), 1.29–1.22 (m, 1H) 1.00 (q, *J* = 11.9 Hz, 1H).

^{13}C{^{1}H} NMR (126 MHz, $CDCl_3$, 25 ºC, δ): 170.7, 165.5, 156.0, 141.2, 138.4, 135.0, 132.9, 130.6, 130.0 ,128.8, 128.4, 126.4, 124.1, 123.8, 121.4, 119.9, 115.6, 115.1, 98.8, 81.1, 66.1, 66.3, 42.7, 40.8, 38.1, 36.0, 30.0, 28.2, 26.2, 21.9, 21.8, 19.8.

HRMS-ESI (m/z) calc'd for $C_{40}H_{48}N_2O_6Na$ $[M+Na]^+$,675.34046; found, 675.34108; deviation: −0.92 ppm.

(Cp)Ruthenium-Atorvastatin derivative 135

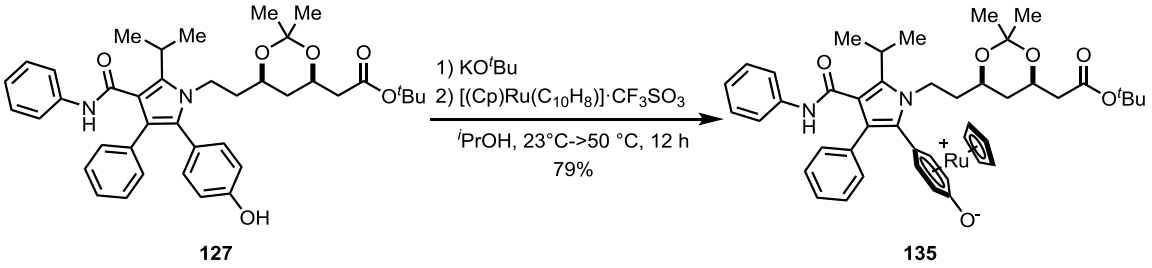

Under inert atmosphere, an oven-dried round-bottom flask (50 mL) equipped with a Teflon-coated egg-shaped magnetic stirring bar was charged with **127** (628 mg, 962 µmol, 1.00 equiv), potassium *tert*-butoxide (113 mg, 1.01 mmol, 1.05 equiv), and isopropanol (20 mL, c = 0.05 mol·L^{-1}). The solution was degassed by bubbling argon through it for 20 min while stirring. To the solution was added [(Cp)Ru(η^6-naphthalene)]·CF_3SO_3 (512 mg, 1.15 mmol, 1.20 equiv) and the resulting orange solution was stirred at 50 °C for 12 hours. The reaction mixture was concentrated to dryness under reduced pressure. The brown residue was dissolved in dichloromethane (20 mL), and the solution was washed with water (10 mL) and brine (10 mL). The organic layer were dried over sodium sulfate, filtered, and concentrated *in vacuo* to dryness. The brown residue was purified by HPLC on an YMC-Actus Triart C18 column ((30×150 mm, 5 µm + 30×50 mm, 5 µm), flow rate = 42.5 mL·min^{-1}, 35 °C) with a linear gradient from 40:60 (0.1% TFA in H_2O:MeOH, v:v) to 03:97 (0.1% TFA in H_2O:MeOH, v:v) over 8 minutes. The collected fractions containing the product (t ≈ 7.5 min) were combined, diluted with 100 mL brine, basified to pH 10 with saturated aqueous sodium bicarbonate solution, and the resulting solution was concentrated by rotary evaporation (100 mbar, 35 °C) until no more methanol was evaporated. The suspension was extracted with dichloromethane (3 × 100 mL), and the combined organic layers were dried over sodium sulfate, filtered, and concentrated *in vacuo* to dryness to afford **135** as a beige powder (620 mg, 758 µmol, 79% yield).

NMR Spectroscopy:

^{1}H NMR (400 MHz, DMSO-d_6, 25 ºC, δ): 9.76 (s, 1H), 7.48–7.43 (m, 2H), 7.27–7.14 (m, 7H), 7.01–6.96 (m, 1H), 5.51–5.45 (m, 1H), 5.21 (dd, *J* = 6.9, 1.8 Hz, 1H), 4.92 (dd, *J* = 6.9,

2.9 Hz, 1H), 4.90 (s, 5H), 4.79 (dd, *J* = 6.8, 2.0 Hz, 1H), 4.49–4.39 (m, 1H), 4.32–4.23 (m, 1H), 4.16–4.02 (m, 2H), 3.18 (p, *J* = 7.0 Hz, 1H), 2.43 (dd, *J* = 15.2, 4.8 Hz, 1H), 2.27 (dd, *J* = 15.2, 8.1 Hz, 1H), 2.0–1.9 (m, 1H), 1.82–1.71 (m, 1H), 1.64 (dt, *J* = 12.7, 2.5 Hz, 1H), 1.49 (s, 3H), 1.42 (s, 9H), 1.40–1.32 (m, 9H), 1.27–1.18 (m, 1H).

$^{13}C\{^{1}H\}$ NMR (101 MHz, DMSO-d_6, 25 ºC, δ): 169.6, 165.6, 155.9, 139.3, 137.6, 134.8, 130.1, 128.4, 127.9, 126.2, 123.9, 123.0, 121.2, 119.4, 118.6, 98.2, 87.2, 86.1, 85.3, 79.8, 76.7, 71.8, 71.7, 66.4, 65.8, 42.1, 38.7, 35.4, 30.0, 27.8, 25.5, 22.8, 21.7, 20.0.

HRMS-EI (m/z) calc'd for $C_{45}H_{53}N_2O_6Ru$ $[M-OTf]^+$, 819.29416; found, 819.29557; deviation: −1.72 ppm.

IV.1.3. **Radiochemistry general methods**

No-carrier-added [^{18}F]fluoride was purchased from Advanced Accelerator Applications SA. Liquid chromatographic (LC) analysis was performed with Thermo Scientific Dionex UltiMate 3000 dual channel HPLC system connected to LabLogic NaI/PMT-radiodetectors with Flow-Ram output. A Thermo Scientific™ Accucore™ XL C18, 4 µm, 3×150 mm HPLC column was used for analysis and a Thermo Scientific Hypersil Gold column™, 5 µm, 10×250 mm HPLC column was used for preparative HPLC. Analytical and preparative HPLC used the following mobile phases: 0.1% CF_3CO_2H in water (A), 0.1% CF_3CO_2H in acetonitrile (B).

Gradient 1

time [min]	A [%]	B [%]
0	95	5
2	95	5
22	50	50
22.5	5	95
27	5	95
28	95	5
32	95	5

Gradient 2

time [min]	A [%]	B [%]
0	95	5
2	95	5
10	5	95
14	5	95
15	95	5
18	95	5

All ^{18}F-labeled molecules were characterized by comparing the HPLC radio-trace of the isolated compound to the HPLC UV-trace of an authentic reference sample. Radioactivity was measured in a Veenstra Instruments, VIK-203 ionization-chamber.

Note: radioactivity chromatographs are offset by 0.1 or 0.3 minutes on account of the delay introduced by the spatial separation between the diode array detectors and the radioactivity detectors.

General procedure for pre-conditioning of Sep-Pak cartridges

Waters Sep-Pak light C18 cartridge (part # WAT023501) was pre-conditioned by sequentially pushing MeOH (2 mL) and water (10 mL) through the cartridge unless otherwise indicated.

General procedure for pre-conditioning of QMA cartridges

Chromafix PS-HCO_3 ^{18}F separation cartridge (45 mg) (Product No. 731876 from ABX) was pre-conditioned by sequentially pushing potassium oxalate solution (3 mL, 10 mg·mL^{-1} H_2O) and H_2O (2 mL) through the cartridge at a flow rate of 5 mL·min^{-1} unless otherwise indicated.

[^{18}F]Atorvastatin derivative 128

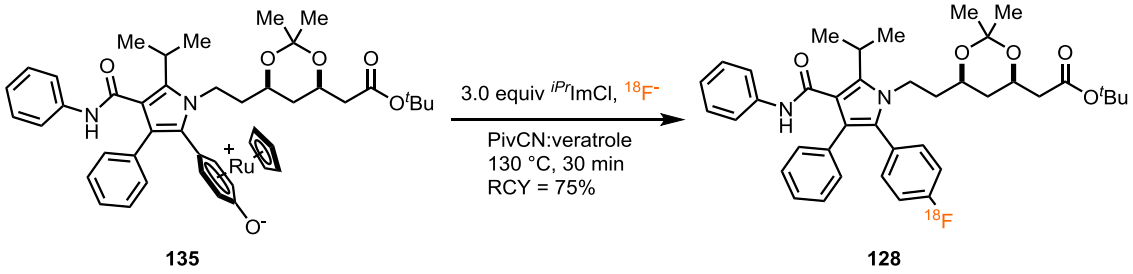

135 128

Aqueous ^{18}F-fluoride solution (700 µL) was loaded with a syringe onto a QMA anion-exchange cartridge that was pre-conditioned according to the general procedure, and then the cartridge was washed with MeCN (1 mL). The cartridge was dried by pushing air (2 mL) through the cartridge. The [^{18}F]fluoride was eluted from the cartridge with a solution of ruthenium complex **135** (1.6 mg, 2.0 µmol, 1.0 equiv) and imidazolium chloride **40** (2.8 mg, 6.0 µmol, 3.0 equiv) in methanol (300 µL), into a 4 mL borosilicate vial (95% elution efficiency). The methanol was removed by heating at 80 °C under a stream of nitrogen (~5 min). To the vial was added a mixture of veratrole and pivalonitrile (400 µL, 1:1, v:v). After sealing of the vial with a Teflon-lined cap it was stirred

at 130 °C for 30 minutes. The vial was removed from the hot plate, diluted with methanol (1 mL) and the resulting solution was analyzed by radio-HPLC and radio-TLC. The product was obtained in 75% RCY.

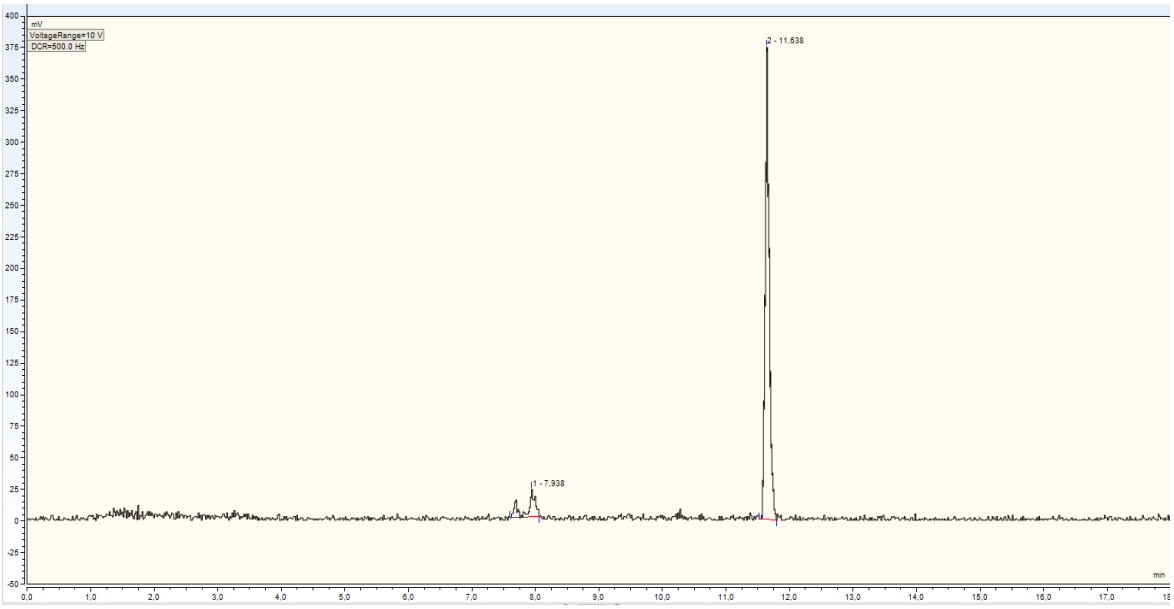

Figure S1. Crude radio-HPLC trace (gradient 1) of [^{18}F]atorvastatin derivative **128**.

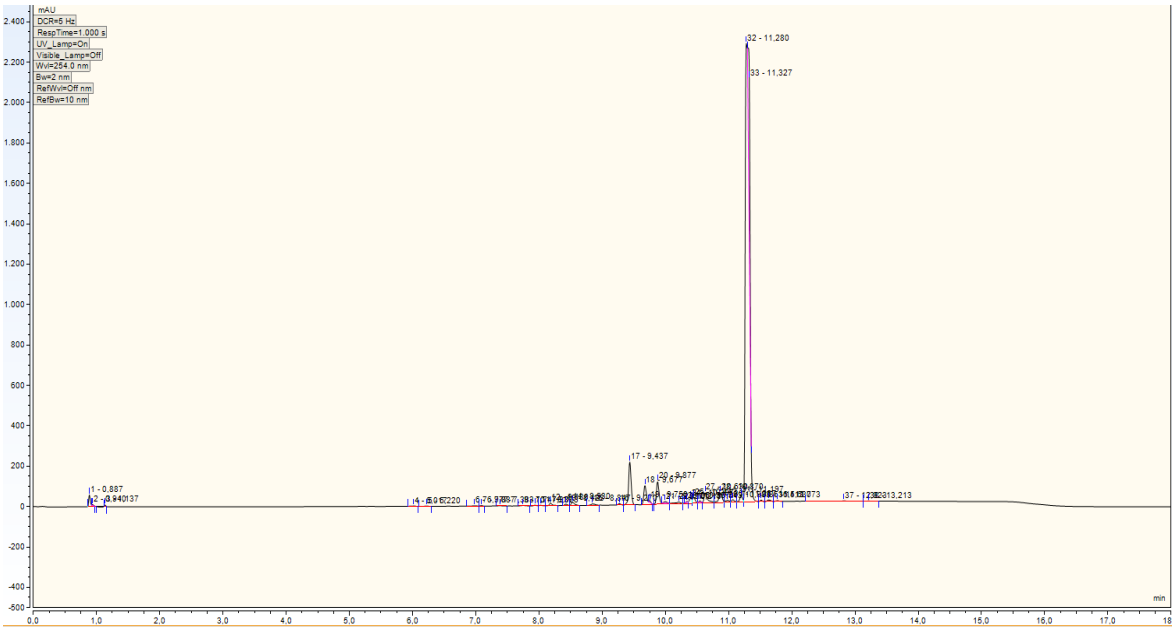

Figure S2. UV-HPLC trace (gradient 1) of acetal ester protected atorvastatin [^{19}F]**128**.

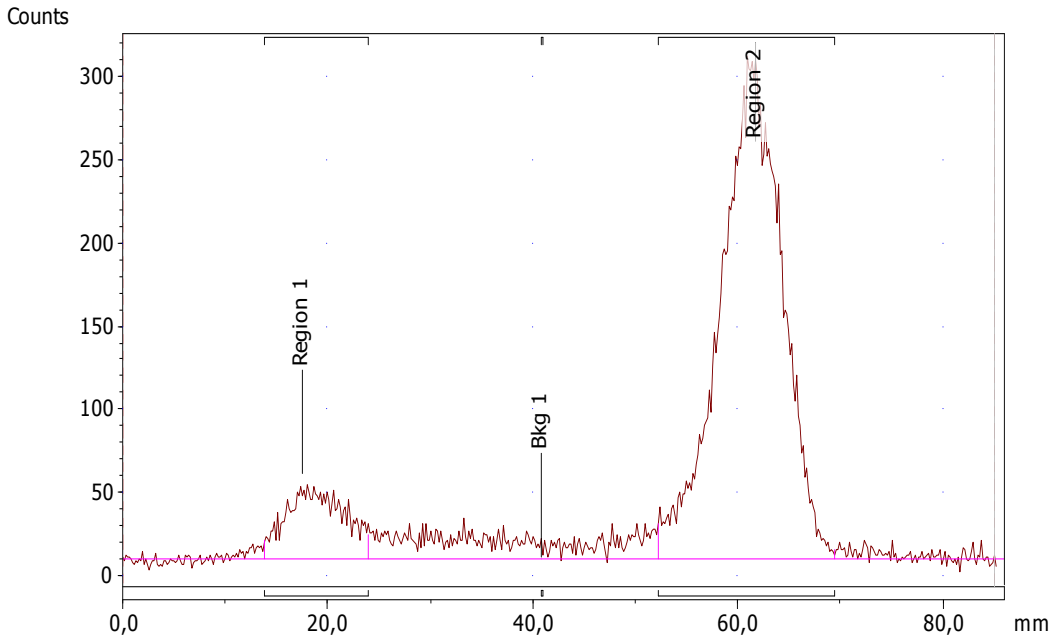

Figure S 3. Crude radio-TLC trace of [^{18}F]atorvastatin derivative **128**.

[^{18}F]Atorvastatin 120

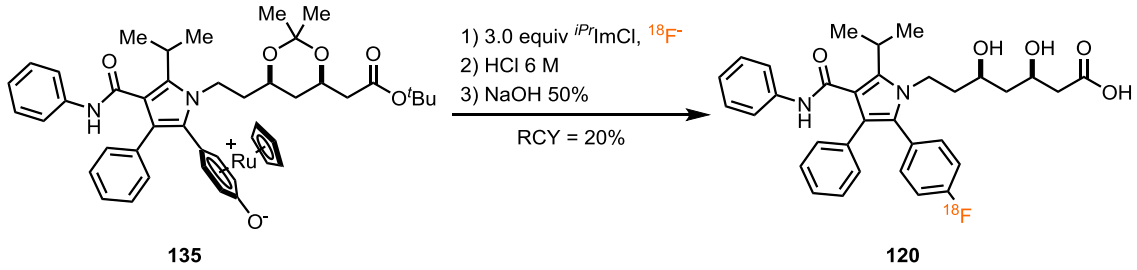

Reactions were performed on a Synthra RNplus module. Aqueous [^{18}F]fluoride solution (500 µL) was trapped on a short PTFE tubing (1/16 inch) filled with MP-1 resin (10 mg), and then the resin dried under a flow of helium for two minutes. The [^{18}F]fluoride was eluted from the cartridge with a solution of ruthenium complex **135** (4.1 mg, 5.0 µmol, 1.0 equiv), and ^{iPr}ImCl (6.9 mg, 15 µmol, 3.0 equiv) in ethanol, MeCN, and DMSO (v:v:v, 1:3:6, 500 µL), into a V-shaped vial (5 mL). The reaction mixture was stirred at 130 °C for 30 minutes. The reaction mixture was allowed to cool to 60 °C, followed by addition of methanol (950 µL), and hydrochloric acid (6 M in water, 50 µL, 0.30 mmol, 60 euqiv). The reaction mixture was stirred at 60 °C for 5 minutes. Afterwards, methanol (350 µL) and sodium hydroxide (50% in water, 0.13 mL, 0.20 g, 2.5 mmol, 490 equiv) was added, and the reaction mixture was stirred at 60 °C. After 5 minutes the reaction mixture was passed through a filter (0.22 µm pore size) and was purified by semi-preparative HPLC on a

SymmetryPrep™ C18 column (300×7.8 mm, 7 µm, flow rate = 5 mL·min^{-1}). The activity of the product containing fraction was diluted with water (45 mL) and loaded onto an Oasis HLB Plus cartridge. The cartridge was washed with water (10 mL) and the product was sequentially eluted with ethanol (1 mL) into a vial containing calcium acetate solution (0.05 M in water, 10 mL) affording [^{18}F]atorvastatin in 20% decay corrected radiochemical yield. The molar activity of [^{18}F]atorvastatin was 112 ± 77 GBq µmol^{-1}.

Lipophilicity (log *P*):

To a microcentrifuge tube containing phosphate-buffered saline (PBS, 455 µL, pH 7.4) and n-octanol (495 µL) was added [^{18}F]atorvastatin in ethanolic saline (v:v, 1:10, 50 µL). The mixture was vortexed for 2 minutes at room temperature, and centrifuged at 3000 rpm for 5 minutes. From both the organic and aqueous layer (100 µL) were removed and measured on a ɣ-counter. The log D value was calculated by dividing the ɣ-counts in octanol by the ɣ-counts in PBS. The log P value was obtained by three independent measurements and was 1.61±0.12.

Stability in human serum at 37 °C:

To an Eppendorf tube with 300 µL of human serum was added 50 µL of the radiotracer. The tube was left at 37˚C under gentle shaking and periodic radio-TLC measurements were performed.

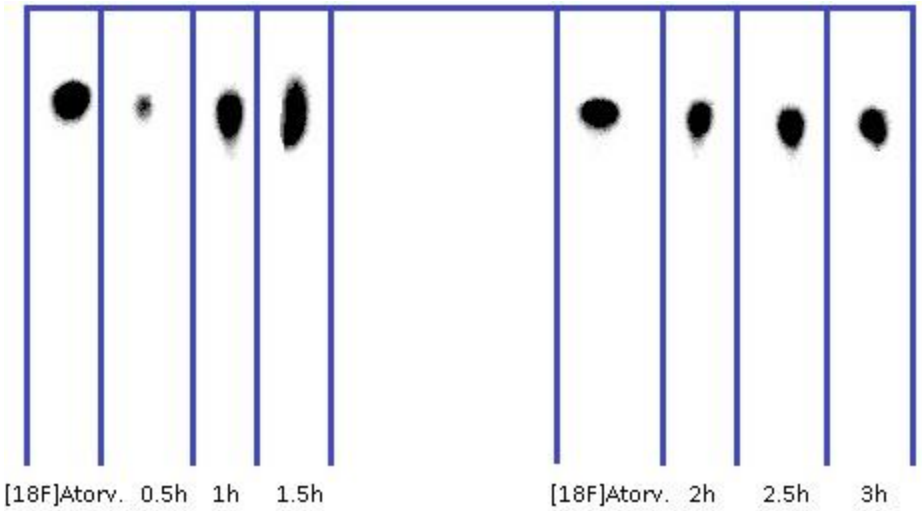

Rat serum plasma protein binding:

To a microcentrifuge tube containing rat plasma (300 µL, normal or fat diet) was added [^{18}F]atorvastatin in ethanolic saline (25 µL). The mixture was incubated for 1 hour and afterwards acetonitrile (900 µL) was added to precipitate the plasma protein. The suspension was centrifuged at 3000 rpm for 5 minutes. The precipitate (proteins) was separated from the supernatant and was measured on a ɣ-counter. Plasma proteins binding for normal rats was 16.7% and for fat rats 13.8%.

Liver homogenate binding assay

Tris-HCl (0.05 M, pH 7.4) was added to the extracted rat liver (normal and fat rats, fed with high-calorie food) to obtain a final concentration of 20 mg liver tissue per mL. The mixture was homogenized, using a Heidolph DIAX 600 homogenizer, for 30 seconds while being cooled in an ice bath. The rat liver homogenate was stored at –80°C.

Rat liver homogenate (300 µL or Tris-HCl solution for non-specific binding) was added to each assay tube. Tris-HCl solution (0.05M, pH 7.4) containing 0.3% human serum albumin was added to reach a final volume of 475 µL (175 µL) and left for pre-incubation for 15 minutes at room temperature. Then, 25 µL of [^{18}F]atorvastatin in ethanolic saline was added to each assay tube (8 x control, 12 x fat liver, 6 x non-specific binding). Assay tubes were briefly vortexed and then incubated for 60 minutes under gentle shaking at 37 ºC.

Incubation was terminated by centrifuging the assay tubes at 4°C for 15 min (3500 RPM). The supernatant of each tube was taken leaving the pellet in the original tube. Supernatants and pellets were measured on a ɣ-counter.

% of tracer in cell debris (pellet) of control rats: 5.2%

% of tracer in S9 fraction (supernatant) of control rats: 94.8%

% in cell debris (pellet) of fat diet rats: 9.2%

% in S9 fraction (supernatant) of fat diet rats: 90.8%

IV.2. Peptide Labeling

IV.2.1. **Experimental Data**

[(Cp)Ru(η^6-naphthalene)]·BF_4 (141)

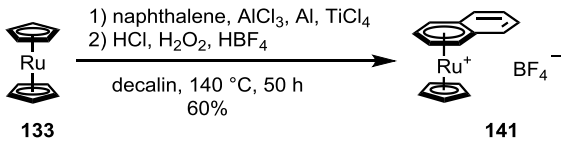

133 **141**

Under inert atmosphere, an oven-dried two-neck round-bottom flask (500 mL) equipped with a reflux condenser and a Teflon-coated egg-shaped magnetic stirring bar was charged with ruthenocene (**133**) (4.52 g, 19.5 mmol, 1.00 equiv), naphthalene (25.0 g, 195 mmol, 10.0 equiv), $AlCl_3$ (2.61 g, 19.5 mmol, 1.00 equiv), and aluminum powder (~325 mesh, 99.7%, 264 mg, 9.77 mmol, 0.500 equiv). Then dry decalin (0.13 L, c = 0.15 M) was added, followed by dropwise addition of $TiCl_4$ (1.07 mL, 1.85 g, 9.77 mmol, 0.500 equiv) via a syringe. The resulting red suspension was heated to 140 °C and was then stirred for 50 hours at 140 °C. The oil bath was removed, and after cooling to room temperature, the reaction mixture was poured onto a mixture of ice (0.15 kg), aqueous concentrated HCl-solution (28 mL), and H_2O_2 (35% solution in H_2O, 28 mL). The aqueous layer was separated from the organic layer with the aid of a separatory funnel, and the aqueous layer was washed with pentane (2 × 0.1 L). The combined organic layers were extracted with water (50 mL). The combined aqueous layers were added back to the reaction flask, and then fluoroboric acid (48% solution in water, 5.1 mL, 7.2 g, 39 mmol, 2.0 equiv) was added to the combined aqueous layers. The resulting orange solution was stirred for 15 minutes, and then the suspension was extracted with dichloromethane (4 × 100 mL). The combined organic layers were dried over sodium sulfate, filtered, and concentrated *in vacuo* to dryness. The brown residue was dissolved in dichloromethane (15 mL) and was then added dropwise through a syringe-filter to vigorously stirred diethyl ether (150 mL). The suspension was filtered through a 60 mL Büchner funnel with micro porosity (code M), and the pale yellow solid was washed with diethyl ether (2 × 30 mL), and dried *in vacuo* to afford **141** as a yellow solid (4.50 g, 11.8 mmol, 60% yield).

NMR Spectroscopy:[142]

^{1}H NMR (500 MHz, $CDCl_3$, 25 °C, δ): 7.75 (dd, *J* = 6.7, 3.3 Hz, 2H), 7.59 (dd, *J* = 6.8, 3.1 Hz, 2H), 7.08–7.02 (m, 2H), 6.44–6.37 (m, 2H), 5.05 (s, 5H).

^{13}C{^{1}H} NMR (126 MHz, $CDCl_3$, 25 °C, δ): 131.5, 129.5, 97.2, 86.4, 84.0, 80.2.

^{19}F NMR (471 MHz, $CDCl_3$, 25 °C, δ): −152.3.

HRMS-ESI (m/z) calc'd for $C_{15}H_{13}Ru$ $[M-BF_4]^+$, 295.00553; found, 295.00578; deviation: −0.86 ppm.[157]

[Fmoc-tyrosine(RuCp)-O]·H_2O (140)

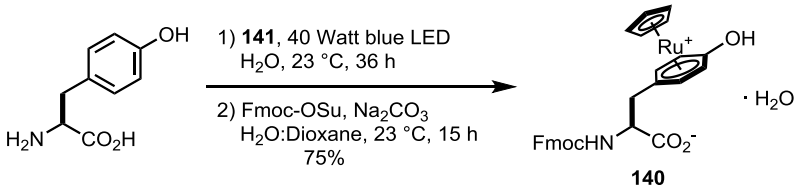

140

A round-bottom flask (250 mL) equipped with a Teflon-coated magnetic stirring bar was charged with [(Cp)Ru(η^6-naphthalene)]·BF_4 (**131**) (4.61 g, 12.1 mmol, 1.10 equiv), *L*-tyrosine (1.99 g, 11.0 mmol, 1.00 equiv), water (0.11 L, c = 0.10 M), and fluoroboric acid (48% in water, 2.9 mL, 4.0 g, 22 mmol, 2.0 equiv). The yellow suspension was irradiated for 36 h with blue LED light (Kessil A 160WE Tuna Blue, 40 W). It is crucial that the tyrosine is fully consumed at this point; failure will result in tyrosine contamination, which challenges the purification procedure, and column chromatography must be used instead. If required, the reaction time needs to be adjusted and more ruthenium precursor needs to be added. The resulting beige suspension was basified with sodium carbonate (3.85 g, 36.3 mmol, 3.30 equiv). The suspension was cooled to 0 °C with an ice bath, and then a solution of Fmoc-OSu (4.45 g, 13.2 mmol, 1.20 equiv) in dioxane (55 mL) was added. The reaction mixture was stirred at 0 °C for 1 hour, then at 23 °C for 14 hours. The solution was concentrated by rotary evaporation to two-thirds of the original volume, and then the aqueous layer was washed with dichloromethane (2 × 30 mL). The aqueous layer was acidified with HCl (4 M solution in H_2O) to pH 4, and was then extracted with DCM (3 × 0.1 L). The combined organic layers were dried over sodium sulfate, filtered, and concentrated *in vacuo* to

dryness. The brown residue was dissolved in dichloromethane (15 mL) and filtered through a 15 mL Büchner funnel with fine porosity (code f) into vigorously stirred acetonitrile (150 mL). The suspension was cooled to 0 °C and filtered over a 60 mL Büchner funnel with micro porosity (code M), and the beige solid was washed with acetonitrile (2 × 10 mL), and dried *in vacuo* to dryness to afford **140** as a beige solid (4.83 g, 8.24 mmol, 75% yield).

R_f = 0.36 (DCM:MeOH:TFA, 92:8:1, v:v:v).

NMR Spectroscopy:

^{1}H NMR (500 MHz, CD_3OD, 60 ºC, δ): 7.78 (d, *J* = 7.5, 2H), 7.62 (t, *J* = 6.5, 2H), 7.38 (t, *J* = 7.4, 2H), 7.30 (t, *J* = 7.4 Hz, 2H), 5.83 (br, 1H), 5.74–5.64 (m, 3H), 5.14 (s, 5H), 4.47 (br, 1H), 4.36 (br, 1H), 4.27–4.14 (m, 2H) 2.88 (br, 1H), 2.68 (br, 1H).

^{13}C{^{1}H} NMR (126 MHz, CD_3OD, 25 ºC, δ): 175.5, 158.0, 145.3, 145.1, 142.7, 142.6, 141.2, 128.8_2, 128.8_1, 128.1_9, 128.1_7, 126.2, 126.1, 120.9_7, 120.9_5, 97.7, 86.9, 86.8, 80.2, 75.9, 75.8, 67.5, 57.8, 37.9. 2 Rotamers of the Fmoc-protecting group are observed at 25 °C and one carbon resonance is not observed, presumably due to overlap with a solvent carbon resonance.

HRMS-ESI (m/z) calc'd for $C_{29}H_{26}NO_5Ru$ $[M-OH]^+$,570.08490; found, 570.08502; deviation: 0.21 ppm.

Elemental Analysis calc'd for $C_{29}H_{27}NO_6Ru$: C, 59.38; H, 4.64; found: C, 59.06; H, 4.31.

[Fmoc-tyrosine(RuCp)-OH]·CF_3CO_2 (156)

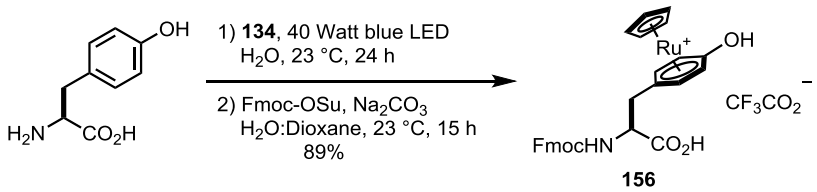

156

A round-bottom flask (2 L) equipped with a Teflon-coated magnetic stirring bar was charged with [(Cp)Ru(η^6-naphthalene)]·CF_3SO_3 (**134**) (6.65 g, 15.0 mmol, 1.00 equiv), *L*-tyrosine (3.40 g, 18.8 mmol, 1.25 equiv), water (0.75 L, c = 0.02 M), and trifluoroacetic acid (2.87 mL, 4.27 g, 37.5 mmol, 2.50 equiv). The yellow suspension was irradiated for 24 h with blue LED light (Kessil A

160WE Tuna Blue, 40 W), then the resulting beige suspension was extracted with hexane (2 × 200 mL), and the combined organic layers were extracted with water (50 mL). The combined aqueous layers were basified with Na_2CO_3 (7.95 g, 75.0 mmol, 5.00 equiv) and dioxane (0.25 L) was added. The suspension was cooled to 0 °C with an ice bath, and then a solution of Fmoc-OSu (7.59 g, 22.5 mmol, 1.50 equiv) in dioxane (0.25 L) was added. The reaction mixture was stirred at 0 °C for 1 hour, then at 23 °C for 14 hours. The solution was concentrated by rotary evaporation to half the original volume, and then the aqueous layer was washed with dichloromethane (3 × 0.2 L). The aqueous layer was acidified with trifluoroacetic acid to pH 3 and then extracted with dichloromethane (4 × 0.3 L). The combined organic layers were dried over sodium sulfate, filtered, and concentrated *in vacuo* to dryness. The residual brown solid was purified by column chromatography (EtOAc:MeCN:TFA, 90:9:0.1, v:v:v) to afford **156** as a yellow powder (9.15 g, 13.4 mmol, 89% yield).

R_f = 0.26 (EtOAc:MeCN:TFA, 9:1:0.1, v:v:v).

R_f = 0.56 (EtOAc:MeCN:TFA, 8:2:0.1, v:v:v).

NMR Spectroscopy:

^{1}H NMR (500 MHz, CD_3CN, 25 ºC, δ): 7.85 (dt, *J* = 7.5, 0.9 Hz, 2H), 7.70–7.60 (m, 2H), 7.47–7.40 (m, 2H), 7.35 (td, *J* = 7.5, 1.1 Hz, 2H), 6.08 (d, *J* = 8.7 Hz, 1H), 6.07–6.05 (m, 1H), 6.02 (dd, *J* = 6.2, 1.8 Hz, 1H), 5.83 (d, *J* = 16.8, 6.2 Hz, 1H), 5.21 (s, 5H), 4.38 (m, 3H), 4.21 (t, *J* = 6.5 Hz, 1H), 2.91 (dd, *J* = 13.8, 4.6 Hz, 1H), 2.70 (dd, *J* = 14.2, 8.9 Hz, 1H).

^{13}C{^{1}H} NMR (126 MHz, CD_3CN, 25 ºC, δ): 172.3, 156.9, 145.0, 144.9, 142.2, 134.1, 128.8, 128.1, 126.1, 121.1, 98.3, 86.5, 86.4, 75.9, 75.7, 67.2, 55.7, 48.0, 36.3.

^{19}F NMR (471 MHz, CD_3CN, 25 ºC, δ): −77.3.

HRMS-ESI (m/z) calc'd for $C_{29}H_{26}NO_5Ru$ $[M-CF_3CO_2]^+$,570.08490; found, 570.08505; deviation: 0.26 ppm.

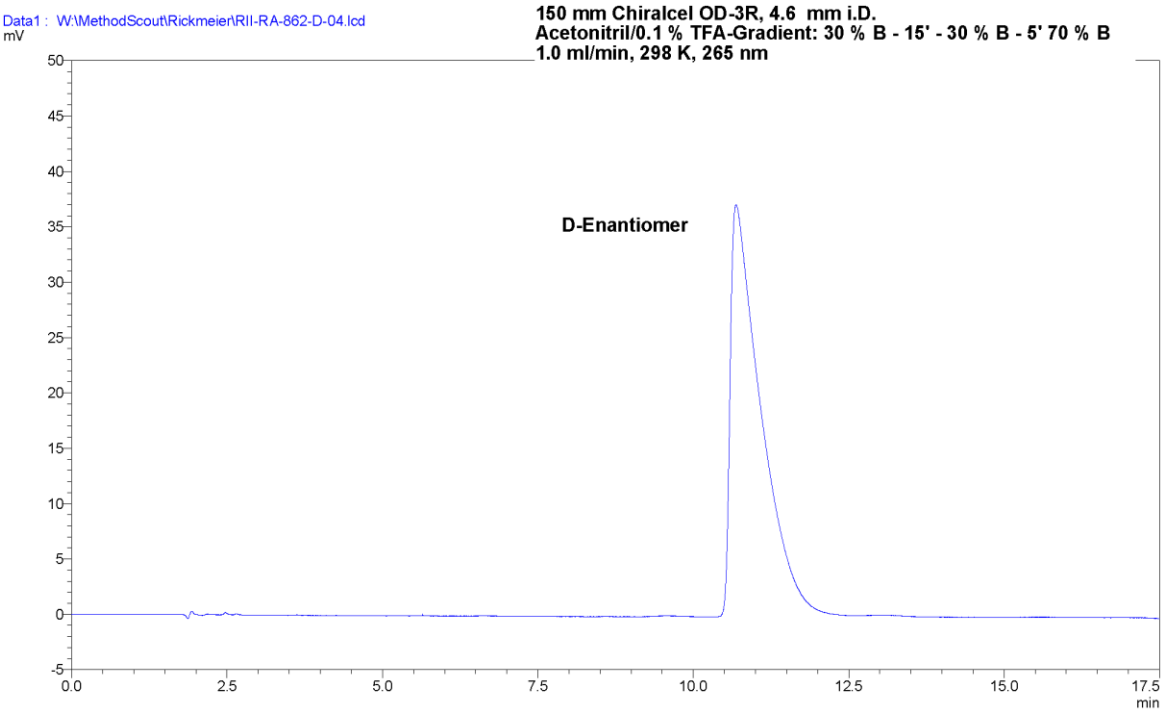

Figure S4. Analytical HPLC trace of **156** (Chiralcel OD-3R, 4.6 × 150 mm, flow rate = 1.0 mL·min^{-1}) with an isocratic eluent 70:30 (0.1% TFA in H_2O:MeCN, v:v) for 15 min followed by a linear gradient to 30:70 (0.1% TFA in H_2O:MeCN, v:v) over 5 minutes.

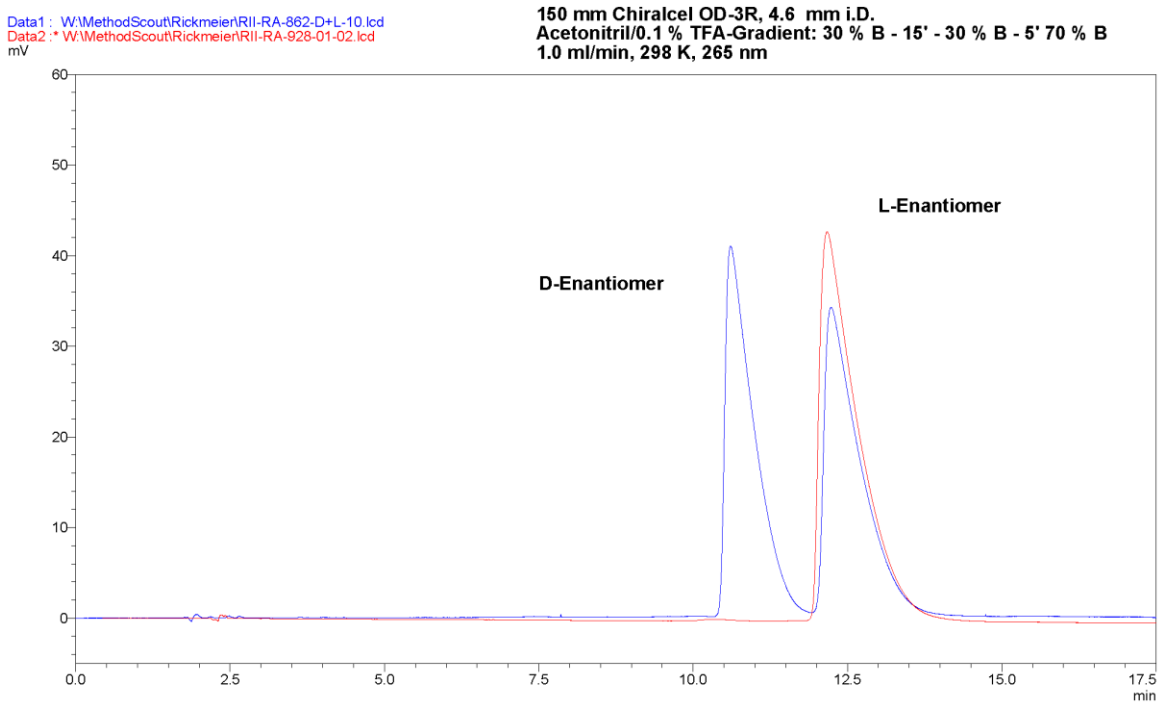

Figure S5. Analytical HPLC trace of **156** (red) and a mixed sample of **156** and **157** (blue) (Chiralcel OD-3R, 4.6 × 150 mm, flow rate = 1.0 mL·min^{-1}) with an isocratic eluent 70:30 (0.1% TFA in H_2O:MeCN, v:v) for 15 min followed by a linear gradient to 30:70 (0.1% TFA in H_2O:MeCN, v:v) over 5 minutes.

[Fmoc-*D*-tyrosine(RuCp)-OH]·CF_3CO_2 (157)

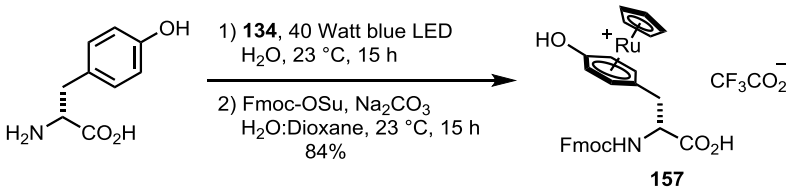

A round-bottom flask (1 L) equipped with a Teflon-coated magnetic stirring bar was charged with [(Cp)Ru(η^6-naphthalene)]·CF_3SO_3 (**134)** (3.00 g, 6.77 mmol, 1.00 equiv), *D*-tyrosine (1.35 g, 7.44 mmol, 1.10 equiv), water (0.27 L, c = 0.025 M), and hydrochloric acid (37% in water, 1.1 mL, 1.3 g, 7.4 mmol, 2.0 equiv). The yellow suspension was irradiated for 15 h with blue LED light (Kessil A 160WE Tuna Blue, 40 W), then the resulting beige suspension was extracted with hexane (2 × 120 mL), and the combined organic layers were extracted with water (50 mL). The combined aqueous layers were basified with Na_2CO_3 (2.15 g, 20.3 mmol, 3.00 equiv) and dioxane (0.12 L) was added. The suspension was cooled to 0 °C with an ice bath and then a solution of Fmoc-OSu (2.74 g, 8.12 mmol, 1.20 equiv) in dioxane (0.12 L) was added. The reaction mixture was stirred at 0 °C for 1 hour, then at 23 °C for 14 hours. The solution was concentrated by rotary evaporation to half the original volume, and then the aqueous layer was washed with dichloromethane (3 × 0.12 L). The aqueous layer was acidified with trifluoroacetic acid to pH 3 and then extracted with dichloromethane (4 × 0.12 L). The combined organic layers were dried over sodium sulfate, filtered, and concentrated *in vacuo* to dryness. The residual beige solid was purified by column chromatography (EtOAc:MeCN:TFA, 90:9:0.1 v:v:v) to afford **157** as a yellow powder (3.89 g, 5.70 mmol, 84% yield).

R_f = 0.26 (EtOAc:MeCN:TFA, 9:1:0.1, v:v:v).

R_f = 0.56 (EtOAc:MeCN:TFA, 8:2:0.1, v:v:v).

NMR Spectroscopy:

^{1}H NMR (500 MHz, CD_3CN, 25 ºC, δ): 7.83 (d, *J* = 7.4 Hz, 2H), 7.67–7.59 (m, 2H), 7.42 (t, *J* = 7.3 Hz, 2H), 7.33 (t, *J* = 7.2 Hz, 2H), 6.14 (d, *J* = 7.6 Hz, 1H), 6.02 (d, *J* = 17.0 Hz, 2H), 5.83 (br, 2H), 5.18 (s, 5H), 4.36 (dd, *J* = 14.7, 7.2 Hz, 3H), 4.21 (t, *J* = 6.50Hz, 1H), 2.92 (d,

J = 13.8, 1H), 2.71 (br, 1H).

$^{13}C\{^{1}H\}$ NMR (126 MHz, CD_3CN, 25 ºC, δ): 172.3, 156.8, 145.0, 144.8, 142.1, 134.4, 128.7, 128.1, 126.1, 121.0, 98.1, 86.5, 86.4, 81.1, 75.9, 75.7, 67.2, 55.7, 48.0, 36.3.

^{19}F NMR (471 MHz, CD3CN, 25 ºC, δ): −77.2.

HRMS-ESI (m/z) calc'd for $C_{29}H_{26}NO_5Ru$ $[M-CF_3CO_2]^+$,570.08490; found, 570.08507; deviation: 0.30 ppm.

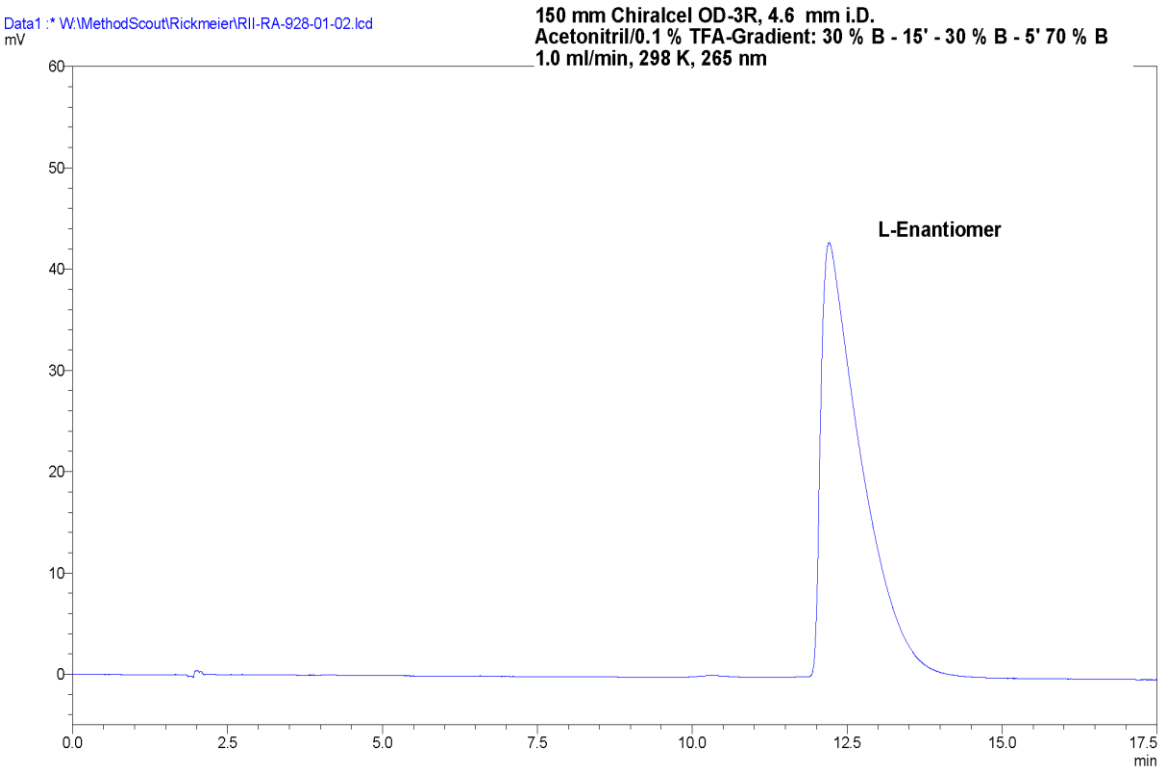

Figure S6. Analytical HPLC trace of **157** (Chiralcel OD-3R, 4.6 × 150 mm, flow rate = 1.0 mL·min^{-1}) with an isocratic eluent 70:30 (0.1% TFA in H_2O:MeCN, v:v) for 15 min followed by a linear gradient to 30:70 (0.1% TFA in H_2O:MeCN, v:v) over 5 minutes.

Neopentyltrimethylammonium iodide (159)

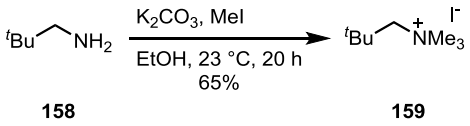

158 **159**

A round-bottom flask (250 mL) equipped with a Teflon-coated magnetic stirring bar was charged with neopentylamine (7.04 mL, 5.25 g, 60.3 mmol, 1.00 equiv) and ethanol (95 mL, c = 0.63 M). Potassium carbonate (11.0 g, 79.6 mmol, 1.32 equiv) and methyl iodide (12.0 mL, 27.3 g, 193 mmol, 3.20 equiv) were added sequentially to the reaction mixture, and then the reaction mixture was stirred at 23 °C for 20 hours. The suspension was filtered through a 60 mL Büchner funnel with micro porosity (code M), and the filtrate was concentrated *in vacuo* to dryness to give a yellow solid. Recrystallization from isopropanol (200 mL) afforded **159** as a colorless crystalline solid (10.1 g, 39.2 mmol, 65% yield).

NMR Spectroscopy:[172]

^{1}H NMR (500 MHz, $(CD_3)_2SO$, 25 ºC, δ): 3.32 (s, 2H), 3.17 (s, 9h), 1.12 (s, 9H).

^{13}C{^{1}H} NMR (126 MHz, $(CD_3)_2SO$, 25 ºC, δ): 75.3, 54.5, 32.9, 29.3.

HRMS-ESI (m/z) calc'd for $C_8H_{20}N$ $[M-I]^+$, 130.15902; found,130.15901; deviation: 0.11 ppm.

Bis(neopentyltrimethylammonium) oxalate (160)

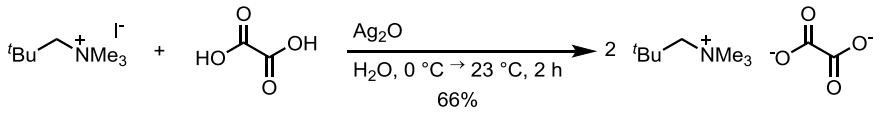

159 **160**

A round-bottom flask (100 mL) equipped with a Teflon-coated magnetic stirring bar and a thermometer was charged with neopentyltrimethylammonium iodide (**159**) (3.00 g, 11.7 mmol, 1.00 equiv) and water (21 mL, c = 0.55 M). The reaction flask was placed in an ice bath, and the reaction mixture was cooled to 0 °C then silver(I) oxide (1.49 g, 6.42 mmol, 0.550 equiv) was added. The suspension was allowed to warm to 23 °C. After 1.5 h, oxalic acid (578 mg, 6.42 mmol, 0.550 equiv) was added, and the reaction mixture was stirred for 30 minutes. The suspension was filtered over a 60 mL Büchner funnel with micro porosity (code M), and the

residual product was extracted with water (3 × 30 mL). The filtrate was concentrated by rotary evaporation to afford an oily residue. The oil was dissolved in acetonitrile (20 mL), filtered, and recrystallized by vapor diffusion with diethyl ether (20 mL). The colorless crystalline solid (**160**) was collected by filtration and dried *in vacuo* for 15 h at 75 °C (1.34 g, 3.85 mmol, 66%).

Note: Compound **160** is hygroscopic and should be stored in a closed vial or in a desiccator.

NMR Spectroscopy:

^{1}H NMR (500 MHz, $(CD_3)_2SO$, 25 ºC, δ): 3.28 (s, 2H), 3.14 (s, 9h), 1.12 (s, 9H).

^{13}C{^{1}H} NMR (126 MHz, $(CD_3)_2SO$, 25 ºC, δ): 166.4, 75.4, 54.5 , 32.9, 29.3.

General procedure for peptide synthesis.

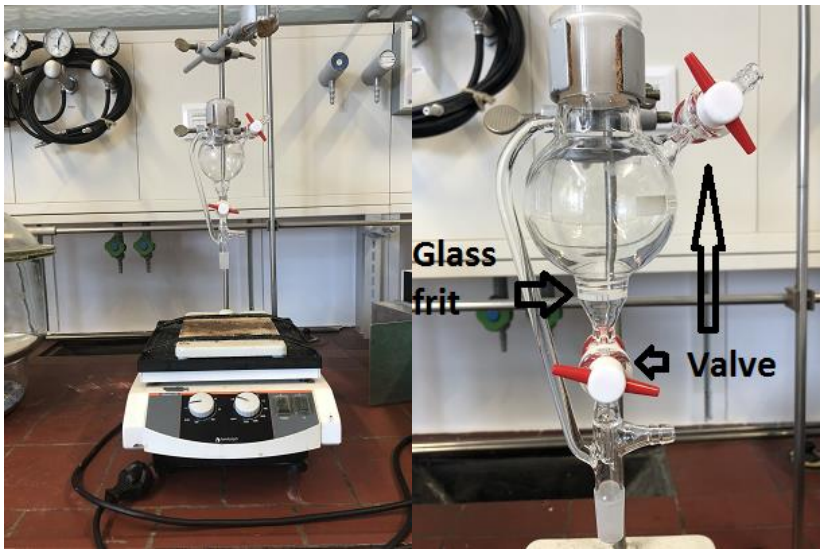

Figure S7. Peptide synthesis set-up.

Peptides were synthesized by solid phase peptide synthesis using the Fmoc/^{t}Bu-orthogonal strategy on a 2-chlorotritly chloride resin (100–200 mesh, 1% DVB, 1.6 mmol·g^{-1}) or a Fmoc-Rink-Amid-2CT resin (200–400 mesh, 1% DVB, 0.68 mmol·g^{-1}).[173] All manipulations were performed under argon atmosphere unless otherwise stated.

General washing procedure: Into the peptide synthesis vessel (Figure S7) containing resin was added the stated washing-solvent (20 mL·g^{-1} resin). The suspension was shaken with the aid

of a Heidolph Vibramax 100 (Figure S7) for 2 minutes at 23 °C, and then the liquid was removed via vacuum filtration.

General loading procedure (2-CTC resin):

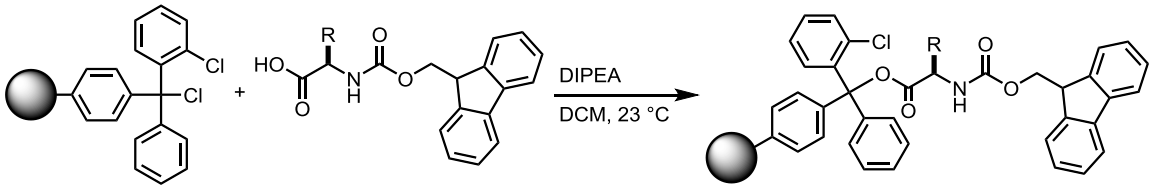

A peptide synthesis vessel (Figure S7) was charged with 2-chlorotrityl chloride resin and DCM (30 mL·g^{-1} resin). The suspension was shaken with the aid of a Heidolph Vibramax 100 (Figure S7) for 30 min at 23 °C. The liquid was removed via vacuum filtration, and a solution of Fmoc-protected amino acid (4.00 equiv) and DIPEA (10.0 equiv) in DCM (30 mL·g^{-1} resin) was added into the peptide synthesis vessel. The resulting suspension was shaken for 15 hours at 23 °C, and then the liquid was removed via vacuum filtration. The resin was washed with DCM (3 × 20 mL·g^{-1} resin × 2 min), and a solution of DIPEA, MeOH, and DCM (1:2:17, v:v:v, 30 mL·g^{-1} resin) was added into the peptide synthesis vessel. The suspension was shaken for 1 hour at 23 °C, and then the resin was washed sequentially with DMF (2 × 20 mL·g^{-1} resin), DCM (2 × 20 mL·g^{-1} resin), MeOH (2 × 20 mL·g^{-1} resin), and Et_2O (2 × 20 mL·g^{-1} resin). The resin was dried *in vacuo*, and the loading efficiency was determined by UV/vis spectroscopy at 289.8 nm.[174]

General deprotection procedure:

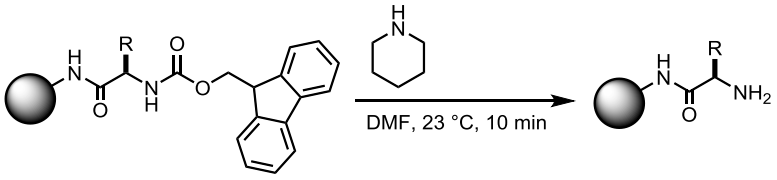

Into the peptide synthesis vessel containing resin-bound Fmoc-protected peptide was added 20% piperidine in DMF (v:v, 20 mL·g^{-1} resin), and the suspension was shaken for 5 minutes at 23 °C. Then the liquid was removed via vacuum filtration. This deprotection sequence was repeated once, and then the resin was washed with DMF (3 × 20 mL·g^{-1} resin × 2 min).

General HBTU/HOBt coupling procedure:

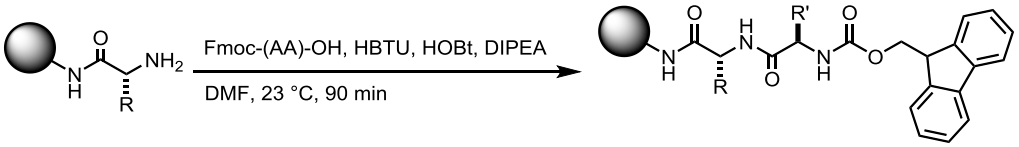

A round-bottom flask equipped with a Teflon-coated magnetic stirring bar was charged with Fmoc-protected amino acid (Fmoc-(AA)-OH, 4.00 equiv), HBTU (3.90 equiv), HOBt hydrate (3.90 equiv), DIPEA (8.00 equiv), and DMF (10 $mL \cdot g^{-1}$ resin). The solution was stirred for 15 minutes at 23 °C and was then added into the peptide synthesis vessel. The vessel was shaken for 90 minutes at 23 °C, and then the liquid was removed via vacuum filtration. The resin was washed with DMF (3 × 10 $mL \cdot g^{-1}$ resin × 2 min).

General [Fmoc-Tyr(RuCp)-OH]·CF_3CO_2 coupling procedure:

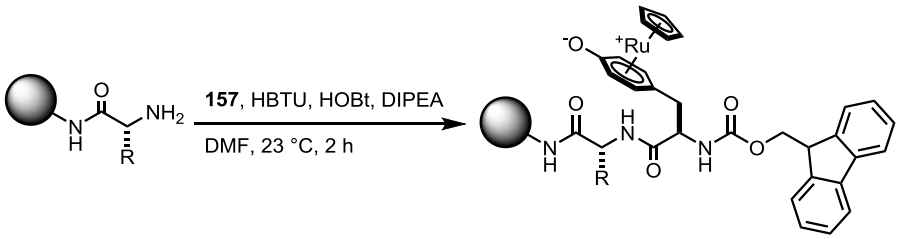

A round-bottom flask equipped with a Teflon-coated magnetic stirring bar was charged with [Fmoc-Tyr(RuCp)-OH]·CF_3CO_2 (**157**) (2.00 equiv), HBTU (1.90 equiv), HOBt hydrate (1.90 equiv), DIPEA (16.0 equiv), and DMF (10 $mL \cdot g^{-1}$ resin). The solution was stirred for 1 minute at 23 °C and was then added into the peptide synthesis vessel. The vessel was shaken for 2 h at 23 °C, and then the liquid was removed via vacuum filtration. The resin was washed with DMF (3 × 10 $mL \cdot g^{-1}$ resin × 2 min).

General [Fmoc-Tyr(RuCp)-O]·H_2O coupling procedure:

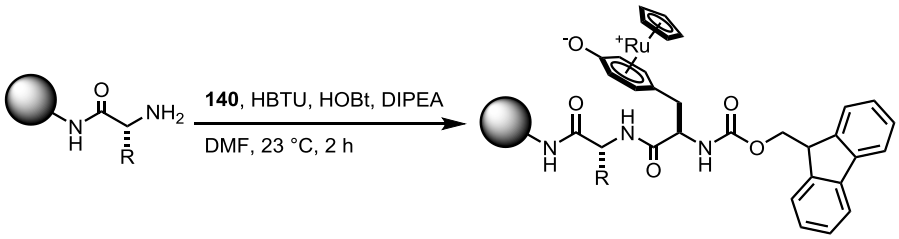

A round-bottom flask equipped with a Teflon-coated magnetic stirring bar was charged with [Fmoc-Tyr(RuCp)-O]·H_2O (**140**) (2.00 equiv), HBTU (1.90 equiv), HOBt hydrate (1.90 equiv), DIPEA (16.0 equiv), and DMF (10 mL·g^{-1} resin). The solution was stirred for 1 minute at 23 °C, and was then added into the peptide synthesis vessel. The vessel was shaken for 2 h at 23 °C, and then the liquid was removed via vacuum filtration. The resin was washed with DMF (3 × 10 mL·g^{-1} resin × 2 min).

General Boc protection procedure:

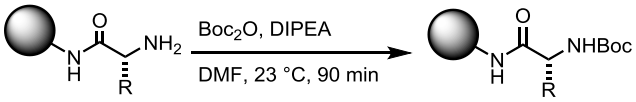

To the resin bound peptide was added a solution of di-*tert*-butyldicarbonate (Boc_2O) (4.00 equiv) and DIPEA (8.00 equiv) in DMF (20.0 mL·g^{-1} resin), then the peptide synthesis vessel was shaken for 2 hours at 23 °C. The liquid was removed via vacuum filtration, and the resin was washed with DMF (3 × 20 mL·g^{-1} × 2 min).

General cleavage conditions:

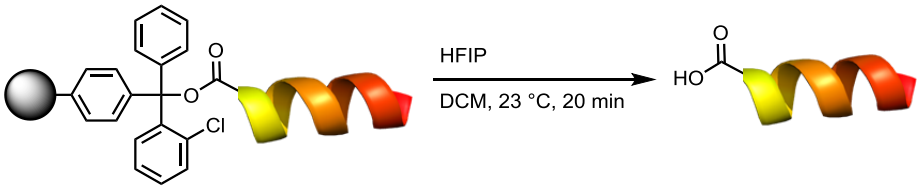

The resin was washed with DCM (3 × 20 mL·g^{-1} resin × 2 min). Then a solution of 20% of hexafluoroisopropanol (HFIP) in DCM (v:v, 50 mL·g^{-1} resin) was added to the resin, and the suspension was shaken for 20 minutes at 23 °C. The liquid was collected via vacuum filtration, and a solution of 20% of HFIP in DCM (v:v, 50 mL·g^{-1} resin) was added to the resin, and the suspension was shaken for 50 minutes at 23 °C. The liquid was collected via vacuum filtration, and the combined organic layers were concentrated *in vacuo* to dryness and were analyzed via LC-MS.

[H-Asp(^{t}Bu)-*D*-Phe(4-F)-Lys(Boc)-Arg(Pbf)-Gly-OH]·CF_3CO_2H (161)

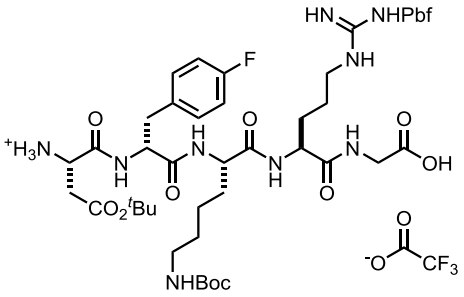

161 (75%)

Representative Example: A peptide synthesis vessel (100 mL) was charged with 2-chlorotritly-chloride resin (100–200 mesh, 1% DVB, 1.6 mmol·g^{-1}, 1.0 g, 1.6 mmol, 1.0 equiv) and DCM (45 mL, 22 g·L^{-1}). The suspension was shaken with the aid of a Heidolph Vibramax 100 (Figure S7) for 30 minutes at 23 °C. The liquid was removed via vacuum filtration, and a solution of Fmoc-Gly-OH (1.9 g, 6.4 mmol, 4.0 equiv) and DIPEA (2.8 mL, 2.1 g, 16 mmol, 10 equiv) in DCM (30 mL) was added into the peptide synthesis vessel. The resulting suspension was shaken for 15 hours at 23 °C, and then the liquid was removed via vacuum filtration. The resin was washed with DCM (3 × 20 mL × 2 min), and a solution of DIPEA, MeOH, and DCM (1:2:17, v:v:v, 30 mL) was added into the peptide synthesis vessel. The suspension was shaken for 1 hour at 23 °C, and then the resin was washed sequentially with DMF (2 × 20 mL), DCM (2 × 20 mL), MeOH (2 × 20 mL), and Et_2O (2 × 20 mL). The resin was dried *in vacuo* to afford Fmoc-Gly-O-2CT resin. The resin loading was determined to be 0.86 mmol·g^{-1} by UV/vis spectroscopy.

A peptide synthesis vessel (100 mL) was charged with Fmoc-Gly-O-2CT resin (0.86 mmol·g^{-1}, 1.2 g, 1.0 mmol, 1.0 equiv) and DCM (45 mL, 26 g·L^{-1}). The resulting suspension was shaken for 30 minutes at 23 °C, and then the liquid was removed via vacuum filtration. The resin was washed with DMF (3 × 10 mL × 2 min). Into the peptide synthesis vessel was added 20% piperidine in DMF (v:v, 20 mL), and the suspension was shaken for 5 minutes at 23 °C. Then the liquid was removed via vacuum filtration. This deprotection sequence was repeated once, and then the resin was washed with DMF (3 × 20 mL × 2 min). A round-bottom flask (20 mL) equipped with a Teflon-coated magnetic stirring bar was charged with Fmoc-Asp(^{t}Bu)-OH (1.6 g, 4.0 mmol, 4.0 equiv), HBTU (1.5 g, 3.9 mmol, 3.9 equiv), HOBt hydrate (0.53 g, 3.9 mmol, 3.9

equiv), DIPEA (1.4 mL, 1.0 g, 8.0 mmol, 8.0 equiv), and DMF (10 mL). The yellow solution was stirred for 15 minutes at 23 °C and was then added into the peptide synthesis vessel. The vessel was shaken for 90 minutes at 23 °C, and then the liquid was removed via vacuum filtration. The resin was washed with DMF (3 × 10 mL × 2 min). Into the peptide synthesis vessel was added 20% piperidine in DMF (v:v, 20 mL), and the suspension was shaken for 5 minutes at 23 °C. Then the liquid was removed via vacuum filtration. This deprotection sequence was repeated once, and then the resin was washed with DMF (3 × 20 mL × 2 min). A round-bottom flask (20 mL) equipped with a Teflon-coated magnetic stirring bar was charged with Fmoc-*D*-Phe(4-F)-OH (1.6 g, 4.0 mmol, 4.0 equiv), HBTU (1.5 g, 3.9 mmol, 3.9 equiv), HOBt hydrate (0.53 g, 3.9 mmol, 3.9 equiv), DIPEA (1.4 mL, 1.0 g, 8.0 mmol, 8.0 equiv), and DMF (10 mL). The yellow solution was stirred for 15 minutes at 23 °C and was then added into the peptide synthesis vessel. The vessel was shaken for 90 minutes at 23 °C, and then the liquid was removed via vacuum filtration. The resin was washed with DMF (3 × 10 mL × 2 min). Into the peptide synthesis vessel was added 20% piperidine in DMF (v:v, 20 mL), and the suspension was shaken for 5 minutes at 23 °C. Then the liquid was removed via vacuum filtration. This deprotection sequence was repeated once, and then the resin was washed with DMF (3 × 20 mL × 2 min). A round-bottom flask (20 mL) equipped with a Teflon-coated magnetic stirring bar was charged with Fmoc-Lys(Boc)-OH (1.9 g, 4.0 mmol, 4.0 equiv), HBTU (1.5 g, 3.9 mmol, 3.9 equiv), HOBt hydrate (0.53 g, 3.9 mmol, 3.9 equiv), DIPEA (1.4 mL, 1.0 g, 8.0 mmol, 8.0 equiv), and DMF (10 mL). The yellow solution was stirred for 15 minutes at 23 °C and was then added into the peptide synthesis vessel. The vessel was shaken for 90 minutes at 23 °C, and then the liquid was removed via vacuum filtration. The resin was washed with DMF (3 × 10 mL × 2 min). Into the peptide synthesis vessel was added 20% piperidine in DMF (v:v, 20 mL), and the suspension was shaken for 5 minutes at 23 °C. Then the liquid was removed via vacuum filtration. This deprotection sequence was repeated once, and then the resin was washed with DMF (3 × 20 mL × 2 min). A round-bottom flask (20 mL) equipped with a Teflon-coated magnetic stirring bar was charged with Fmoc-Arg(Pbf)-OH (2.6 g, 4.0 mmol, 4.0 equiv), HBTU (1.5 g, 3.9 mmol, 3.9 equiv), HOBt hydrate (0.53 g, 3.9 mmol, 3.9 equiv), DIPEA (1.4 mL, 1.0 g, 8.0 mmol, 8.0 equiv), and DMF (10

mL). The yellow solution was stirred for 15 minutes at 23 °C and was then added into the peptide synthesis vessel. The vessel was shaken for 90 minutes at 23 °C, and then the liquid was removed via vacuum filtration. The resin was washed with DMF (3 × 10 mL × 2 min). Into the peptide synthesis vessel was added 20% piperidine in DMF (v:v, 20 mL), and the suspension was shaken for 5 minutes at 23 °C. Then the liquid was removed via vacuum filtration. This deprotection sequence was repeated once, and then the resin was washed with DMF (3 × 20 mL × 2 min). The resin was washed with DCM (3 × 20 mL × 2 min). Then a solution of 20% of hexafluoroisopropanol (HFIP) in DCM (v:v, 50 mL) was added to the resin, and the suspension was shaken for 20 minutes at 23 °C. The liquid was collected via vacuum filtration, and a solution of 20% of HFIP in DCM (v:v, 50 mL) was added to the resin, and the suspension was shaken for 50 minutes at 23 °C. The liquid was collected via vacuum filtration, and the combined organic layers were concentrated *in vacuo* to dryness, and were analyzed via LC-MS. The beige residue was purified by HPLC with an YMC-Actus Triart C18 column ((30 × 150 mm, 5 µm + 30 × 50 mm, 5 µm), flow rate = 42.5 mL·min^{-1}, 35 °C) with a linear gradient from 40:60 (0.1% TFA in H_2O:MeOH, v:v) to 10:90 (0.1% TFA in H_2O:MeOH, v:v) over 10 minutes. The collected fractions containing the product (t ≈ 8.5 min) were combined and concentrated *in vacuo* to dryness to afford **161** as a colorless solid (0.87 g, 0.75 mmol, 75% yield).

HRMS-ESI (m/z) calc'd for $C_{49}H_{73}FN_9O_{13}S$ $[M-CF_3CO_2H-H]^-$, 1046.50381; found, 1046.50464; deviation: −0.79 ppm.

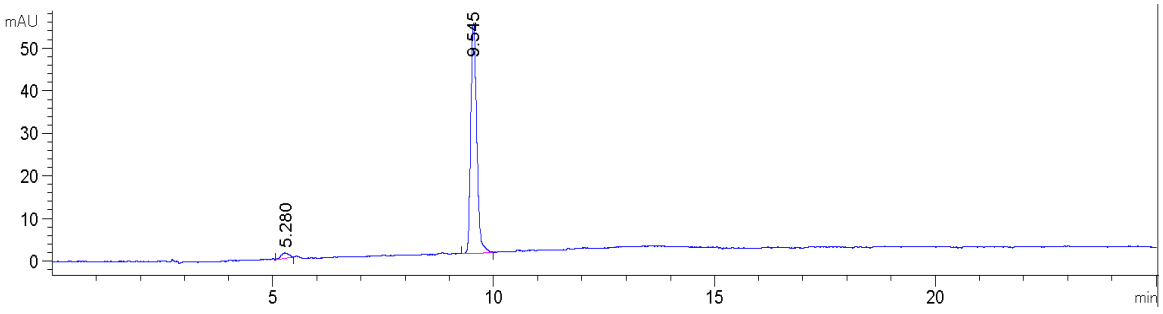

Figure S8. Analytical HPLC trace of **161** (YMC-Triart C18 column, 150 x 4.6 mm, flow rate = 0.8 mL·min^{-1}) with a linear gradient from 30:70 (0.1% TFA in H_2O:MeOH, v:v) to 05:95 (0.1% TFA in H_2O:MeOH, v:v) over 10 minutes.

[c(Asp(ᵗBu)-*D*-Phe(4-F)-Lys(Boc)-Arg(Pbf)-Gly)]·CF_3CO_2H (162)

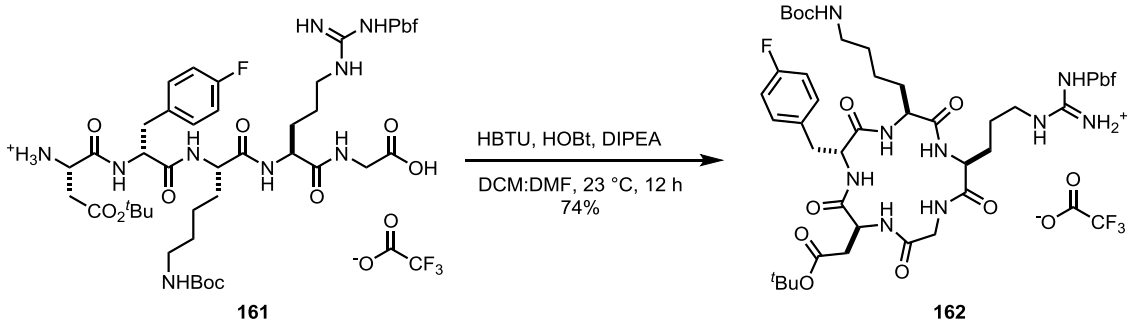

161 162

A round-bottom flask (1 L) equipped with a Teflon-coated magnetic stirring bar was charged with HOBt (0.12 g, 0.88 mmol, 1.2 equiv), HBTU (0.33 g, 0.88 mmol, 1.2 equiv), DIPEA (0.38 mL, 0.28 g, 2.2 mmol, 3.0 equiv), DCM (0.4 L), and DMF (0.1 L). The reaction mixture was cooled to 0°C and a solution of linear peptide **161** (0.85 g, 0.73 mmol, 1.0 equiv) in DMF (20 mL) was added dropwise via a syringe over 20 minutes. The reaction mixture was allowed to warm to 23 °C and was afterwards stirred for 12 hours at 23 °C. The solution was concentrated by rotary evaporation to 5 mL and was then diluted with ethyl acetate (50 mL). The solution was washed with water (2 × 30 mL), and the combined aqueous layers were extracted with ethyl acetate (10 mL). The combined organic layers were dried over sodium sulfate, filtered, and concentrated *in vacuo* to dryness. The beige residue was purified by HPLC on an YMC-Actus Triart C18 column ((30 × 150 mm, 5 µm + 30 × 50 mm, 5 µm), flow rate = 42.5 mL·min^{-1}, 35 °C) with a linear gradient from 30:70 (0.1% TFA in H_2O:MeOH, v:v) to 05:95 (0.1% TFA in H_2O:MeOH, v:v) over 10 minutes. The collected fractions containing the product **162** (t ≈ 9.5 min) were combined, neutralized to pH 7 with saturated aqueous sodium bicarbonate solution, diluted with 100 mL brine, and the resulting suspension was concentrated by rotary evaporation (100 mbar, 35 °C) until no more methanol was evaporated. The suspension was extracted with dichloromethane (3 × 100 mL), and the combined organic layers were dried over sodium sulfate, filtered, and concentrated *in vacuo* to dryness to afford **162** a colorless powder (0.62 g, 0.54 mmol, 74% yield).

HRMS-ESI (m/z) calc'd for $C_{49}H_{72}FN_9O_{12}SNa$ $[M+Na-CF_3CO_2H]^+$, 1052.48974; found, 1052.49063; deviation: −0.85 ppm.

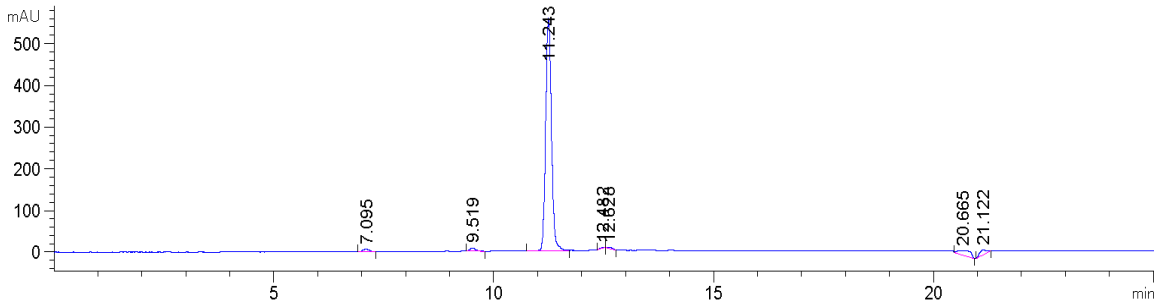

Figure S9. Analytical HPLC trace of **162** (YMC-Triart C18 column, 150 x 4.6 mm, flow rate = 0.8 mL·min^{-1}) with a linear gradient from 30:70 (0.1% TFA in H_2O:MeOH, v:v) to 05:95 (0.1% TFA in H_2O:MeOH, v:v) over 10 minutes.

[c(Asp-*D*-Phe(4-F)-Lys-Arg-Gly]·2CF_3CO_2H ([^{19}F]149)

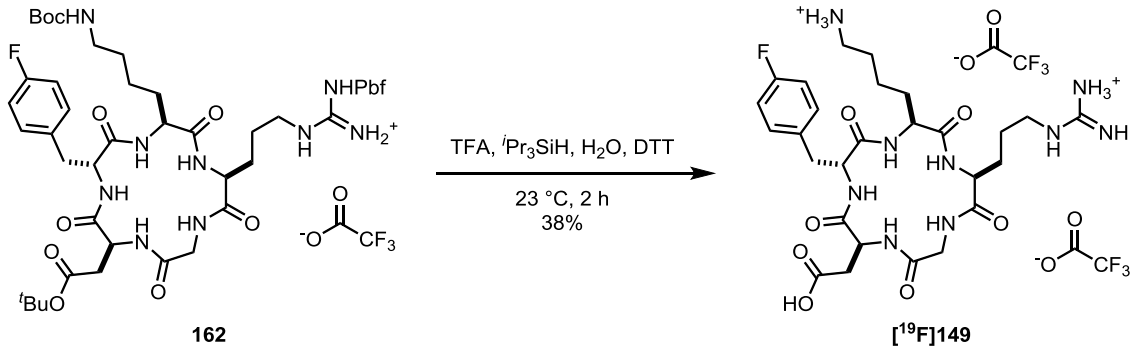

A vial (4 mL) equipped with a Teflon-coated magnetic stirring bar was charged with TFA (0.41 mL), DTT (35 mg, 0.23 mmol, 4.3 equiv), water (35 µL, 35 mg, 1.9 mmol, 37 equiv), and triisopropylsilane (18 µL, 14 mg, 85 µmol, 1.6 equiv). Cyclic peptide **162** (60 mg, 53 µmol, 1.0 equiv) was added to the emulsion, and the reaction mixture was stirred at 23 °C for 2 hours. Afterwards, the reaction mixture was concentrated *in vacuo* to dryness. The residual beige solid was purified by HPLC on an YMC-Actus Triart C18 column ((30 × 150 mm, 5 µm + 30 × 50 mm, 5 µm), flow rate = 42.5 mL·min^{-1}, 35 °C) with a linear gradient from 70:30 (0.1% TFA in H_2O:MeOH, v:v) to 35:65 (0.1% TFA in H_2O:MeOH, v:v) over 10 minutes. The collected fractions containing the product (t ≈ 4.6 min) were combined and concentrated *in vacuo* to dryness to afford **[^{19}F]149** as a colorless solid (17 mg, 20 µmol, 38% yield).

NMR Spectroscopy:

^{1}H NMR (500 MHz, CD_3OD, 25 °C, δ): 7.29–7.21 (m, 2H), 7.06–6.99 (m, 2H), 4.77 (dd, *J* = 7.9, 6.4 Hz, 1H), 4.49 (t, *J* = 7.9 Hz, 1H), 4.31–4.22 (m, 2H), 4.00 (dd, *J* = 11.0, 4.0 Hz, 1H),

3.19 (qt, *J* = 13.7, 7.0 Hz, 2H), 2.99 (d, *J* = 7.9 Hz, 2H), 2.88–2.77 (m, 3H), 2.59 (dd, *J* = 16.5, 6.4 Hz, 1H), 1.88 (ddt, *J* = 13.1, 9.2, 6.5 Hz, 1H), 1.76 (dddd, *J* = 13.6, 9.4, 7.2, 4.0 Hz, 1H) 1.66 (dddd, *J* = 13.1, 10.0, 7.7, 5.2 Hz, 1H), 1.60–1.41 (m, 5H), 1.07–0.98 (m, 2H). One proton resonance is not observed, presumably due to overlap with a solvent proton resonance.

$^{13}C\{^{1}H\}$ NMR (126 MHz, CD_3OD, 25 ºC, δ): 174.6, 173.8, 173.7, 173.4, 172.8, 172.2, 163.2 ($^{1}J_{C–F}$ = 243 Hz), 158.6, 134.0 ($^{4}J_{C–F}$ = 3 Hz), 132.3 ($^{3}J_{C–F}$ = 8 Hz), 116.2 ($^{2}J_{C–F}$ = 21 Hz), 56.9, 55.8, 53.9, 51.0, 44.9, 42.0, 40.3, 37.3, 36.2, 31.7, 29.4, 27.9, 26.3, 24.1.

^{19}F NMR (471 MHz, CD_3OD, 25 ºC, δ): −77.7, −118.9.

HRMS-ESI (m/z) calc'd for $C_{27}H_{42}FN_9O_7$ $[M-2CF_3CO_2]^{2+}$, 311.65901; found, 311.65885; deviation: 0.52 ppm.

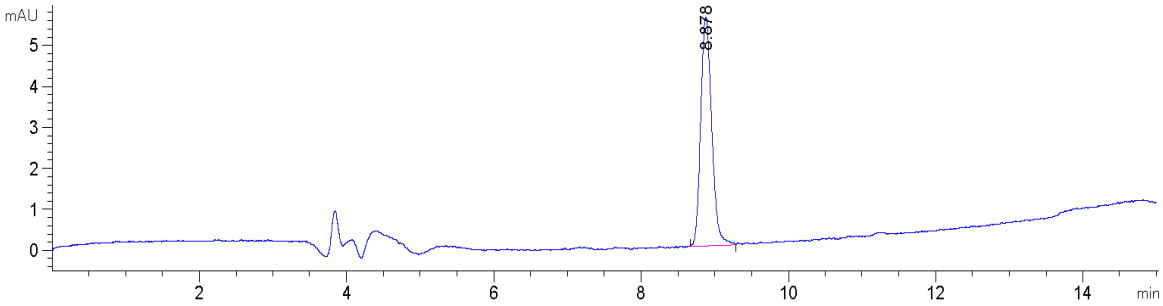

Figure S10. Analytical HPLC trace of **[^{19}F]149** (YMC-Triart C18 column, 150 x 4.6 mm, flow rate = 0.8 mL·min^{-1}) with a linear gradient from 70:30 (0.1% TFA in H_2O:MeOH, v:v) to 40:60 (0.1% TFA in H_2O:MeOH, v:v) over 10 minutes.

[H-Asp(^{t}Bu)-*D*-Tyr(RuCp)-Lys(Boc)-Arg(Pbf)-Gly-OH]·CF_3CO_2H·CF_3CO_2 (163)

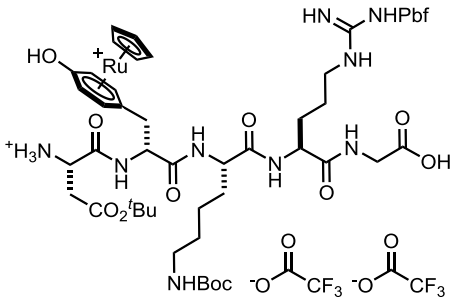

163 (73%)

The peptide was synthesized according to the general procedure for peptide synthesis starting with 1 mmol Fmoc-Gly-O-2CT resin. The beige residue was purified by HPLC with an YMC-Actus Triart C18 column ((30×150 mm, 5 µm + 30×50 mm, 5 µm), flow rate = 42.5 mL·min^{-1}, 35 °C) with a linear gradient from 40:60 (0.1% TFA in H_2O:MeOH, v:v) to 10:90 (0.1% TFA in H_2O:MeOH, v:v) over 10 minutes. The collected fractions containing the product (t ≈ 6.5 min) were combined and concentrated *in vacuo* to dryness to afford **163** as a colorless solid (1.1 g, 0.73 mmol, 73% yield).

HRMS-ESI (m/z) calc'd for $C_{54}H_{81}O_{14}N_9RuS$ $[M-2CF_3CO_2]^{2+}$, 606.73281; found, 606.73366; deviation: 1.40 ppm.

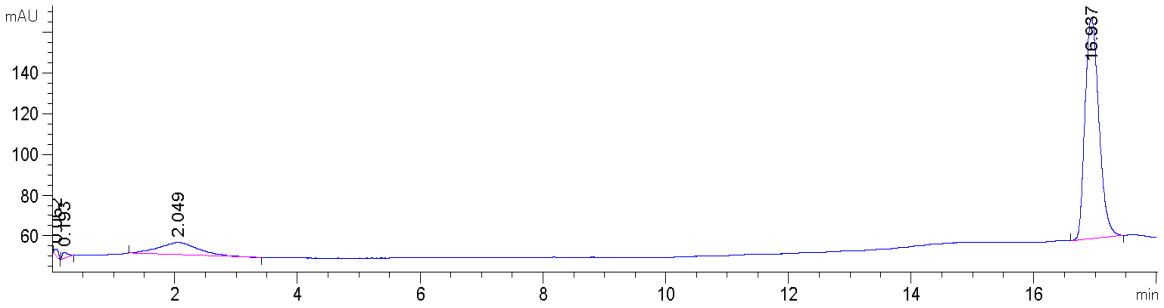

Figure S11. Analytical HPLC trace of **163** (YMC-Triart C18 column, 150 x 4.6 mm, flow rate = 0.8 mL·min^{-1}) with a linear gradient from 30:70 (0.1% TFA in H_2O:MeOH, v:v) to 05:95 (0.1% TFA in H_2O:MeOH, v:v) over 10 minutes.

[c(Asp(ᵗBu)-*D*-Tyr(RuCp)-Lys(Boc)-Arg(Pbf)-Gly)] (164)

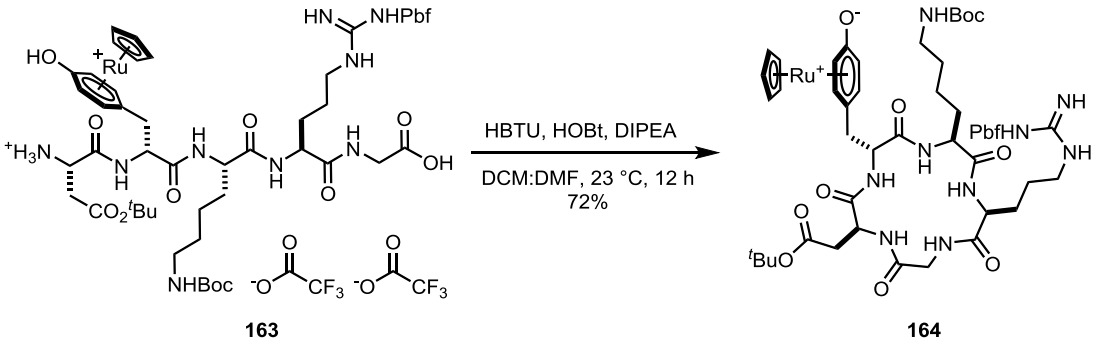

163 **164**

A round-bottom flask (1 L) equipped with a Teflon-coated magnetic stirring bar was charged with HOBt (0.10 g, 0.77 mmol, 1.2 equiv), HBTU (0.29 g, 0.77 mmol, 1.2 equiv), DIPEA (0.33 mL, 0.25 g, 1.9 mmol, 3.0 equiv), DCM (0.4 L), and DMF (0.1 L). The reaction mixture was cooled to 0 °C and a solution of linear peptide **163** (0.92 g, 0.64 mmol, 1.0 equiv) in DMF (20 mL) was added dropwise via a syringe over 20 min. The reaction mixture was allowed to warm to 23 °C and was afterwards stirred for 12 hours at 23 °C. The solution was concentrated by rotary evaporation to 5 mL and afterwards diluted with ethyl acetate (50 mL). The solution was extracted with water (2 × 30 mL), and the combined aqueous layers were extracted with ethyl acetate (10 mL). The combined organic layers were dried over sodium sulfate, filtered, and concentrated *in vacuo* to dryness. The beige residue was purified by HPLC on an YMC-Actus Triart C18 column ((30×150 mm, 5 µm + 30×50 mm, 5 µm), flow rate = 42.5 mL·min^{-1}, 35 °C) with a linear gradient from 20:80 (0.1% TFA in H_2O:MeOH, v:v) to 10:90 (0.1% TFA in H_2O:MeOH, v:v) over 10 minutes. The collected fractions containing the product (t ≈ 8.0 min) were combined, basified to pH 8 with saturated aqueous sodium bicarbonate solution, diluted with 100 mL brine and the resulting solution was concentrated by rotary evaporation (100 mbar, 35 °C) until no more methanol was evaporated. The suspension was extracted with dichloromethane (3 × 100 mL), and the combined organic layers were dried over sodium sulfate, filtered, and concentrated *in vacuo* to dryness to afford **164** a colorless powder (0.55 g, 0.46 mmol, 72% yield).

NMR Spectroscopy:

^{1}H NMR (500 MHz, (CD_3OD, 25 ºC, δ): 8.27 (s, 1H), 5.87 (dd, *J* = 6.5, 1.5 Hz, 1H), 5.79 (dd, *J* = 6.5, 1.6 Hz, 1H), 5.58 (ddd, *J* = 12.7, 6.4, 1.9 Hz, 2H), 5.15 (s, 5H), 4.71 (dd, *J* = 9.1, 5.5 Hz, 1H), 4.58 (t, *J* = 7.3 Hz, 1H), 4.19–4.07 (m, 3H), 3.24–3.5 (m, 2H), 3.03–2.98 (m, 4H), 2.83–2.65 (m, 3H), 2.57 (s, 3H), 2.54–2.47 (m, 4H), 2.08 (s, 3H), 1.91–1.82 (m, 1H), 1.79–1.56 (m, 3H), 1.56–1.38 (m, 29H), 1.30 (td, *J* = 15.9, 14.1, 5.9 Hz, 2H). One proton resonance is not observed, presumably due to overlap with a solvent proton resonance.

^{13}C{^{1}H} NMR (126 MHz, (CD_3OD, 25 ºC, δ): 174.8, 173.7, 172.9, 172.4, 172.1, 171.4, 166.9, 159.9, 158.5, 158.1, 139.4, 134.4, 133.5, 126.0, 118.4, 94.9, 87.7, 87.2, 86.9, 82.3, 79.9, 79.6, 76.1, 76.0, 65.0 , 56.5, 56.0, 54.3, 50.9, 44.7, 44.0, 41.1, 36.9, 36.6, 32.4, 30.5, 29.0, 28.9, 28.7, 28.4, 24.7, 19.6, 18.4, 12.5. One carbon resonance is not observed, presumably due to overlap with a solvent carbon resonance.

HRMS-ESI (m/z) calc'd for $C_{54}H_{78}O_{13}N_9RuS$ $[M+H]^+$, 1194.44778; found, 1194.44979; deviation: 1.68 ppm.

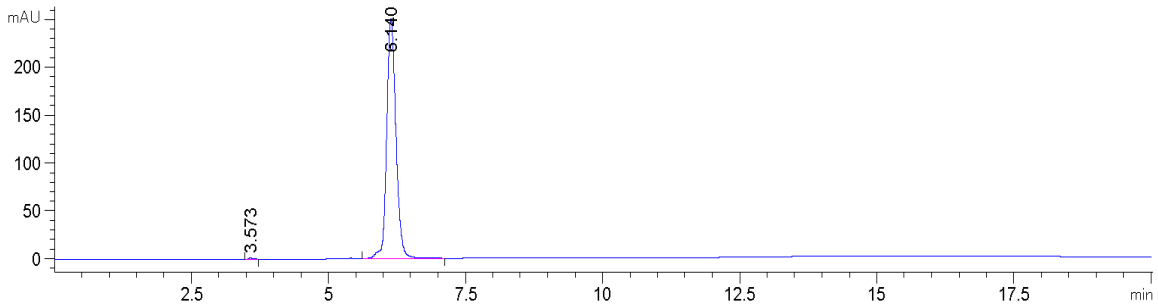

Figure S12. Analytical HPLC trace of **164** (YMC-Triart C18 column, 150 x 4.6 mm, flow rate = 0.8 $mL \cdot min^{-1}$) with a linear gradient from 20:80 (0.1% TFA in H_2O:MeOH, v:v) to 03:97 (0.1% TFA in H_2O:MeOH, v:v) over 10 minutes.

[Boc-*D*-Glu(*t*Bu)-Ala-Tyr(*t*Bu)-Gly-Trp(Boc)-Met-Asp(*t*Bu)-Phe(4-F)-OH] (165)

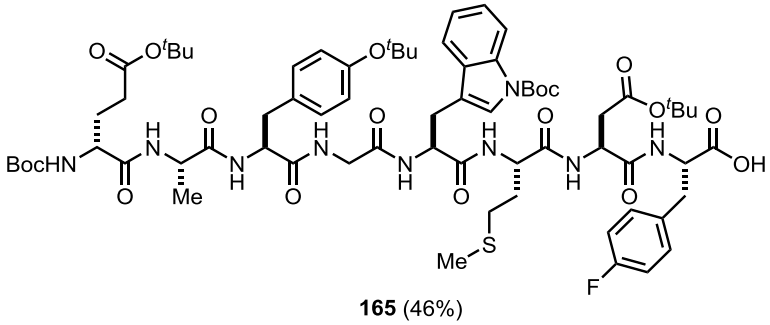

165 (46%)

The peptide was synthesized according to the general procedure for peptide synthesis starting with 0.5 mmol Fmoc-Phe(4-F)-O-2CT resin. The beige residue was purified by HPLC with an YMC-Actus Triart C18 column ((30×150 mm, 5 µm + 30×50 mm, 5 µm), flow rate = 42.5 mL·min^{-1}, 35 °C) with a linear gradient from 15:85 (0.1% TFA in H_2O:MeOH, v:v) to 05:95 (0.1% TFA in H_2O:MeOH, v:v) over 10 minutes. The collected fractions containing the product (t ≈ 9.0 min) were combined, basified to pH 7 with saturated aqueous sodium bicarbonate solution, diluted with 100 mL brine, and the resulting solution was concentrated by rotary evaporation (100 mbar, 35 °C) until no more methanol was evaporated. The suspension was extracted with dichloromethane (3 × 100 mL), and the combined organic layers were dried over sodium sulfate, filtered, and concentrated *in vacuo* to dryness to afford the title compound **165** as a colorless solid (0.32 g, 0.23 mmol, 46% yield).

HRMS-ESI (m/z) calc'd for $C_{70}H_{97}FN_9O_{18}S$ $[M-H]^-$, 1402.66618; found, 1402.66603; deviation: 0.11 ppm.

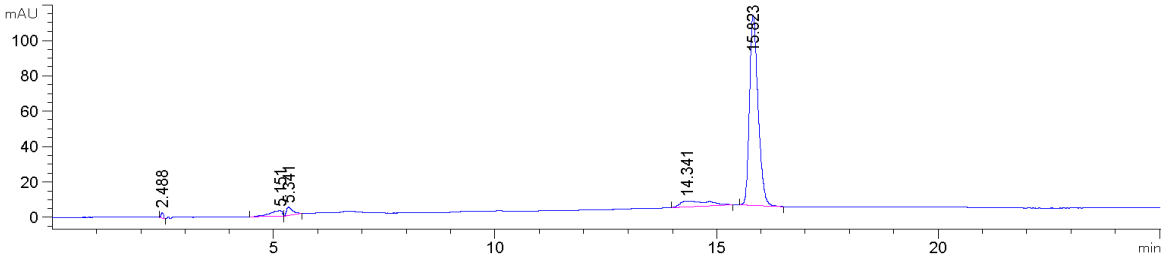

Figure S13. Analytical HPLC trace of **165** (YMC-Triart C18 column, 150 x 4.6 mm, flow rate = 0.8 mL·min^{-1}) with a linear gradient from 30:70 (0.1% TFA in H_2O:MeOH, v:v) to 05:95 (0.1% TFA in H_2O:MeOH, v:v) over 10 minutes.

[Boc-*D*-Glu(ᵗBu)-Ala-Tyr(ᵗBu)-Gly-Trp(Boc)-Met-Asp(ᵗBu)-Phe(4-F)-NHTmob] (166)

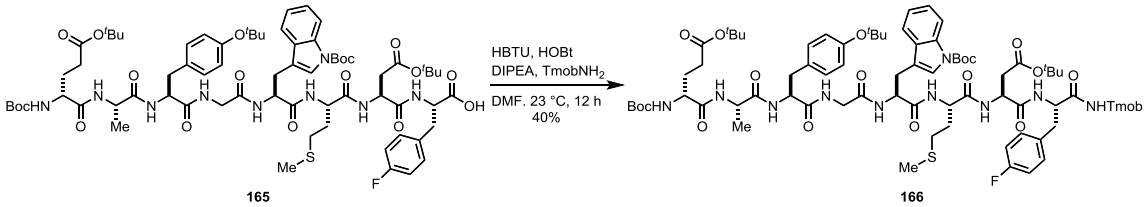

A vial (20 mL) equipped with a Teflon-coated magnetic stirring bar was charged with **165** (0.26 g, 0.19 mmol, 1.0 equiv), HOBt (26 mg, 0.19 mmol, 1. equiv), $TmobNH_2$ (38 mg, 0.19 mmol, 1.0 equiv), DIPEA (0.10 mL, 74 mg, 0.57 mmol, 3.1 equiv), and DMF (17 mL, 0.010 $mol \cdot L^{-1}$). The reaction mixture was cooled to 0 °C and then HBTU (73 mg, 0.19 mmol, 1.0 equiv) was added. The reaction mixture was allowed to warm to room temperature and was stirred at 23 °C for 12 hours. The solution was concentrated by rotary evaporation to 5 mL, and was afterwards diluted with ethyl acetate (50 mL). The solution was extracted with water (2 × 30 mL), and the combined aqueous layers were extracted with ethyl acetate (10 mL). The combined organic layers were concentrated *in vacuo* to dryness. The beige residue was purified by HPLC on an YMC-Actus Triart C18 column ((30×150 mm, 5 µm + 30×50 mm, 5 µm), flow rate = 42.5 $mL \cdot min^{-1}$, 35 °C) with a linear gradient from 25:75 (0.1% TFA in H_2O:MeOH, v:v) to 03:97 (0.1% TFA in H_2O:MeOH, v:v) over 10 minutes. The collected fractions containing the product (t ≈ 9.8 min) were combined, basified to pH 7 with saturated aqueous sodium bicarbonate solution, diluted with 100 mL brine and the resulting solution was concentrated by rotary evaporation (100 mbar, 35 °C) until no more methanol was evaporated. The suspension was extracted with dichloromethane (3 × 100 mL), and the combined organic layers were dried over sodium sulfate, filtered, and concentrated *in vacuo* to dryness to afford **166** a colorless powder (0.12 g, 76 µmol, 40% yield).

HRMS-ESI (m/z) calc'd for $C_{80}H_{110}FN_{10}O_{20}S$ $[M-H-CF_3CO_2H]^-$, 1581.76081; found, 1581.76160.

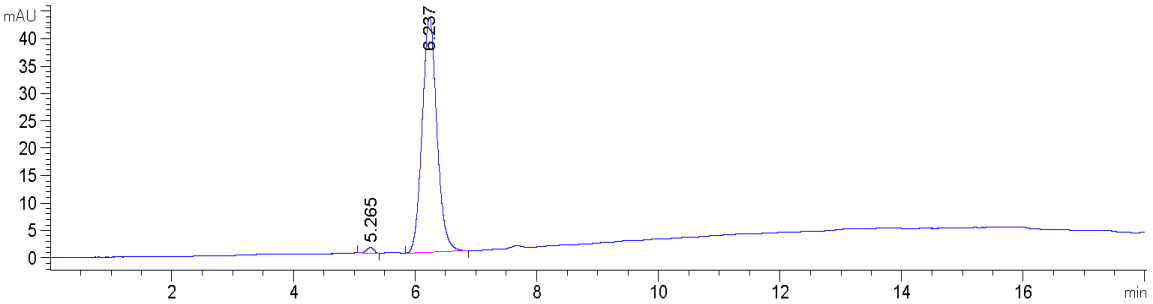

Figure S14. Analytical HPLC trace of **166** (YMC-Triart C18 column, 150 x 4.6 mm, flow rate = 0.8 mL·min^{-1}) with a linear gradient from 50:50 (0.1% TFA in H_2O:MeOH, v:v) to 10:90 (0.1% TFA in H_2O:MeOH, v:v) over 10 minutes.

[H-*D*-Glu-Ala-Tyr-Gly-Trp-Met-Asp-Phe(4-F)-NH_2]·2CF_3CO_2H ([^{18}F]148)

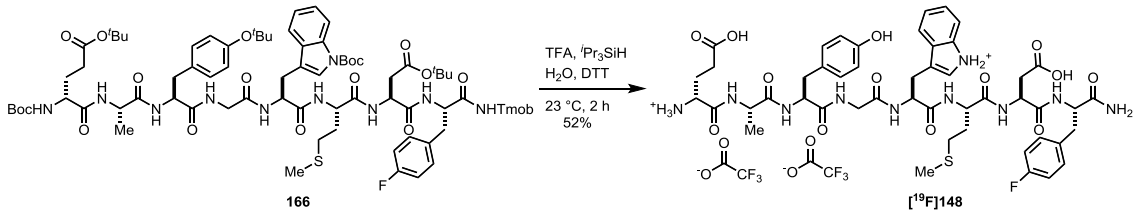

A vial (4 mL) equipped with a Teflon-coated magnetic stirring bar was charged with TFA (0.41 mL, 0.61 g), DTT (35 mg, 0.23 mmol, 6.0 equiv), water (35 µL, 35 mg, 1.9 mmol, 51 equiv), and triisopropylsilane (18 µL, 14 mg, 85 µmol, 2.3 equiv). Linear peptide **166** (60 mg, 38 µmol, 1.0 equiv) was added to the emulsion, and the reaction mixture was stirred at 23 °C for 2 hours. The reaction mixture was concentrated *in vacuo* to dryness, and the resulting beige solid was purified by HPLC on an YMC-Actus Triart C18 column ((30×150 mm, 5 µm + 30×50 mm, 5 µm), flow rate = 42.5 mL·min^{-1}, 35 °C) with a linear gradient from 50:50 (0.1% TFA in H_2O:MeOH, v:v) to 15:85 (0.1% TFA in H_2O:MeOH, v:v) over 10 minutes. The collected fractions containing **[^{19}F]148** (t ≈ 6.3 min) were combined and concentrated *in vacuo* to dryness to afford the **[^{19}F]148** as a colorless solid (25 mg, 20 µmol, 52% yield).

NMR Spectroscopy:

^{1}H NMR (500 MHz, CD_3OD, 25 °C, δ): 7.57 (d, *J* = 7.9 Hz, 1H), 7.32 (d, *J* = 8.1 Hz, 1H), 7.28–7.23 (m, 2H), 7.19 (s, 1H), 7.08 (ddd, *J* = 8.2, 7.0, 1.2 Hz, 1H), 7.04–6.92 (m, 5H), 6.75–6.67 (m, 2H), 4.62 (dd, *J* = 7.5, 6.1 Hz, 1H), 4.58–4.52 (m, 2H), 4.32 (dd, *J* = 9.1, 6.0 Hz, 1H), 4.28–4.20 (m, 2H), 4.02–3.95 (m, 2H), 3.65 (d, *J* = 16.5 Hz, 1H), 3.19 (dd, *J* = 14.1,

5.3 Hz, 1H), 3.07 (dd, *J* = 14.0, 5.9 Hz, 1H), 2.97 (dd, *J* = 14.0, 8.9 Hz, 1H), 2.90–2.76 (m, 2H), 2.68 (dd, *J* = 16.9, 7.5 Hz, 1H), 2.47 (dt, *J* = 7.5, 1.8 Hz, 2H), 2.25 (ddd, *J* = 13.6, 8.5, 5.5 Hz, 1H), 2.18–2.08 (m, 3H), 1.99 (s, 3H), 1.89 (ddt, *J* = 14.3, 10.8, 6.6 Hz, 2H), 1.29 (d, *J* = 7.2 Hz, 3H). The resonance for two protons was not observed, presumably due to overlap with the solvent proton resonance.

$^{13}C\{^{1}H\}$ NMR (126 MHz, CD_3OD, 25 ºC, δ):175.7, 175.6, 175.0, 174.8, 174.1, 174.0, 173.8, 172.6, 172.3, 170.1, 163.2 ($^{1}J_{C\text{-}F}$ = 244 Hz), 157.3, 138.0, 134.4 ($^{4}J_{C\text{-}F}$ = 3 Hz), 132.1 ($^{3}J_{C\text{-}F}$ = 243 Hz), 131.3, 129.2, 128.7, 124.9, 122.6, 119.9, 119.3, 116.2, 116.1 ($^{2}J_{C\text{-}F}$ = 22 Hz), 112.5, 110.5, 57.1, 56.4, 56.0, 54.6, 53.8, 51.7, 51.3, 44.0, 37.8, 36.8, 36.4, 31.3, 30.9, 30.1, 28.2, 27.6, 17.8, 15.2.

^{19}F NMR (471 MHz, CD_3OD, 25 ºC, δ): −77.1, −118.3.

HRMS-ESI (m/z) calc'd for $C_{48}H_{58}F\ N_{10}O_{13}S$ $[M-H-2CF_3CO_2H]^-$, 1033.38950; found, 1033.39025; deviation: −0.72 ppm.

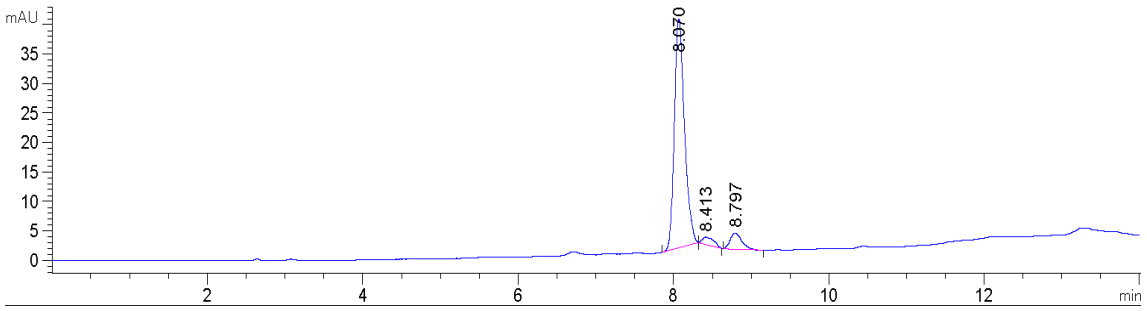

Figure S15. Analytical HPLC trace of **[^{19}F]148** (YMC-Triart C18 column, 150 x 4.6 mm, flow rate = 0.8 mL·min^{-1}) with a linear gradient from 50:50 (0.1% TFA in H_2O:MeOH, v:v) to 10:90 (0.1% TFA in H_2O:MeOH, v:v) over 10 minutes.

[Boc-*D*-Glu(*t*Bu)-Ala-Tyr(*t*Bu)-Gly-Trp(Boc)-Met-Asp(*t*Bu)-Tyr(RuCp)-OH] (167)

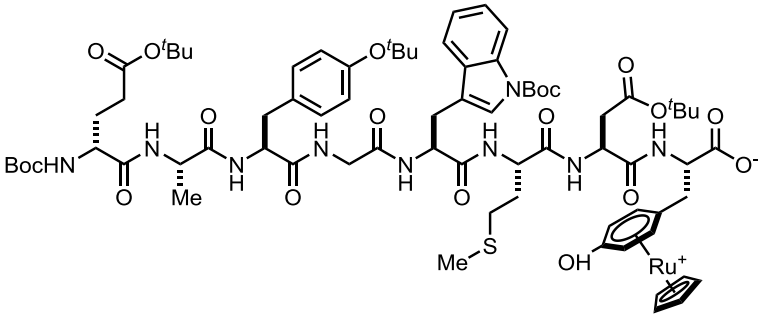

167 (41%)

A peptide synthesis vessel (100 mL) was charged with 2-chlorotritly-chloride resin (100–200 mesh, 1% DVB, 1.6 mmol·g^{-1}, 1.0 g, 1.6 mmol, 1.0 equiv) and DCM (45 mL, 22 g·L^{-1}). The suspension was shaken with the aid of a Heidolph Vibramax 100 (Figure S7) for 30 minutes at 23 °C. The liquid was removed via vacuum filtration, and a solution of [Fmoc-Tyr(RuCp)-O]·H_2O (1.9 g, 3.2 mmol, 2.0 equiv) and DIPEA (1.4 mL, 1.0 g, 8.0 mmol, 5.0 equiv) in DCM (30 mL) was added into the peptide synthesis vessel. The resulting suspension was shaken for 15 hours at 23 °C, and then the liquid was removed via vacuum filtration. The resin was washed with DCM (3 × 20 mL × 2 min), and a solution of DIPEA, MeOH, and DCM (1:2:17, v:v:v, 30 mL) was added into the peptide synthesis vessel. The suspension was shaken for 1 hour at 23 °C, and then the resin was washed sequentially with DMF (2 × 20 mL), DCM (2 × 20 mL), MeOH (2 × 20 mL), and Et_2O (2 × 20 mL). The resin was dried *in vacuo* to afford Fmoc-Tyr(RuCp)-O-2CT resin. The resin loading was determined to be 0.30 mmol·g^{-1} by UV/vis spectroscopy.

The peptide was synthesized according to the general procedure for peptide synthesis starting with 1.0 mmol Fmoc-Tyr(RuCp)-O-2CT resin. The beige residue was purified by HPLC with an YMC-Actus Triart C18 column ((30×150 mm, 5 µm + 30×50 mm, 5 µm), flow rate = 42.5 mL·min^{-1}, 35 °C) with a linear gradient from 25:75 (0.1% TFA in H_2O:MeOH, v:v) to 15:85 (0.1% TFA in H_2O:MeOH, v:v) over 10 minutes. The collected fractions containing the product (t ≈ 9.5 min) were combined, neutralized to pH 7 with saturated aqueous sodium bicarbonate solution, diluted with 100 mL brine, and the resulting solution was concentrated by rotary evaporation (100 mbar, 35 °C) until no more methanol was evaporated. The suspension was extracted with dichloromethane (3 × 100 mL), and the combined organic layers were dried over

sodium sulfate, filtered, and concentrated *in vacuo* to dryness to afford **167** as a colorless solid (0.65 g, 0.41 mmol, 41% yield).

HRMS-ESI (m/z) calc'd for $C_{75}H_{102}O_{19}N_9RuS$ $[M-H]^-$, 1566.60617; found, 1566.60617; deviation: −0 ppm.

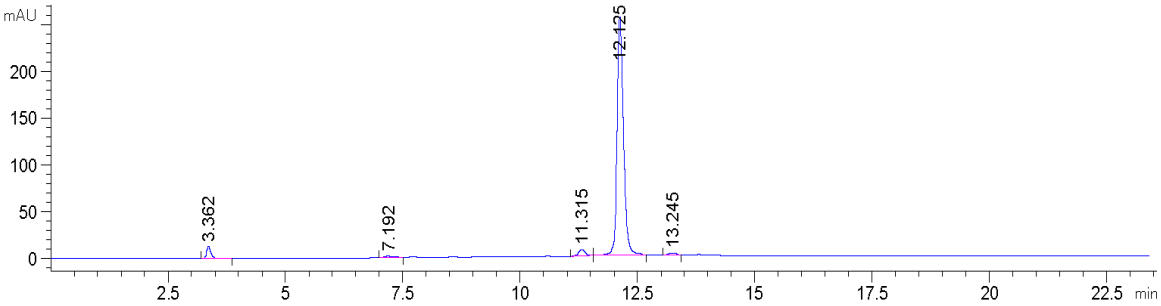

Figure S16. Analytical HPLC trace of **167** (YMC-Triart C18 column, 150 x 4.6 mm, flow rate = 0.8 mL·min^{-1}) with a linear gradient from 30:70 (0.1% TFA in H_2O:MeOH, v:v) to 05:95 (0.1% TFA in H_2O:MeOH, v:v) over 10 minutes.

[Boc-*D*-Glu(*t*Bu)-Ala-Tyr(*t*Bu)-Gly-Trp(Boc)-Met-Asp(*t*Bu)-Tyr(RuCp)-NHTmob]·CF_3CO_2 (168)

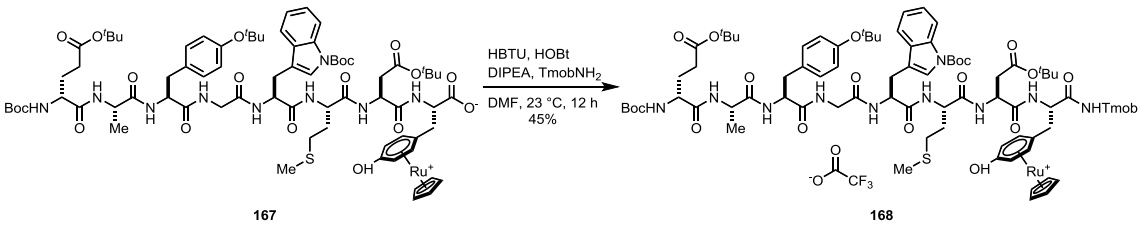

A 50 mL round-bottom flask equipped with a magnetic stirring bar was charged with **167** (0.60 g, 0.38 mmol, 1.0 equiv), HOBt (53 mg, 0.39 mmol, 1.0 equiv), $TmobNH_2$ (77 mg, 0.39 mmol, 1.0 equiv), DIPEA (0.20 mL, 0.15 g, 1.2 mmol, 3.1 equiv) and DMF (17 mL, 20 mmol·L^{-1}). The reaction mixture was cooled to 0 °C and then HBTU (0.15 g, 0.39 mmol, 1.0 equiv) was added. The reaction mixture was allowed to warm to room temperature and was stirred at 23 °C for 12 hours. The solution was concentrated by rotary evaporation to 5 mL, and was afterwards diluted with ethyl acetate (50 mL). The solution was extracted with water (2 × 30 mL), and the combined aqueous layers were extracted with ethyl acetate (10 mL). The combined organic layers were dried over sodium sulfate, filtered, and concentrated *in vacuo* to dryness. The beige residue was purified by HPLC on an YMC-Actus Triart C18 column ((30×150 mm, 5 µm + 30×50 mm, 5

µm), flow rate = 42.5 mL·min^{-1}, 35 °C) with a linear gradient from 20:80 (0.1% TFA in H_2O:MeOH, v:v) to 10:90 (0.1% TFA in H_2O:MeOH, v:v) over 10 minutes. The collected fractions containing the product (t ≈ 8 min) were combined, basified to pH 8 with saturated aqueous sodium bicarbonate solution, diluted with 100 mL brine and the resulting solution was concentrated by rotary evaporation (100 mbar, 35 °C) until no more methanol was evaporated. The suspension was extracted with dichloromethane (3 × 100 mL), and the combined organic layers were dried over sodium sulfate, filtered, and concentrated *in vacuo* to dryness to afford **168** a colorless powder (0.32 g, 0.17 mmol, 45% yield).

NMR Spectroscopy:

^{1}H NMR (500 MHz, $(CD_3)_2SO$, 25 ºC, δ): 8.30 (d, *J* = 7.7 Hz, 1H), 8.23 (d, *J* = 7.6 Hz, 1H), 8.18 (d, *J* = 7.7 Hz, 1H), 8.06 (br, 1H), 8.00 (t, *J* = 8.6 Hz, 2H), 7.88 (d, *J* = 7.2 Hz, 1H), 7.75–7.68 (m, 2H), 7.56 (s, 1H), 7.37–7.28 (m, 1H), 7.24 (t, *J* = 7.5 Hz, 1H), 7.09 (d, *J* = 8.1 Hz, 2H), 6.92 (d, *J* = 7.6 Hz, 1H), 6.81 (d, *J* = 8.0 Hz, 2H), 6.24 (s, 2H), 6.02 (t, *J* = 4.9 Hz, 2H), 5.95 (d, *J* = 5.7 Hz, 1H), 5.89 (d, *J* = 6.3 Hz, 1H), 5.25 (s, 5H), 4.63 (q, *J* = 8.2 Hz, 1H), 4.55 (q, *J* = 7.3 Hz, 1H), 4,51–4.39 (m, 2H), 4.34 (dt, *J* = 13.3, 6.2 Hz, 1H), 4.28–4.09 (m, 3H), 3.97–3.88 (m, 1H), 3.78 (s, 3H), 3.75 (s, 6H), 3.74–3.69 (m, 1H), 3.63 (t, *J* = 16.9, 5.4 Hz, 1H), 3.12 (d, *J* = 14.4 Hz, 1H), 3.01–2.89 (m, 2H), 2.75 (dd, *J* = 14.0, 9.5 Hz, 1H), 2.66–2.57 (m, 2H), 2.44–2.31 (m, 2H), 2.18 (t, *J* = 7.8 Hz, 2H), 2.01 (s, 3H), 1.92 (t, *J* = 7.0 Hz, 1H), 1.82 (dd, *J* = 8.6, 3.9 Hz, 2H), 1.71–1.64 (m, 1H) ,1.61 (s, 9H), 1.37 (s, 9H), 1.36 (s, 9H), 1.34 (s, 9H), 1.23 (s, 9H),1.09 (d, *J* = 7.1 Hz, 3H). One proton resonance is not observed, presumably due to overlap with a solvent proton resonance.

^{13}C{^{1}H} NMR (126 MHz, $(CD_3)_2SO$, 25 ºC, δ):171.9, 171.6, 171.3, 171.2, 170.9, 169.9, 169.2, 168.9, 168.7, 160.7, 159.1, 155.3, 153.4, 149.0, 134.6, 132.4, 130.3, 129.6, 124.2, 124.1, 123.4, 122.4, 119.4, 116.4, 114.6, 105.2, 96.1, 85.5, 85.3, 83.5, 80.3, 79.6, 79.1, 78.3, 77.5, 74.1, 74.0, 55.8, 55.3, 54.1, 53.5_0, 53.4_5, 52.6, 52.1, 49.6, 48.1, 42.0, 37.0, 36.6_2, 36.5_6, 31.7, 31.2, 29.4, 28.5, 28.1, 27.7_0, 27.7_3, 27.6, 27.3, 27.2, 18.1, 14.6. Three carbon resonances are not observed, presumably due to overlap with other carbon resonances.

^{19}F NMR (471 MHz, $(CD_3)_2SO$, 25 °C, δ): −74.1.

HRMS-ESI (m/z) calc'd for $C_{85}H_{115}O_{21}N_{10}RuS$ $[M-H-CF_3CO_2H]^-$, 1745.70079; found, 1745.70213; deviation: −0.77 ppm.

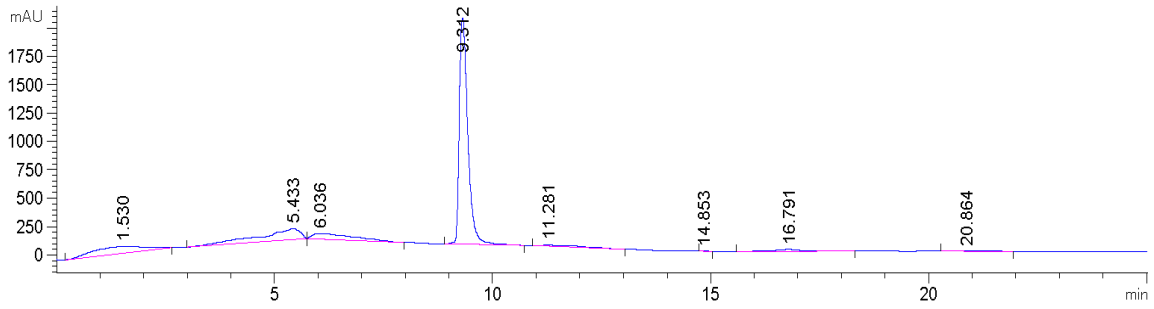

Figure S17. Analytical HPLC trace of **168** (YMC-Triart C18 column, 150 x 4.6 mm, flow rate = 0.8 mL·min^{-1}) with a linear gradient from 30:70 (0.1% TFA in H_2O:MeOH, v:v) to 05:95 (0.1% TFA in H_2O:MeOH, v:v) over 10 minutes.

Boc-Gly-Asn(Trt)-Leu-Trp(Boc)-Ala-Thr(^{t}Bu)-Gly-His(Trt)-Phe(4-F)-Met-OH (169)

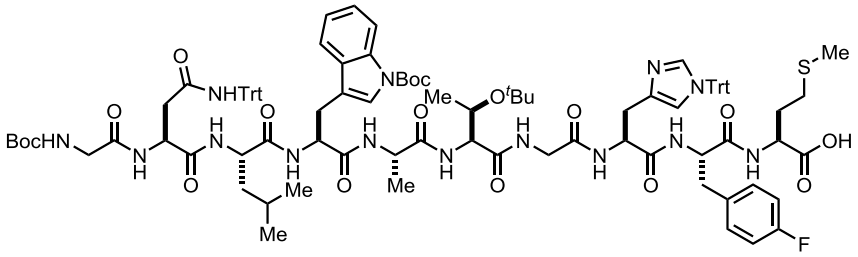

169 (86%)

The peptide was synthesized according to the general procedure for peptide synthesis starting with 1.0 mmol Fmoc-Met-O-2CT resin. The beige residue was purified by HPLC with an YMC-Actus Triart C18 column ((30×150 mm, 5 µm + 30×50 mm, 5 µm), flow rate = 42.5 mL·min^{-1}, 35 °C) with a linear gradient from 20:80 (0.1% TFA in H_2O:MeOH, v:v) to 03:97 (0.1% TFA in H_2O:MeOH, v:v) over 6 minutes. The collected fractions containing the product (t ≈ 7.5 min) were combined, neutralized to pH 7 with saturated aqueous sodium bicarbonate solution, diluted with 100 mL brine and the resulting solution was concentrated by rotary evaporation (100 mbar, 35 °C) until no more methanol was evaporated. The suspension was extracted with dichloromethane (3 × 100 mL), and the combined organic layers were dried over sodium sulfate, filtered, and concentrated *in vacuo* to dryness to afford **169** as a colorless solid (1.6 g, 0.86 mmol, 86% yield).

HRMS-ESI (m/z) calc'd for $C_{104}H_{122}FN_{14}O_{17}S$ $[M-H]^-$, 1889.88226; found, 1889.88141; deviation: 0.45 ppm.

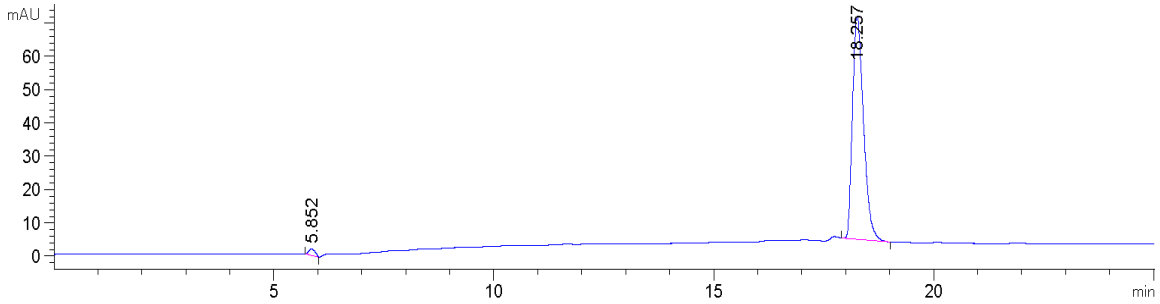

Figure S18. Analytical HPLC trace of **169** (YMC-Triart C18 column, 150 x 4.6 mm, flow rate = 0.8 mL·min^{-1}) with a linear gradient from 30:70 (0.1% TFA in H_2O:MeOH, v:v) to 05:95 (0.1% TFA in H_2O:MeOH, v:v) over 10 minutes.

Boc-Gly-Asn(Trt)-Leu-Trp(Boc)-Ala-Thr(^{t}Bu)-Gly-His(Trt)-Phe(4-F)-Met-NHTmob (170)

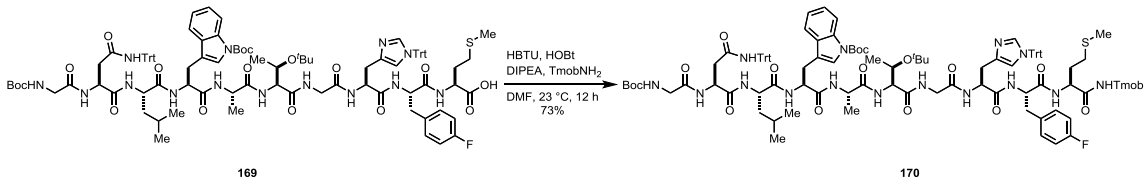

A 50 mL round-bottom flask equipped with a magnetic stirring bar was charged with **169** (1.6 g, 0.86 mmol, 1.0 equiv), HOBt (0.12 g, 0.89 mmol, 1.0 equiv), $TmobNH_2$ (0.18 mg, 0.89 mmol, 1.0 equiv), DIPEA (0.50 mL, 0.37 g, 2.9 mmol, 3.4 equiv), and DMF (43 mL, 18 mmol·L^{-1}). The reaction mixture was cooled to 0 °C and then HBTU (0.34 g, 0.89 mmol, 1.0 equiv) was added. The reaction mixture was allowed to warm to 23 °C and was stirred at 23 °C for 12 hours. The solution was concentrated by rotary evaporation to 5 mL and was afterwards diluted with ethyl acetate (50 mL). The solution was extracted with water (2 × 30 mL), and the combined aqueous layers were extracted with ethyl acetate (10 mL). The combined organic layers were dried over sodium sulfate, filtered, and concentrated *in vacuo* to dryness. The beige residue was purified by HPLC on an YMC-Actus Triart C18 column ((30×150 mm, 5 µm + 30×50 mm, 5 µm), flow rate = 42.5 mL·min^{-1}, 35 °C) with a linear gradient from 20:80 (0.1% TFA in H_2O:MeOH, v:v) to 03:97 (0.1% TFA in H_2O:MeOH, v:v) over 10 minutes. The collected fractions containing the product (t ≈ 7.5 min) were combined, basified to pH 8 with saturated aqueous sodium bicarbonate

solution, diluted with 100 mL brine and the resulting solution was concentrated by rotary evaporation (100 mbar, 35 °C) until no more methanol was evaporated. The suspension was extracted with dichloromethane (3 × 100 mL), and the combined organic layers were dried over sodium sulfate, filtered, and concentrated *in vacuo* to dryness to afford **170** as a colorless powder (1.3 g, 0.63 mmol, 73% yield).

HRMS-ESI (m/z) calc'd for $C_{114}H_{135}FN_{15}O_{19}S$ $[M-H]^-$, 2068.97689; found, 2068.97487; deviation: 0.98 ppm.

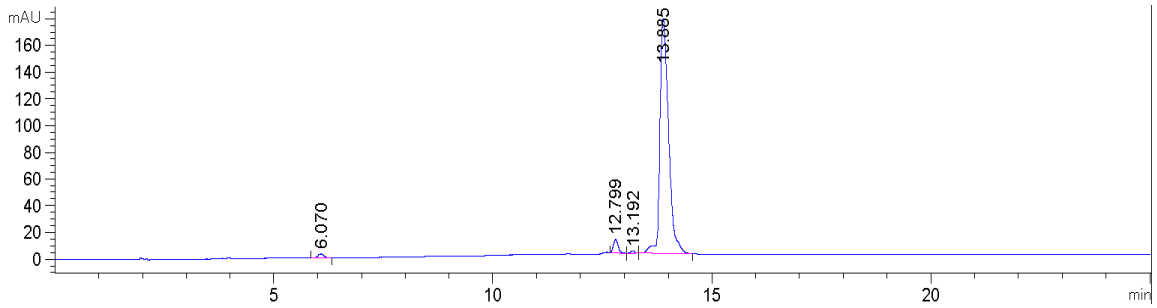

Figure S19. Analytical HPLC trace of **170** (YMC-Triart C18 column, 150 x 4.6 mm, flow rate = 0.8 mL·min^{-1}) with a linear gradient from 30:70 (0.1% TFA in H_2O:MeOH, v:v) to 05:95 (0.1% TFA in H_2O:MeOH, v:v) over 10 minutes.

[H-Gly-Asn-Leu-Trp-Ala-Thr-Gly-His-Phe(4-F)-Met-NH_2]·4CF_3CO_2H ([^{19}F]150)

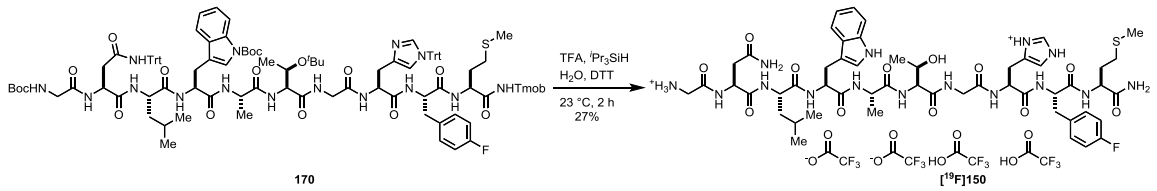

A vial (4 mL) equipped with a Teflon-coated magnetic stirring bar was charged with TFA (6.8 mL, 10 g), DTT (0.58 g, 3.7 mmol, 6.4 equiv), water (0.58 mL, 0.58 g, 32 mmol, 55 equiv), and triisopropylsilane (0.28 mL, 0.22 g, 1.4 mmol, 2.4 equiv). Linear peptide **170** (1.2 g, 0.58 µmol, 1.0 equiv) was added to the emulsion, and the reaction mixture was stirred at 23 °C for 2 hours. The product was precipitated by addition to rapidly stirring Et_2O (100 mL), and the off-white solid was collected by filtration. The solid was purified by HPLC on an YMC-Actus Triart C18 column ((30×150 mm, 5 µm + 30×50 mm, 5 µm), flow rate = 42.5 mL·min^{-1}, 35 °C) with a linear gradient from 50:50 (0.1% TFA in H_2O:MeOH, v:v) to 25:75 (0.1% TFA in H_2O:MeOH, v:v)

over 10 minutes. The collected fractions containing the product (t ≈ 5.0 min) were combined and concentrated *in vacuo* to dryness to afford **[^{19}F]150** as a colorless solid (0.25 mg, 0.16 mmol, 27% yield).

NMR Spectroscopy:

^{1}H NMR (500 MHz, CD_3OD, 25 ºC, δ): 8.33 (d, *J* = 2.8 Hz, 1H), 7.56 (d, *J* = 7.8 Hz, 1H), 7.28 (d, *J* = 8.1 Hz, 1H), 7.27–7.20 (m, 3H), 7.19 (s, 1H), 7.07 (ddd, *J* = 8.1, 6.9, 1.2 Hz, 1H), 7.05–6.92 (m, 4H), 4.78 (dd, *J* = 8.6, 5.0 Hz, 1H), 4.58–4.39 (m, 3H), 4.30–4.18 (m, 2H), 4.18–4.03 (m, 2H), 3.81 (q, *J* = 16.8 Hz, 2H), 3.72 (s, 2H), 3.48–3.32 (m, 2H), 3.18 (m, 2H), 3.04–2.96 (m, 2H), 2.88 (dd, *J* = 15.5, 8.7 Hz, 1H), 2.76 (dd, *J* = 15.5, 5.0 Hz, 1H), 2.58–2.36 (m, 2H), 2.16–1.89 (m, 5H), 1.62 (dt, *J* = 13.0, 6.5 Hz, 1H), 1.50–1.36 (m, 5H), 1.24 (d, *J* = 6.5 Hz, 3H), 0.82 (dd, *J* = 23.8, 6.5 Hz, 3H).

^{13}C{^{1}H} NMR (126 MHz, CD_3OD, 25 ºC, δ): 176.4, 176.1, 176.0, 175.8, 174.4 174.0, 174.0_2, 174.0_0, 173.2, 171.9, 167.2, 163.3 ($^{1}J_{C\text{-}F}$ = 244 Hz), 138.1, 134.6, 134.2 ($^{4}J_{C\text{-}F}$ = 3 Hz), 132.1 ($^{3}J_{C\text{-}F}$ = 243 Hz), 130.9, 128.7, 124.8, 122.6, 120.0, 119.2, 118.6, 116.2 ($^{2}J_{C\text{-}F}$ = 22 Hz), 112.5, 111.1, 68.0, 62.5, 57.7, 56.9, 55.6, 54.2, 53.9, 52.3, 51.6, 44.4, 41.7, 41.1, 37.9, 37.4, 32.6, 31.2, 27.8, 27.5, 25.8, 23.1, 22.0, 20.3, 17.2, 15.3. One carbon resonance is not observed, presumably due to overlap with a solvent carbon resonance.

^{19}F NMR (471 MHz, CD_3OD, 25 ºC, δ): −78.0, −118.8.

HRMS-ESI (m/z) calc'd for $C_{52}H_{73}F_1N_{15}O_{12}S_1$ $[M-3CF_3CO_2H-CF_3CO_2]^+$, 1150.52623; found, 1150.52721; deviation: −0.85 ppm.

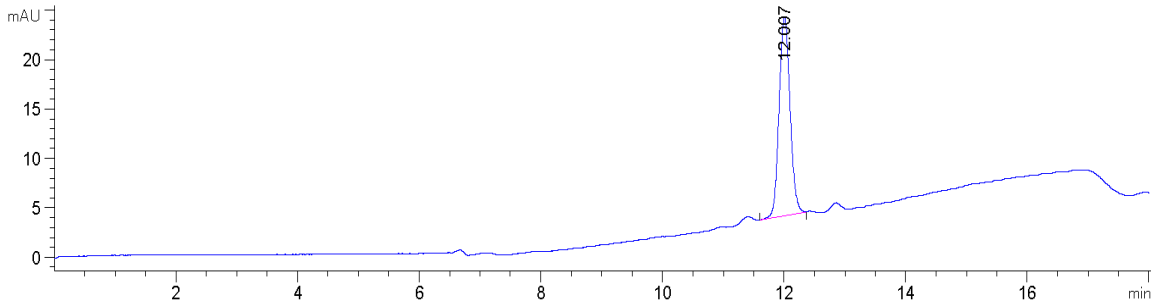

Figure S20. Analytical HPLC trace of **[^{19}F]150** (YMC-Triart C18 column, 150 x 4.6 mm, flow rate = 0.8 mL·min^{-1}) with a linear gradient from 50:50 (0.1% TFA in H_2O:MeOH, v:v) to 10:90 (0.1% TFA in H_2O:MeOH, v:v) over 10 minutes.

[Boc-Gly-Asn(Trt)-Leu-Trp(Boc)-Ala-Thr(^{t}Bu)-Gly-His(Trt)-Tyr(RuCp)-Met-OH]·CF_3CO_2 (171)

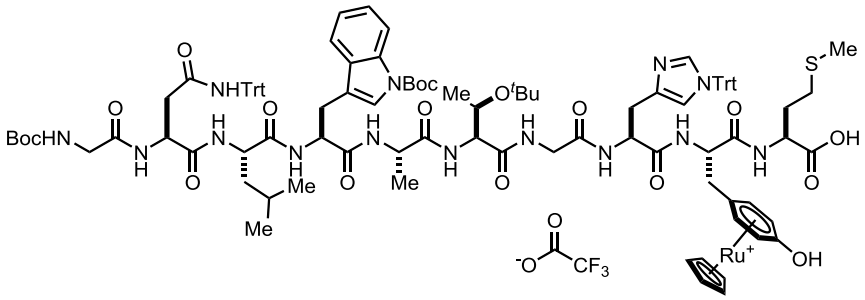

171 (62%)

The peptide was synthesized according to the general procedure for peptide synthesis starting with 1.0 mmol Fmoc-Met-O-2CT resin. The beige residue was purified by HPLC with an YMC-Actus Triart C18 column ((30×150 mm, 5 µm + 30×50 mm, 5 µm), flow rate = 42.5 mL·min^{-1}, 35 °C) with a linear gradient from 27:63 (0.1% TFA in H_2O:MeOH, v:v) to 03:97 (0.1% TFA in H_2O:MeOH, v:v) over 10 minutes. The collected fractions containing the product (t ≈ 7.5 min) were combined, neutralized to pH 7 with saturated aqueous sodium bicarbonate solution, diluted with 100 mL brine, and the resulting solution was concentrated by rotary evaporation (100 mbar, 35 °C) until no more methanol was evaporated. The suspension was extracted with dichloromethane (3 × 100 mL), and the combined organic layers were dried over sodium sulfate, filtered, and concentrated *in vacuo* to dryness to afford **171** as a colorless solid (1.4 g, 0.62 mmol, 62% yield).

HRMS-ESI (m/z) calc'd for $C_{109}H_{120}O_{18}N_{14}SRu$ $[M-CF_3CO_2]^+$, 2055.83680; found, 2055.84021; deviation: −1.66 ppm.

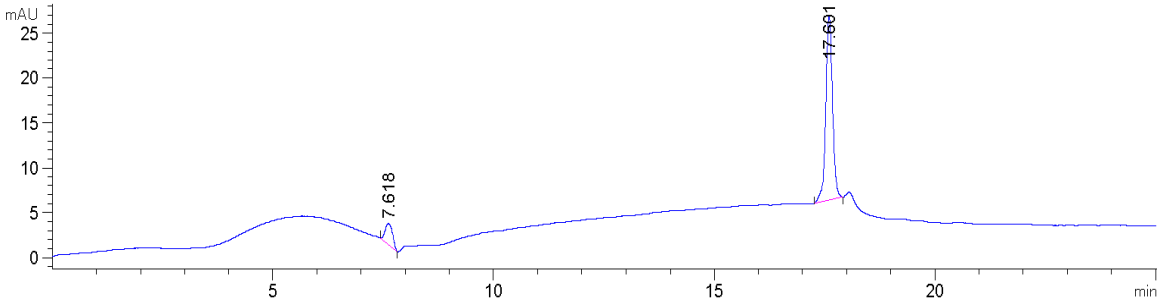

Figure S21. Analytical HPLC trace of **171** (YMC-Triart C18 column, 150 x 4.6 mm, flow rate = 0.8 mL·min^{-1}) with a linear gradient from 30:70 (0.1% TFA in H_2O:MeOH, v:v) to 05:95 (0.1% TFA in H_2O:MeOH, v:v) over 10 minutes.

[Boc-Gly-Asn(Trt)-Leu-Trp(Boc)-Ala-Thr(ᵗBu)-Gly-His(Trt)-Tyr(RuCp)-Met-NHTmob]·CF_3CO_2 (172)

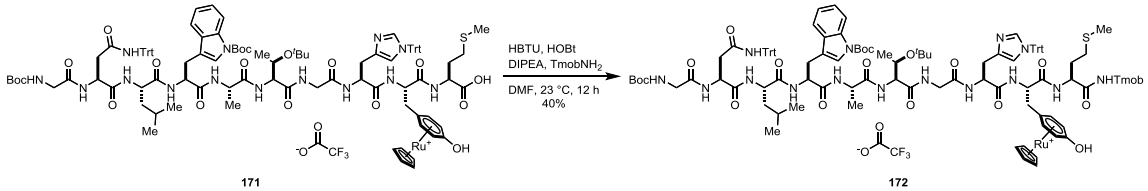

A 50 mL round-bottom flask equipped with a magnetic stirring bar was charged with **171** (1.3 g, 0.59 mmol, 1.0 equiv), HOBt (88 mg, 0.65 mmol, 1.1 equiv), $TmobNH_2$ (0.13 g, 0.65 mmol, 1.1 equiv), DIPEA (0.34 mL, 0.25 g, 2.0 mmol, 3.3 equiv), and DMF (30 mL, 20 mmol·L^{-1}). The reaction mixture was cooled to 0 °C and then HBTU (0.25 g, 0.65 mmol, 1.1 equiv) was added. The reaction mixture was allowed to warm to room temperature and was stirred at 23 °C for 12 hours. The solution was concentrated by rotary evaporation to 5 mL, and afterwards diluted with ethyl acetate (50 mL). The solution was extracted with water (2 × 30 mL), and the combined aqueous layers were extracted with ethyl acetate (10 mL). The combined organic layers were concentrated *in vacuo* to dryness. The beige residue was purified by HPLC on an YMC-Actus Triart C18 column ((30×150 mm, 5 µm + 30×50 mm, 5 µm), flow rate = 42.5 mL·min^{-1}, 35 °C) with a linear gradient from 17:83 (0.1% TFA in H_2O:MeOH, v:v) to 14:86 (0.1% TFA in H_2O:MeOH, v:v) over 10 minutes. The collected fractions containing the product (t ≈ 9.3 min) were combined, basified to pH 8 with saturated aqueous sodium bicarbonate solution, diluted with

100 mL brine and the resulting solution was concentrated by rotary evaporation (100 mbar, 35 °C) until no more methanol was evaporated. The suspension was extracted with dichloromethane (3 × 100 mL), and the combined organic layers were dried over sodium sulfate, filtered, and concentrated *in vacuo* to dryness to afford **172** as a colorless powder (0.56 g, 0.24 mmol, 40% yield).

NMR Spectroscopy:

^{1}H NMR (500 MHz, CD_3OD, 25 ºC, δ): 8.88, (s, 1H), 8.50 (br, 1H), 8.38 (br, 1H), 8.11 (d, *J* = 7.6 Hz, 1H), 8.08–8.01 (m, 2H), 7.93 (d, *J* = 7.7 Hz, 1H), 7.77 (d, *J* = 6.1 Hz, 1H), 7.63 (d, *J* = 6.8 Hz, 1H), 7.59 (t, *J* = 4.8 Hz, 1H), 7.47–7.34 (m, 6H), 7.32–7.24 (m, 2H), 7.22–7.13 (m, 25H), 6.14 (s, 2H), 6.10–5.99 (m, 4H), 5.28 (s, 5H), 4.61 (dd, *J* = 9.2, 4.3 Hz, 1H), 4.57 (dd, *J* = 9.2, 4.5 Hz, 1H), 4.46 (t, *J* = 6.4 Hz, 1H), 4.43–4.28 (m, 5H), 4.26–4.16 (m, 2H), 4.14 (dd, *J* = 6.3, 3.5 Hz, 1H), 4.06 (dt, *J* = 9.8, 4.9 Hz, 1H), 3.81–3.76 (m, 2H), 3.75 (s, 6H), 3.72 (s, 3H), 3.67 (s, 2H), 3.14 (dd, *J* = 15.8, 4.5 Hz, 1H), 3.10–3.03 (m, 1H), 2.98–2.91 (m, 3H), 2.87–2.83 (m, 1H), 2.80–2.74 (m, 1H), 2.48 (t, *J* = 13.5 Hz, 1H), 2.36 (t, *J* = 8.1 Hz, 2H), 2.02 (s, 3H), 1.83 (dq, *J* = 14.3, 8.0 Hz, 1H), 1.68 (s, 9H), 1.53 (td, *J* = 9.5, 9.1, 3.5 Hz, 1H), 1.46 (d, *J* = 7.1 Hz, 3H), 1.39 (s, 9H), 1.20–1.14 (m, 12H), 0.88 (d, *J* = 6.6 Hz, 3H), 0.81 (d, *J* = 6.5 Hz, 3H).

^{13}C{^{1}H} NMR (126 MHz, CD_3OD, 25 ºC, δ): 176.0, 175.4, 174.5, 174.3, 173.8, 172.6, 172.3, 171.9, 171.7, 171.6, 171.5, 162.8, 160.9, 158.6, 151.0, 145.7, 141.6, 134.5, 131.5, 130.8, 130.1 129.9, 129.8, 129.3, 128.8, 128.7, 128.6, 128.0, 127.9, 125.6, 123.7, 120.2, 118.3, 116.2, 106.6, 98.8, 91.6, 87.2, 87.0, 85.1, 81.3, 80.9, 79.8, 76.1, 76.0, 75.7, 71.7, 67.8, 61.6, 56.3, 55.9, 55.6, 55.4, 54.0, 53.7, 51.9, 51.8, 44.8, 44.3, 40.8, 38.9, 36.5, 33.5, 32.8, 31.0, 30.7, 28.9, 28.8, 28.7, 28.6, 26.8, 25.8, 23.4, 22.0, 20.4, 17.5, 15.2. One carbon resonance is not observed, presumably due to overlap with a solvent carbon resonance.

^{19}F NMR (471 MHz, CD_3OD, 25 ºC, δ): −77.4.

HRMS-ESI (m/z) calc'd for $C_{119}H_{142}N_{15}O_{20}RuS$ $[M\text{-}CF_3CO_2]^+$, 2234.93143; found, 2234.93487; deviation: −1.54 ppm.

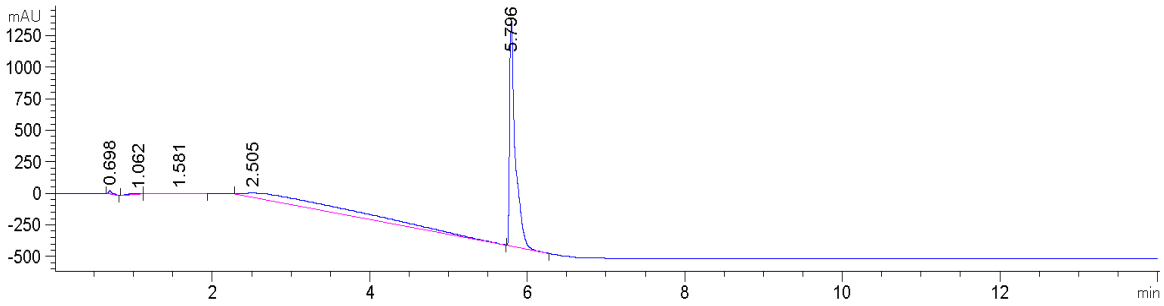

Figure S22. Analytical HPLC trace of **172** (Agilent Poroshell 120, 50 x 3.0 mm, flow rate = 1 mL·min^{-1}) with a linear gradient from 100:0 (0.1% TFA in H_2O:MeOH, v:v) to 05:99 (0.1% TFA in H_2O:MeOH, v:v) over 5 minutes.

[H-Phe(4-F)-Ile-Cys-Val-Gln-Pro-Ser-Phe-OH]·CF_3CO_2H ([^{19}F]151)

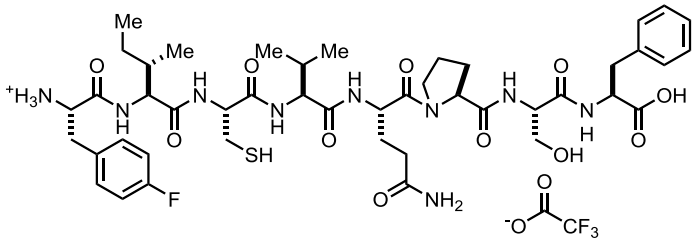

[^{19}F]151 (12%)

The peptide was synthesized according to the general procedure for peptide synthesis starting with 1.0 mmol Fmoc-Phe-O-2CT resin. To the beige residue was added a mixture of TFA (6.8 mL, 10 g), DTT (0.58 g, 3.7 mmol, 3.7 equiv), water (0.58 mL, 0.58 g, 32 mmol, 32 equiv), and triisopropylsilane (0.29 mL, 0.22 g, 1.4 µmol, 1.4 equiv), and the reaction mixture was stirred at 23 °C for 2 hours. The reaction mixture was added dropwise into a round-bottom flask (100 mL) containing vigorously stirred diethyl ether (80 mL). The resulting suspension was filtered and the filter cake was purified by HPLC on an YMC-Actus Triart C18 column ((30×150 mm, 5 µm + 30×50 mm, 5 µm), flow rate = 42.5 mL·min^{-1}, 35 °C) with a linear gradient from 27:73 (0.1% TFA in H_2O:MeOH, v:v) to 03:97 (0.1% TFA in H_2O:MeOH, v:v) over 10 minutes. The collected fractions containing the product (t ≈ 7.5 min) were combined and concentrated *in vacuo* to dryness to afford **[^{19}F]151** as a colorless solid (0.13 g, 0.12 mmol, 12% yield).

NMR Spectroscopy:

^{1}H NMR (500 MHz, $(CD_3)_2SO$, 25 ºC, δ): 8.57 (d, *J* = 8.7 Hz, 1H), 8.35 (d, *J* = 7.9 Hz, 1H), 8.17 (d, *J* = 5.6 Hz, 1H), 8.15–8.05 (m, 2H), 7.92 (dd, *J* = 13.0, 7.8 Hz, 1H), 7.85 (d, *J* = 8.7

Hz, 1H), 7.28–7.23 (m, 4H), 7.22–7.18 (m, 3H), 7.17–7.11 (m, 2H), 6.80 (s, 1H), 4.53–4.40 (m, 3H), 4.36 (dd, *J* = 8.5, 3.8 Hz, 1H), 4.30 (td, *J* = 8.5, 6.0 Hz, 1H), 4.25 (td, *J* = 5.7, 2.3 Hz, 1H), 4.18 (d, *J* = 8.7, 6.3 Hz, 1H), 4.14–4.07 (m,1H), 3.70–3.57 (m, 1H), 3.54 (dd, *J* = 5.8, 2.7 Hz, 2H), 3.04 (ddd, *J* = 13.5, 8.0, 5.5 Hz, 2H), 2.93 (dd, *J* = 13.9, 7.8 Hz, 2H), 2.78 (ddd, *J* = 13.8, 8.9, 5.3 Hz, 1H) 2.71–2.65 (m, 1H), 2.29 (t, *J* = 8.4 Hz, 1H), 2.18–2.09 (m, 2H), 2.02–1.92 (m, 2H), 1.90–1.84 (m, 2H), 1.83–1.75 (m, 2H), 1.49 (dp, *J* = 10.8, 3.3 Hz, 1H), 1.09 (ddd, *J* = 13.3, 9.3, 7.0 Hz, 1H), 0.83 (ddd, *J* = 17.7, 11.9, 6.7 Hz, 12H).

^{13}C{^{1}H} NMR (126 MHz, $(CD_3)_2SO$, 25 ºC, δ): 173.9, 172.6 171.6, 170.6, 170.5, 169.9_0, 169.8_4, 169.5, 167.7. 161.5 ($^{1}J_{C-F}$ = 243 Hz), 137.2, 131.6 ($^{4}J_{C-F}$ = 8 Hz), 130.8 ($^{3}J_{C-F}$ = 3 Hz), 129.2, 128.2, 126.5, 115.3 ($^{2}J_{C-F}$ = 21 Hz), 61.6, 59.2, 57.4, 57.0, 55.2, 55.1, 53.4, 53.1, 49.9, 46.9, 37.0, 36.8, 36.1, 30.9, 30.7, 29.2, 27.1, 26.0, 24.3, 24.4, 19.1, 17.9, 15.2, 11.1.

^{19}F NMR (471 MHz, $(CD_3)_2SO$, 25 ºC, δ): −74.0, −116.4.

HRMS-ESI (m/z) calc'd for $C_{45}H_{63}FN_9O_{11}S$ $[M-H-CF_3CO_2H]^-$, 956.43573; found, 956.43639; deviation: −0.69 ppm.

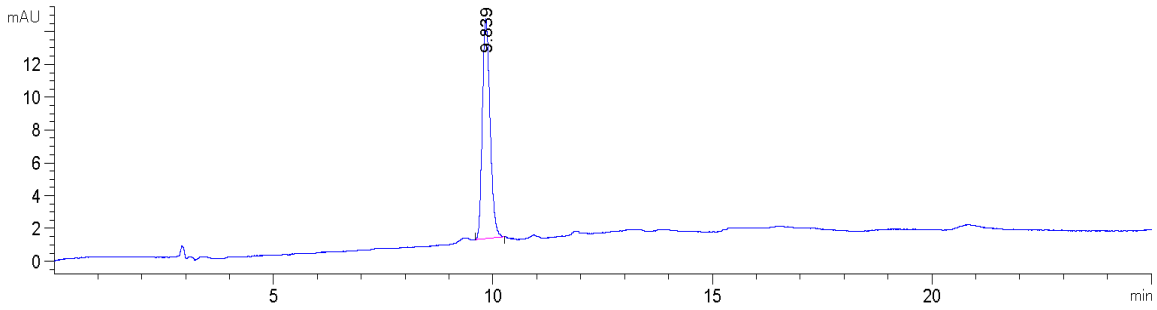

Figure S23. Analytical HPLC trace of **[^{19}F]151** (YMC-Triart C18 column, 150 x 4.6 mm, flow rate = 0.8 mL·min^{-1}) with a linear gradient from 50:50 (0.1% TFA in H_2O:MeOH, v:v) to 25:75 (0.1% TFA in H_2O:MeOH, v:v) over 10 minutes.

[Boc-Tyr(RuCp)-Ile-Cys(Trt)-Val-Gln(Trt)-Pro-Ser(^{t}Bu)-Phe-OH]·CF_3CO_2 (173)

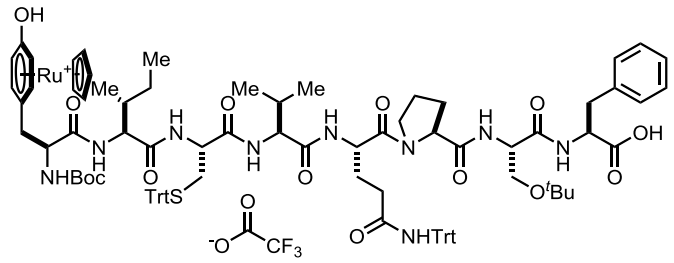

173 (14%)

The peptide was synthesized according to the general procedure for peptide synthesis starting with 1.0 mmol Fmoc-Phe-O-2CT resin. The beige residue was purified by HPLC with an YMC-Actus Triart C18 column ((30×150 mm, 5 µm + 30×50 mm, 5 µm), flow rate = 42.5 mL·min^{-1}, 35 °C) with a linear gradient from 25:75 (0.1% TFA in H_2O:MeOH, v:v) to 15:85 (0.1% TFA in H_2O:MeOH, v:v) over 10 minutes. The collected fractions containing the product (t ≈ 6.5 min) were combined, neutralized to pH 7 with saturated aqueous sodium bicarbonate solution, diluted with 100 mL brine, and the resulting solution was concentrated by rotary evaporation (100 mbar, 35 °C) until no more methanol was evaporated. The suspension was extracted with dichloromethane (3 × 100 mL), and the combined organic layers were dried over sodium sulfate, filtered, and concentrated *in vacuo* to dryness to afford **173** as a colorless solid (0.25 g, 0.14 mmol, 14% yield).

NMR Spectroscopy:

^{1}H NMR (500 MHz, CD_3OD, 25 ºC, δ): 7.46–7.32 (m, 6H), 7.32–7.07 (m, 29H), 6.05–5.72 (m, 4H), 5,04 (s, 5H), 4.63 (t, *J* = 6.0 Hz, 1H), 4.51–4.38 (m, 4H), 4.29 (d, *J* = 4.6 Hz, 1H), 4.27 (d, *J* = 4.8 Hz, 1H), 4.17 (t, *J* = 7.6 Hz, 1H), 3.66–3.60 (m, 1H), 3.60–3.53 (m, 3H), 3.28–3.22 (m, 1H), 3.15 (dd, *J* = 13.7, 5.6 Hz, 1H), 3.06 (dd, *J* = 13.8, 6.5 Hz, 1H), 2.75 (dd, *J* = 14.1, 3.5 Hz, 1H), 2.62–2.45 (m, 3H), 2.38 (dt, *J* = 14.9, 7.7 Hz, 2H), 2.19–2.07 (m, 1H), 2.08–1.68 (m, 6H), 1.40 (s, 9H), 1.29 (br, 2H), 1.09 (s, 9H), 0.95–0.80 (m, 12H).

^{13}C{^{1}H} NMR (126 MHz, CD_3OD, 25 ºC, δ):174.2$_2$, 174.1$_8$, 173.1, 172.9, 172.6, 172.2, 171.7$_0$, 171.6$_6$, 157.6, 146.0$_4$, 145.9$_7$, 138.1, 138.1, 130.7, 130.6, 130.1, 129.5, 129.2, 128.9, 128.0, 127.8, 98.1, 87.1, 86.7, 81.1, 80.6$_4$, 80.6$_2$, 76.0, 75.8, 74.8, 68.0, 62.8, 61.6, 59.6, 59.0,

57.1, 55.0, 53.7, 51.7, 38.6, 38.5, 37.3, 33.5, 32.4, 30.9, 30.8, 29.0, 28.7, 27.8, 25.8, 25.7, 19.7, 19.0, 16.0, 11.6. Two carbon resonances are not observed, presumably due to overlap with a solvent carbon resonance.

^{19}F NMR (471 MHz, CD_3OD, 25 ºC, δ): −77.6.

HRMS-ESI (m/z) calc'd for $C_{97}H_{112}O_{14}N_9RuS$ $[M-H-CF_3CO_2H]^-$, 1760.70984; found, 1760.71274; deviation: −1.65 ppm.

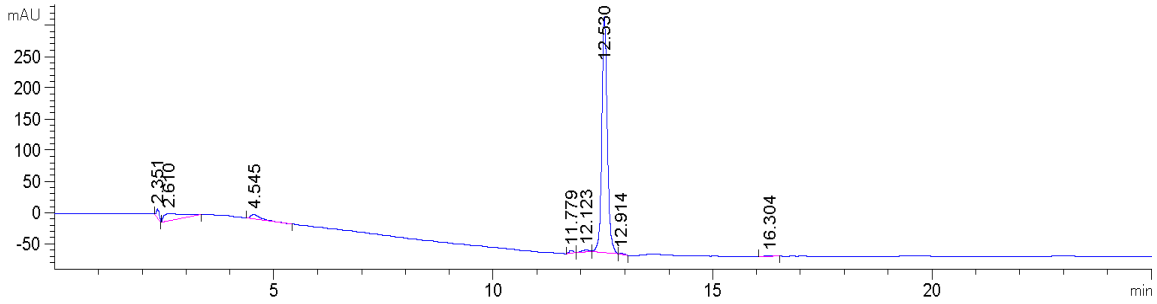

Figure S24. Analytical HPLC trace of **173** (YMC-Triart C18 column, 150 x 4.6 mm, flow rate = 0.8 mL·min^{-1}) with a linear gradient from 30:70 (0.1% TFA in H_2O:MeOH, v:v) to 05:95 (0.1% TFA in H_2O:MeOH, v:v) over 10 minutes.

[Boc-Tyr(RuCp)-Ile-Cys(Trt)-Val-Gln(Trt)-Pro-Ser(^{t}Bu)-Phe-OPMB]·CF_3CO_2 (174)

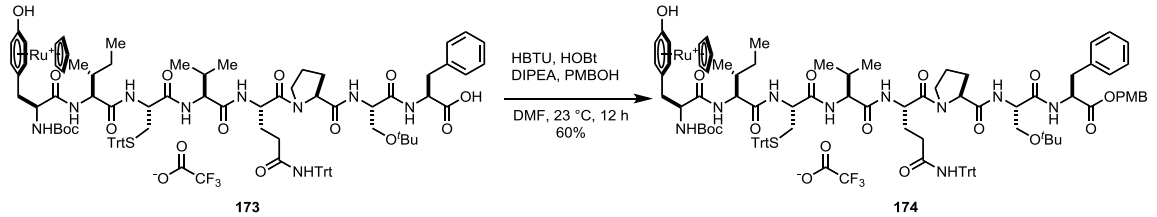

A round-bottom flask (25 mL) equipped with a Teflon-coated magnetic stirring bar was charged with **173** (0.15 g, 80 µmol, 1.0 equiv), HOBt (13 mg, 96 µmol, 1.2 equiv), PMBOH (0.10 mL, 0.11 g, 0.80 mmol, 10 equiv), DIPEA (50 µL, 37 mg, 0.29 mmol, 3.6 equiv) and DMF (4.3 mL, 20 mmol·L^{-1}). The reaction mixture was cooled to 0 °C and then HBTU (33 mg, 88 µmol, 1.1 equiv) was added. The reaction mixture was allowed to warm to room temperature and was stirred at 23 °C for 12 hours. The reaction mixture was cooled to 0 °C and then HBTU (33 mg, 88 µmol, 1.1 equiv) was added. The reaction mixture was allowed to warm to room temperature and was stirred at 23 °C for 3 hours. The solution was diluted with ethyl acetate (50 mL). The solution was extracted with water (2 × 30 mL), and the combined aqueous layers were extracted with ethyl

acetate (10 mL). The combined organic layers were dried over sodium sulfate, filtered, and concentrated *in vacuo* to dryness. The beige residue was purified by HPLC on an YMC-Actus Triart C18 column ((30×150 mm, 5 µm + 30×50 mm, 5 µm), flow rate = 42.5 mL·min^{-1}, 35 °C) with a linear gradient from 25:75 (0.1% TFA in H_2O:MeOH, v:v) to 03:97 (0.1% TFA in H_2O:MeOH, v:v) over 10 minutes. The collected fractions containing the product (t ≈ 8.5 min) were combined, basified to pH 10 with saturated aqueous sodium bicarbonate solution, diluted with 100 mL brine and the resulting solution was concentrated by rotary evaporation (100 mbar, 35 °C) until no more methanol was evaporated. The suspension was extracted with dichloromethane (3 × 50 mL), and the combined organic layers were dried over sodium sulfate, filtered, and concentrated *in vacuo* to dryness to afford **174** a colorless powder (96 mg, 48 µmol, 60% yield).

NMR Spectroscopy:

^{1}H NMR (500 MHz, CD_3OD, 25 ºC, δ): 7.40–7.34 (m, 6H), 7.28–7.14 (m, 29H), 7.13–7.09 (m, 2H), 6.89–6.84 (m, 2H), 5.68–5.62 (m, 2H), 5.40–5.30 (m, 2H), 5.04–5.00 (m, 2H), 4.92–4.88 (m, 5H), 4.69–4.61 (m, 1H), 4.45–4.38 (m, 3H), 4.36–4.30 (m, 1H), 4.29–4.20 (m, 2H), 4.20–4.14 (m, 1H), 3.76 (m, 3H), 3.58–3.51 (m, 1H), 3.50–3.41 (m, 2H), 3.11 (dd, *J* = 13.9, 5.9 Hz, 1H), 3.06–2.96 (m, 1H), 2.69 (dd, *J* = 14.6, 4.3 Hz, 1H), 2.59–2.45 (m, 3H), 2.36 (dt, *J* = 14.8, 7.4 Hz, 1H), 2.15–1.71 (m, 8H), 1.57–1.50 (m, 1H) 1.40 (s, 9H),1.39–1.34 (m, 2H) 1.29 (br, 2H), 1.06 (s, 2H), 1.09 (s, 9H), 0.93–0.80 (m, 12H).

^{13}C{^{1}H} NMR (126 MHz, CD_3OD, 25 ºC, δ):174.0_8, 174.0_6, 173.3, 173.0, 172.6_6, 172.5_4, 172.5_0, 171.9, 171.8, 161.3, 157.7, 150.5, 146.1, 146.0, 137.8, 131.5, 131.4, 130.7, 130.4, 130.1, 129.6, 129.2, 128.9, 128.8, 128.0, 127.9, 127.8, 114.9, 94.6, 87.3, 86.8, 81.0, 78.8, 76.1, 75.9, 74.8, 74.7, 71.5, 68.02, 67.96, 62.7, 62.0, 59.7, 59.0, 57.3, 55.8, 55.5, 55.0, 53.7, 51.8, 38.7, 38.5, 37.5, 34.8, 33.6, 32.3, 30.7, 28.8, 27.8, 25.8, 19.7, 18.9, 16.0, 11.6.

^{19}F NMR (471 MHz, CD_3OD, 25 ºC, δ): −80.8.

HRMS-ESI (m/z) calc'd for $C_{105}H_{123}O_{15}N_9RuS$ $[M-CF_3CO_2]^+$, 1883.78974; found, 1883.79122; deviation: −0.79 ppm.

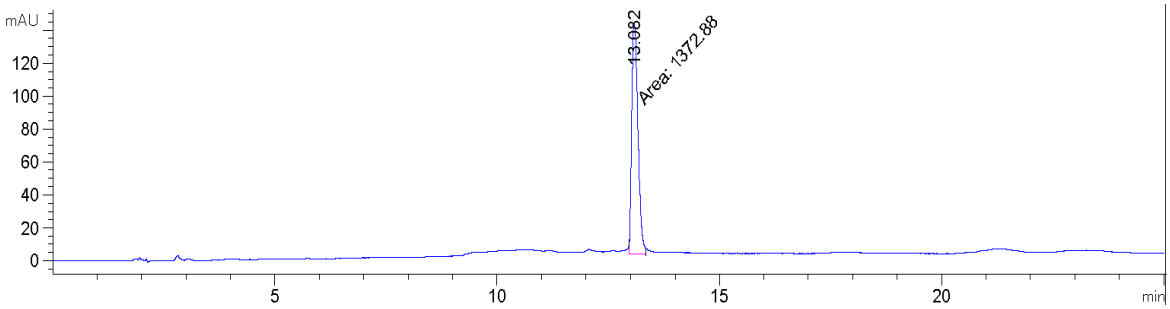

Figure S25. Analytical HPLC trace of **174** (YMC-Triart C18 column, 150 x 4.6 mm, flow rate = 0.8 mL·min^{-1}) with a linear gradient from 30:70 (0.1% TFA in H_2O:MeOH, v:v) to 05:95 (0.1% TFA in H_2O:MeOH, v:v) over 10 minutes.

Boc-Leu-(4-F-Phe)-Glu(^{t}Bu)-Met-Lys(Boc)-OH (175)

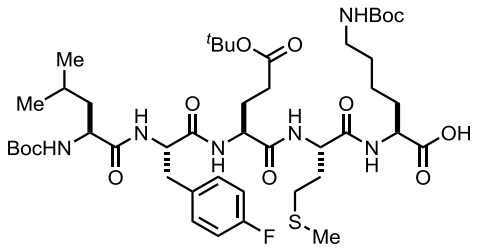

175 (55%)

The peptide was synthesized according to the general procedure for peptide synthesis starting with 0.88 mmol Fmoc-Lys-O-2CT resin. The beige residue was purified by HPLC with an YMC-Actus Triart C18 column ((30×150 mm, 5 µm + 30×50 mm, 5 µm), flow rate = 42.5 mL·min^{-1}, 35 °C) with a linear gradient from 20:80 (0.1% TFA in H_2O:MeOH, v:v) to 03:97 (0.1% TFA in H_2O:MeOH, v:v) over 6 minutes. The collected fractions containing the product (t ≈ 7.5 min) were combined, neutralized to pH 7 with saturated aqueous sodium bicarbonate solution, diluted with 100 mL brine and the resulting solution was concentrated by rotary evaporation (100 mbar, 35 °C) until no more methanol was evaporated. The suspension was extracted with dichloromethane (3 × 100 mL), and the combined organic layers were dried over sodium sulfate, filtered, and concentrated *in vacuo* to dryness to afford **175** as a colorless solid (0.45 mg, 0.48 mmol, 55% yield).

HRMS-ESI (m/z) calc'd for $C_{45}H_{73}O_{12}N_6FSNa$ $[M+Na]^+$, 963.4883; found 963.4884; deviation: −0.08 ppm.

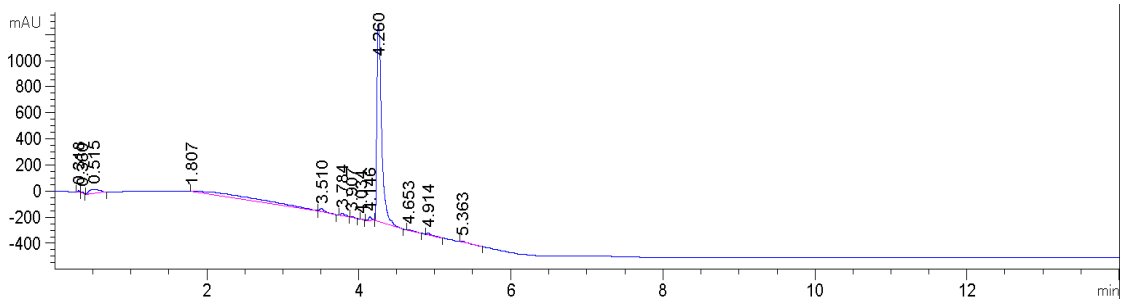

Figure S26. Analytical HPLC trace of 175 (Agilent Poroshell 120, 50 x 3.0 mm, flow rate = 1 mL·min^{-1}) with a linear gradient from 100:0 (0.1% TFA in H_2O:MeOH, v:v) to 05:95 (0.1% TFA in H_2O:MeOH, v:v) over 5 minutes.

Boc-Leu-(4-F-Phe)-Glu(^{t}Bu)-Met-Lys(Boc)-NHTmob ([^{19}F]143)

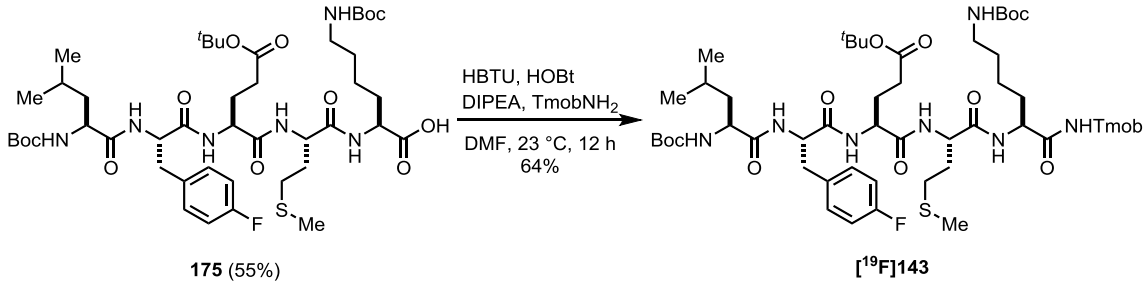

175 (55%) **[^{19}F]143**

A 10 mL round-bottom flask equipped with a magnetic stirring bar was charged with **175** (50 mg, 53 µmol, 1.0 equiv), HOBt (8.6 mg, 64 µmol, 1.2 equiv), $TmobNH_2$ (13 mg, 64 µmol, 1.2 equiv), DIPEA (33 µL, 25 mg, 0.19 mmol, 3.30 equiv), and DMF (2.7 mL, 20 mmol·L^{-1}). The reaction mixture was cooled to 0 °C and then HBTU (24 mg, 64 µmol, 1.2 equiv) was added. The reaction mixture was allowed to warm to room temperature and was stirred at 23 °C for 12 hours. The solution was diluted with ethyl acetate (50 mL). The solution was extracted with water (2 × 30 mL), and the combined aqueous layers were extracted with ethyl acetate (10 mL). The combined organic layers were concentrated *in vacuo* to dryness. The beige residue was purified by HPLC on an YMC-Actus Triart C18 column ((30×150 mm, 5 µm + 30×50 mm, 5 µm), flow rate = 42.5 mL·min^{-1}, 35 °C) with a linear gradient from 17:83 (0.1% TFA in H_2O:MeOH, v:v) to 14:86 (0.1% TFA in H_2O:MeOH, v:v) over 10 minutes. The collected fractions containing the product (t ≈ 9.3 min) were combined, basified to pH 8 with saturated aqueous sodium bicarbonate solution, diluted with 100 mL brine and the resulting solution was concentrated by rotary evaporation (100 mbar, 35 °C) until no more methanol was evaporated. The suspension was extracted with dichloromethane (3 × 100 mL), and the combined organic layers were dried over sodium sulfate,

filtered, and concentrated *in vacuo* to dryness to afford **[^{19}F]143** as a colorless powder (38 mg, 34 µmol, 64% yield).

HRMS-ESI (m/z) calc'd for $C_{55}H_{86}O_{14}N_7FSNa$ $[M+Na]^+$, 1142.58297; 1142.58386; deviation: −0.78 ppm.

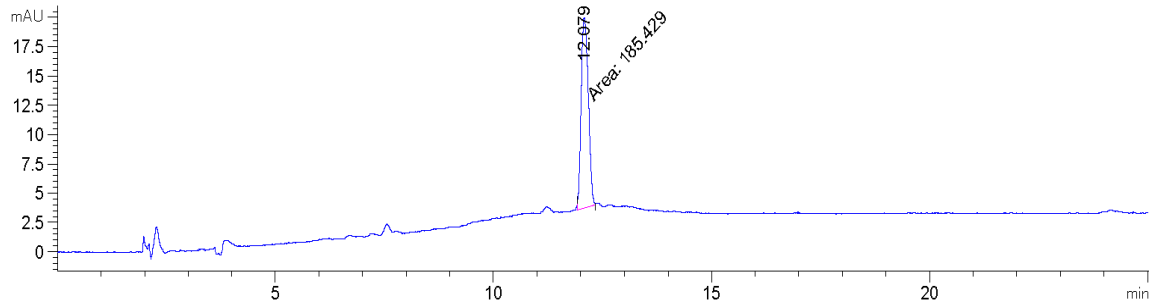

Figure S27. Analytical HPLC trace of **[^{19}F]143** (YMC-Triart C18 column, 150 x 4.6 mm, flow rate = 0.8 mL·min^{-1}) with a linear gradient from 30:70 (0.1% TFA in H_2O:MeOH, v:v) to 05:95 (0.1% TFA in H_2O:MeOH, v:v) over 10 minutes.

[H-Leu-Phe(4-F)-Glu-Met-Lys-NH_2]·3CF_3CO_2H ([^{19}F]147)

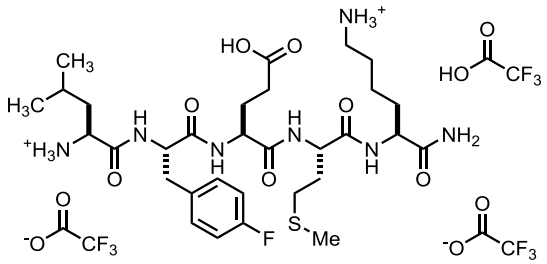

[^{19}F]147 (45%)

The peptide was synthesized according to the general procedure for peptide synthesis on Fmoc-Rink-Amid-2CT resin (200–400 mesh, 1% DVB, 0.68 mmol·g^{-1}, 0.37 g, 0.25 mmol, 1.0 equiv). Different to the regular cleavage process a mixture of TFA (8.8 mL, 13 g), DTT (0.50 g), water (0.50 mL, 0.50 g), and triisopropylsilane (0.25 mL, 0.19 g) was added, and the suspension was shaken at 23 °C for 2 hours. The reaction mixture was filtered into a round-bottom flask (100 mL) containing diethyl ether (80 mL). The resulting suspension was filtered and the filter cake was purified by HPLC on an YMC-Actus Triart C18 column ((30×150 mm, 5 µm + 30×50 mm, 5 µm), flow rate = 42.5 mL·min^{-1}, 35 °C) with a linear gradient from 50:50 (0.1% TFA in H_2O:MeOH, v:v) to 03:97 (0.1% TFA in H_2O:MeOH, v:v) over 10 minutes. The collected

fractions containing the product (t ≈ 5.0 min) were combined and concentrated *in vacuo* to dryness to afford **[^{19}F]147** as a colorless solid (0.11 g, 0.11 mmol, 45% yield).

NMR Spectroscopy:

^{1}H NMR (500 MHz, CD_3OD, 25 ºC, δ):8.33 (d, *J* = 7.2 Hz, 1H), 8.27 (d, *J* = 7.3 Hz, 1H), 8.14 (d, *J* = 7.8 Hz, 1H), 7.30–7.24 (m, 2H), 7.08–6.94 (m, *2*H), 4.62 (dd, *J* = 8.8, 6.1 Hz, 1H), 4.43 (td, *J* = 7.5, 3.7 Hz, 1H), 4.39–4.32 (m, 2H), 3.87–3.81 (m, 1H), 3.14 (dd, *J* = 14.1, 6.2 Hz, 1H), 3.00–2.90 (m, 3H), 2.63–2.50 (m, 2H), 2.42–2.32 (m, 2H), 2.15–2.03 (m, 5H), 2.02–1.82 (m, 2H), 1.77–1.61 (m, 6H), 1.53–1.42 (m, 2H), 1.35–1.26 (m, 1H), 0.98 (t, *J* = 6.0, 6H).

^{13}C{^{1}H} NMR (126 MHz, CD_3OD, 25 ºC, δ): 176.6, 176.4, 173.6, 173.5, 172.9 170.9, 163.3 ($^{1}J_{C\text{-}F}$ = 244 Hz), 134.1 ($^{4}J_{C\text{-}F}$ = 3 Hz), 132.0 ($^{3}J_{C\text{-}F}$ = 8.0 Hz), 116.2 ($^{2}J_{C\text{-}F}$ = 21.5 Hz), 56.3, 54.0_8, 54.0_5, 54.0, 52.8, 41.7, 40.6, 37.5, 32.5, 32.3, 31.1_1, 31.0_8, 28.2, 28.0, 25.3, 23.7, 23.2, 21.8, 15.3.

^{19}F NMR (471 MHz, CD_3OD, 25 ºC, δ): −76.9, –118.2.

HRMS-ESI (m/z) calc'd for $C_{31}H_{51}FN_7O_7S$ $[M-CF_3CO_2-2CF_3CO_2H]^+$, 684.35492; found, 684.35508; deviation: −0.23 ppm.

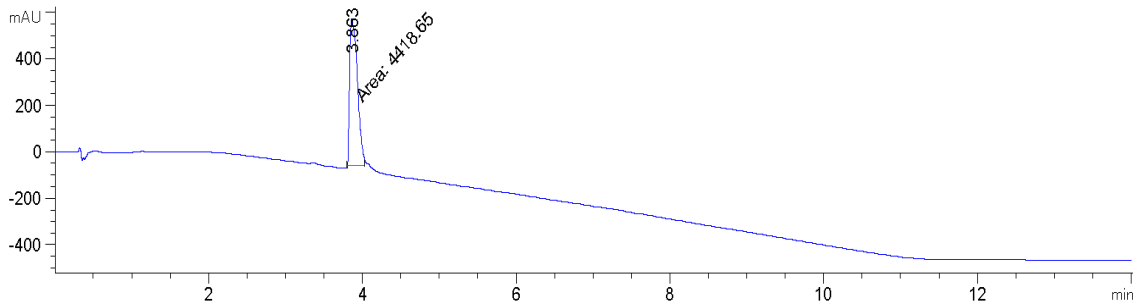

Figure S28. Analytical HPLC trace of **[^{19}F]147** (Agilent Poroshell 120, 50 x 3.0 mm, flow rate = 1 mL·min^{-1}) with a linear gradient from 100:0 (0.1% TFA in H_2O:MeOH, v:v) to 05:95 (0.1% TFA in H_2O:MeOH, v:v) over 10 minutes.

[Boc-Leu-Tyr(RuCp)-Glu(^{t}Bu)-Met-Lys(Boc)-OH]·CF_3CO_2 (176)

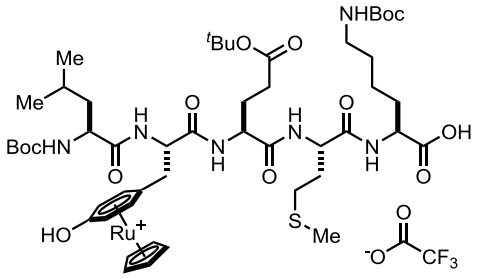

176 (66%)

The peptide was synthesized according to the general procedure for peptide synthesis starting with 1.0 mmol Fmoc-Lys(Boc)-O-2CT resin. The beige residue was purified by HPLC with an YMC-Actus Triart C18 column ((30×150 mm, 5 µm + 30×50 mm, 5 µm), flow rate = 42.5 mL·min^{-1}, 35 °C) with a linear gradient from 30:70 (0.1% TFA in H_2O:MeOH, v:v) to 10:90 (0.1% TFA in H_2O:MeOH, v:v) over 10 minutes. The collected fractions containing the product (t ≈ 6.5 min) were combined, neutralized to pH 7 with saturated aqueous sodium bicarbonate solution, diluted with 100 mL brine, and the resulting solution was concentrated by rotary evaporation (100 mbar, 35 °C) until no more methanol was evaporated. The suspension was extracted with dichloromethane (3 × 100 mL), and the combined organic layers were dried over sodium sulfate, filtered, and concentrated *in vacuo* to dryness to afford **176** as a colorless solid (0.80 g, 0.66 mmol, 66% yield).

HRMS-ESI (m/z) calc'd for $C_{50}H_{79}O_{13}N_6RuS$ $[M-CF_3CO_2]^+$, 1105.44638; found, 1105.44811; deviation: −1.56 ppm.

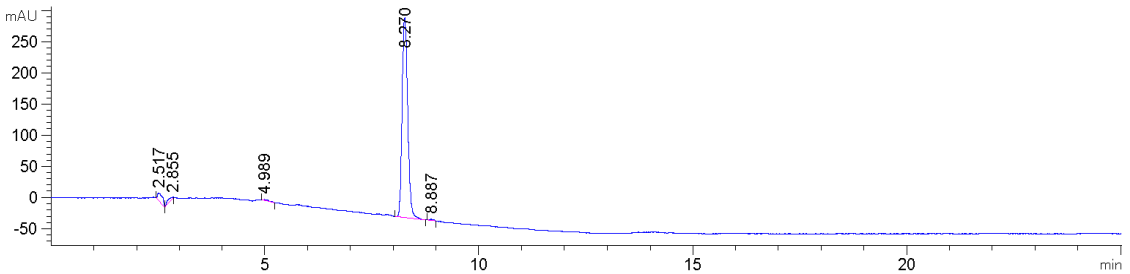

Figure S29. Analytical HPLC trace of **176** (YMC-Triart C18 column, 150 x 4.6 mm, flow rate = 0.8 mL·min^{-1}) with a linear gradient from 30:70 (0.1% TFA in H_2O:MeOH, v:v) to 05:95 (0.1% TFA in H_2O:MeOH, v:v) over 10 minutes.

Boc-Leu-Tyr(RuCp)-Glu(ᵗBu)-Met-Lys(Boc)-NHTmob (177)

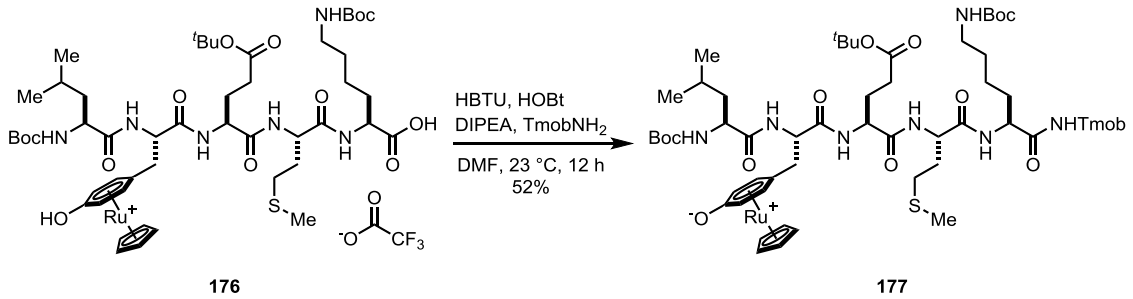

176 177

A 50 mL round-bottom flask equipped with a magnetic stirring bar was charged with **177** (0.80 g, 0.66 mmol, 1.0 equiv), HOBt (0.10 g, 0.76 mmol, 1.2 equiv), $TmobNH_2$ (0.16 g, 0.79 mmol, 1.2 equiv), DIPEA (0.41 mL, 0.31 g, 2.3 mmol, 3.6 equiv), and DMF (33 mL, 20 mmol·L^{-1}). The reaction mixture was cooled to 0 °C and then HBTU (0.29 g, 0.76 mmol, 1.2 equiv) was added. The reaction mixture was allowed to warm to room temperature and was stirred at 23 °C for 12 hours. The solution was concentrated by rotary evaporation to 5 mL, and was afterwards diluted with ethyl acetate (50 mL). The solution was extracted with water (2 × 30 mL), and the combined aqueous layers were extracted with ethyl acetate (10 mL). The combined organic layers were dried over sodium sulfate, filtered, and concentrated *in vacuo* to dryness. The beige residue was purified by HPLC on an YMC Pro C18 column ((30×150 mm, 5 µm + 30×50 mm, 5 µm), flow rate = 42.5 mL·min^{-1}, 35 °C) with an isocratic eluent 30:70 (0.1% TFA in H_2O:MeOH, v:v). The collected fractions containing the product (t ≈ 14.5 min) were combined, basified to pH 8 with saturated aqueous sodium bicarbonate solution, diluted with 100 mL brine and the resulting solution was concentrated by rotary evaporation (100 mbar, 35 °C) until no more methanol was evaporated. The suspension was extracted with dichloromethane (3 × 100 mL), and the combined organic layers were dried over sodium sulfate, filtered, and concentrated *in vacuo* to dryness to afford **177** as a colorless powder (0.48 g, 0.35 mmol, 52% yield).

NMR Spectroscopy:

^{1}H NMR (500 MHz, CD_3OD, 25 ºC, δ): 6.20 (s, 2H), 5.41–5.35 (m, 2H), 5.07 (s, 5H), 4.62–4.59 (m, 1H), 4.48 (dd, *J* = 9.0, 5.0 Hz, 1H), 4.38 (d, *J* = 13.4 Hz, 1H), 4.34–4.24 (m, 3H), 4.10–4.02 (m, 1H), 3.81 (s, 6H), 3.80 (s, 3H), 3.00 (t, *J* = 7.1 Hz, 2H), 2.84 (dd, *J* = 14.4, 5.0

Hz, 1H), 2.66 (dd, *J* = 14.4, 8.0 Hz, 1H), 2.61–2.45 (m, 2H), 2.39–2.25 (m, 2H), 2.13–2.01 (m, 5H), 1.94–1.84 (m, 2H), 1.82–1.71 (m, 1H), 1.70–1.59 (m, 2H), 1.52–1.40 (m, 30H), 1.38–1.27 (m, 2H), 0.93 (dd, *J* = 16.2, 6.6 Hz, 6H).

$^{13}C\{^{1}H\}$ NMR (126 MHz, CD_3OD, 25 °C, δ): 175.7, 173.7, 173.4, 173.3$_2$, .173.2$_5$, 172.3, 162.8, 160.8, 158.4, 158.0, 150.8, 106.7, 93.7, 91.6, 87.5, 87.1, 81.9, 80.8, 79.8, 78.9, 76.2, 76.1, 56.3, 55.8, 55.5, 54.8, 54.6, 54.2, 53.9, 42.0, 41.3, 37.8, 33.2, 32.9, 32.6$_8$,32.6$_5$, 31.1, 30.6, 28.9, 28.8, 28.4, 28.3, 25.9, 24.1, 23.4, 22.0.

HRMS-ESI (m/z) calc'd for $C_{36}H_{54}N_7O_8RuS$ $[M–H–3(CF_3CO_2H)]^-$, 846.28111; found, 846.28111; deviation: −0.89 ppm.

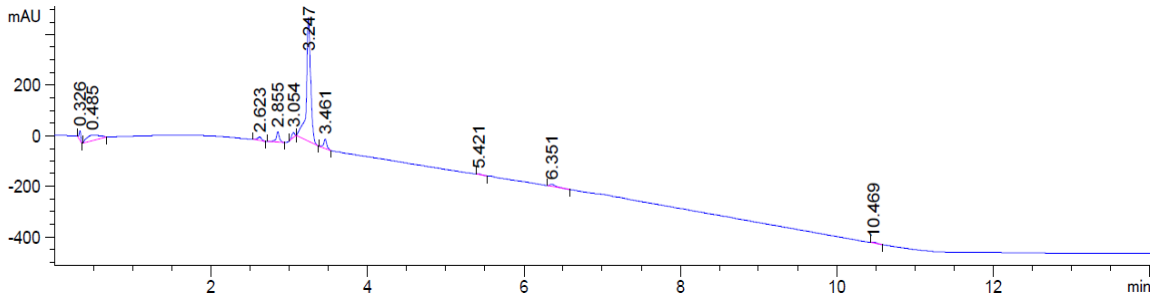

Figure S30. Analytical HPLC trace of **177** (Agilent Poroshell 120, 50 x 3.0 mm, flow rate = 1 mL·min^{-1}) with a linear gradient from 100:0 (0.1% TFA in H_2O:MeOH, v:v) to 05:95 (0.1% TFA in H_2O:MeOH, v:v) over 10 minutes.

[H-Leu-Tyr(RuCp)-Glu-Met-Lys-NH_2]·3CF_3CO_2H (146)

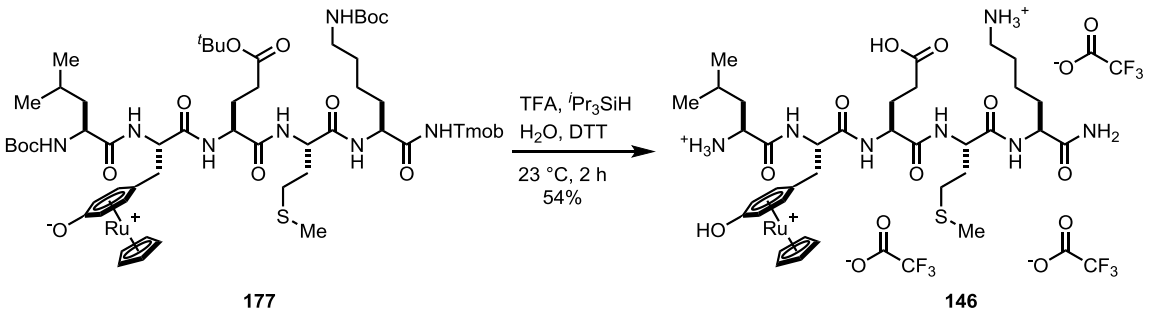

177 **146**

A vial (4 mL) equipped with a Teflon-coated magnetic stirring bar was charged with TFA (0.24 mL, 0.37 g, 3.2 mmol, 152 equiv), DTT (23 mg, 0.15 mmol, 7.0 equiv), water (21 µL, 21 mg, 1.2 mmol, 55 euqiv), and triisopropylsilane (13 µL, 10 mg, 63 µmol, 3.0 equiv). Peptide **177** (27 mg, 21 µmol, 1.0 equiv) was added to the emulsion, and the reaction mixture was stirred at 23 °C for 2

hours. To the emulsion was added diethyl ether (1 mL) and the precipitate was collected by filtration. The white precipitate was purified by HPLC on an YMC Triart C18 column ((30×150 mm, 5 µm + 30×50 mm, 5 µm), flow rate = 42.5 mL·min^{-1}, 35 °C) with a linear gradient from 80:20 (0.1% TFA in H_2O:MeOH, v:v) to 60:40 (0.1% TFA in H_2O:MeOH, v:v) over 10 minutes. The collected fractions containing the product (t ≈ 8.1 min) were combined, and concentrated by rotary evaporation to afford **146** as a white powder (14 mg, 11 µmol, 54% yield).

NMR Spectroscopy:

^{1}H NMR (500 MHz, CD_3OD, 25 ºC, δ):8.48 (d, *J* = 7.0, Hz, 1H), 8.39 (d, *J* = 7.5 Hz, 1H), 6.13–6.09 (m, 4H), 5.34 (s, 5H), 4.65 (t, *J* = 6.8 Hz, 1H), 4.54–4.49 (m, 1H), 4.38–4.31 (m, 2H), 3.97–3.92 (m, 1H), 2.97–2.90 (m, 3H), 2.75 (dd, *J* = 14.1, 7.5 Hz, 1H), 2.63–2.51 (m, 2H), 2.47–2.34 (m, 2H), 2.18–2.03 (m, 5H), 2.02–1.82 (m, 2H), 1.77–1.63 (m, 6H), 1.54–1.40 (m, 2H), 1.35–1.25 (m, 1H), 1.01–0.96 (m, 6H).

^{13}C{^{1}H} NMR (126 MHz, CD_3OD, 25 ºC, δ): 176.4, 176.3, 173.6, 173.5, 171.4, 170.9, 134.8, 98.1, 87.1, 86.8, 81.3, 76.0, 75.9, 55.6, 54.3, 54.0, 53.8, 52.8, 41.7, 40.5, 37.3, 32.6, 32.4, 31.1, 31.0, 28.2, 28.1, 25.4, 23.7, 23.1, 22.0, 15.2.

^{19}F NMR (471 MHz, CD_3OD, 25 ºC, δ): −76.9.

HRMS-ESI (m/z) calc'd for $C_{36}H_{54}N_7O_8SRu$ $[M-3CF_3CO_2H]^-$, 846.28111; found, 846.28111; deviation: −0.89 ppm.

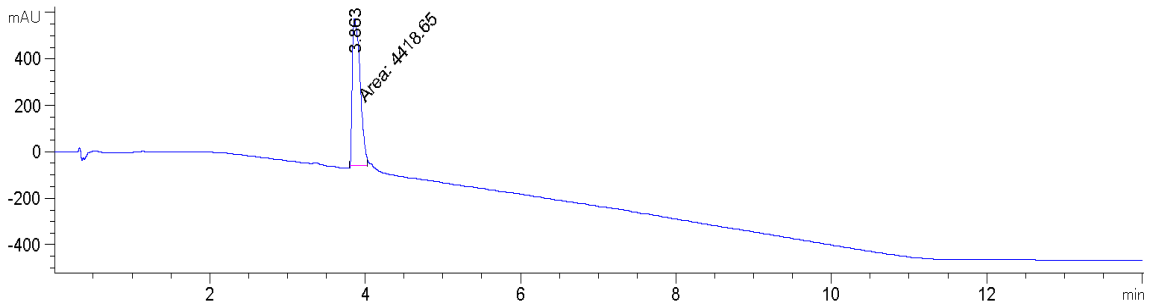

Figure S31. Analytical HPLC trace of **146** (Agilent Poroshell 120, 50 x 3.0 mm, flow rate = 1 mL·min^{-1}) with a linear gradient from 100:0 (0.1% TFA in H_2O:MeOH, v:v) to 05:95 (0.1% TFA in H_2O:MeOH, v:v) over 10 minutes.

Boc-Gly-His(Trt)-Gly-*D*-Phe(4-F)-Gly-NHTmob (178)

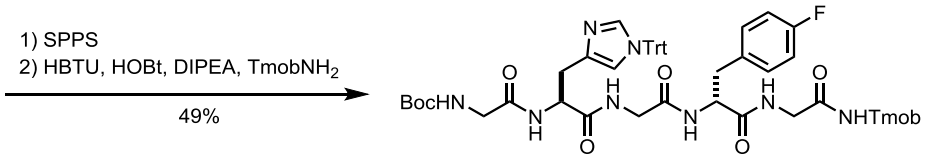

178

The peptide was synthesized according to the general procedure for peptide synthesis starting with 0.25 mmol Fmoc-Gly-O-2CT resin. A 50 mL round-bottom flask equipped with a magnetic stirring bar was charged with the solid residue from SPPS, HOBt (41 mg, 0.30 mmol, 1.2 equiv), $TmobNH_2$ (54 mg, 0.28 mmol, 1.1 equiv), DIPEA (0.13 mL, 97 mg, 0.75 mmol, 3.0 equiv), and DMF (13 mL, 20 $mmol \cdot L^{-1}$). The reaction mixture was cooled to 0 °C and then HBTU (0.11 g, 0.30 mmol, 1.2 equiv) was added. The reaction mixture was allowed to warm to room temperature and was stirred at 23 °C for 12 hours. The solution was concentrated by rotary evaporation to 5 mL, and afterwards diluted with ethyl acetate (50 mL). The solution was extracted with water (2 × 30 mL), and the combined aqueous layers were extracted with ethyl acetate (10 mL). The combined organic layers were dried over sodium sulfate, filtered, and concentrated *in vacuo* to dryness. The beige residue was purified by HPLC with an YMC Pro C18 column ((30×150 mm, 5 µm + 30×50 mm, 5 µm), flow rate = 42.5 $mL \cdot min^{-1}$, 35 °C) with a linear gradient from 40:60 (0.1% TFA in H_2O:MeOH, v:v) to 20:80 (0.1% TFA in H_2O:MeOH, v:v) over 10 minutes. The collected fractions containing the product (t ≈ 8.0 min) were combined, neutralized to pH 7 with saturated aqueous sodium bicarbonate solution, diluted with 100 mL brine and the resulting solution was concentrated by rotary evaporation (100 mbar, 35 °C) until no more methanol was evaporated. The suspension was extracted with dichloromethane (3 × 100 mL), and the combined organic layers were dried over sodium sulfate, filtered, and concentrated *in vacuo* to dryness to afford **178** as a colorless solid (0.12 g, 0.12 mmol, 49% yield).

HRMS-ESI (m/z) calc'd for $C_{55}H_{62}FN_8O_{10}$ $[M+H]^+$, 1013.45674; found, 1013.45712; deviation: −0.37 ppm.

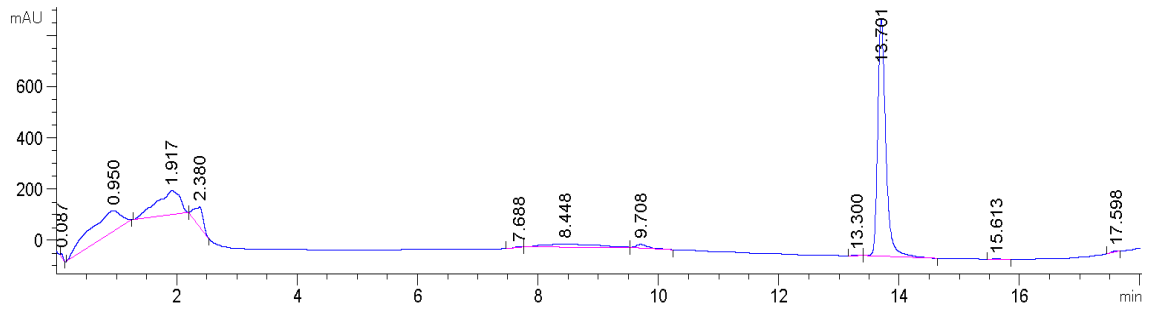

Figure S32. Analytical HPLC trace of **178** (YMC-Triart C18 column, 150 x 4.6 mm, flow rate = 0.8 mL·min^{-1}) with a linear gradient from 30:70 (0.1% TFA in H_2O:MeOH, v:v) to 05:95 (0.1% TFA in H_2O:MeOH, v:v) over 10 minutes.

[H-Gly-His-Gly-*D*-Phe(4-F)-Gly-NH_2]·2CF_3CO_2H (179)

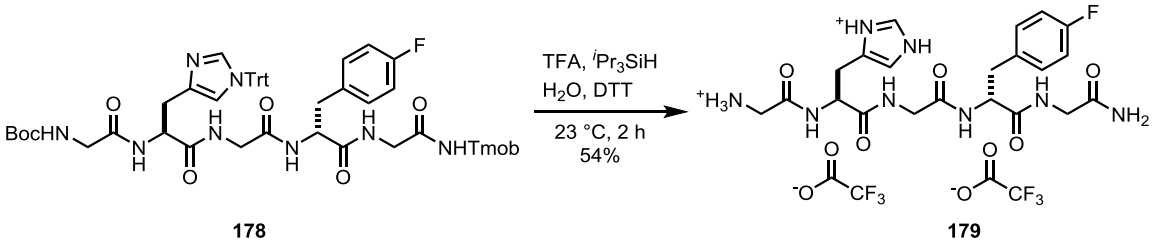

178 **179**

A vial (4 mL) equipped with a Teflon-coated magnetic stirring bar was charged with TFA (4.4 mL, 6.55 g), DTT (0.25 g, 1.6 mmol, 16 equiv), water (0.25 mL, 0.25 g), and triisopropylsilane (0.13 mL, 97 mg, 0.61 mmol, 6.2 equiv). Peptide **178** (0.10 g, 99 µmol, 1.0 equiv) was added to the emulsion, and the reaction mixture was stirred at 23 °C for 2 hours. The reaction mixture was concentrated *in vacuo* and the solid residue was purified by HPLC on an Chiralpak® ZWIX (+) ((10×250 mm, 5 µm), flow rate = 6.0 mL·min^{-1}, 35 °C) with an isocratic eluent 49:49:2 (MeOH:MeCN:H_2O+50 mM formic acid, 25 mM diethylamine). The collected fractions containing the product (t ≈ 15.0 min) were combined and concentrated *in vacuo* to dryness to afford **179** as a colorless solid (38 mg, 53 µmol, 54% yield).

NMR Spectroscopy:

^{1}H NMR (500 MHz, CD_3OD, 25 ºC, δ): 8.78 (d, *J* = 1.4 Hz, 1H), 7.38 (d, *J* =1.4 Hz, 1H), 7.34–7.18 (m, 2H), 7.07–6.88 (m, 2H), 4.68 (dd, *J* = 7.2, 5.6 Hz, 1H), 4.58 (dd, *J* = 9.0, 5.6 Hz, 1H), 3.97–3.95 (m, 1H), 3.93–3.90 (m, 1H), 3.88–3.80 (m, 1H), 3.79–3.73 (m, 3H), 3.37–3.30 (m, 1H), 3.19 (ddd, *J* =13.8, 10.0, 6.4 Hz, dH), 2.97 (dd, *J* =13.9, 9.0 Hz, 1H).

$^{13}C\{^{1}H\}$ NMR (126 MHz, CD_3OD, 25 ºC, δ): 174.0, 173.8, 172.6, 171.7, 168.1 163.3 ($^{1}J_{C\text{-}F}$ = 243.5 Hz), 135.3, 134.4 ($^{4}J_{C\text{-}F}$ = 3.2 Hz), 132.1 ($^{3}J_{C\text{-}F}$ = 8 Hz), 130.3, 118.9, 116.1 ($^{2}J_{C\text{-}F}$ = 21.5 Hz), 56.4, 54.3, 43.3, 43.0, 41.6, 37.6, 27.9.

^{19}F NMR (471 MHz, CD_3OD, 25 ºC, δ): −77.6, −119.2.

HRMS-ESI (m/z) calc'd for $C_{21}H_{28}FN_8O_5$ $[M-CF_3CO_2-CF_3CO_2H]^+$, 491.21612; found, 491.21618; deviation: −0.13 ppm.

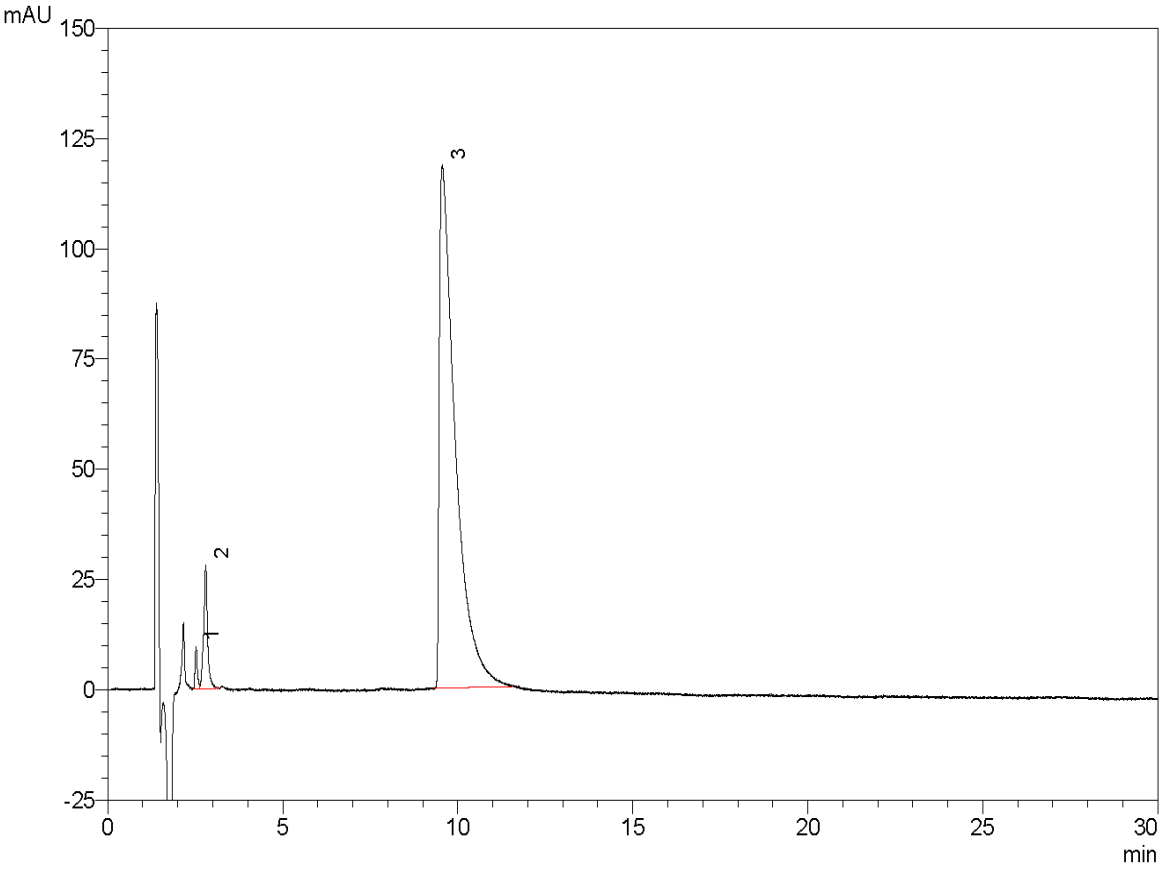

Figure S33. Analytical HPLC trace of **179** (Chiralpak® ZWIX(+) 3 µm, flow rate = 1 mL·min^{-1}) with an isocratic eluent 49:49:2 (MeOH:MeCN:H_2O+50 mM formic acid, 25 mM diethylamine).

Boc-Gly-His(Trt)-Gly-Phe(4-F)-Gly-NHTmob (180)

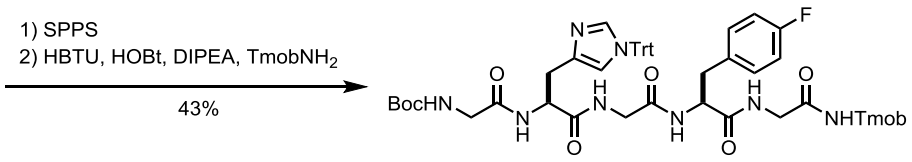

180

The peptide was synthesized according to the general procedure for peptide synthesis starting with 0.25 mmol Fmoc-Gly-O-2CT resin. A 50 mL round-bottom flask equipped with a magnetic stirring bar was charged solid residue from SPPS, HOBt (41 mg, 0.30 mmol, 1.2 equiv), $TmobNH_2$ (54 mg, 0.28 mmol, 1.1 equiv), DIPEA (0.41 mL, 0.31 g, 2.4 mmol, 3.6 equiv), and DMF (13 mL, 20 mmol·L^{-1}). The reaction mixture was cooled to 0 °C and then HBTU (0.11 g, 0.30 mmol, 1.2 equiv) was added. The reaction mixture was allowed to warm to room temperature and was stirred at 23 °C for 12 hours. The solution was concentrated by rotary evaporation to 5 mL, and afterwards diluted with ethyl acetate (50 mL). The solution was extracted with water (2 × 30 mL), and the combined aqueous layers were extracted with ethyl acetate (10 mL). The combined organic layers were dried over sodium sulfate, filtered, and concentrated *in vacuo* to dryness. The beige residue was purified by HPLC with an YMC Pro C18 column ((30×150 mm, 5 µm + 30×50 mm, 5 µm), flow rate = 42.5 mL·min^{-1}, 35 °C) with a linear gradient from 40:60 (0.1% TFA in H_2O:MeOH, v:v) to 20:80 (0.1% TFA in H_2O:MeOH, v:v) over 10 minutes. The collected fractions containing the product (t ≈ 8.0 min) were combined, neutralized to pH 7 with saturated aqueous sodium bicarbonate solution, diluted with 100 mL brine and the resulting solution was concentrated by rotary evaporation (100 mbar, 35 °C) until no more methanol was evaporated. The suspension was extracted with dichloromethane (3 × 100 mL), and the combined organic layers were dried over sodium sulfate, filtered, and concentrated *in vacuo* to dryness to afford **180** as a colorless solid (0.11 g, 0.10 mmol, 43% yield).

HRMS-ESI (m/z) calc'd for $C_{55}H_{62}FN_8O_{10}$ $[M+H]^+$, 1013.45674; found, 1013.45774; deviation: −0.98 ppm.

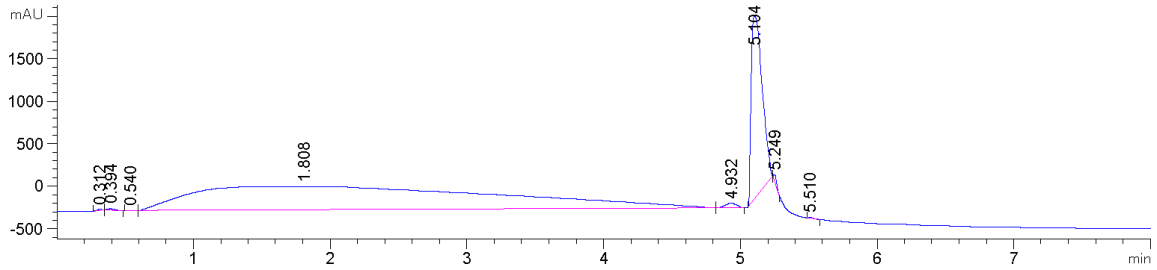

Figure S34. Analytical HPLC trace of **180** (Agilent Poroshell 120, 50 x 3.0 mm, flow rate = 1 mL·min^{-1}) with a linear gradient from 100:0 (0.1% TFA in H_2O:MeOH, v:v) to 05:95 (0.1% TFA in H_2O:MeOH, v:v) over 5 minutes.

[H-Gly-His-Gly-Phe(4-F)-Gly-NH$_2$]·2CF$_3$CO$_2$H ([^{19}F]152)

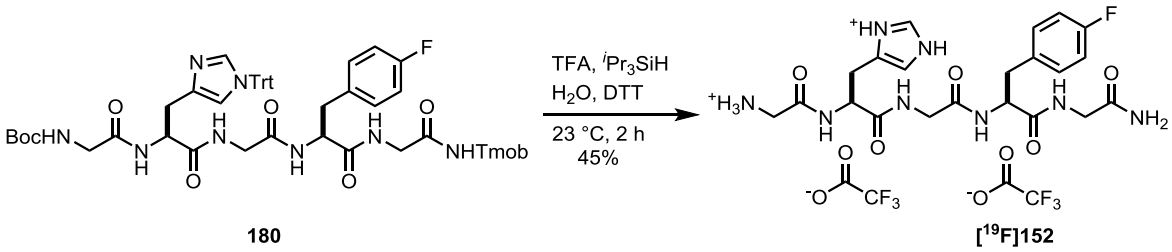

180 **[^{19}F]152**

A vial (4 mL) equipped with a Teflon-coated magnetic stirring bar was charged with TFA (4.4 mL, 6.6 g), DTT (0.25 g, 1.6 mmol, 16 equiv), water (0.25 mL, 0.25 g), and triisopropylsilane (0.13 mL, 97 mg, 0.61 mmol, 6.2 equiv). Peptide **180** (0.10 g, 99 µmol, 1.0 equiv) was added to the emulsion, and the reaction mixture was stirred at 23 °C for 2 hours. The reaction mixture was concentrated *in vacuo* and the solid residue was purified by HPLC on an Chiralpak® ZWIX (+) ((10×250 mm, 5 µm), flow rate = 6.0 mL·min^{-1}, 35 °C) with an isocratic eluent 49:49:2 (MeOH:MeCN:H_2O+50 mM formic acid, 25 mM diethylamine). The collected fractions containing the product (t ≈ 17.5 min) were combined and concentrated *in vacuo* to dryness to afford **[^{19}F]152** as a colorless solid (32 mg, 45 µmol, 45% yield).

NMR Spectroscopy:

^{1}H NMR (500 MHz, CD_3OD, 25 ºC, δ): 8.80 (d, *J* = 1.5 Hz, 1H), 7.39 (d, *J* =1.4 Hz, 1H), 7.27 (ddd, *J* = 8.5, 5.4, 2.7 Hz, 2H), 7.03–6.95 (m, 2H), 4.70 (t, *J* = 6.6 Hz, 1H), 4.60 (dd, *J* = 9.4, 5.4 Hz, 1H), 3.99–3.88 (m, 2H), 3.83–3.70 (m, 4H), 3.30–3.24 (m, 1H), 3.24–3.15 (m, 2H), 2.98 (dd, *J* =14.0, 9.5 Hz, 1H).

$^{13}C\{^{1}H\}$ NMR (126 MHz, CD_3OD, 25 ºC, δ): 174.0, 173.8, 172.1, 171.8, 167.9 163.3 ($^{1}J_{C\text{-}F}$ = 243.6 Hz), 135.3, 134.3 ($^{4}J_{C\text{-}F}$ = 3.0 Hz), 132.1 ($^{3}J_{C\text{-}F}$ = 8.1 Hz), 130.6, 118.8, 116.1 ($^{2}J_{C\text{-}F}$ = 21.4 Hz), 56.6, 53.9, 43.3, 43.0, 41.6, 37.6, 27.9.

^{19}F NMR (471 MHz, CD_3OD, 25 ºC, δ): −77.9, −119.1.

HRMS-ESI (m/z) calc'd for $C_{21}H_{28}FN_8O_5$ $[M-CF_3CO_2H-CF_3CO_2]^+$, 491.21611; found, 491.21605; deviation: 0.14 ppm.

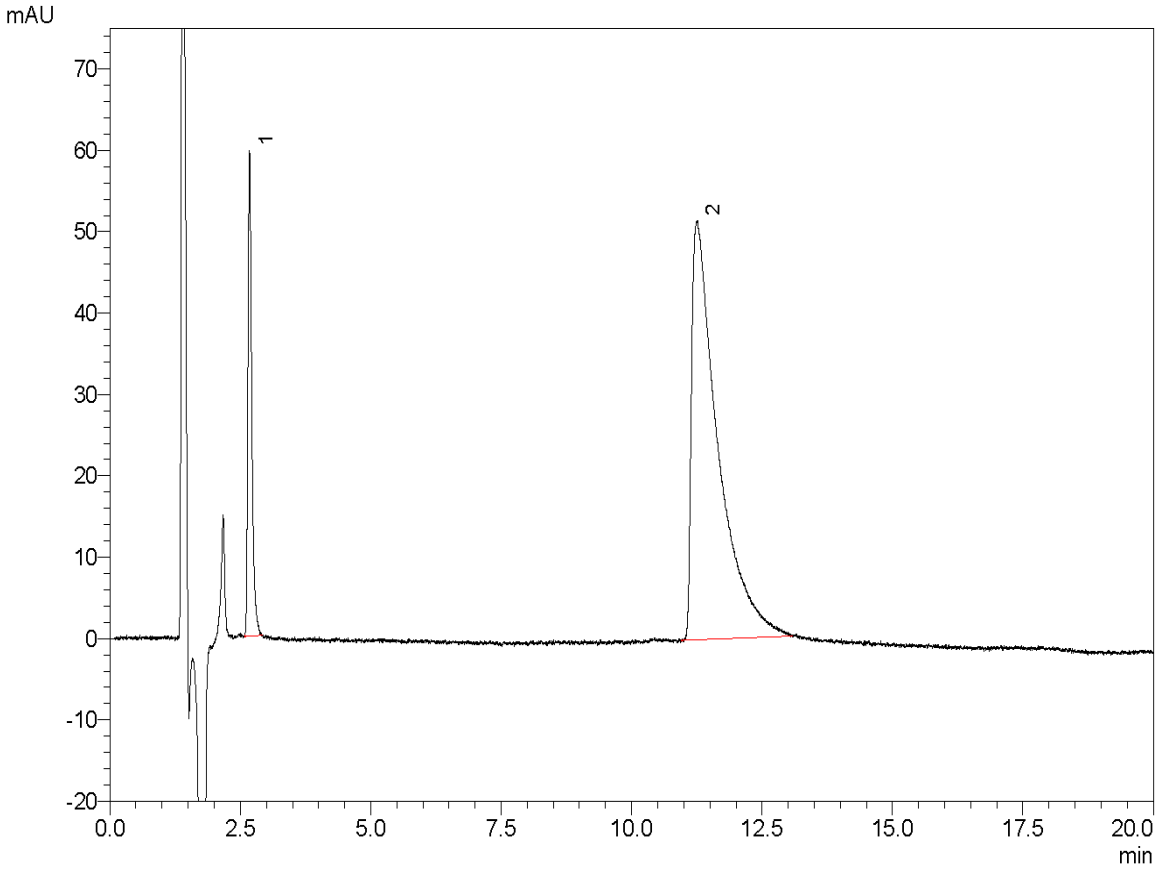

Figure S35. Analytical HPLC trace of **[^{19}F]152** (Chiralpak® ZWIX(+) 3 µm, flow rate = 1 mL·min^{-1}) with an isocratic eluent 49:49:2 (MeOH:MeCN:H_2O+50 mM formic acid, 25 mM diethylamine).

[Boc-Gly-His(Trt)-Gly-Tyr(RuCp)-Gly-OH]·CF_3CO_2 (181)

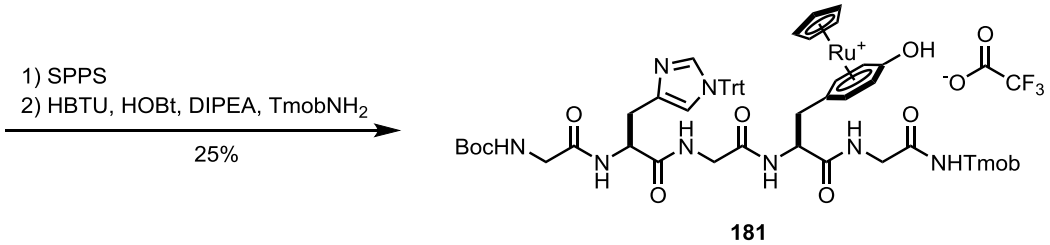

181

The peptide was synthesized according to the general procedure for peptide synthesis starting with 0.5 mmol Fmoc-Gly-O-2CT resin. The beige residue was purified by HPLC with an YMC Pro C18 column ((30×150 mm, 5 µm + 30×50 mm, 5 µm), flow rate = 42.5 mL·min^{-1}, 35 °C) with a linear gradient from 30:70 (0.1% TFA in H_2O:MeOH, v:v) to 05:95 (0.1% TFA in H_2O:MeOH, v:v) over 10 minutes. The collected fractions containing the product (t ≈ 4.5 min) were combined, neutralized to PH 7 with saturated aqueous sodium bicarbonate solution, diluted with 100 mL brine and the resulting solution was concentrated by rotary evaporation (100 mbar, 35 °C) until no more methanol was evaporated. The suspension was extracted with dichloromethane (3 × 100 mL), and the combined organic layers were dried over sodium sulfate, filtered, and concentrated *in vacuo* to dryness to afford **181** as a colorless solid (0.16 g, 0.12 mmol, 25% yield).

NMR Spectroscopy:

^{1}H NMR (500 MHz, CD_3OD, 25 ºC, δ): 7.42 (s, 1H), 7.37 (dd, *J* = 5.2, 2.0 Hz, 9H), 7.18–7.09 (m, 6H), 6.77 (s, 1H), 6.19 (s, 2H), 5.71 (dd, *J* = 5.8, 3.7 Hz, 2H), 5.46–5.28 (m, 2H), 5.05 (s, 4H), 4.55 (dd, *J* = 9.1, 4.6 Hz, 1H), 4.49 (t, *J* = 6.6 Hz, 1H), 4.35 (d, *J* = 2.2 Hz, 1H), 3.94–3.80 (m, 2H), 3.78 (d, *J* = 1.1 Hz, 9H), 3.74–3.61 (m, 3H), 3.05 (dd, *J* = 14.7, 5.7 Hz, 1H), 2.96 (dd, *J* = 14.7, 7.2 Hz, 1H), 2.86 (dd, *J* = 14.3, 4.6 Hz, 1H), 2.66 (dd, *J* = 14.3, 9.2 Hz, 1H), 1.39 (s, 9H).

^{13}C{^{1}H} NMR (126 MHz, CD_3OD, 25 ºC, δ): 174.2, 172.8, 172.7, 171.7, 170.4, 162.8, 160.8, 158.5, 150.6, 143.6, 139.8, 137.3, 130.9, 129.4, 129.3, 121.5, 106.7, 94.5, 91.6, 87.6, 86.8, 80.9, 78.9, 76.8, 76.1, 56.3, 55.8, 55.4, 44.9, 44.0, 43.4, 37.2, 33.3, 30.6, 28.8. Two carbon resonances are not observed, presumably due to overlap with a solvent carbon resonance.

^{19}F NMR (471 MHz, CD_3OD, 25 ºC, δ): −77.5.

HRMS-ESI (m/z) calc'd for $C_{60}H_{67}O_{11}N_8Ru$ $[M-CF_3CO_2]^+$, 1177.39776; found, 1177.3978; deviation: −0.87 ppm.

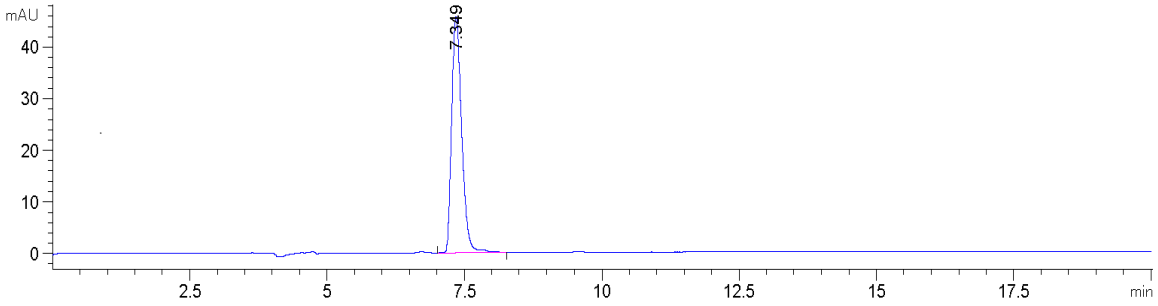

Figure S36. Analytical HPLC trace of **181** (YMC-Triart C18 column, 150 x 4.6 mm, flow rate = 0.8 $mL \cdot min^{-1}$) with a linear gradient from 45:55 (0.1% TFA in H_2O:MeCN, v:v) to 30:70 (0.1% TFA in H_2O:MeCN, v:v) over 10 minutes.

IV.2.2. **General procedure for radio-deoxyfluorination of peptides**

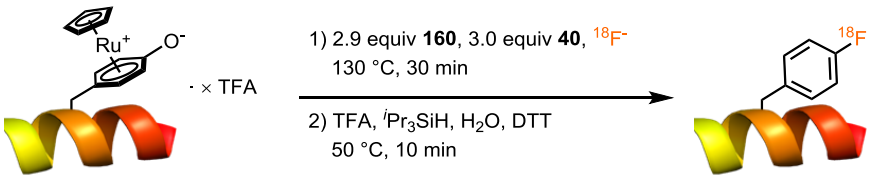

Aqueous [^{18}F]fluoride solution (700 µL) was loaded with a syringe onto a QMA anion-exchange cartridge that was pre-conditioned according to the general procedure, and then the cartridge was washed with MeCN (1 mL). The cartridge was dried by pushing air (2 mL) through the cartridge. The [^{18}F]fluoride was eluted from the cartridge with a solution of tracer precursor (5.0 µmol, 1.0 equiv), imidazolium chloride **40** (6.9 mg, 15 µmol, 3.0 equiv), and bis(neopentyltrimethylammonium) oxalate **160** (5.0 mg, 14 µmol, 2.9 equiv) in a mixture of ethanol and pivalonitrile (200 µL, 1:3, v:v), into a 4 mL borosilicate vial. The remaining substrate was eluted from the cartridge with a mixture of veratrole and pivalonitrile (250 µL, 4:1, v:v) into the same vial. The reaction vial containing 450 µL reaction mixture was sealed with a Teflon-lined cap and was stirred at 130 °C for 30 minutes. The vial was removed from the hot plate, and after 2 minutes the reaction mixture was concentrated by heating at 80 °C under a stream of nitrogen (~5 min). To the remaining solution was added a mixture of TFA (0.42 mL), triisopropylsilane (40 µL), *DL*-1,4-dithiothreitol (35 mg), and water (20 µL), then the mixture was stirred at 50 °C for 10 minutes. The reaction mixture was diluted with water and was purified by HPLC on a Hypersil Gold column (250×10 mm, 5 µm). The activity of the product containing fraction was measured and the product identity and purity was determined by comparison of the HPLC radio-trace with the HPLC UV-trace of the authentic reference sample.

c(Asp-*D*-Phe(4-[^{18}F]F)-Lys-Arg-Gly) (149)

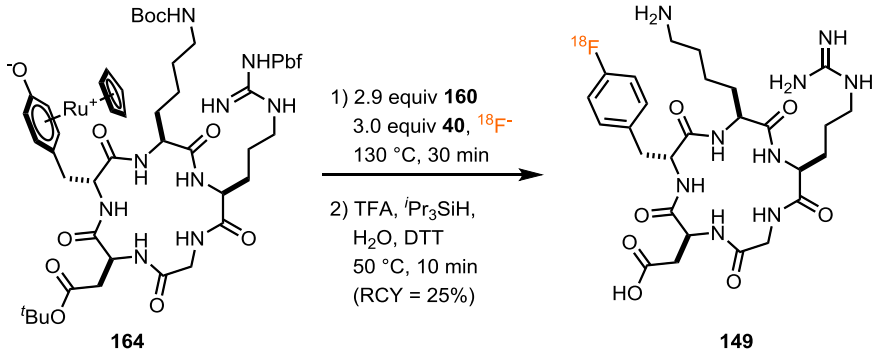

Aqueous [^{18}F]fluoride solution (700 µL) was loaded with a syringe onto a QMA anion-exchange cartridge that was pre-conditioned according to the general procedure. The cartridge was dried by sequentially pushing MeCN (1 mL) and air (2 mL) through the cartridge. The [^{18}F]fluoride was eluted from the cartridge with a solution of **164** (6.0 mg, 5.0 µmol, 1.0 equiv), imidazolium chloride **40** (6.9 mg, 15 µmol, 3.0 equiv), and bis(neopentyltrimethylammonium) oxalate **160** (5.0 mg, 14 µmol, 2.9 equiv) in a mixture of ethanol and pivalonitrile (200 µL, 1:3, v:v), into a 4 mL borosilicate vial. The cartridge was eluted a second time with a mixture of veratrole and pivalonitrile (250 µL, 4:1, v:v) into the same vial. The reaction vial containing 450 µL reaction mixture was sealed with a Teflon-lined cap and was stirred at 130 °C for 30 minutes. The vial was removed from the hot plate, and after 2 minutes the reaction mixture was concentrated by heating at 80 °C under a stream of nitrogen (5 min). To the remaining solution was added a mixture of TFA (0.42 mL), triisopropylsilane (40 µL), *DL*-1,4-dithiothreitol (35 mg), and water (20 µL). The mixture was stirred at 50 °C for 10 minutes. The reaction mixture was diluted with water (2 mL) and purified by HPLC on a Hypersil Gold column (250×10 mm, 5 µm, flow rate = 4 mL·min^{-1}) with an isocratic mixture of 05:95 (MeCN:water, 0.1% TFA, v:v) for 5 minutes, followed by a linear gradient to 35:65 (MeCN:water, 0.1% TFA, v:v) within 18 minutes. The activity of the product **149** containing fraction (≈ 22 min) was measured and the product identity and purity was determined by comparison of the HPLC radio-trace with the HPLC UV-trace of the authentic reference sample **149**.

Table S1. Radiochemical yield of **149**.

reaction	starting activity / (MBq)	isolated acitivty after / HPLC (MBq)	synthesis time / (min)	RCY
1	60.1	7.5	146	31%
2	64.8	6.66	100	19%
average RCY				25%

Figure S37. HPLC γ-trace (gradient 2) of the isolated compound c(Asp-*D*-Phe(4-[^{18}F]F)-Lys-Arg-Gly) **149**.

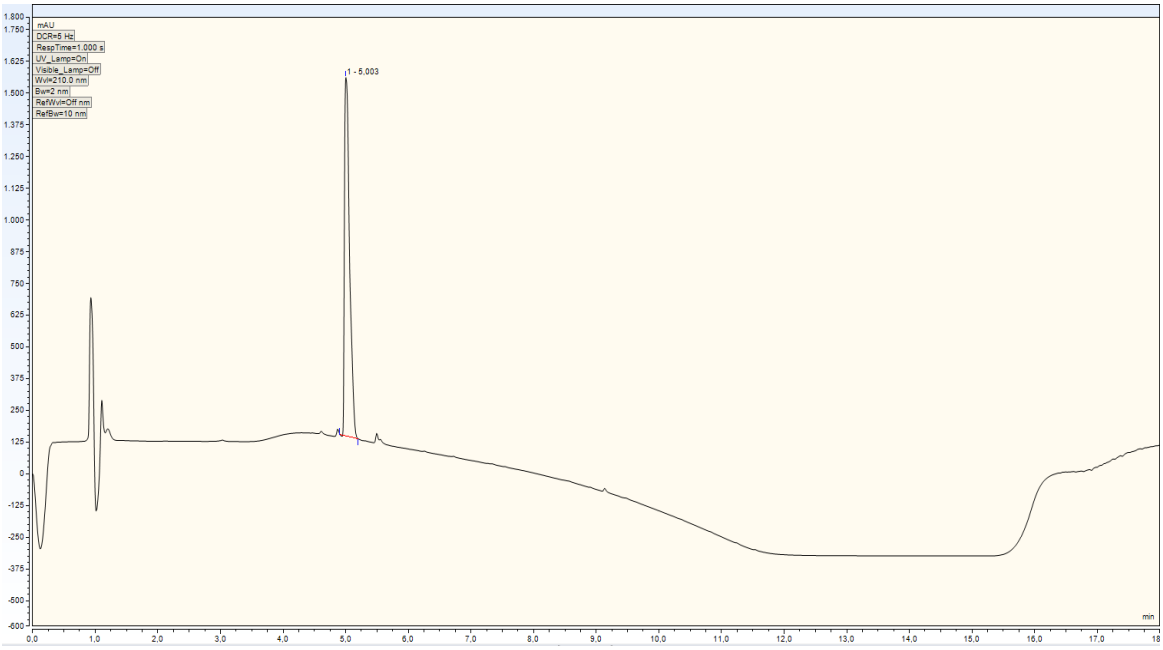

Figure S38. HPLC UV-trace (gradient 2) of c(Asp-*D*-Phe(4-F)-Lys-Arg-Gly) **[^{19}F]149** as the reference.

H-Phe(4-[^{18}F]F)-Ile-Cys-Val-Gln-Pro-Ser-Phe-OH (151)

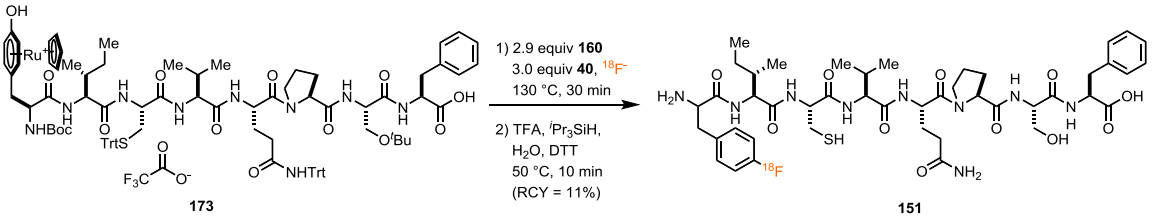

173 151

Aqueous [^{18}F]fluoride solution (700 µL) was loaded with a syringe onto a QMA anion-exchange cartridge that was pre-conditioned according to the general procedure. The cartridge was dried by sequentially pushing MeCN (1 mL) and air (2 mL) through the cartridge. The [^{18}F]fluoride was eluted from the cartridge with a solution of **171** (8.8 mg, 5.0 µmol, 1.0 equiv), imidazolium chloride **40** (6.9 mg, 15 µmol, 3.0 equiv), and bis(neopentyltrimethylammonium) oxalate **160** (5.0 mg, 14 µmol, 2.9 equiv) in a mixture of ethanol and pivalonitrile (200 µL, 1:3, v:v), into a 4 mL borosilicate vial. The cartridge was eluted a second time with a mixture of veratrole and pivalonitrile (250 µL, 4:1, v:v) into the same vial. The reaction vial containing 450 µL reaction mixture was sealed with a Teflon-lined cap and was stirred at 130 °C for 30 minutes. The vial was removed from the hot plate, and after 2 minutes the reaction mixture was concentrated by heating at 80 °C under a stream of nitrogen (5 min). To the remaining solution was added a mixture of TFA (0.42 mL), triisopropylsilane (40 µL), *DL*-1,4-dithiothreitol (35 mg), and water (20 µL). The mixture was stirred at 50 °C for 10 minutes. The reaction mixture was diluted with water and methanol (2 mL, 2:1, v:v) and purified by HPLC on a Hypersil Gold column (250×10 mm, 5 µm, flow rate = 4 mL·min^{-1}) with an isocratic mixture of 25:75 (MeCN:water, 0.1% TFA, v:v) for 2 minutes, followed by a linear gradient to 50:50:0.1 (MeCN:water, 0.1% TFA, v:v) within 20 minutes. The activity of the product **151** containing fraction (≈ 21 min) was measured and the product identity and purity was determined by comparison of the HPLC radio-trace with the HPLC UV-trace of the authentic reference sample **151**.

Table S2. Radiochemical yield of **151**.

reaction	starting activity / (MBq)	isolated acitivty after HPLC / (MBq)	synthesis time / (min)	RCY
1	63.1	2.56	115	8%
2	49.2	3.12	120	14%
average RCY				11%

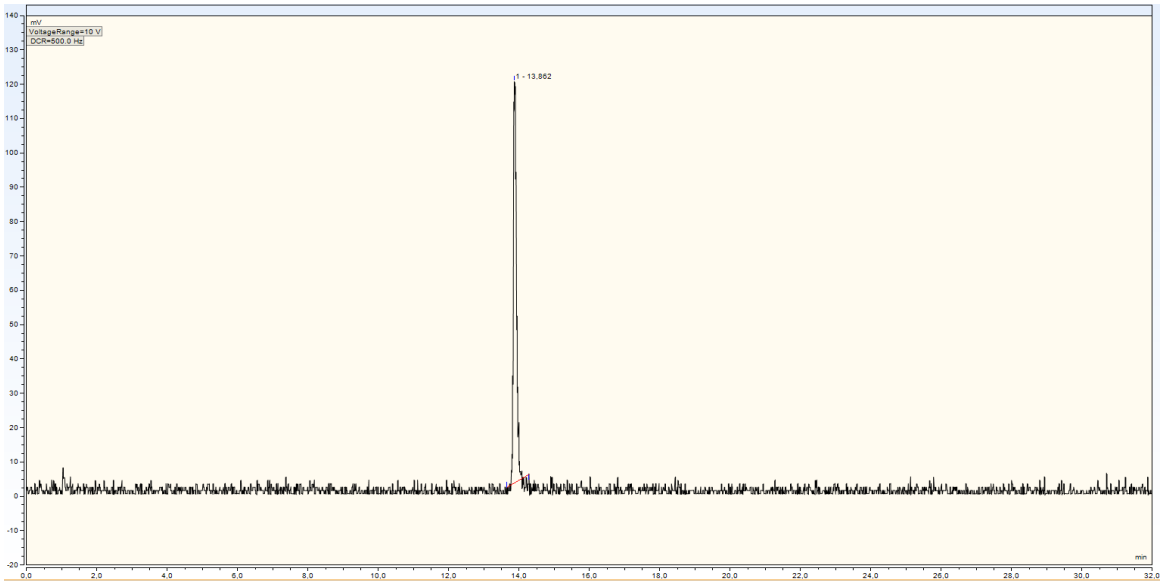

Figure S39. Radio-HPLC trace (gradient 1) of the isolated compound H-Phe(4-[^{18}F]F)-Ile-Cys-Val-Gln-Pro-Ser-Phe-OH **151**.

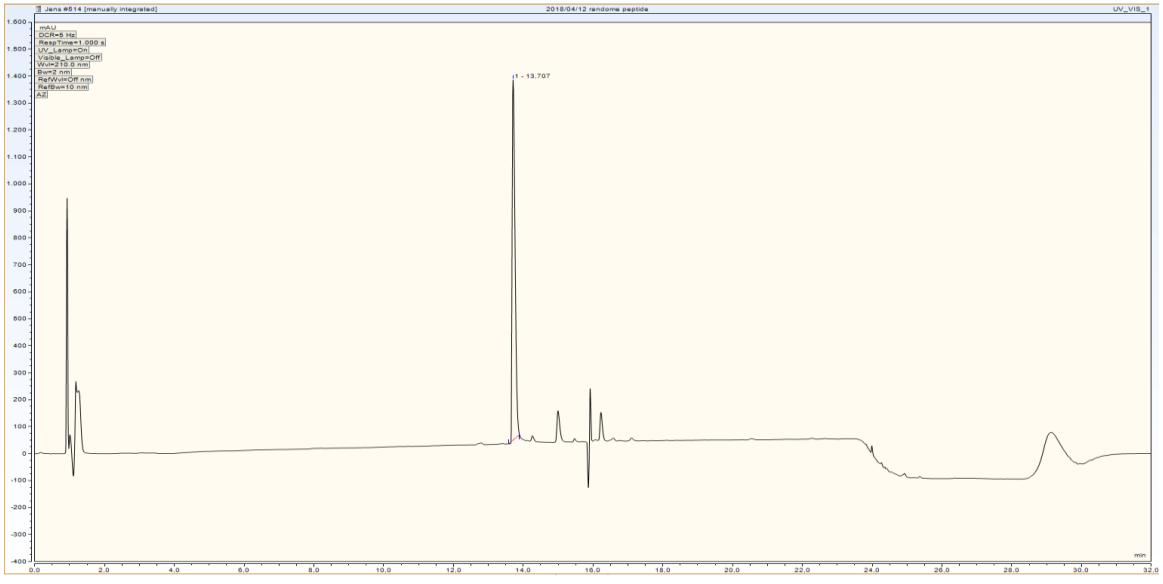

Figure S40. UV-HPLC trace (gradient 1) of H-Phe(4-F)-Ile-Cys-Val-Gln-Pro-Ser-Phe-OH as the reference **[^{19}F]151**.

H-Phe(4-[^{18}F]F)-Ile-Cys-Val-Gln-Pro-Ser-Phe-OH (151)

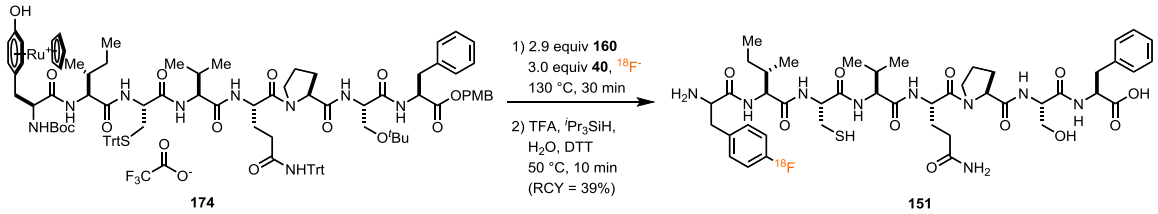

174 151

Aqueous [^{18}F]fluoride solution (700 µL) was loaded with a syringe onto a QMA anion-exchange cartridge that was pre-conditioned according to the general procedure. The cartridge was dried by sequentially pushing MeCN (1 mL) and air (2 mL) through the cartridge. The [^{18}F]fluoride was eluted from the cartridge with a solution of **174** (10 mg, 5.0 µmol, 1.0 equiv), imidazolium chloride **40** (6.9 mg, 15 µmol, 3.0 equiv), and bis(neopentyltrimethylammonium) oxalate **160** (5.0 mg, 14 µmol, 2.9 equiv) in a mixture of ethanol and pivalonitrile (200 µL, 1:3, v:v), into a 4 mL borosilicate vial. The cartridge was eluted a second time with a mixture of veratrole and pivalonitrile (250 µL, 4:1, v:v) into the same vial. The reaction vial containing 450 µL reaction mixture was sealed with a Teflon-lined cap and was stirred at 130 °C for 30 minutes. The vial was removed from the hot plate, and after 2 minutes the reaction mixture was concentrated by heating at 80 °C under a stream of nitrogen (5 min). To the remaining solution was added a mixture of TFA (0.42 mL), triisopropylsilane (40 µL), *DL*-1,4-dithiothreitol (35 mg), and water (20 µL). The mixture was stirred at 50 °C for 10 minutes. The reaction mixture was diluted with water and methanol (2 mL, 2:1, v:v) and purified by HPLC on a Hypersil Gold column (250×10 mm, 5 µm, flow rate = 4 mL·min^{-1}) with an isocratic mixture of 25:75 (MeCN:water, 0.1% TFA, v:v) for 2 minutes, followed by a linear gradient to 50:50:0.1 (MeCN:water, 0.1% TFA, v:v) within 20 minutes. The activity of the product **151** containing fraction (≈ 21 min) was measured and the product identity and purity was determined by comparison of the HPLC radio-trace with the HPLC UV-trace of the authentic reference sample **151**.

Table S3. Radiochemical yield of **151**.

reaction	starting activity / (MBq)	isolated acitivty after HPLC / (MBq)	aynthesis time / (min)	RCY
1	54.1	13.1	81	40%
2	51.5	10.9	91	38%
average RCY				39%

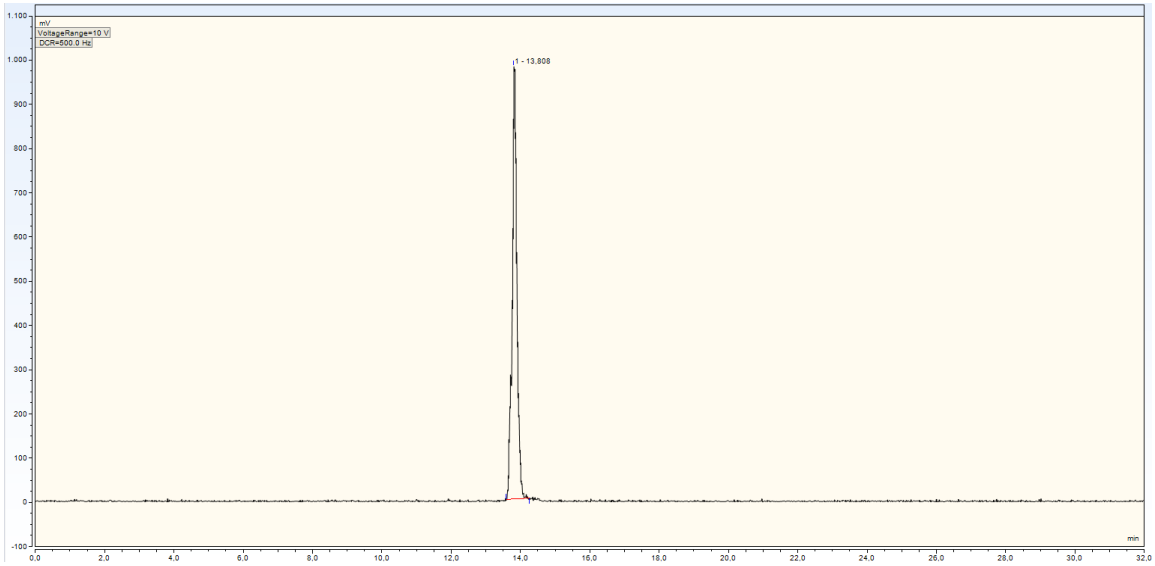

Figure S41. Radio-HPLC trace (gradient 1) of the isolated compound H-Phe(4-[^{18}F]F)-Ile-Cys-Val-Gln-Pro-Ser-Phe-OH **151**.

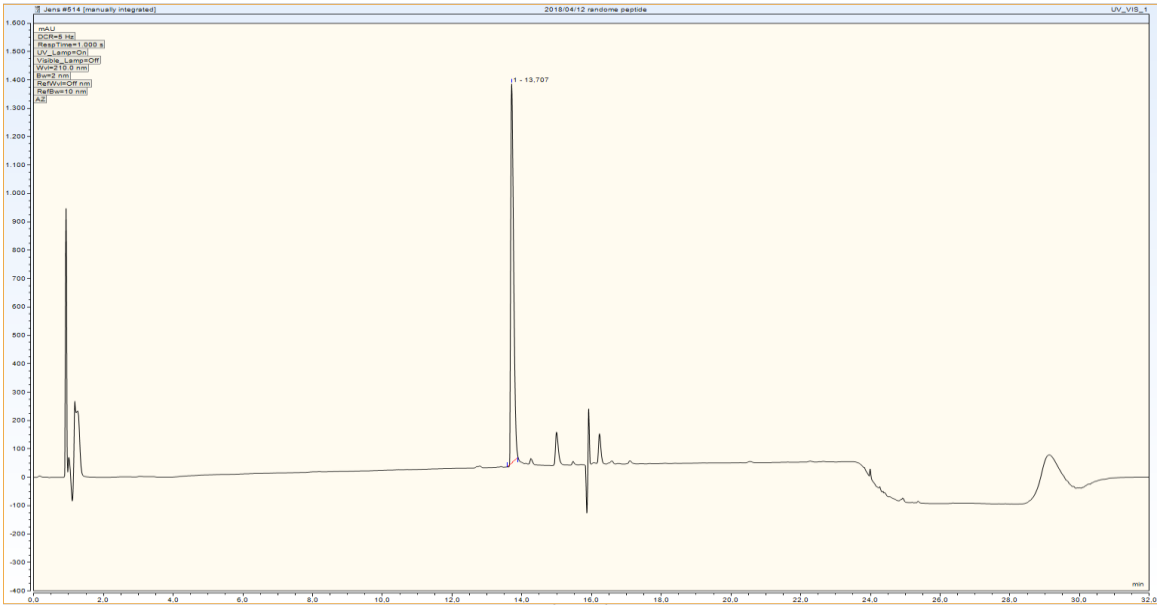

Figure S42. UV-HPLC trace (gradient 1) of H-Phe(4-F)-Ile-Cys-Val-Gln-Pro-Ser-Phe-OH as the reference **[^{19}F]151**.

H-*D*-Glu-Ala-Tyr-Gly-Trp-Met-Asp-Phe(4-[^{18}F]F)-NH$_2$ (148)

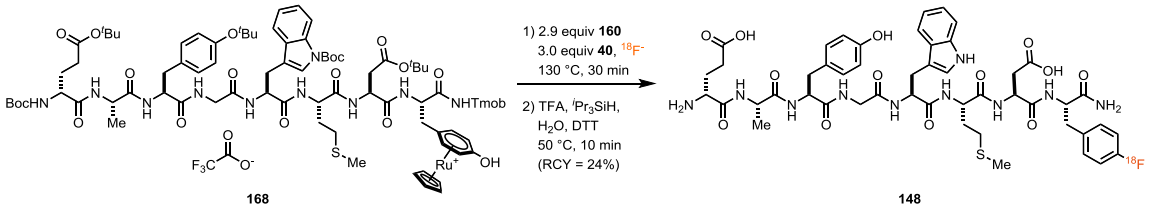

Aqueous [^{18}F]fluoride solution (700 µL) was loaded with a syringe onto a QMA anion-exchange cartridge that was pre-conditioned according to the general procedure. The cartridge was dried by sequentially pushing MeCN (1 mL) and air (2 mL) through the cartridge. The [^{18}F]fluoride was eluted from the cartridge with a solution of **168** (9.3 mg, 5.0 µmol, 1.0 equiv), imidazolium chloride **40** (6.9 mg, 15 µmol, 3.0 equiv), and bis(neopentyltrimethylammonium) oxalate **160** (5.0 mg, 14 µmol, 2.9 equiv) in a mixture of ethanol and pivalonitrile (200 µL, 1:3, v:v), into a 4 mL borosilicate vial. The cartridge was eluted a second time with a mixture of veratrole and pivalonitrile (250 µL, 4:1, v:v) into the same vial. The reaction vial containing 450 µL reaction mixture was sealed with a Teflon-lined cap and was stirred at 130 °C for 30 minutes. The vial was removed from the hot plate, and after 2 minutes the reaction mixture was concentrated by heating at 80 °C under a stream of nitrogen (5 min). To the remaining solution was added a mixture of TFA (0.42 mL), triisopropylsilane (40 µL), *DL*-1,4-dithiothreitol (35 mg), and water (20 µL). The mixture was stirred at 50 °C for 10 minutes. The reaction mixture was diluted with water (2 mL) and purified by HPLC on a Hypersil Gold column (250×10 mm, 5 µm, flow rate = 4 mL·min^{-1}) with an isocratic mixture of 20:80 (MeCN:water, 0.1% TFA, v:v) for 5 minutes, followed by a linear gradient to 50:50 (MeCN:water, 0.1% TFA, v:v) within 20 minutes. The activity of the product **148** containing fraction (≈ 24 min) was measured and the product identity and purity was determined by comparison of the HPLC radio-trace with the HPLC UV-trace of the authentic reference sample **148**.

Table S4. Radiochemical yield of **148**.

reaction	starting activity / (MBq)	isolated acitivty after HPLC / (MBq)	synthesis time / (min)	RCY
1	58.8	5.7	168	28%
2	57.2	7.01	114	24%
3	59.4	4.95	148	21%
average RCY				24%

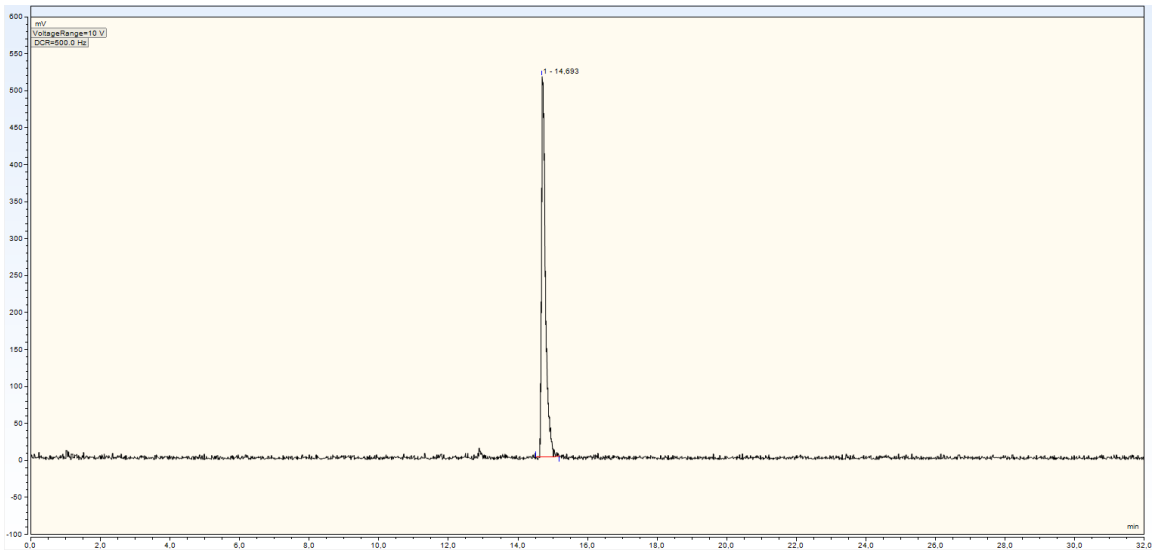

Figure S43. Radio-HPLC trace (gradient 1) of the isolated compound H-*D*-Glu-Ala-Tyr-Gly-Trp-Met-Asp-Phe(4-[^{18}F]F)-NH_2 **148**.

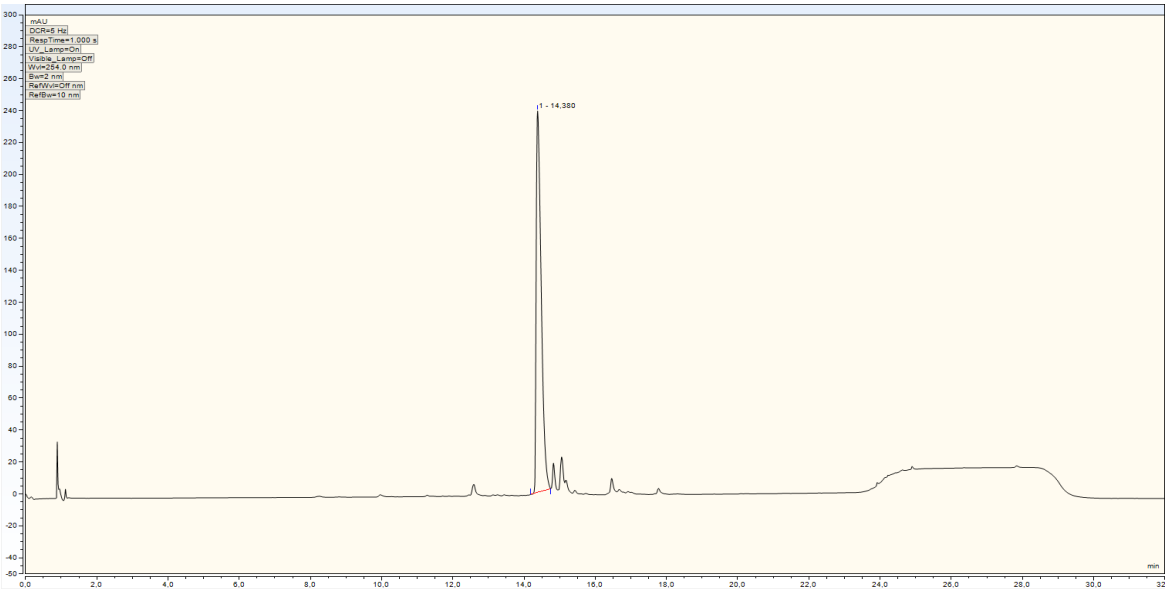

Figure S44. UV-HPLC trace (gradient 1) of H-*D*-Glu-Ala-Tyr-Gly-Trp-Met-Asp-Phe(4-F)-NH_2 **[^{19}F]148** as the reference.

H-Gly-Asn-Leu-Trp-Ala-Thr-Gly-His-Phe(4-[^{18}F]F)-Met-NH$_2$ (150)

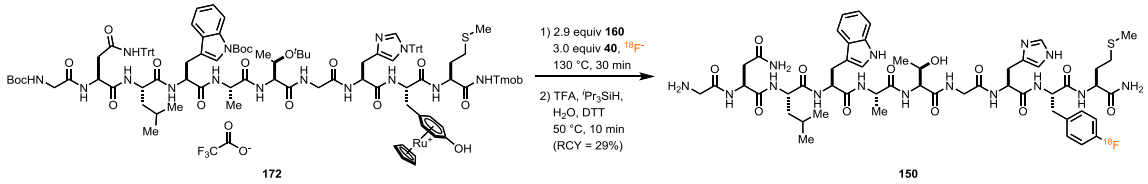

Aqueous [^{18}F]fluoride solution (700 µL) was loaded with a syringe onto a QMA anion-exchange cartridge that was pre-conditioned according to the general procedure. The cartridge was dried by sequentially pushing MeCN (1 mL) and air (2 mL) through the cartridge. The [^{18}F]fluoride was eluted from the cartridge with a solution of **172** (12 mg, 5.0 µmol, 1.0 equiv), imidazolium chloride **40** (6.9 mg, 15 µmol, 3.0 equiv), and bis(neopentyltrimethylammonium) oxalate **160** (5.0 mg, 14 µmol, 2.9 equiv) in a mixture of ethanol and pivalonitrile (200 µL, 1:3, v:v), into a 4 mL borosilicate vial. The cartridge was eluted a second time with a mixture of veratrole and pivalonitrile (250 µL, 4:1, v:v) into the same vial. The reaction vial containing 450 µL reaction mixture was sealed with a Teflon-lined cap and was stirred at 130 °C for 30 minutes. The vial was removed from the hot plate, and after 2 minutes the reaction mixture was concentrated by heating at 80 °C under a stream of nitrogen (5 min). To the remaining solution was added a mixture of TFA (0.42 mL), triisopropylsilane (40 µL), *DL*-1,4-dithiothreitol (35 mg), and water (20 µL). The mixture was stirred at 50 °C for 10 minutes. The reaction mixture was diluted with water (2 mL) and purified by HPLC on a Hypersil Gold column (250×10 mm, 5 µm, flow rate = 4 mL·min^{-1}) with an isocratic mixture of 10:90 (MeCN:water, 0.1% TFA v:v:v) for 2 minutes, followed by a linear gradient to 50:50 (MeCN:water, 0.1% TFA, v:v) within 18 minutes. The activity of the product **150** containing fraction (≈ 23 min) was measured and the product identity and purity was determined by comparison of the HPLC radio-trace with the HPLC UV-trace of the authentic reference sample **150**.

Table S5. Radiochemical yield of **150**.

reaction	starting Activity / (MBq)	isolated acitivty after HPLC / (MBq)	synthesis time / (min)	RCY
1	56.8	5.16	163	25%
2	68.9	11.4	119	33%
average RCY				29%

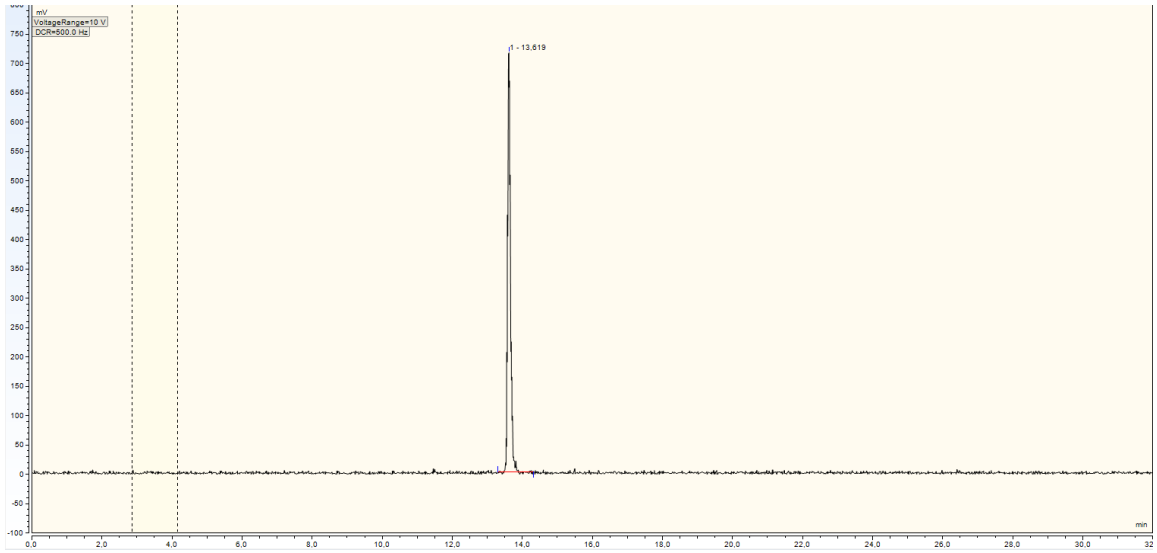

Figure S45. Radio-HPLC trace (gradient 1) of the isolated compound H-Gly-Asn-Leu-Trp-Ala-Thr-Gly-His-Phe(4-[^{18}F]F)-Met-NH_2 **150**.

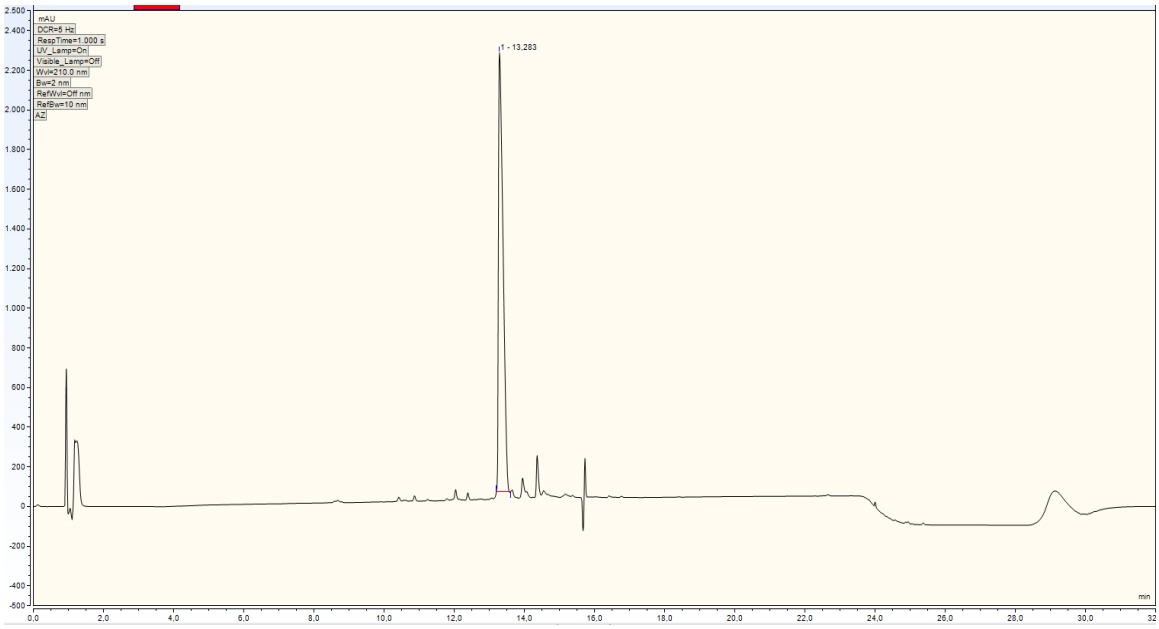

Figure S46. UV-HPLC trace (gradient 1) of H-Gly-Asn-Leu-Trp-Ala-Thr-Gly-His-Phe(4-F)-Met-NH_2 **[^{19}F]150** as the reference.

H-Gly-His-Gly-Phe(4-[^{18}F]F)-Gly-NH$_2$ (152)

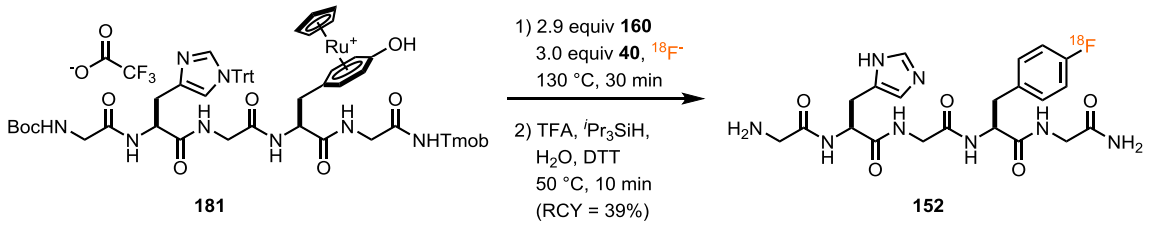

Aqueous [^{18}F]fluoride solution (700 µL) was loaded with a syringe onto a QMA anion-exchange cartridge that was pre-conditioned according to the general procedure. The cartridge was dried by sequentially pushing MeCN (1 mL) and air (2 mL) through the cartridge. The [^{18}F]fluoride was eluted from the cartridge with a solution of **181** (6.0 mg, 5.0 µmol, 1.0 equiv), imidazolium chloride **40** (6.9 mg, 15 µmol, 3.0 equiv), and bis(neopentyltrimethylammonium) oxalate **160** (5.0 mg, 14 µmol, 2.9 equiv) in a mixture of ethanol and pivalonitrile (200 µL, 1:3, v:v), into a 4 mL borosilicate vial. The cartridge was eluted a second time with a mixture of veratrole and pivalonitrile (250 µL, 4:1, v:v) into the same vial. The reaction vial containing 450 µL reaction mixture was sealed with a Teflon-lined cap and was stirred at 130 °C for 30 minutes. The vial was removed from the hot plate, and after 2 minutes the reaction mixture was concentrated by heating at 80 °C under a stream of nitrogen (5 min). To the remaining solution was added a mixture of TFA (0.42 mL), triisopropylsilane (40 µL), *DL*-1,4-dithiothreitol (35 mg), and water (20 µL). The mixture was stirred at 50 °C for 10 minutes. The reaction mixture was diluted with water (2 mL) and purified by HPLC on a Hypersil Gold column (250×10 mm, 5 µm, flow rate = 4 mL·min^{-1}) with an isocratic mixture of 05:95 (MeCN:water, 0.1% TFA, v:v) for 2 minutes, followed by a linear gradient to 50:50 (MeCN:water, 0.1% TFA, v:v) within 20 minutes. The activity of the product **152** containing fraction (≈ 19 min) was measured and the product identity and purity was determined by comparison of the HPLC radio-trace with the HPLC UV-trace of the authentic reference sample **152**.

Table S6. Radiochemical yield of **152**.

reaction	starting activity / (MBq)	isolated acitivty after HPLC / (MBq)	synthesis time / (min)	RCY
1	13.3	3.17	84	41%
2	46.6	8.84	110	37%
average RCY				39%

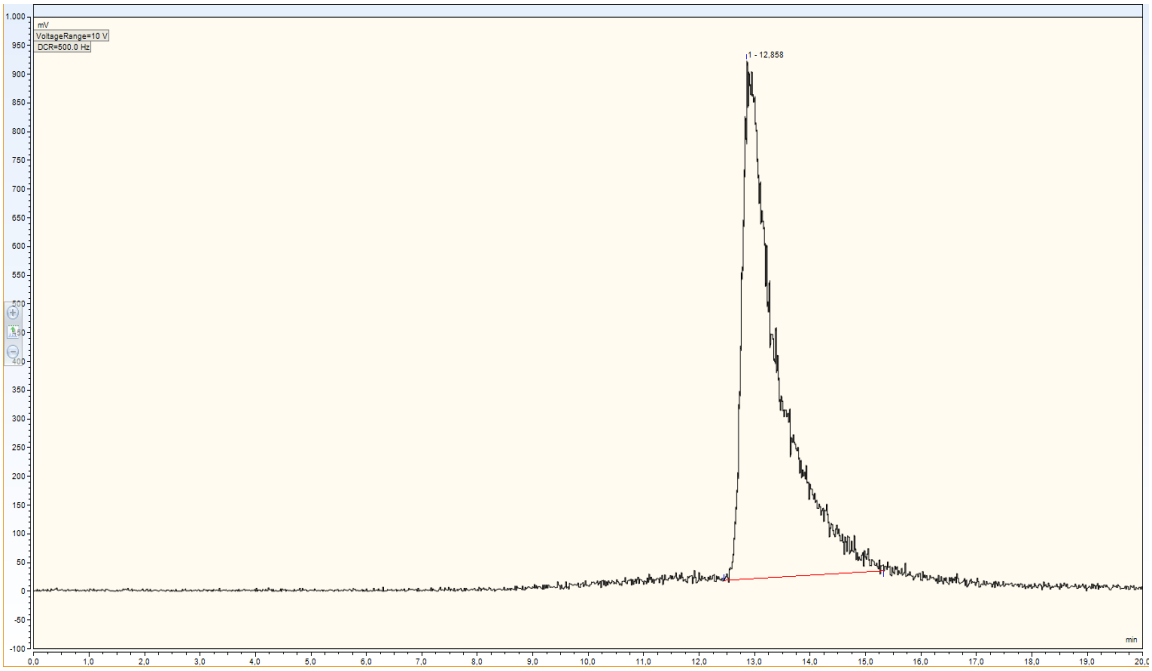

Figure S47. Radio-HPLC trace (Chiralpak® ZWIX (+) ((10×250 mm, 5 µm), flow rate = 1.0 mL·min^{-1}, 35 °C) with an isocratic eluent 49:49:2 (MeOH:MeCN:H_2O+50 mM formic acid, 25 mM diethylamine) of the isolated compound H-Gly-His-Gly-Phe(4-[^{18}F]F)-Gly-NH_2 **152**.

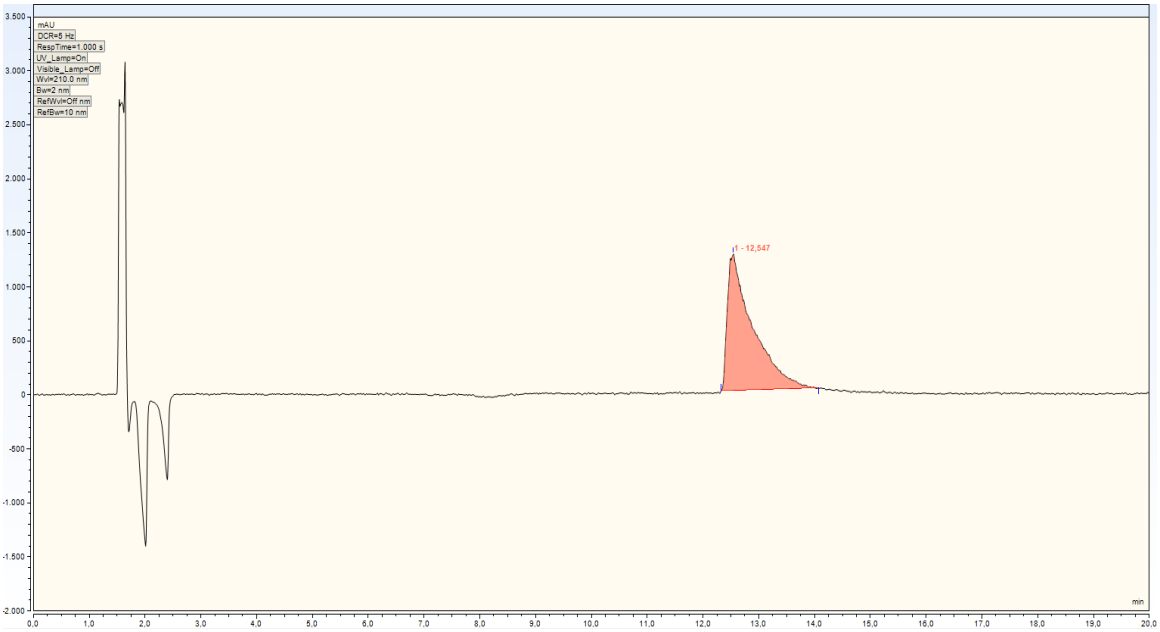

Figure S48. UV-HPLC trace (Chiralpak® ZWIX (+) ((10×250 mm, 5 µm), flow rate = 1.0 mL·min^{-1}, 35 °C) with an isocratic eluent 49:49:2 (MeOH:MeCN:H_2O+50 mM formic acid, 25 mM diethylamine) of H-Gly-His-Gly-Phe(4-F)-Gly-NH_2 as the reference **[^{19}F]152**.

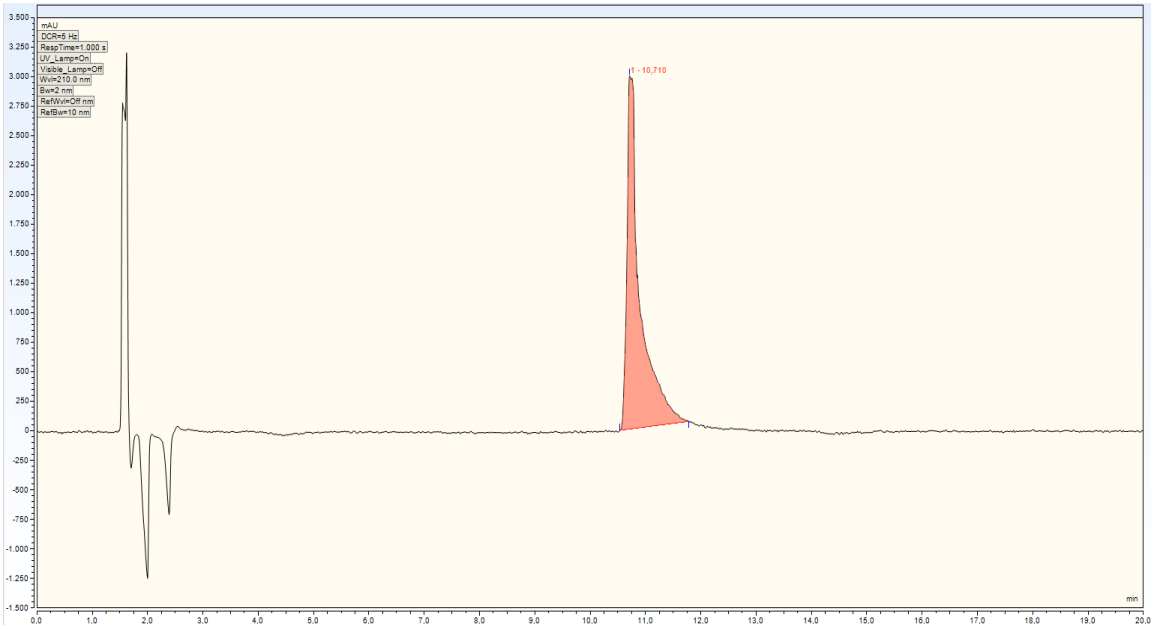

Figure S49. UV-HPLC trace (Chiralpak® ZWIX (+) ((10×250 mm, 5 µm), flow rate = 1.0 mL·min^{-1}, 35 °C) with an isocratic eluent 49:49:2 (MeOH:MeCN:H_2O+50 mM formic acid, 25 mM diethylamine) of H-Gly-(*D*-His)-Gly-Phe(4-F)-Gly-NH_2 as the reference **179**.

H-Leu-Phe(4-[^{18}F]F)-Glu-Met-Lys-NH$_2$ (147)

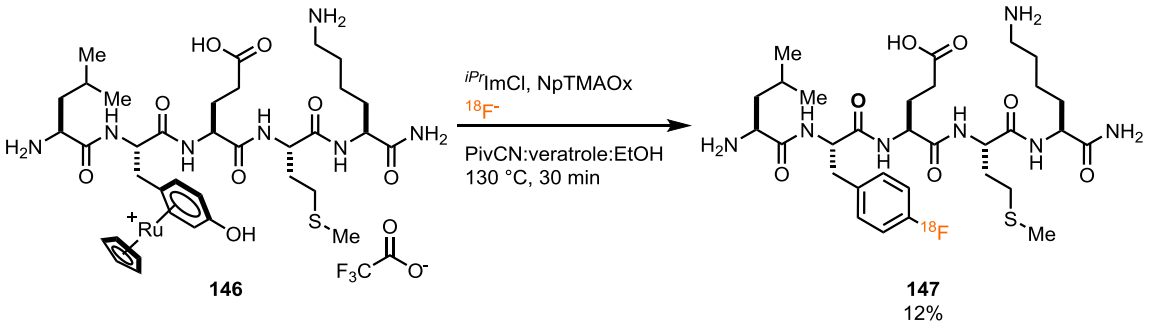

Aqueous [^{18}F]fluoride solution (700 µL) was loaded with a syringe onto a QMA anion-exchange cartridge that was pre-conditioned according to the general procedure. The cartridge was dried by sequentially pushing MeCN (1 mL) and air (2 mL) through the cartridge. The [^{18}F]fluoride was eluted from the cartridge with a solution of **146** (4.9 mg, 5.0 µmol, 1.0 equiv), imidazolium chloride **40** (6.9 mg, 15 µmol, 3.0 equiv), and bis(neopentyltrimethylammonium) oxalate **160** (5.0 mg, 14 µmol, 2.9 equiv) in methanol (400 µL), into a 4 mL borosilicate vial. The reaction mixture was concentrated by heating at 80 °C under a stream of nitrogen (5 min). To the vial was added a mixture of veratrole, pivalonitrile and ethanol (450 µL, 4:4:1, v:v:v). The reaction vial containing 450 µL reaction mixture was sealed with a Teflon-lined cap and was stirred at 130 °C for 30 minutes. The reaction mixture was diluted with methanol (1 mL) and was analysed by radio-HPLC.

Figure S50. Radio-HPLC trace (gradient 1) of the crude reaction mixture.

H-Leu-Phe(4-[^{18}F]F)-Glu-Met-Lys-NH$_2$ (147)

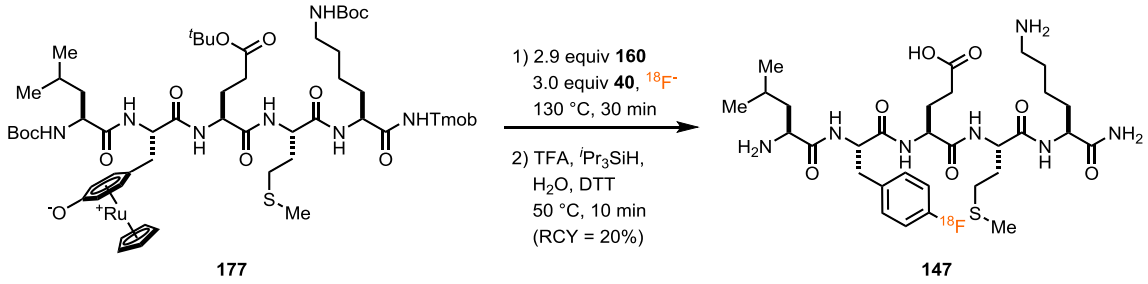

Aqueous [^{18}F]fluoride solution (700 µL) was loaded with a syringe onto a QMA anion-exchange cartridge that was pre-conditioned according to the general procedure. The cartridge was dried by sequentially pushing MeCN (1 mL) and air (2 mL) through the cartridge. The [^{18}F]fluoride was eluted from the cartridge with a solution of **177** (7.0 mg, 5.0 µmol, 1.0 equiv), imidazolium chloride **40** (6.9 mg, 15 µmol, 3.0 equiv), and bis(neopentyltrimethylammonium) oxalate **160** (5.0 mg, 14 µmol, 2.9 equiv) in a mixture of ethanol and pivalonitrile (200 µL, 1:3, v:v), into a 4 mL borosilicate vial. The cartridge was eluted a second time with a mixture of veratrole and pivalonitrile (250 µL, 4:1, v:v) into the same vial. The reaction vial containing 450 µL reaction mixture was sealed with a Teflon-lined cap and was stirred at 130 °C for 30 minutes. The vial was removed from the hot plate, and after 2 minutes the reaction mixture was concentrated by heating at 80 °C under a stream of nitrogen (5 min). To the remaining solution was added a mixture of TFA (0.42 mL), triisopropylsilane (40 µL), *DL*-1,4-dithiothreitol (35 mg), and water (20 µL). Then the mixture was stirred at 50 °C for 10 minutes. The reaction mixture was diluted with water (2 mL) and purified by HPLC on a Hypersil Gold column (250×10 mm, 5 µm, flow rate = 4 mL·min^{-1}) with an isocratic mixture of 15:85 (MeCN:water, 0.1% TFA, v:v) for 2 minutes, followed by a linear gradient to 35:65:0.1 (MeCN:water, 0.1% TFA, v:v) within 16 minutes. The activity of the product **147** containing fraction (≈ 18 min) was measured and the product identity and purity was determined by comparison of the HPLC radio-trace with the HPLC UV-trace of the authentic reference sample **147**.

Table S7. Radiochemical yield of **147**.

reaction	starting activity / (MBq)	isolated acitivty after HPLC / (MBq)	synthesis time / (min)	RCY
1	56.1	4.54	110	16%
2	63.1	8.16	98	24%
average RCY				20%

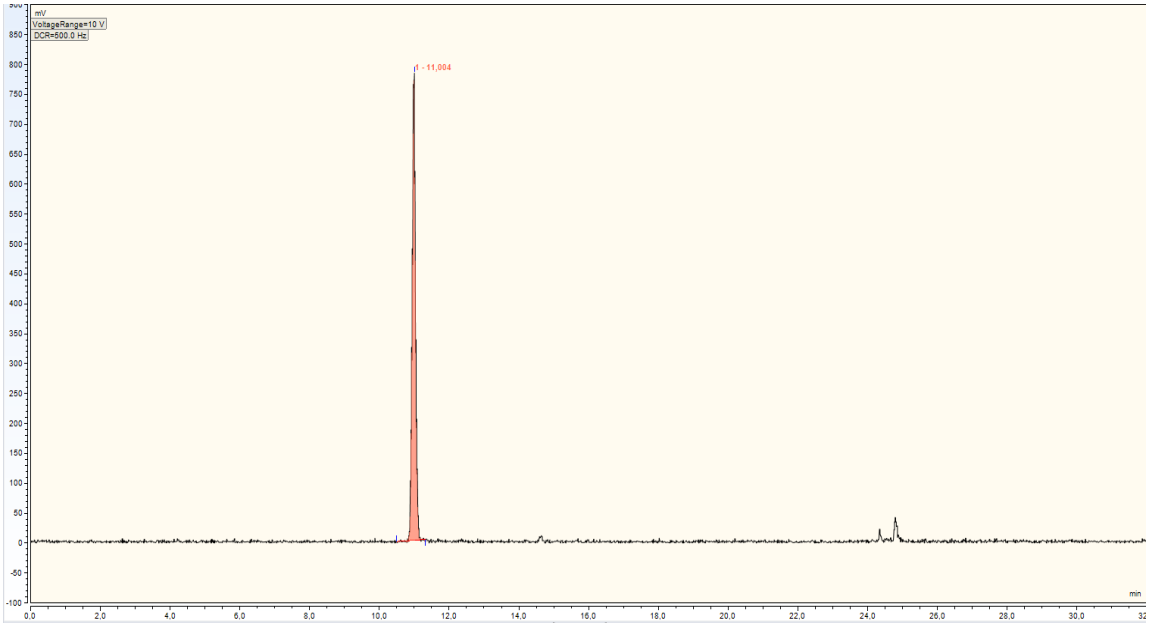

Figure S51. Radio-HPLC trace (gradient 1) of the isolated compound H-Leu-Phe(4-[^{18}F]F)-Glu-Met-Lys-NH_2 **147**.

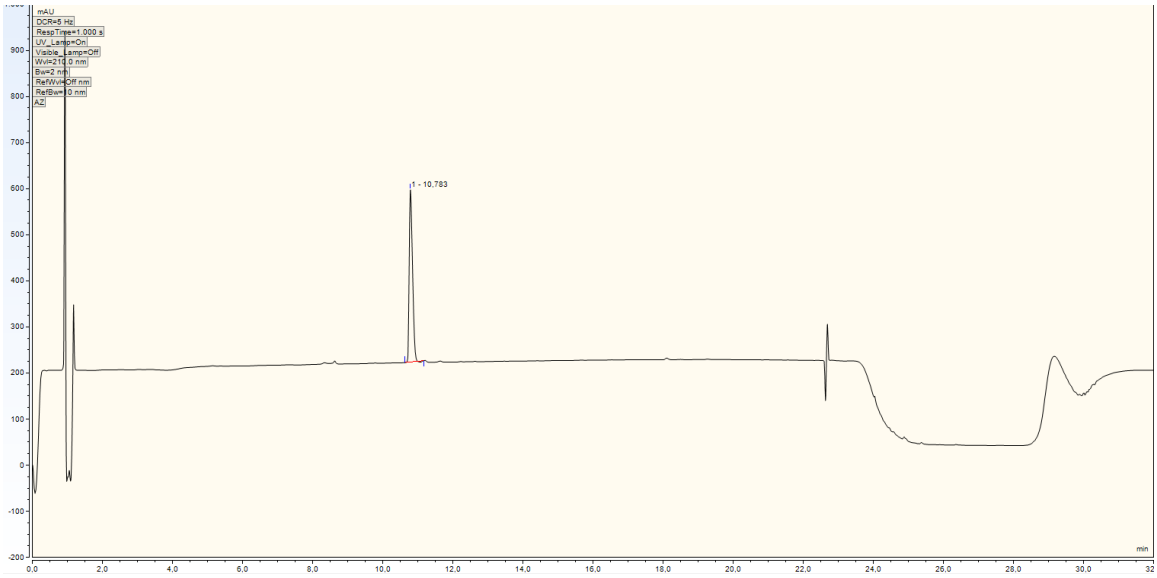

Figure S52. UV-HPLC trace (gradient 1) of H-Leu-Phe(4-F)-Glu-Met-Lys-NH_2 as the reference **[^{19}F]147**.

Automated H-Leu-Phe(4-[^{18}F]F)-Glu-Met-Lys-NH$_2$ (147) synthesis

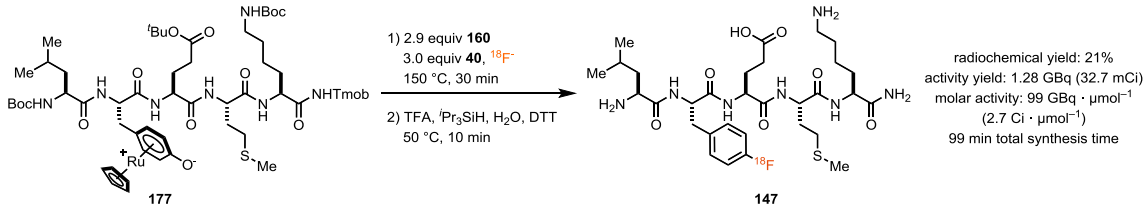

Reactions were performed on an automated cassette-based radiochemical synthesizer ELIXYS FLEX/CHEM connected to a PURE/FORM purification and formulation unit (Sofie Biosciences). Aqueous [^{18}F]fluoride (11.4 GBq, (308 mCi), t = 0) was trapped onto a QMA anion-exchange cartridge that was pre-conditioned according to the general procedure, the cartridge was then washed with MeCN (1.0 mL). The [^{18}F]fluoride was eluted from the cartridge with a solution of **177** (6.0 mg, 5.0 µmol, 1.0 equiv), imidazolium chloride **40** (6.9 mg, 15 µmol, 3.0 equiv), and bis(neopentyltrimethylammonium) oxalate **160** (5.0 mg, 14 µmol, 2.9 equiv) in a mixture of ethanol and but-2-one (200 µL, 1:3, v:v), into a 3 mL V-vial (an aluminum cylinder 15.0 mm height and 15.0 mm diameter was placed underneath the V-vial in the reactor to fit the 3 mL V-vial in the 5 mL V-vial sample holder). The cartridge was eluted a second time with a mixture of veratrole and but-2-one (250 µL, 4:1, v:v) into the same vial. The reaction vial containing 450 µL reaction mixture was sealed against a Teflon-liner and was stirred at elevated temperature (set-point at 150 °C) for 30 minutes and subsequently cooled to 50 °C. The solvent was evaporated at 100 °C under reduced pressure for 5 minutes. To the remaining solution was added a mixture of TFA (0.42 mL), triisopropylsilane (40 µL), *DL*-1,4-dithiothreitol (35 mg), and water (20 µL). Then the mixture was stirred at 50 °C for 10 minutes. The reaction mixture was cooled to room temperature and then diluted with a solution of water (1.5 mL) and methanol (0.75 mL). The reaction mixture was transferred from the ELIXYS FLEX/CHEM system to the PURE/FORM, and was purified by HPLC with a Hypersil Gold (250×10 mm, 5 µm, flow rate = 4 mL·min^{-1}) column with an isocratic mixture of 15:85 (MeCN:water, 0.1% TFA, v:v) for 2 minutes, followed by a linear gradient to 45:55 (MeCN:water, 0.1% TFA, v:v) within 18 minutes. The product was collected from 18 min to 19 min. The activity of the product containing fraction was diluted with water (40 mL) and loaded onto a C-18 light SepPak cartridge. The C-18 cartridge was washed

with water (3 mL) and the product was sequentially eluted with ethanol (1 mL) and saline (1.7 mL). The ethanolic saline solution contained 1.28 GBq (34.6 mCi, t = 99 min). The total decay corrected radio chemical yield is 21 %.The radiochemical identity was confirmed by analytical HPLC.

To determine the molar activity of **147**, 22.1 MBq of purified compound **147** (Figure S54, 87% purity was observed and therefore calculations were proceeded with 19.3 MBq. However, the observed low purity was presumably due to saturation of the detector. If a smaller amount of sample was injected 100% purity was observed. (Figure S56)) was injected into an analytical HPLC and the UV absorption corresponding to the radio-peak was measured. To determine the amount of **147** the molar response of **[^{19}F]147** was determined (Figure S58) with the authentic standard H-Leu-Phe(4-F)-Glu-Met-Lys-NH_2 **[^{19}F]147**. It was calculated that the absorption of 2.5629 mAU·min (Figure S58) corresponds to 0.20 nmol of **147** and therefore the molar activity of **147** was determined to be 99 GBq·µmol^{-1} (2.7 Ci·µmol^{-1}).

The ruthenium content in the reformulated sample was 1.8 µg, which is more than fivefold below the specified limit of 10 µg per day considered safe for injection into humans. If an additional reformulation with a C-18 cartridge was performed before injection into the preparative HPLC, the ruthenium content dropped to 0.09 µg. If desired, the residual ruthenium can be reduced by the use of commercial metal scavengers. To achieve this 200 mg Quadrasil™ AP were added to the reaction mixture before concentration under a stream of nitrogen. After addition of Quadrasil™ AP the reaction mixture was stirred at 50 °C for 10 min. The reaction mixture was filtered and the filter cake was eluted with methanol (0.5 mL). The filtrate was concentrated by heating at 80 °C under a stream of nitrogen (5 min). To the remaining solution was added a mixture of TFA (0.42 mL), triisopropylsilane (40 µL), *DL*-1,4-dithiothreitol (35 mg), and water (20 µL). Then the mixture was stirred at 50 °C for 10 minutes. The reaction mixture was diluted with water (2 mL) and purified by HPLC. The use of Quadrasil™ AP lowered the ruthenium content to 0.11 µg. A blank sample of the HPLC eluent contained 0.03 µg of ruthenium.

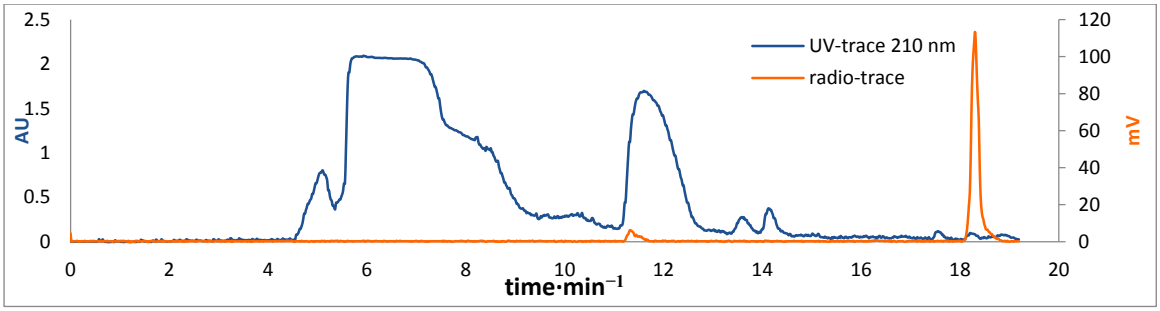

Figure S53. Overlay of radio-trace (orange) and UV-trace (blue) of the crude reaction mixture.

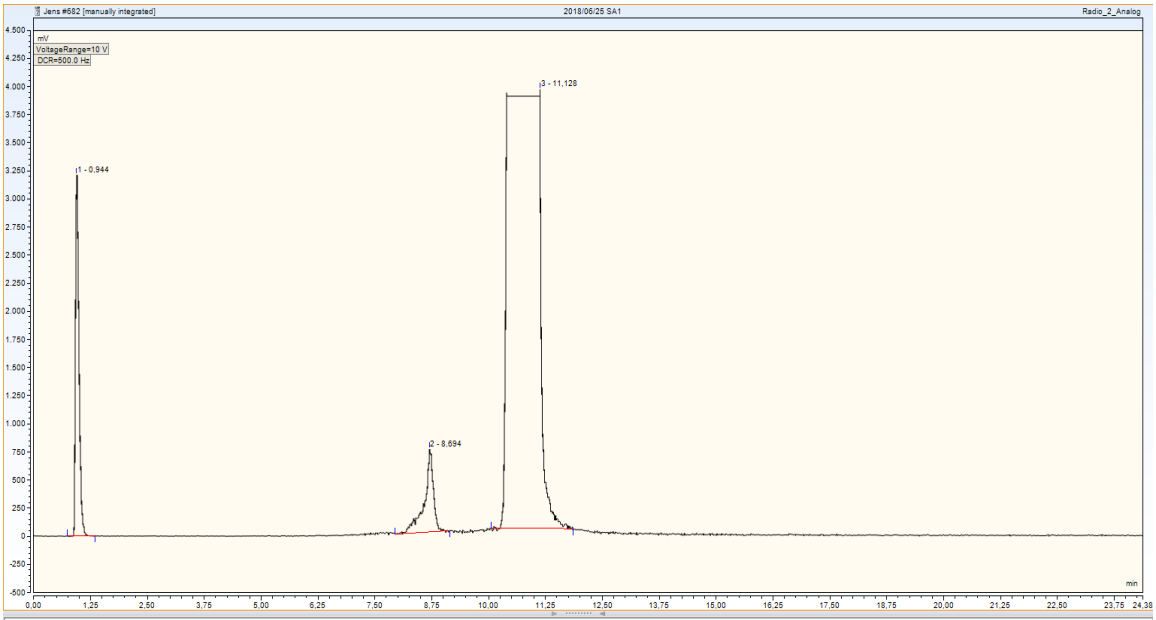

No.	Peakname	Ret.Time min	Area mV*min	Amount n.a.	Type	Height mV	Rel.Area %	Resolution
1		0,944	290,2351	n.a.	BMB*	3210,912	8,07	39,19
2		8,694	166,6496	n.a.	BMB*	736,112	4,63	3,13
3		11,128	#########	n.a.	BMB*	3906,548	87,30	n.a.
Total:			#########	0,0000		7853,572	100,00	

Figure S54. Determination of molar activity (gradient 1); radio-trace (22.1 MBq).

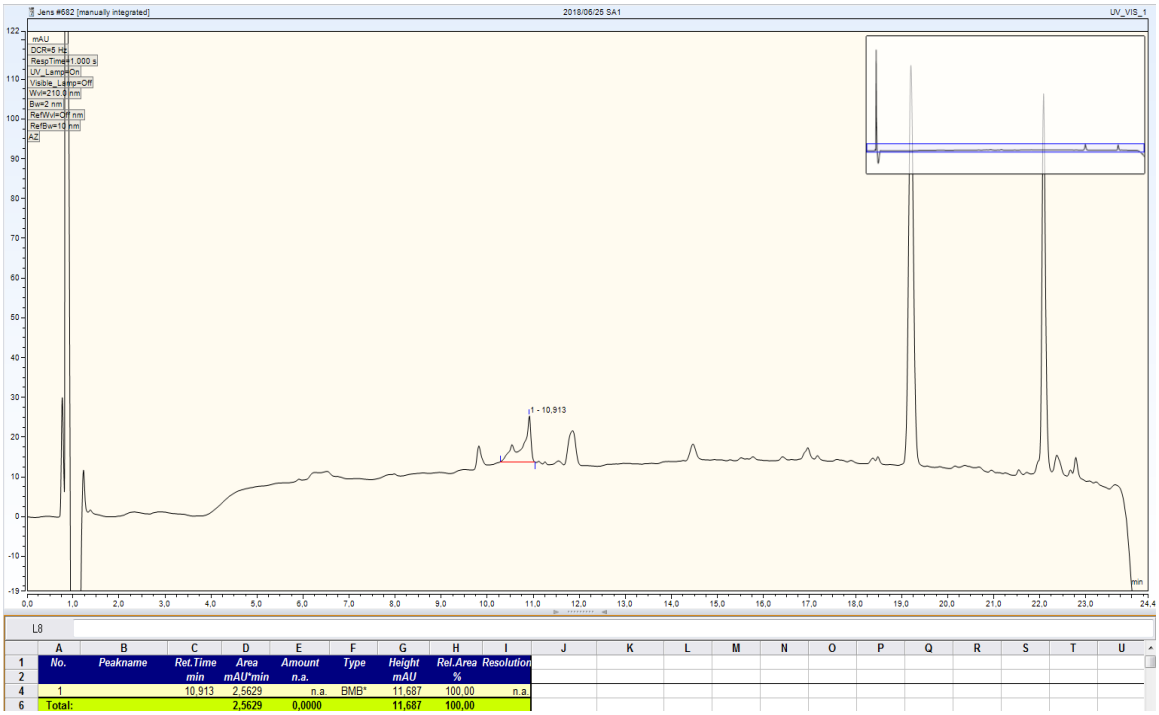

L8

	A	B	C	D	E	F	G	H	I	J	K	L	M	N	O	P	Q	R	S	T	U
1	No.	Peakname	Ret.Time min	Area mAU*min	Amount n.a.	Type	Height mAU	Rel.Area %	Resolution												
2																					
4	1		10,913	2,5629	n.a.	BMB*	11,687	100,00	n.a.												
6	Total:			2,5629	0,0000		11,687	100,00													

Figuer S55. Determination of molar activity (gradient 1); UV-trace (22.1 MBq).

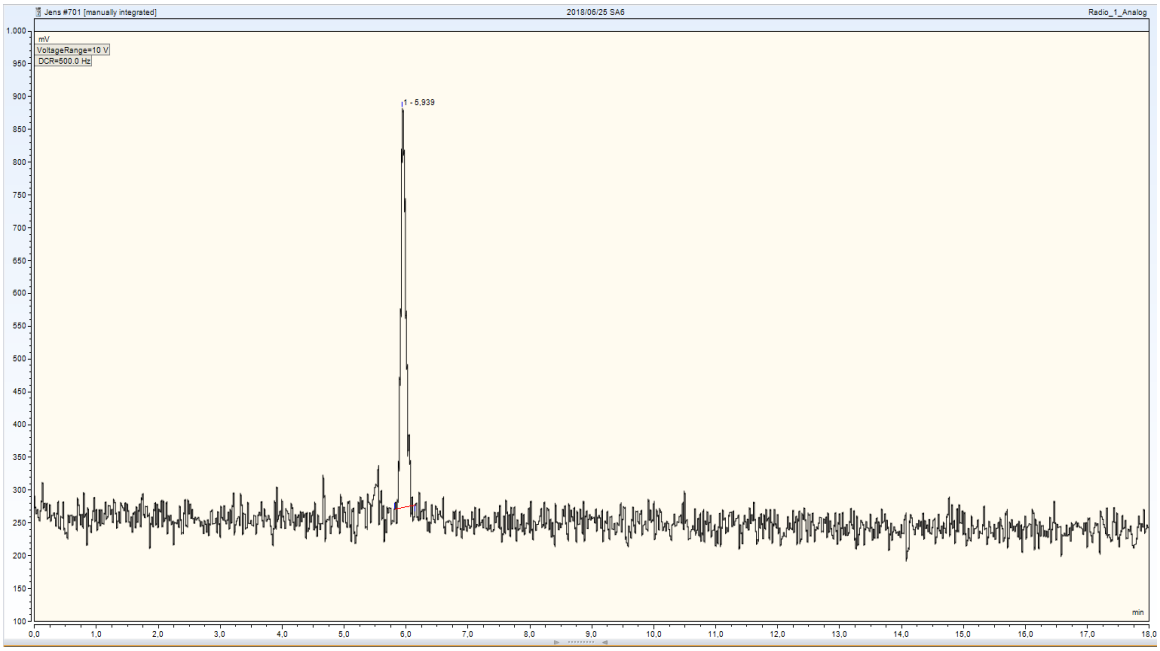

Figure S56. Determination of molar activity (gradient 2); radio-trace @ 210 nm.

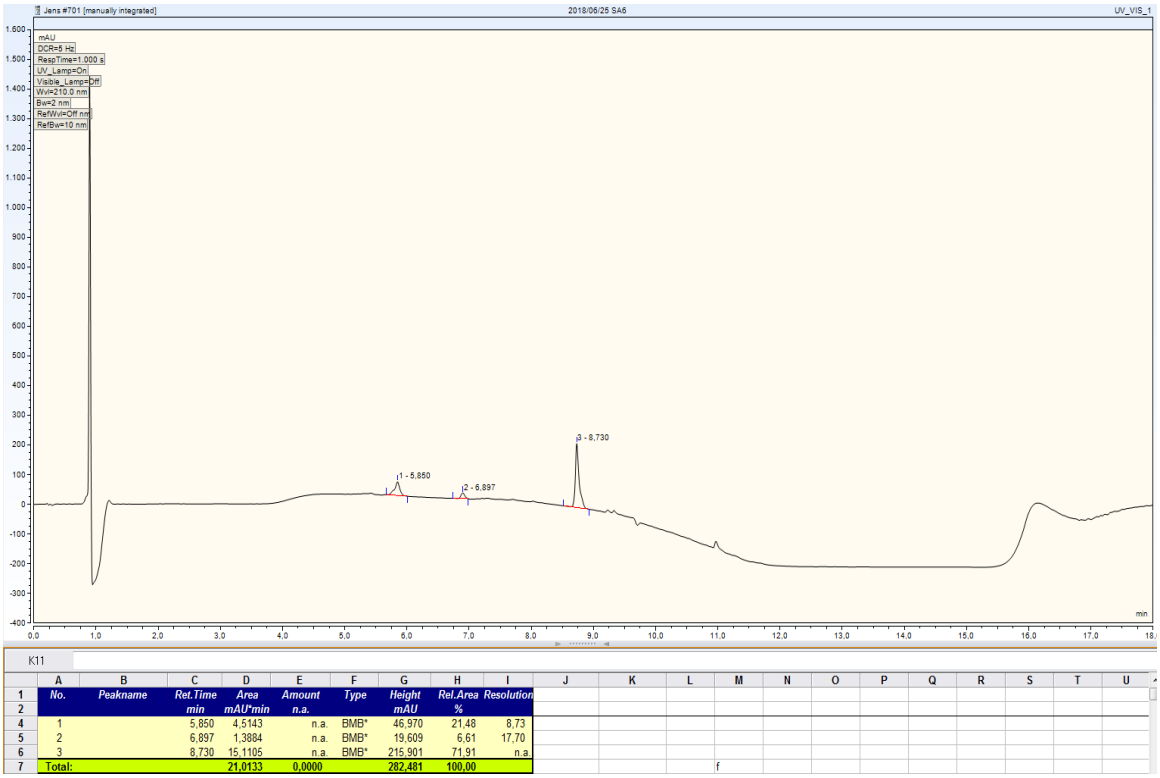

K11

	A	B	C	D	E	F	G	H	I	J	K	L	M	N	O	P	Q	R	S	T	U
1	No.	Peakname	Ret.Time	Area	Amount	Type	Height	Rel.Area	Resolution												
2			min	mAU*min	n.a.		mAU	%													
4	1		5,850	4,5143	n.a.	BMB*	46,970	21,48	8,73												
5	2		6,897	1,3884	n.a.	BMB*	19,609	6,61	17,70												
6	3		8,730	15,1105	n.a.	BMB*	215,901	71,91	n.a.												
7	Total:			21,0133	0,0000		282,481	100,00													

Figure S57. Determination of molar activity (gradient 2); UV-trace @ 210 nm.

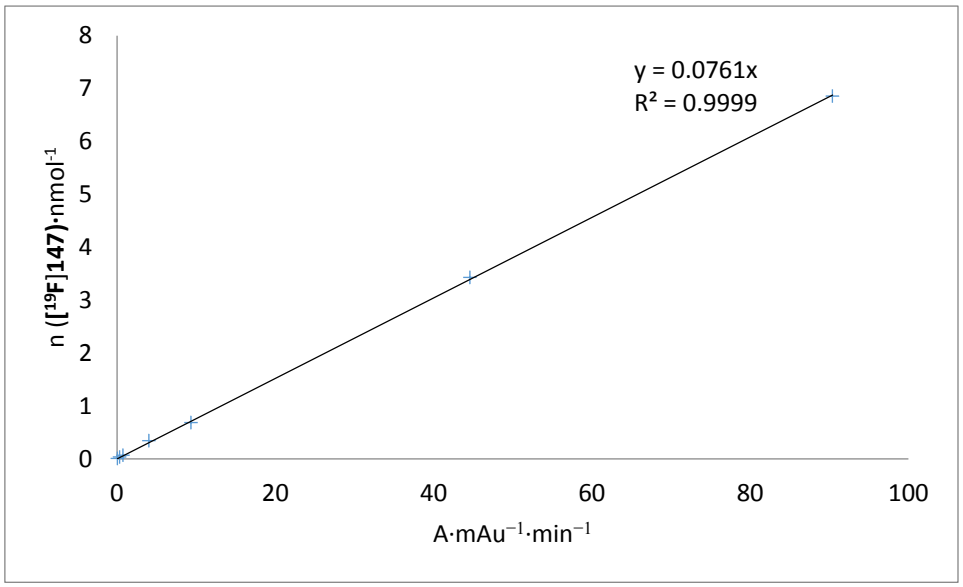

Figure S58. Calibration curve acquired with **[^{19}F]147** at 210 nm for determination of molar activity.

.

V. References

[1] G. Hevesy, *Biochem. J.* **1923**, *17*, 439-445.
[2] W. G. Myers, *J. Nucl. Med.* **1979**, *20*, 590-698.
[3] O. Chiewitz, G. Hevesy, *Nature* **1935**, *136*, 754-755.
[4] F. Joliot, I. Curie, *Nature* **1934**, *133*, 201-202.
[5] E. O. Lawrence, D. Cooksey, *Phys. Rev.* **1936**, *50*, 1131-1140.
[6] P. M. Matthews, E. A. Rabiner, J. Passchier, R. N. Gunn, *Br. J. Clin. Pharmacol.* **2012**, *73*, 175-186.
[7] H. Herzog, *Radiochim. Acta* **2001**, *89*, 203-214.
[8] P. W. Miller, N. J. Long, R. Vilar, A. D. Gee, *Angew. Chem., Int. Ed.* **2008**, *47*, 8998-9033.
[9] (a) D. W. Townsend, S. R. Cherry, *Eur. Radiol.* **2001**, *11*, 1968-1974; (b) Y. Berker, Y. Li, *Med. Phys.* **2016**, *43*, 807-832; (c) P. E. Kinahan, B. H. Hasegawa, T. Beyer, *Semin. Nucl. Med.* **2003**, *33*, 166-179.
[10] A. L. Feliu, *J. Chem. Educ.* **1988**, *65*, 655-660.
[11] H. J. Ache, *Angew. Chem., Int. Ed.* **1972**, *11*, 179-199.
[12] S. Patching, *J. Diagn. Imaging Ther.* **2015**, *2*, 30-102.
[13] H. H. Coenen, P. H. Elsinga, R. Iwata, M. R. Kilbourn, M. R. Pillai, M. G. Rajan, H. N. Wagner, Jr., J. J. Zaknun, *Nucl. Med. Biol.* **2010**, *37*, 727-740.
[14] S. N. Reske, J. Kotzerke, *Eur. J. Nucl. Med.* **2001**, *28*, 1707-1723.
[15] (a) T. Ido, C. N. Wan, V. Casella, J. S. Fowler, A. P. Wolf, M. Reivich, D. E. Kuhl, *J. Labelled Compd. Radiopharm.* **1978**, *14*, 175-183; (b) H. H. C. K. Hamacher, and G. Stocklin, *J. Nucl. Med.* **1986**, *27*, 235-238.
[16] H. H. Coenen, V. W. Pike, G. Stöcklin, R. Wagner, *Int. J. Radiat. Appl. Instrum. Part A* **1987**, *38*, 605-610.
[17] G. A. van Dongen, G. W. Visser, M. N. Lub-de Hooge, E. G. de Vries, L. R. Perk, *Oncologist* **2007**, *12*, 1379-1389.
[18] S. C. Jones, J. H. Greenberg, R. Dann, G. D. Robinson, Jr., M. Kushner, A. Alavi, M. Reivich, *J. Cereb. Blood Flow Metab.* **1985**, *5*, 566-575.

[19] M. M. Khalil, *Basic Sciences of Nuclear Medicine*, Springer, Berlin, Heidelberg, **2011**.
[20] L. Cunha, I. Horvath, S. Ferreira, J. Lemos, P. Costa, D. Vieira, D. S. Veres, K. Szigeti, T. Summavielle, D. Máthé, L. F. J. M. D. Metello, Therapy, *Mol. Diagn. Ther.* **2014**, *18*, 153-173.
[21] W. F. Walsh, H. R. Fill, P. V. Harper, *Semin. Nucl. Med.* **1977**, *7*, 59-66.
[22] E. Britannica, *https://www.britannica.com/technology/cyclotron/images-videos/media/1/148211/18064*.
[23] A. Pekosak, U. Filp, A. J. Poot, A. D. Windhorst, *Mol. Imaging Biol.* **2018**, *20*, 510-532.
[24] F. Wuest, M. Berndt, T. Kniess, *Carbon-11 Labeling Chemistry Based upon [11C]Methyl Iodide*, Springer Berlin Heidelberg, Berlin, Heidelberg, **2007**, 183-213.
[25] S. Faulkner, N. J. Long, *Dalton Trans.* **2011**, *40*, 6067-6067.
[26] S. R. Banerjee, M. G. Pomper, *Appl. Radiat. Isot.* **2013**, *76*, 2-13.
[27] B. N. Clarke, *J. Nucl. Med. Technol.* **2018**, *46*, 12-16.
[28] A. Sanchez-Crespo, P. Andreo, S. A. Larsson, *Eur. J. Nucl. Med. Mol. Imaging* **2004**, *31*, 44-51.
[29] D. O'Hagan, D. B. Harper, *J. Fluorine Chem.* **1999**, *100*, 127-133.
[30] L. M. Jarvis, *Chem. Eng. News* **2019**, *97*, 33-37.
[31] N. A. Meanwell, *J. Med. Chem.* **2011**, *54*, 2529-2591.
[32] D. O'Hagan, *Chem. Soc. Rev.* **2008**, *37*, 308-319.
[33] S. C. P. Williams, *Nat. Med.* **2013**, *19*, 1551.
[34] R. van Grieken, M. de Bruin, *Pure Appl. Chem.* **1994**, *66*, 2513-2526.
[35] L. Cai, S. Lu, V. W. Pike, *Eur. J. Org. Chem.* **2008**, *2008*, 2853-2873.
[36] V. Casella, T. Ido, A. P. Wolf, J. S. Fowler, R. R. MacGregor, T. J. Ruth, *J. Nucl. Med.* **1980**, *21*, 750-757.
[37] O. Matsson, J. Persson, B. S. Axelsson, B. Långström, *J. Am. Chem. Soc.* **1993**, *115*, 5288-5289.
[38] J. Bergman, O. Solin, *Nucl. Med. Biol.* **1997**, *24*, 677-683.

[39] M. S. Berridge, S. M. Apana, J. M. Hersh, *J. Labelled Compd. Radiopharm.* **2009**, *52*, 543-548.
[40] G. Firnau, R. Chirakal, E. S. Garnett, *J. Nucl. Med.* **1984**, *25*, 1228-1233.
[41] M. J. Adam, J. R. Grierson, T. J. Ruth, S. Jivan, *Int. J. Radiat. Appl. Instrum. Part A* **1986**, *37*, 877-882.
[42] H. H. Coenen, K. Franken, P. Kling, G. Stöcklin, *Int. J. Radiat. Appl. Instrum. Part A* **1988**, *39*, 1243-1250.
[43] M. J. Adam, B. F. Abeysekera, T. J. Ruth, S. Jivan, B. D. Pate, *J. Labelled Compd. Radiopharm.* **1984**, *21*, 1227-1228.
[44] H. H. Coenen, S. M. Moerlein, *J. Fluorine Chem.* **1987**, *36*, 63-75.
[45] O. Solin, J. Bergman, M. Haaparanta, A. Reissell, *Int. J. Radiat. Appl. Instrum. Part A* **1988**, *39*, 1065-1071.
[46] D. M. Jewett, S. A. Toorongian, G. K. Mulholland, G. L. Watkins, M. R. Kilbourn, *Int. J. Radiat. Appl. Instrum. Part A* **1988**, *39*, 1109-1111.
[47] C. L. Liotta, H. P. Harris, *J. Am. Chem. Soc.* **1974**, *96*, 2250-2252.
[48] J. Emsley, *Chem. Soc. Rev.* **1980**, *9*, 91-124.
[49] X. Chen, J. I. Brauman, *J. Am. Chem. Soc.* **2008**, *130*, 15038-15046.
[50] M. R. Kilbourn, J. R. Huizenga, *Fluorine-18 Labeling of Radiopharmaceuticals*, National Academies, **1990**.
[51] B. Langlois, L. Gilbert, G. Forat, in *The Roots of Organic Development, Vol. 8*, Elsevier, **1996**, 244-292.
[52] E. E. Kwan, Y. Zeng, H. A. Besser, E. N. Jacobsen, *Nat. Chem.* **2018**, *10*, 917-923.
[53] S. Preshlock, M. Tredwell, V. Gouverneur, *Chem. Rev.* **2016**, *116*, 719-766.
[54] H. H. Coenen, PET Chemistry The Driving Force in Molecular Imaging, *Fluorine-18 Labeling Methods: Features and Possibilities of Basic Reactions*, Springer Berlin, Heidelberg, **2007**, 15-50.
[55] M. S. Haka, M. R. Kilbourn, L. G. Watkins, S. A. Toorongian, *J. Labelled Compd. Radiopharm.* **1989**, *27*, 823-833.

[56] H. Sun, S. G. DiMagno, *J. Fluorine Chem.* **2007**, *128*, 806-812.
[57] J. Ermert, C. Hocke, T. Ludwig, R. Gail, H. H. Coenen, *J. Labelled Compd. Radiopharm.* **2004**, *47*, 429-441.
[58] L. Allain-Barbier, M.-C. Lasne, C. Perrio-Huard, B. Moreau, L. Barré, *Acta Chem. Scand.* **1998**, *52*, 480-489.
[59] (a) O. Wallach, *Liebigs Ann.* **1886**, *235*, 255-271; (b) G. Balz, G. Schiemann, *Ber. Dtsch. Chem. Ges.* **1927**, *60*, 1186-1190.
[60] B. Langlois, in *Organo-Fluorine Compounds, Vol. E 10 a*, 4th Edition ed., Georg Thieme Verlag, **1998**, 686-709.
[61] R. M. Hoyte, S. S. Lin, D. R. Christman, H. L. Atkins, W. Hauser, A. P. Wolf, *J. Nucl. Med.* **1971**, *12*, 280-286.
[62] M. Argentini, C. Wiese, R. Weinreich, *J. Fluorine Chem.* **1994**, *68*, 141-144.
[63] H. Hayashi, H. Sonoda, K. Fukumura, T. Nagata, *Chem. Commun.* **2002**, 1618-1619.
[64] P. Tang, W. Wang, T. Ritter, *J. Am. Chem. Soc.* **2011**, *133*, 11482-11484.
[65] C. N. Neumann, J. M. Hooker, T. Ritter, *Nature* **2016**, *534*, 369-373.
[66] A. Böttcher, A. Chlenov, B. Gotov, W. D. Harman, M. A. Kondratenkov, E. P. Kündig, K. Muñz, A. Pape, J. H. Rigby, H.-G. Schmalz, M. F. Semmelhack, M. Uemura, *Transition Metal Arene π-Complexes in Organic Synthesis and Catalysis, Vol. 7*, Springer-Verlag Berlin Heidelberg, **2004**.
[67] E. M. D'Amato, C. N. Neumann, T. Ritter, *Organometallics* **2015**, *34*, 4626-4631.
[68] J. D. Holmes, D. A. K. Jones, R. Pettit, *J. Organomet. Chem.* **1965**, *4*, 324-331.
[69] M. F. Semmelhack, in *Comprehensive Organometallic Chemistry II*, Elsevier, **1995**, 979-1015.
[70] B. Nicholls, M. C. Whiting, *J. Chem. Soc.* **1959**, *31*, 551-556.
[71] A. J. Pearson, S. Cui, *Tetrahedron Lett.* **2005**, *46*, 2639-2642.
[72] M. H. Beyzavi, D. Mandal, M. G. Strebl, C. N. Neumann, E. M. D'Amato, J. Chen, J. M. Hooker, T. Ritter, *ACS Cent. Sci.* **2017**, *3*, 944-948.

[73] C. Hartmann, V. Meyer, *Ber. Dtsch. Chem. Ges.* **1894**, *27*, 426-432.
[74] F. M. Beringer, A. Brierley, M. Drexler, E. M. Gindler, C. C. Lumpkin, *J. Am. Chem. Soc.* **1953**, *75*, 2708-2712.
[75] A. Shah, V. W. Pike, D. A. Widdowson, *J. Chem. Soc., Perkin Trans. 1* **1998**, *1*, 2043-2046.
[76] T. L. Ross, J. Ermert, C. Hocke, H. H. Coenen, *J. Am. Chem. Soc.* **2007**, *129*, 8018-8025.
[77] J.-H. Chun, S. Lu, Y.-S. Lee, V. W. Pike, *J. Org. Chem.* **2010**, *75*, 3332-3338.
[78] N. Ichiishi, A. F. Brooks, J. J. Topczewski, M. E. Rodnick, M. S. Sanford, P. J. H. Scott, *Org. Lett.* **2014**, *16*, 3224-3227.
[79] N. Ichiishi, A. J. Canty, B. F. Yates, M. S. Sanford, *Org. Lett.* **2013**, *15*, 5134-5137.
[80] A. Casitas, M. Canta, M. Solà, M. Costas, X. Ribas, *J. Am. Chem. Soc.* **2011**, *133*, 19386-19392.
[81] (a) M. F. Ghorab, J. M. Winfield, *J. Fluorine Chem.* **1990**, *49*, 367-383; (b) M. Jauregui-Osoro, K. Sunassee, A. J. Weeks, D. J. Berry, R. L. Paul, M. Cleij, J. P. Banga, M. J. O'Doherty, P. K. Marsden, S. E. Clarke, J. R. Ballinger, I. Szanda, S. Y. Cheng, P. J. Blower, *Eur. J. Nucl. Med. Mol. Imaging* **2010**, *37*, 2108-2116.
[82] I. A. I. Mkhalid, J. H. Barnard, T. B. Marder, J. M. Murphy, J. F. Hartwig, *Chem. Rev.* **2010**, *110*, 890-931.
[83] (a) D. M. T. Chan, K. L. Monaco, R.-P. Wang, M. P. Winters, *Tetrahedron Lett.* **1998**, *39*, 2933-2936; (b) D. A. Evans, J. L. Katz, T. R. West, *Tetrahedron Lett.* **1998**, *39*, 2937-2940; (c) P. Y. S. Lam, C. G. Clark, S. Saubern, J. Adams, M. P. Winters, D. M. T. Chan, A. Combs, *Tetrahedron Lett.* **1998**, *39*, 2941-2944.
[84] J. X. Qiao, P. Y. S. Lam, *Synthesis* **2011**, *6*, 829-856.
[85] P. S. Fier, J. Luo, J. F. Hartwig, *J. Am. Chem. Soc.* **2013**, *135*, 2552-2559.
[86] M. Tredwell, S. M. Preshlock, N. J. Taylor, S. Gruber, M. Huiban, J. Passchier, J. Mercier, C. Génicot, V. Gouverneur, *Angew. Chem., Int. Ed.* **2014**, *53*, 7751-7755.
[87] B. D. Wright, S. E. Lapi, *J. Nucl. Med.* **2013**, *54*, 1171-1174.

[88] S. Lee, J. Xie, X. Chen, *Chem. Rev.* **2010**, *110*, 3087-3111.
[89] L. Gentilucci, R. De Marco, L. Cerisoli, *Curr. Pharm. Des.* **2010**, *16*, 3185-3203.
[90] A. N. Eberle, G. Mild, S. Froidevaux, *J. Recept. Signal Transduction* **2004**, *24*, 319-455.
[91] (a) J. C. Reubi, A. M. Landolt, *J. Clin. Endocrinol. Metab.* **1984**, *59*, 1148-1151; (b) D. Storch, M. Béhé, M. A. Walter, J. Chen, P. Powell, R. Mikolajczak, H. R. Mäcke, *J. Nucl. Med.* **2005**, *46*, 1561-1569.
[92] W. Zhao, H. G. Lee, S. L. Buchwald, J. M. Hooker, *J. Am. Chem. Soc.* **2017**, *139*, 7152-7155.
[93] M. Nič, J. Jirát, B. Košata, A. Jenkins, A. McNaught, *IUPAC Compendium of Chemical Terminology*, **2009**.
[94] D. Brasse, A. Nonat, *Dalton Trans.* **2015**, *44*, 4845-4858.
[95] H. R. Maecke, J. C. Reubi, *J. Nucl. Med.* **2011**, *52*, 841-844.
[96] S. Froidevaux, A. Heppeler, A. N. Eberle, A. M. Meier, M. Hausler, C. Beglinger, M. Behe, P. Powell, H. R. Macke, *Endocrinology* **2000**, *141*, 3304-3312.
[97] S. Richter, F. Wuest, *Molecules* **2014**, *19*, 20536-20556.
[98] S. Vallabhajosula, *Molecular Imaging*, Springer-Verlag Berlin Heidelberg, **2009**.
[99] C. L. Charron, J. L. Hickey, T. K. Nsiama, D. R. Cruickshank, W. L. Turnbull, L. G. Luyt, *Nat. Prod. Rep.* **2016**, *33*, 761-800.
[100] (a) J. A. Dean, N. A. Lange, *Lange's Handbook of Chemistry*, McGraw-Hill, **1999**; (b) R. Schirrmacher, G. Bradtmöller, E. Schirrmacher, O. Thews, J. Tillmanns, T. Siessmeier, H. G. Buchholz, P. Bartenstein, B. Wängler, C. M. Niemeyer, K. Jurkschat, *Angew. Chem., Int. Ed.* **2006**, *45*, 6047-6050.
[101] M. S. Rosenthal, A. L. Bosch, R. J. Nickles, S. J. Gatley, *Int. J. Appl. Radiat. Isot.* **1985**, *36*, 318-319.
[102] A. Höhne, L. Yu, L. Mu, M. Reiher, U. Voigtmann, U. Klar, K. Graham, P. A. Schubiger, S. M. Ametamey, *Chem. Eur. J.* **2009**, *15*, 3736-3743.
[103] A. Höhne, L. Mu, M. Honer, P. A. Schubiger, S. M. Ametamey, K. Graham, T. Stellfeld, S. Borkowski, D. Berndorff, U. Klar, U. Voigtmann, J. E. Cyr, M. Friebe, L.

Dinkelborg, A. Srinivasan, *Bioconjugate Chem.* **2008**, *19*, 1871-1879.

[104] Z. Liu, Y. Li, R. Ting, D. M. Perrin, *J. Phys. Org. Chem.* **2015**, *28*, 210-214.

[105] (a) R. Ting, C. W. Harwig, J. Lo, Y. Li, M. J. Adam, T. J. Ruth, D. M. Perrin, *J. Org. Chem.* **2008**, *73*, 4662-4670; (b) R. Ting, C. Harwig, U. auf dem Keller, S. McCormick, P. Austin, C. M. Overall, M. J. Adam, T. J. Ruth, D. M. Perrin, *J. Am. Chem. Soc.* **2008**, *130*, 12045-12055.

[106] D. M. Perrin, *Acc Chem Res* **2016**, *49*, 1333-1343.

[107] Z. Liu, D. Chao, Y. Li, R. Ting, J. Oh, D. M. Perrin, *Chem. Eur. J.* **2015**, *21*, 3924-3928.

[108] Z. Liu, M. Pourghiasian, M. A. Radtke, J. Lau, J. Pan, G. M. Dias, D. Yapp, K.-S. Lin, F. Bénard, D. M. Perrin, *Angew. Chem., Int. Ed.* **2014**, *53*, 11876-11880.

[109] Z. Liu, M. Pourghiasian, F. Benard, J. Pan, K. S. Lin, D. M. Perrin, *J. Nucl. Med.* **2014**, *55*, 1499-1505.

[110] (a) V. V. Rostovtsev, L. G. Green, V. V. Fokin, K. B. Sharpless, *Angew. Chem., Int. Ed.* **2002**, *41*, 2596-2599; (b) C. W. Tornøe, C. Christensen, M. Meldal, *J. Org. Chem.* **2002**, *67*, 3057-3064.

[111] J. Marik, J. L. Sutcliffe, *Tetrahedron Lett.* **2006**, *47*, 6681-6684.

[112] N. J. Agard, J. A. Prescher, C. R. Bertozzi, *J. Am. Chem. Soc.* **2004**, *126*, 15046-15047.

[113] (a) Z. Li, T. S. Seo, J. Ju, *Tetrahedron Lett.* **2004**, *45*, 3143-3146; (b) G. Wittig, A. Krebs, *Chem. Ber.* **1961**, *94*, 3260-3275.

[114] L. S. Campbell-Verduyn, L. Mirfeizi, A. K. Schoonen, R. A. Dierckx, P. H. Elsinga, B. L. Feringa, *Angew. Chem., Int. Ed.* **2011**, *50*, 11117-11120.

[115] K. Sachin, V. H. Jadhav, E.-M. Kim, H. L. Kim, S. B. Lee, H.-J. Jeong, S. T. Lim, M.-H. Sohn, D. W. Kim, *Bioconjugate Chem.* **2012**, *23*, 1680-1686.

[116] O. C. Boerman, W. J. G. Oyen, F. H. M. Corstens, *Semin. Nucl. Med.* **2000**, *30*, 195-208.

[117] G. Vaidyanathan, M. R. Zalutsky, *Int. J. Radiat. Appl. Instrum. Part B* **1992**, *19*, 275-281.
[118] H.-J. Wester, K. Hamacher, G. Stöcklin, *Nucl. Med. Biol.* **1996**, *23*, 365-372.
[119] M. Berndt, J. Pietzsch, F. Wuest, *Nucl. Med. Biol.* **2007**, *34*, 5-15.
[120] R. Schirrmacher, B. Wangler, J. Bailey, V. Bernard-Gauthier, E. Schirrmacher, C. Wangler, *Semin Nucl Med* **2017**, *47*, 474-492.
[121] S. Verhoog, C. W. Kee, Y. Wang, T. Khotavivattana, T. C. Wilson, V. Kersemans, S. Smart, M. Tredwell, B. G. Davis, V. Gouverneur, *J. Am. Chem. Soc.* **2018**, *140*, 1572-1575.
[122] M. Ogawa, K. Hatano, S. Oishi, Y. Kawasumi, N. Fujii, M. Kawaguchi, R. Doi, M. Imamura, M. Yamamoto, K. Ajito, T. Mukai, H. Saji, K. Ito, *Nucl. Med. Biol.* **2003**, *30*, 1-9.
[123] V. M. Labroo, D. Hebel, K. L. Kirk, L. A. Cohen, C. Lemieux, P. W. Schiller, *Int. J. Pept. Protein Res.* **1991**, *37*, 430-439.
[124] X. Huang, W. Liu, H. Ren, R. Neelamegam, J. M. Hooker, J. T. Groves, *J. Am. Chem. Soc.* **2014**, *136*, 6842-6845.
[125] W. Liu, X. Huang, M. S. Placzek, S. W. Krska, P. McQuade, J. M. Hooker, J. T. Groves, *Chem. Sci.* **2018**, *9*, 1168-1172.
[126] M. B. Nodwell, H. Yang, M. Čolović, Z. Yuan, H. Merkens, R. E. Martin, F. Bénard, P. Schaffer, R. Britton, *J. Am. Chem. Soc.* **2017**, *139*, 3595-3598.
[127] H. Teare, E. G. Robins, E. Årstad, S. K. Luthra, V. Gouverneur, *Chem. Commun.* **2007**, 2330-2332.
[128] Z. Yuan, M. B. Nodwell, H. Yang, N. Malik, H. Merkens, F. Bénard, R. E. Martin, P. Schaffer, R. Britton, *Angew. Chem., Int. Ed.* **2018**, *57*, 12733-12736.
[129] G. Clemente, J. Rickmeier, T. Zarganes-Tzitzikas, I. Antunes, R. Slart, A. Dömling, T. Ritter, P. Elsinga, *J. Labelled Compd. Radiopharm.* **2019**, *62*, S84-S85.
[130] G. A. Roth, C. Johnson, A. Abajobir, F. Abd-Allah, S. F. Abera, G. Abyu, M. Ahmed, B. Aksut, T. Alam, K. Alam, F. Alla, N. Alvis-Guzman, S. Amrock, H. Ansari, J. Ärnlöv, H.

Asayesh, T. M. Atey, L. Avila-Burgos, A. Awasthi, A. Banerjee, et al., *J. Am. Coll. Cardiol.* **2017**, *70*, 1-25.
[131] D. P. Barr, E. M. Russ, H. A. Eder, *Am. J. Med.* **1951**, *11*, 480-493.
[132] A. Endo, M. Kuroda, K. Tanzawa, *FEBS Lett.* **1976**, *72*, 323-326.
[133] N. A. McGrath, M. Brichacek, J. T. Njardarson, *J. Chem. Educ.* **2010**, *87*, 1348-1349.
[134] J. K. Liao, U. Laufs, *Annu. Rev. Pharmacol. Toxicol.* **2005**, *45*, 89-118.
[135] A. Oesterle, U. Laufs, J. K. Liao, *Circ. Res.* **2017**, *120*, 229-243.
[136] G. Weitz-Schmidt, K. Welzenbach, V. Brinkmann, T. Kamata, J. Kallen, C. Bruns, S. Cottens, Y. Takada, U. Hommel, *Nat. Med.* **2001**, *7*, 687-692.
[137] Ž. Reiner, *Nutr., Metab. Cardiovasc. Dis.* **2014**, *24*, 1057-1066.
[138] H. Lennernäs, *Clin. Pharmacokinet.* **2003**, *42*, 1141-1160.
[139] B.-C. Chen, J. E. Sundeen, P. Guo, M. S. Bednarz, J. J. Hangeland, S. Z. Ahmed, M. Jemal, *J. Labelled Compd. Radiopharm.* **2000**, *43*, 261-270.
[140] H. Stetter, M. Schreckenberg, *Angew. Chem., Int. Ed.* **1973**, *12*, 81-81.
[141] L. Knorr, *Ber. Dtsch. Chem. Ges.* **1885**, *18*, 299-311.
[142] N. A. Vol'kenau, I. N. Bolesova, L. S. Shul'pina, A. N. Kitaigorodskii, D. M. Kravtsov, *J. Organomet. Chem.* **1985**, *288*, 341-348.
[143] E. E. Karslyan, D. S. Perekalin, P. V. Petrovskii, K. A. Lyssenko, A. R. Kudinov, *Russ. Chem. Bull.* **2009**, *57*, 2201.
[144] R. Richarz, P. Krapf, F. Zarrad, E. A. Urusova, B. Neumaier, B. D. Zlatopolskiy, *Org. Biomol. Chem.* **2014**, *12*, 8094-8099.
[145] A. V. Mossine, A. F. Brooks, N. Ichiishi, K. J. Makaravage, M. S. Sanford, P. J. H. Scott, *Sci. Rep.* **2017**, *7*, 233.
[146] J. Rickmeier, T. Ritter, *Angew. Chem., Int. Ed.* **2018**, *57*, 14207-14211.

[147] M. Fani, H. R. Maecke, S. M. Okarvi, *Theranostics* **2012**, *2*, 481-501.
[148] M. R. Kilbourn, M. J. Welch, *Int. J. Radiat. Appl. Instrum. Part A* **1986**, *37*, 677-683.
[149] S. M. Okarvi, *Eur. J. Nucl. Med.* **2001**, *28*, 929-938.
[150] H.-W. Kim, J. A. Perez, S. J. Ferguson, I. D. Campbell, *FEBS Lett.* **1990**, *272*, 34-36.
[151] M. A. Danielson, J. J. Falke, *Annu. Rev. Biophys. Biomol. Struct.* **1996**, *25*, 163-195.
[152] (a) D. S. Perekalin, E. E. Karslyan, P. V. Petrovskii, Y. V. Nelyubina, K. A. Lyssenko, A. S. Kononikhin, E. N. Nikolaev, A. R. Kudinov, *Chem. Eur. J.* **2010**, *16*, 8466-8470; (b) B. Albada, N. Metzler-Nolte, *Chem. Rev.* **2016**, *116*, 11797-11839.
[153] N. A. Vol'kenau, I. N. Bolesova, L. S. Shul'pina, A. N. Kitaigorodskii, *J. Organomet. Chem.* **1984**, *267*, 313-321.
[154] (a) D. P. Cox, J. Terpinski, W. Lawrynowicz, *J. Org. Chem.* **1984**, *49*, 3216-3219; (b) H. Sun, S. G. DiMagno, *J. Am. Chem. Soc.* **2005**, *127*, 2050-2051.
[155] A. R. Mahjoub, X. Zhang, K. Seppelt, *Chem. Eur. J.* **1995**, *1*, 261-265.
[156] M. G. Marino, K. D. Kreuer, *ChemSusChem* **2015**, *8*, 513-523.
[157] D. S. Perekalin, V. V. Novikov, A. A. Pavlov, I. A. Ivanov, N. Y. Anisimova, A. N. Kopylov, D. S. Volkov, I. F. Seregina, M. A. Bolshov, A. R. Kudinov, *Chem. Eur. J.* **2015**, *21*, 4923-4925.
[158] S. Good, M. A. Walter, B. Waser, X. Wang, J. Müller-Brand, M. P. Béhé, J. C. Reubi, H. R. Maecke, *Eur. J. Nucl. Med. Mol. Imaging* **2008**, *35*, 1868-1877.
[159] L. Di, *AAPS J.* **2015**, *17*, 134-143.
[160] J. H. Jones, W. I. Ramage, M. J. Witty, *Int. J. Pept. Protein Res.* **2009**, *15*, 301-303.
[161] M. Lazari, J. Irribarren, S. Zhang, R. M. van Dam, *Appl. Radiat. Isot.* **2016**, *108*, 82-91.
[162] (a) https://www.gmp-compliance.org/gmp-news/ich-q3d-implemented-in-the-european-pharmacopoeia-revision-of-

two-general-monographs-with-regard-to-elemental-impurities; (b) w. i. o. International Conference on Harmonization. 2009. Final Concept Paper Q3D: Impurities: Guideline for elemental impurities. Accessed August 08.

[163] Y. Mine, T. Noutomi, N. Haga, *J. Agric. Food Chem.* **1990**, *38*, 2122-2125.

[164] D. F. Shriver, M. A. Drezdzon, *The Manipulation of Air-Sensitive Compounds*, Wiley, **1986**.

[165] G. R. Fulmer, A. J. M. Miller, N. H. Sherden, H. E. Gottlieb, A. Nudelman, B. M. Stoltz, J. E. Bercaw, K. I. Goldberg, *Organometallics* **2010**, *29*, 2176-2179.

[166] R. K. Harris, E. D. Becker, S. M. Cabral de Menezes, R. Goodfellow, P. Granger, *Solid State Nucl. Magn. Reson.* **2002**, *22*, 458-483.

[167] R. B. Moffett, *Org. Synth.* **1952**, *32*, 41-44.

[168] A. Mercier, W. C. Yeo, J. Chou, P. D. Chaudhuri, G. Bernardinelli, E. P. Kündig, *Chem. Commun.* **2009**, 5227-5229.

[169] E. P. Kündig, F. R. Monnier, *Adv. Synth. Catal.* **2004**, *346*, 901-904.

[170] A. Dorcier, P. J. Dyson, J. S. McIndoe, *Eur. J. Inorg. Chem.* **2003**, *2003*, 4294-4297.

[171] D. DiMondo, M. E. Thibault, J. Britten, M. Schlaf, *Organometallics* **2013**, *32*, 6541-6554.

[172] J. B. Edson, C. S. Macomber, B. S. Pivovar, J. M. Boncella, *J. Membr. Sci.* **2012**, *399-400*, 49-59.

[173] W. C. Chan, P. D. White, *Fmoc Solid Phase Peptide Synthesis: A Practical Approach*, Oxford University Press, **2000**.

[174] S. Eissler, M. Kley, D. Bächle, G. Loidl, T. Meier, D. Samson, *J. Pept. Sci.* **2017**, *23*, 757-762.

VI. Appendix

VI.1. Eidesstattliche Erklärung

Henrick Jens Rickmeier

erklärt hiermit, dass diese Dissertation und die darin dargelegten Inhalte die eigenen sind und selbstständig, als Ergebnis der eigenen originären Forschung, generiert wurden.

Hiermit erkläre ich an Eides statt

1.Diese Arbeit wurde vollständig oder größtenteils in der Phase als Doktorand dieser Fakultät und Universität angefertigt;

2.Sofern irgendein Bestandteil dieser Dissertation zuvor für einen akademischen Abschluss oder eine andere Qualifikation an dieser oder einer anderen Institution verwendet wurde, wurde dies klar angezeigt;

3.Wenn immer andere eigene-oder Veröffentlichungen Dritter herangezogen wurden, wurden diese klar benannt;

4.Wenn aus anderen eigenen- oder Veröffentlichungen Dritter zitiert wurde, wurde stets die Quelle hierfür angegeben. Diese Dissertation ist vollständig meine eigene Arbeit, mit der Ausnahme solcher Zitate;

5.Alle wesentlichen Quellen von Unterstützung wurden benannt;

6.Wenn immer ein Teil dieser Dissertation auf der Zusammenarbeit mit anderen basiert, wurde von mir klar gekennzeichnet, was von anderen und was von mir selbst erarbeitet wurde;

7. Ein Teil oder Teile dieser Arbeit wurden zuvor veröffentlicht und zwar in:

Site-Specific Deoxyfluorination of Small Peptides with [^{18}F]Fluoride. **J. Rickmeier**, T. Ritter, *Angew. Chem. Int. Ed.* **2018**, *57*, 14207–14211.

Automated Radiosynthesis of [^{18}F]Atorvastatin via Ru-mediated ^{18}F-deoxyfluorination: a prospective PET-Imaging Tool for the Assessment of Statin related Mechanisms of Action. G. S. Clemente, **J. Rickmeier**, T. Zarganes-Tzitzikas, F. I. Antunes, R. H. J. A. Slart, A. Dömling, T. Ritter, P. H. Elsinga *J. Labelled Compd. Radiopharm.* **2019**, *62*, S84-S85.

"Reagent and process for the site-specific deoxyfluorination of peptides", Tobias Ritter and **Henrick Jens Rickmeier**, EP18181055.7, **2018**

19.06.2019

Jens Rickmeier

VI.2. List of Publication

(5) Gonçalo S. Clemente, **Jens Rickmeier**, Tryfon Zarganes-Tzitzikas, Farinha I. Antunes, Riemer H. J. A. Slart, Alexander Dömling, Tobias Ritter, Philip H. Elsinga, "Automated Radiosynthesis of [^{18}F]Atorvastatin via Ru-mediated ^{18}F-deoxyfluorination: a prospective PET-Imaging Tool for the Assessment of Statin related Mechanisms of Action", *J. Labelled Compd. Radiopharm.* **2019**, *62*, S84-S85.

(4) Goncalo S. Clemente, Farinha I. Antunes, **Jens Rickmeier**, Ben L. Feringa, Philip H. Elsinga, Tobias Ritter, "Automated Synthesis Of 5-[^{18}F]fluoro-tryptophan Via Deoxyfluorination Of A Phenol-derived Ru-coordinated Complex", *Eur. J. Nucl. Med. Mol. Imaging*, **2018**, *45* (1), S223–S223.

(3) **Jens Rickmeier** and Tobias Ritter, "Site-Specific Deoxyfluorination of Small Peptides with [^{18}F]Fluoride" Angew. Chem. Int. Ed., **2018**, *57*, 14207–14211.

(2) Philip C. Hogan, Chi-Li Chen, Kristen M. Mulvihill, Jonathan F. Lawrence, Eric Moorhead, **Jens Rickmeier** and Andrew G. Myers "Large-scale preparation of key building blocks for the manufacture of fully synthetic macrolide antibiotics" *Journal of Antibiotics (Tokyo)* **2018**, *71*, 318–325.

(1) Tatjana Huber, Daniel Kaiser, **Jens Rickmeier** and Thomas Magauer "Experimental Studies on the Selective *β*-C–H Halogenation of Enones" *J. Org. Chem.*, **2015**, *80* (4), 2281–2294.

Patents

"Reagent and process for the site-specific deoxyfluorination of peptides", Tobias Ritter and **Henrick Jens Rickmeier**, EP18181055.7, **2018**

VI.3. Curriculum Vitae

Henrick Jens Rickmeier

Max-Planck-Institut für Kohlenforschung
Kaiser-Wilhelm-Platz 1
45470 Mülheim an der Ruhr

Tel: +49 152 09576492
rickmeier@mpi-muelheim.mpg.de

Date of birth: 4. April 1991
Place of birth: Ahlen

EDUCATION

10/2015–present	**Ph.D. candidate in chemistry** | Max-Planck-Institut für Kohlenforschung, Mülheim *Advisor: Prof. Dr. Tobias Ritter* Doctoral thesis subject: ^{18}F labeling of small molecules and peptides
10/2013–08/2015	**M.Sc. in chemistry (Final grade 1.1)** | Ludwig-Maximilians-Universität, Munich
10/2010–08/2013	**B.Sc. in chemical engineering (Final grade: 1.4)** | University of Applied Science, Münster

VOCATIONAL TRAINING

08/2007–07/2010	Hans-Böckler-Berufskolleg, Münster Trainee as a chemical-technical assistant (Final mark: 1.7) University of applied science entrance qualification (Final mark: 1.7)

RESEARCH EXPERIENCE

02/2015–08/2015	**Master's thesis | Harvard University, Boston** *Advisor: Prof. Dr. Andrew G. Myers* Development of a scalable synthesis of pseudoephenamine
08/2014–09/2014	**Visiting researcher | Ludwig-Maximilians-Universität, Munich** *Advisor: Prof. Dr. Thomas Magauer* The one-pot *β*-chlorination of enones
04/2014–06/2014	**Visiting researcher | Ludwig-Maximilians-Universität, Munich** *Advisor: Prof. Dr. Sonja Herres-Pawlis* Development of new hybrid guanidine-quinoline ligands for ATRP
03/2013–08/2013	**Bachelor's thesis | James Cook University, Townsville** *Advisor: Prof. Dr. Peter Junk* Synthesis of organolanthanoid complexes and crystal structure analysis

SCHOLARSHIPS AND AWARDS

12/10/2017	Lanxess Lecture Award at the Young Chemists' Symposium Ruhr 2017
02/2015–08/2015	PROSA^{LMU} Auslandsstipendium
06/2013–09/2013	DAAD-Schlorschip (PROMOS)